APPSBX 23 1–204(1974)

Scanning Electron Microscopy of Polymers and Coatings. II

Editor:
L. H. Princen

1974: an Interscience® Publication

```
@str@
*MSG DI4 DROLS PROCESSING-LAST INPUT IGNORED

*MSG DI4 DROLS PROCESSING-LAST INPUT IGNORED

*MSG DI4  DROLS PROCESSING - LAST INPUT IGNORED


--    1   OF     5
--                    ***DTIC DOES NOT HAVE THIS ITEM***
-- 1 -  AD NUMBER: D405344
-- 5 -  CORPORATE AUTHOR: AMERICAN CHEMICAL SOCIETY WASHINGTON D C
-- 6 -  UNCLASSIFIED TITLE:     APPLIED POLYMER SYMPOSIA NO. 23. SCANNING
--      ELECTRON MICROSCOPY OF POLYMERS AND COATINGS.
--10 -  PERSONAL AUTHORS: PRINCEN,L.H. ;
--11 -  REPORT DATE:      JAN    , 1974
--12 -  PAGINATION: XXXXXX    MEDIA COST:  $  6.00
--20 -  REPORT CLASSIFICATION:  UNCLASSIFIED
--21 -  SUPPLEMENTARY NOTE:     PROCEEDING: SCANNING ELECTRON MICROSCOPY OF
--      POLYMERS AND COATING. II, 8-13 APR 73, DALLAS, TEXAS. SPONSORED BY
--      ACS, DIV. OF ORG. COATINGS AND PLASTICS CHEM.
--33 -  LIMITATION CODES:  1

-- END             Y  FOR NEXT ACCESSION                END

 Alt-Z FOR HELP3 ANSI     3 HDX 3          3 LOG CLOSED 3 PRINT OFF 3 PARITY
```

APPLIED POLYMER SYMPOSIA NO. 23

Scanning Electron Microscopy of Polymers and Coatings. II

Symposium held at the 165th National Meeting of the American Chemical Society, Dallas, Texas, April 8–13, 1973

Sponsored by *The Division of Organic Coatings and Plastics Chemistry, American Chemical Society*

Editor

L. H. Princen
Northern Regional Research Laboratory
U. S. Department of Agriculture

an Interscience® Publication

published by **JOHN WILEY & SONS**
NEW YORK • LONDON • SYDNEY • TORONTO

JOURNAL OF APPLIED POLYMER SCIENCE
APPLIED POLYMER SYMPOSIA NO. 23

L. H. Princen has been appointed Editor by the Editorial Board of the *Journal of Applied Polymer Science* for this issue of *Applied Polymer Symposia.*

Published at irregular intervals by John Wiley & Sons, Inc. Publication Office at 20th and Northampton Streets, Easton, Pennsylvania 18042. Executive, Editorial, and Circulation Offices at 605 Third Avenue, New York, New York 10016. Subscription price $180.00 per volume. Foreign postage, $11.00 per volume.

Printed in U.S.A.

Preface

While the first symposium on Scanning Electron Microscopy of Polymers and Coatings was being held during the joint meeting of the American Chemical Society and the Chemical Institute of Canada at Toronto in May 1970, I was asked to organize a follow-up. The second symposium was held at the 165th National Meeting of the American Chemical Society in Dallas, Texas, in April 1973, before the Division of Organic Coatings and Plastics Chemistry. The collected papers of the second symposium represent a companion volume to Applied Polymer Symposium No. 16.

Whereas the first program included papers on a wide variety of topics, the second symposium was divided into three main areas of coatings, electron resist polymers, and fibers. Dr. Larry Thompson of Bell Laboratories ably organized the half-day session on electron resist polymers. This new field is especially appropriate, because it uses the scanning electron microscope as a scribing tool coupled with its conventional morphological use. Although published papers on this topic emphasize impact on microelectronics, this is the first time that the chemical and scanning electron microscopic aspects have been presented in so much detail.

As the use of scanning electron microscopy in the field of coatings and polymers increases, scientists become more aware of closely related techniques, such as x-ray spectroscopy. The second symposium includes two papers on this technique: one describes the x-ray unit interfaced with an existing microscope, and the other deals with a closely related tool, the electron microprobe. In the future, we shall see more combining of scanning electron microscopy with other instruments and with other techniques, to arrive at more sophisticated probing of our many problems.

All authors must be commended for meeting deadlines during organization of the symposium and for their cooperation during the editing of their papers for this second volume. Each paper has been extensively revised and updated by the authors. The staff at the Northern Regional Research Laboratory, Agricultural Research Service, U.S. Department of Agriculture, assisted in planning the symposium and in compiling this volume. I appreciate especially the approval and encouragement by my superiors to accept an assignment of this nature.

L. H. PRINCEN

Northern Regional Research Laboratory
Peoria, Illinois

Contributors

F. L. Baker
Northern Regional Research Laboratory, U.S. Department of Agriculture, Peoria, Illinois

J. L. Bartelt
Bell Telephone Laboratories, Murray Hill, New Jersey

M. J. Bowden
Bell Telephone Laboratories, Murray Hill, New Jersey

A. R. Bunsell
School of Applied Sciences, University of Sussex, Falmar, Sussex, England

O. L. Carter
Rohm and Haas Research Laboratories, Spring House, Pennsylvania

R. D. Corneliussen
Department of Metallurgical Engineering, Drexel University, Philadelphia, Pennsylvania

J. C. Dubois
Laboratoire Central de Recherches, Thomson-CSF, Orsay, France

C. Duchesne
Laboratoire Central de Recherches, Thomson-CSF, Orsay, France

G. J. Ebben
Research and Development, American Can Company, Barrington, Illinois

R. L. Eissler
Northern Regional Research Laboratory, U.S. Department of Agriculture, Peoria, Illinois

E. D. Feit
Bell Telephone Laboratories, Murray Hill, New Jersey

F. Figucia
U.S. Army Natick Laboratories, Department of the Army, Natick, Massachusetts

M. Gazard
Laboratoire Central de Recherches, Thomson-CSF, Orsay, France

M. Hatzakis
IBM Thomas J. Watson Research Center, Yorktown Heights, New York

J. W. S. Hearle
Institute of Science and Technology, University of Manchester, Manchester, England

R. D. Heidenreich
Bell Telephone Laboratories, Murray Hill, New Jersey

I. Kamel
Department of Metallurgical Engineering, Drexel University, Philadelphia, Pennsylvania

B. H. KIRKWOOD
U.S. Army Natick Laboratories, Department of the Army, Natick, Massachusetts

M. J. KOCZAK
Department of Metallurgical Engineering, Drexel University, Philadelphia, Pennsylvania

S. S. LABANA
Scientific Research Staff, Ford Motor Company, Dearborn, Michigan

R. C. LAIBLE
U.S. Army Natick Laboratories, Department of the Army, Natick, Massachusetts

L. LANDAUER
Research and Development, American Can Company, Barrington, Illinois

L. H. LEE
Research Laboratory Department, Xerox Corporation, Rochester, New York

B. LOMAS
Institute of Science and Technology, University of Manchester, Manchester, England

H. MORISHITA
Central Research Laboratory, Hitachi, Ltd., Tokyo, Japan

S. NONOGAKI
Central Research Laboratory, Hitachi, Ltd., Tokyo, Japan

L. H. PRINCEN
Northern Regional Research Laboratory, U.S. Department of Agriculture, Peoria, Illinois

A. QUACH
Research and Development Center, PPG Industries, Inc., Springdale, Pennsylvania

E. D. ROBERTS
Mullard Research Laboratories, Redhill, Surrey, England

N. SAITOU
Central Research Laboratory, Hitachi, Ltd., Tokyo, Japan

A. T. SCHINDLER
Rohm and Haas Research Laboratories, Spring House, Pennsylvania

D. T. SMITH
Research and Development, American Can Company, Barrington, Illinois

J. A. STOLP
Northern Regional Research Laboratory, U.S. Department of Agriculture, Peoria, Illinois

L. F. THOMPSON
Bell Telephone Laboratories, Murray Hill, New Jersey

M. WHEELER
Scientific Research Staff, Ford Motor Company, Dearborn, Michigan

E. E. WORMSER
Rohm and Haas Research Laboratories, Spring House, Pennsylvania

Contents

NO Duplicate of Plastec 1990

index

SCANNING ELECTRON MICROSCOPY APPLIED TO ELECTROCOATING PROBLEMS

D. T. SMITH, L. LANDAUER, and G. J. EBBEN

American Can Company–Research and Development, Barrington, Illinois 60010

SYNOPSIS

With the present ecological concern throughout the world, electrocoating has become of great interest in many diverse areas. The scanning electron microscope provides a tool for surface examination which can furnish much more information than simple topography. Variation of accelerating voltage can give information about the sample below the coating surface. Examination of electrocoated samples at different time intervals gives insight into the coating deposition mechanism. With knowledge of the electrocoating mechanism it is possible to tailor the surface to optimum coating conditions. The ease with which the scanning electron microscope allows the determination of many coating and surface characteristics make it an invaluable tool.

INTRODUCTION

The scanning electron microscope (SEM) is an excellent tool for the examination of coating surfaces. The SEM techniques discussed here may be applied to all types of organic coating surfaces, regardless of how the coating has been applied. More specifically, however, this paper deals with the study of electrodeposited organic coating films.

Electrocoating, or electropainting as it is often called, is currently a field of intense study and commercial development. One important reason is the ecological advantage that these water-base electrocoat systems present; industrial solvent-base enamels have always been a prime source of air pollution. To demonstrate the value of SEM, this paper will present several specific examples and problems from our electrocoating studies.

The SEM not only serves as an extension of light microscopy, but also provides several unique features in its applications. Of major importance in examination of nonpigmented coatings is the possibility with the SEM to see only the coating surface. In optical microscopy the base material often interferes with the coating examination, since it is easily seen through a transparent coating. This difference, together with the great depth of field, high magnification, and high resolution makes the SEM very valuable in coatings research.

Preparation of Coatings for SEM Examination

Due to the electrochemical characteristics of an organic coating, special techniques must be used to prepare a sample for the SEM. The coating surface

Applied Polymer Symposium No. 23, 1-12 (1974)

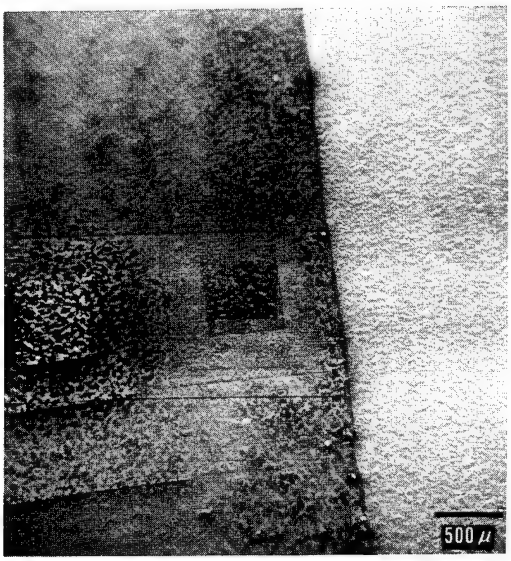

FIG. 1. Coating surface showing charged areas resulting from primary beam; 20X.

is normally a nonconducting material and will build up a charge from the primary electron beam. This charge will then affect the secondary electrons, since their energies are less than 50 eV, and distort the image produced. The result of this charging phenomenon can be seen in Figure 1. The right, lighter portion of the image is that of uncoated metal surface. No charging takes place in this area, and a satisfactory image is produced. The darker area was produced by an organic coating layer. The blotches near the left edge and the dark straight lines are the result of charging that took place during previous raster scans. There are two techniques to correct this condition. The least satisfactory solution is to reduce the accelerating voltage to prevent the charges from building up. This method works only rarely when dealing with organic coatings, since the resolution suffers when the secondary electron signal has been reduced by the reduction of the primary beam voltage. Consequently, high magnification images cannot be produced clearly. Another method to prevent charging is to coat the surface of the sample with a continuous layer of conducting material. This can be done by vacuum deposition of any one of several conducting materials [1, 2]. The most commonly used elements are gold, palladium-gold alloy, aluminum, and carbon. In all our work we have used palladium-gold.

Care must be taken not to produce artifacts when applying the conducting layer. The material must be applied in a thick enough layer to provide a continuous film, yet not so thick that it shows up in the image of the surface. A 100 to 150 Å layer is usually continuous and is thin enough not to be resolved by the SEM. The selection of the metallizing material is important in preventing artifacts. Carbon and palladium-gold appear to present the fewest problems, but often the topography and the chemical make-up of the specimen determine what

coating is most suitable. A problem which may arise as a result of the application of a metallizing layer, and which may be unique to coatings on impervious substrates, is the formation of cracks in the coating. The cracking gives rise to charging in the exposed areas. An example of this problem is shown in Figure 2. This cracking is a direct result of dimensional changes in the sample, caused either by vacuum or heating effects on a sample containing residual moisture. To eliminate the formation of such cracks, moisture-free samples should be used in the vacuum coater or in the SEM. Most cured organic films have given little trouble in this respect.

Accelerating Voltage for Coating Examination

When a sample is mounted and properly coated with a continuous conductive layer, it can be examined in the SEM at any accelerating voltage. The choice of the accelerating voltage is very critical to the information produced [3-5]. By varying the voltage, it is possible to vary the depth of penetration of the beam, and the appearance of the image is changed accordingly. The SEM is often operated at 20 to 30 kV for metal-coated samples, since this voltage range provides the best resolution. If this voltage is used on organic coating samples, a great deal of information may be lost. An example of this can be seen in Figure 3. This series of photomicrographs was taken of the same coating-metal interface on a matte (unmelted) electrolytic tin plate sample. The area at the right side of each micrograph is the uncoated plate surface. In Figure 3a, taken at 30 kV, the coating appears continuous with a number of black spots distributed

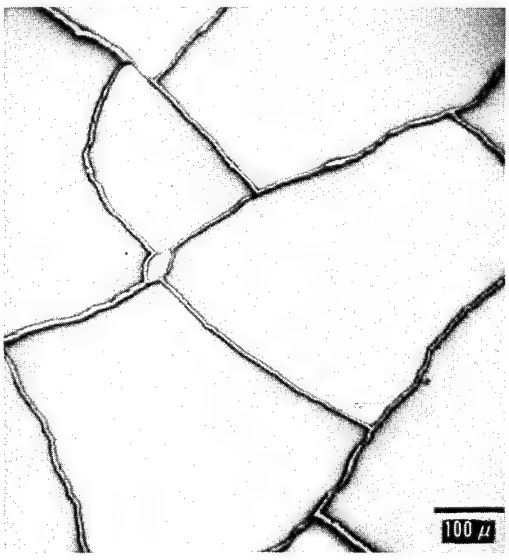

FIG. 2. Cracking in coating surface due to the presence of moisture during metallizing or microscopy; 100X.

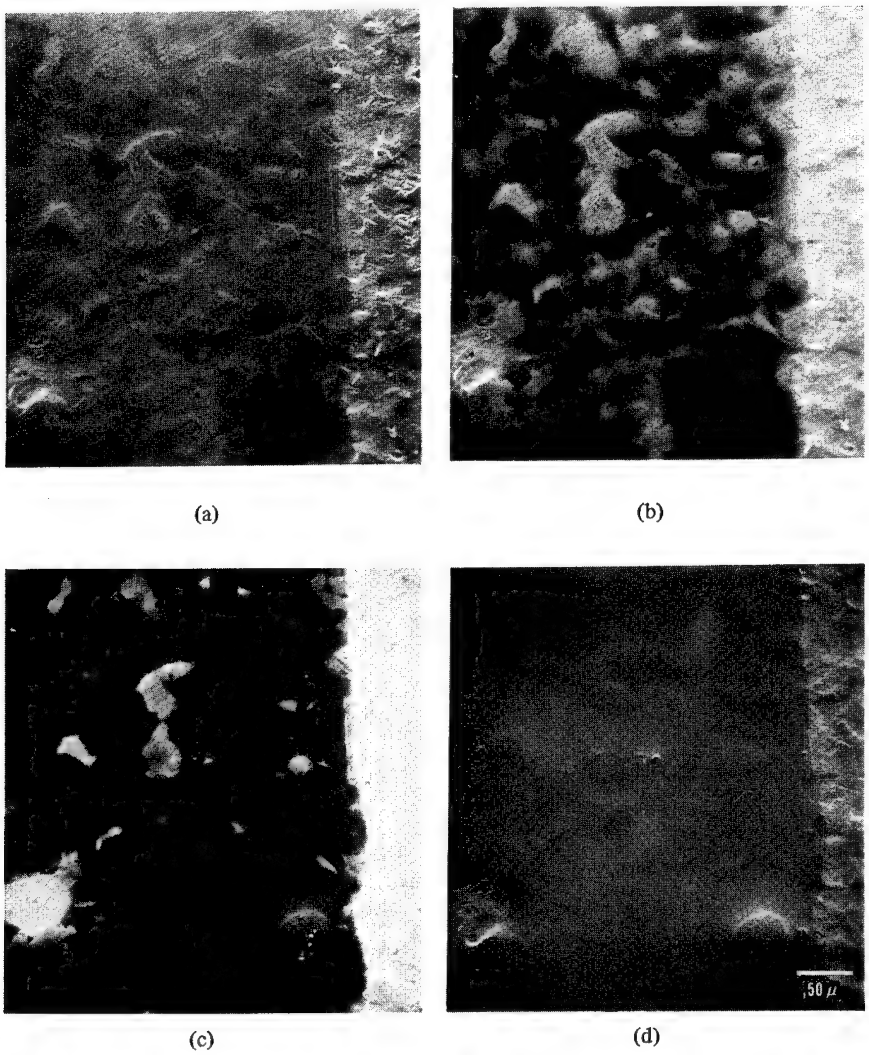

FIG. 3. Clear unpigmented coating on matte tin plate at (a) 30 kV; (b) 20 kV; (c) 10 kV; (d) 2 kV; 200X.

throughout. Much of the matte surface can be seen through the coating, indicating minimal coverage. Figure 3b at 20 kV shows large dark and light areas, which indicate a great variation in the coating thickness over the surface. In addition, a small area of no coverage is coming into view in the lower left corner. At 10 kV, shown in Figure 3c, this void spot is greatly exaggerated, and the areas of very light coating are also pronounced. In Figure 3d the accelerating voltage was 2 kV. The micrograph shows good overall coverage with very little of the features of the matte tin surface showing through. The void area is also easily seen. The series shows that it is possible to get a great deal more information with the SEM than just the surface topography. By varying the accelerating voltage, information about base material, thickness and degree of coverage can be obtained.

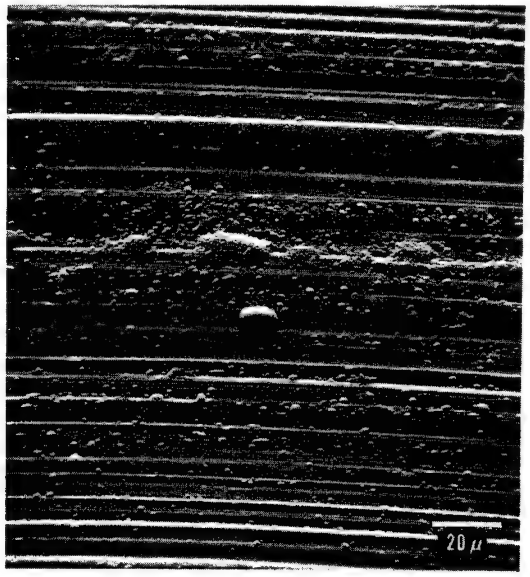

(a)

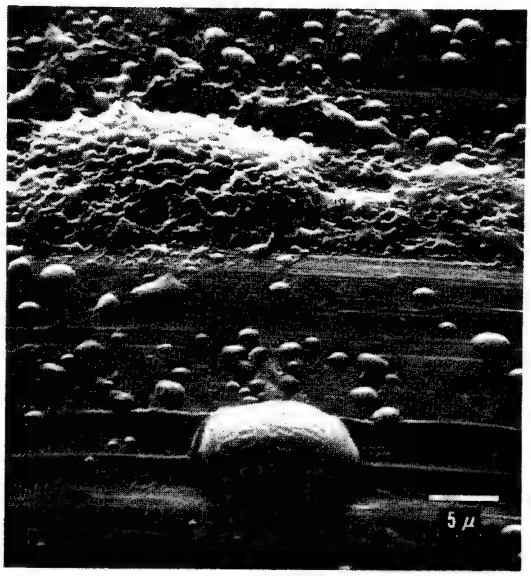

(b)

FIG. 4. Initial electrocoat deposit on aluminum can stock at (a) 500X and (b) 2,000X.

APPLICATION OF SEM TO ELECTROCOATING

In recent years, the electrodeposition of paints has become more and more the subject of extensive research and development efforts. There are many ways the SEM can be used to study the electrodeposition process and to solve specific problems. Several topics pertaining to this field will be discussed below.

Particle Size and Distribution

The SEM offers an interesting approach to the study of the electrocoating mechanism. For example, Figure 4 shows the initial deposition of a clear, nonpigmented electrocoat material on aluminum plate before the coating was baked. This amount was deposited in the first 0.1 sec at 150 V DC. A wide range of particle sizes is observed with distinct differences in texture. The rougher particles are probably the result of gassing, which disrupts the coating as the produced gas is evolved through it. The roughness is apparent only in a small percentage of the coating particles observed. Presumably, the behavior described here represents only one of many chemical mechanisms whereby electrodeposition may take place. We have included these micrographs to illustrate how the SEM may be used to study particle size and distribution during the very early stages of the electrodeposition process. In this way also the effects of surface treatments and contaminants can be studied.

Repair Electrocoating

Since electrodeposition occurs only where exposed bare metal can conduct electric current, the electrodeposition process has the unique ability to repair fractures, scratches, cutedges, and other imperfections in precoated metal pieces. This means that for some applications metal may be sheet or coil coated before fabrication, and any coating damage from fabrication can be repaired after the part is formed.

Figure 5a shows a line of enamel fracture as a result of fabrication damage. Bare metal can be seen exposed at the enamel fracture. Figure 5b shows electrocoating as deposited at such enamel fractures, before the electrocoat deposit was baked. The deposit is somewhat lumpy, as might be expected, since the coating deposits only at the metal exposed through the fractures in the original enamel. Figure 5c represents the same deposit after baking, showing complete flow-out of the electrocoat material and apparent compatibility with the original enamel. A rough estimate of repair coating thickness (or weight) can also be made from this type of examination. In the case of heavy repair beads of electrocoat, failure has sometimes occurred after exposure to certain thermal or mechanical abuses. For example, SEM examination may reveal minute cracks in the repair coating (Fig. 5d), which cannot be observed by other means.

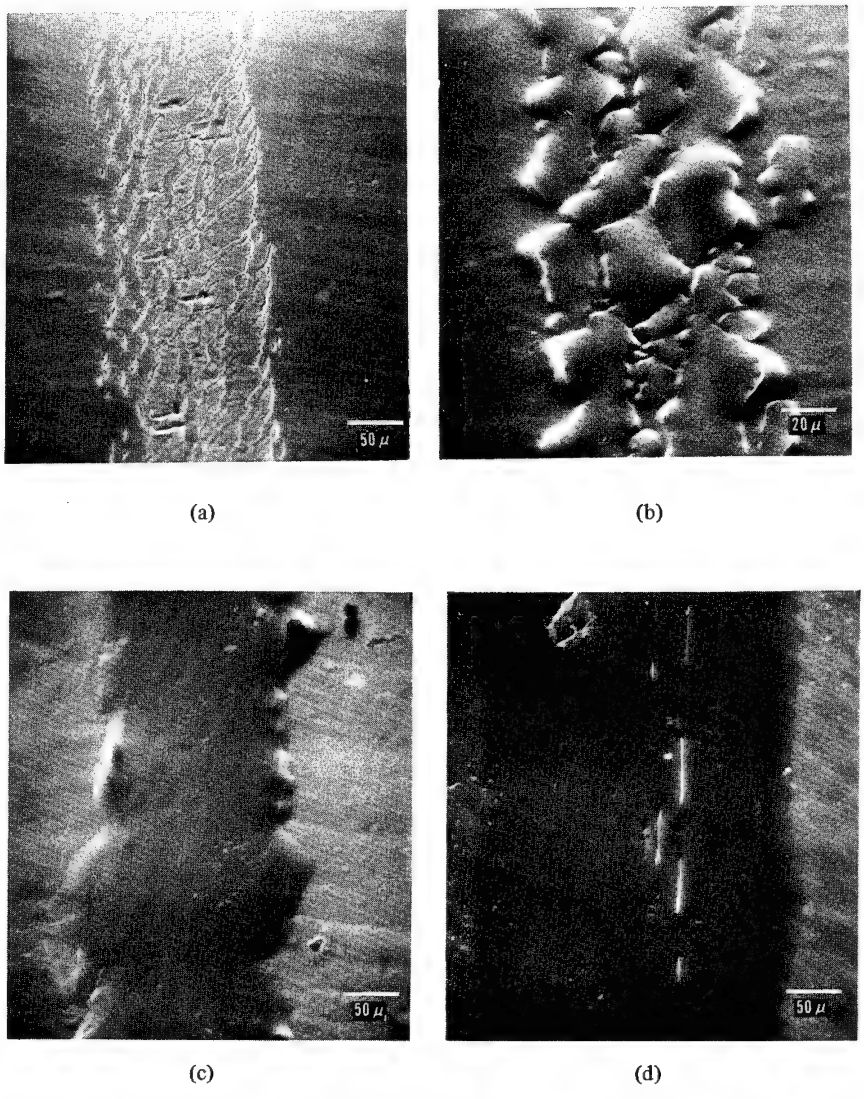

Fig. 5. Repair of fabrication damage in various stages: (a) damage with base metal exposed, 200X; (b) air dried electrocoating deposit on damaged area, 500X; (c) fully cured electrocoating deposite on damaged area, 200X; (d) cured electrocoating deposit showing subsequent damage, 200X.

A Gassing Hole Problem

During the electrodeposition process, gas is generated and evolved through the depositing film. If an anodic deposition is being used, bubbles of oxygen gas must escape. The gas evolution can cause problems as to film continuity, appearance, and corrosion resistance. In our work we have noted the existence

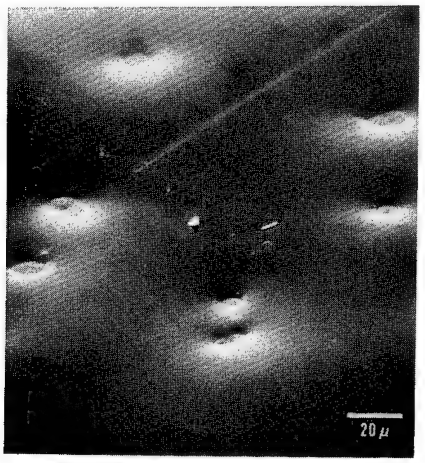

(a)

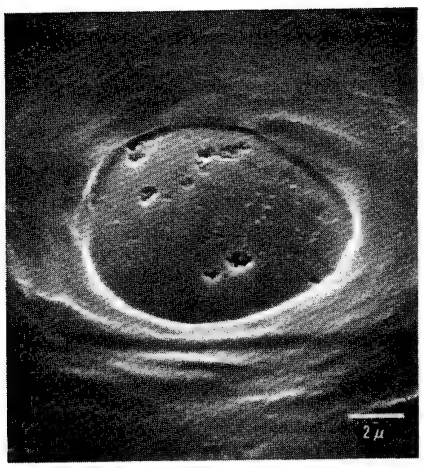

(b)

(c)

FIG. 6. Holes formed in electrocoated surface during coating procedure: (a) overview at 500X; (b) single hole showing discontinuities in base metal, 5,000X; (c) single hole with debris from bubble, 5,000X.

of holes in electrodeposited films, and we believe that they are directly related to gas evolution. The formation of such holes constitutes a major drawback for the application of the electrocoating process where continuous, clear, thin coating films are required. On some plate surfaces the generation of these holes is so profuse as to give the coated surface a nonuniform frosted appearance. There are many factors involved in this problem. They include rinsing and rinse water removal, baking procedures, plate surface conditions, and others.

Of the plates most often used in the container industry, electrolytic tin plate has been consistently the most difficult surface to electrocoat. Aluminum can stock has been consistently the best. This generalization holds true for virtually

all clear, nonpigmented electrocoat materials deposited at thicknesses of ½ mil or less. The SEM was used to study the electrodeposition process in relation to these plate surfaces, to determine what physical plate surface factors might be involved in the generation of these tiny holes.

Figure 6a is a relatively low magnification micrograph of the tiny holes in the electrocoating film with which we are concerned. In many cases, the holes seem to contain a minute dot on the plate surface that is exposed by the hole in the coating. Examination at higher magnification, shown in Figure 6b, indicates these dots are actually microscopic depressions or imperfections in the smooth plate surface. In Figure 6c we can see what appears to be the debris of a gas bubble eruption scattered around the hole in the film. This reinforces the assumption that these holes are caused by gas evolution either before or during the baking of the film. So, at this point it is theorized that the noted defects in an otherwise smooth plate surface serve as nucleation sites for the evolution of gas.

One of the disadvantages of SEM as opposed to transmission electron microscopy (TEM) is the lack of a direct means of measuring surface elevations and depressions. In the TEM surface replication technique, spheres of known size are shadowed at the same angle as the surface being replicated. Shadow lengths are then used to determine heights. SEM samples are viewed directly, and height measurements are usually obtained with stereo pairs and a specially equipped stereoscope. This technique becomes quite involved. When smooth surfaces and low magnification (up to 500X) are involved, it is very convenient to use an interference microscope. The extreme smoothness of coating surfaces and the deposition of highly reflective metals like paladium-gold combine to produce excellent interference patterns for height determinations.

Interference micrographs of the film involved in this study are seen in Figure 7. They show that the holes extend to the metal surface, and that one or more micropits are present in the metal surface in each hole. The holes are steep walled initially from the metal surface. The steep section of wall is followed by a tapered section forming a depression 3 to 4 times the size of the original hole. The depth of the tapered area is easily determined to be 1.2 to 1.9 μm by counting the number of interference rings and combining that number with the half wavelength of the light used, which was 0.244 μm. The thickness of the coating can be estimated as 3.8 μm from the film weight, so the straight wall portion of the hole is estimated to be up to one half of the coating thickness.

If plate surface defects in an otherwise smooth surface can serve as nucleation sites for gas evolution during the electrocoating process, the scattered micropits in the tin plate surface could conceivably cause a tendency toward collection of gas in larger gas bubbles rather than evolution of minute bubbles that would be most desirable for film continuity and reflow during the baking cycle. Our good experience with aluminum plate would fit into this theory. Aluminum plate, as seen in Figure 4b, has a rough rolled surface, and hence would offer a much larger number of nucleation sites to facilitate uniform gas evolution.

The above hypothesis was further explored by working with several tin plate surfaces. It was determined that surface roughness levels as can be obtained by using rougher rolls for final rolling of the steel did not make a difference.

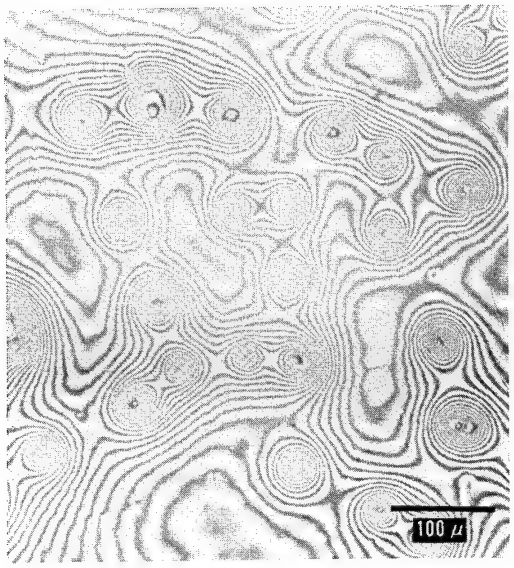

(a)

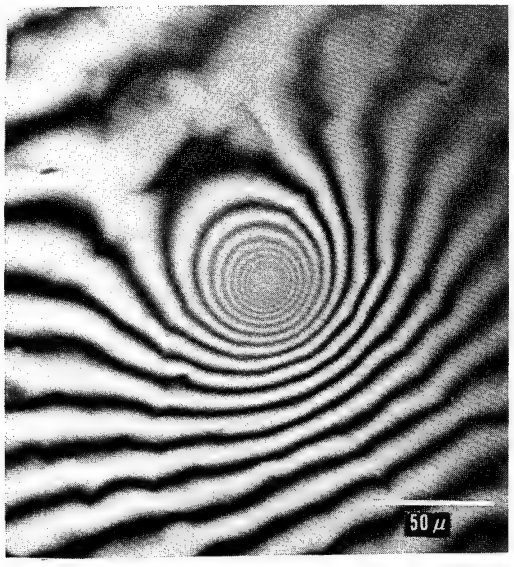

(b)

FIG. 7. Interference micrographs of holes as shown in Figure 6: (a) overview at 150X; (b) single hole at 350X.

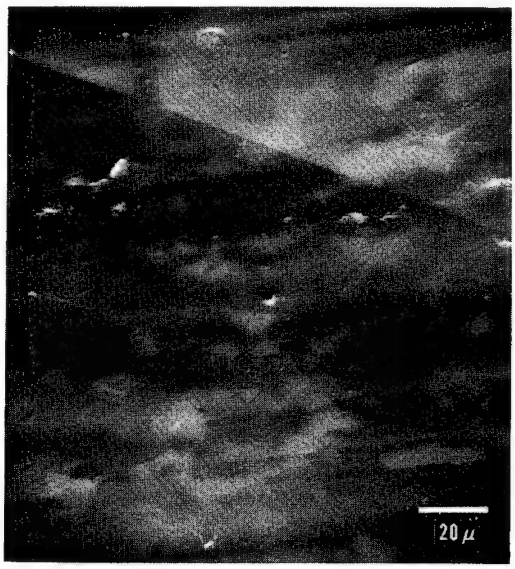

FIG. 8. Untreated reflowed (melted) tin plate surface; 500X.

FIG. 9. Tin plate surface showing pretreatment to eliminate gassing; 500X.

Apparently, the reflowed tin plating shown in Figure 8 smoothed out the micro surface defects, and most of the gas nucleation points are thus eliminated. Use of a matte finish (unmelted) electrolytic tin plate, of which the surface is shown in Figure 3, did offer a significant improvement in coating continuity.

In further experiments, micro defects of the type seen in Figure 9 were developed on conventional tin plate surfaces by mild etching techniques. This procedure provided substantial relief from the gassing hole problem without substantially detracting from the desirable smooth and shiny visual appearance of the plate surface.

SUMMARY

It is important to realize that the SEM may provide a great deal more information than just topography. By varying the beam voltage, information regarding the thickness and the coverage of the coating can be determined. Therefore, it is important to explore all capabilities of the SEM to get the maximum value from its use. Initial electrocoating characteristics have been studied by employing such techniques. Gas formation appears to have a major influence on initial deposition. The substrate topography determines the nature of gas production, but the desired coating deposition can be produced by custom tailoring the surface of the metal substrate.

REFERENCES

[1] C. W. Oatley, W. C. Nixon, and R. F. W. Pease, *Advan. Electron. Electron Phys., 21,* 217 (1965).
[2] J. Sikorski and A. Hepworth, *Proc. 2nd Ann. Scanning Electron Microscope Symp.*, IIT Research Institute, Chicago, Ill., 1969, p. 249.
[3] J. W. S. Hearle, J. T. Sparrow, and P. M. Cross, *The Use of the Scanning Electron Microscope,* Pergamon Press, Elmsford, N.Y., 1972.
[4] A. Boyde and C. Wood, *J. Microsc. (Oxford), 90*(3), 221 (1969).
[5] J. W. S. Hearle, B. Lomas, and J. T. Sparrow, *J. Microsc. (Oxford), 92*(3), 205 (1970).

SCANNING ELECTRON MICROSCOPY FOR EVALUATION OF PAINT FILM WEATHERABILITY

O. L. CARTER, A. T. SCHINDLER, and E. E. WORMSER

Rohm and Haas Research Laboratories,
Spring House, Pennsylvania 19477

SYNOPSIS

Acrylic paint films weather by erosion of the polymeric binder from around the pigment and/or extender particles in the paint formulation. This erosion leads to chalking of flat house paints and to loss of gloss from gloss paints. Scanning electron microscopy provides a means of following this erosion, and thereby predicting the weatherability of paint films. Studies were undertaken to assess the effect of extender on weatherability, to predict relative durability of binders exposed in a modified Xenon Arc Weather-Ometer, and to compare the durability of Weather-Ometer and outdoor exposed flat and gloss paints. With scanning electron microscopy it is possible to rate coatings according to durability, but the technique is not suitable to predict weathering significantly earlier than the conventional chalking and gloss measurements. The greatest potential use for scanning electron microscopy lies probably in the observation of surface structures for elucidation of weathering mechanisms, and for comparison of Weather-Ometer and outdoor exposures to insure that degradation is following the same pathway.

INTRODUCTION

A great deal of time and effort is expended in the coatings industry to evaluate weatherability of paint films. Methods commonly used to assess the degree of weathering include measurement of specular gloss, determination of coating weight loss, and measurement of the degree of chalk formation. These studies have led to the conclusion that film weathering can be described as occurring in three stages: (a) the induction period, (b) the transition interval, and (c) the region of constant rate [1].

Our use of the scanning electron microscope (SEM) to survey areas of general application within the coatings industry have been reported previously [2]. An excellent review of the description and operation of the SEM was reported at the previous symposium [3], and will not be repeated here. This paper describes our efforts to use the SEM as an instrument for early prediction of the weatherability of flat and gloss paint systems. Accurate prediction of long term durability in a short period of time is an industry-wide desire. This study was undertaken to answer the following questions: (a) Can the SEM be used in conjunction with a Weather-Ometer to predict the weatherability of flat and gloss paint systems earlier than is currently possible with conventional tests? (b) Can SEM observations of surface structures be used to study the mechanisms of paint film failure? Particular emphasis was placed on comparing Weather-Ometer and outdoor exposures.

Applied Polymer Symposium No. 23, 13-25 (1974)

Sample Preparation for SEM Examination

Appropriate sections 0.5 cm by 0.5 cm were cut from the weathered sample chips. These sections were mounted with glue onto copper specimen holders. A gold coating of approximately 400 Å thick was deposited on the surface in a vacuum evaporator. This gold layer makes the surface conductive, and minimizes the damage to the surface by the electron beam. The micrographs were recorded with a JEOL JSM-2 instrument, operating at 25 kV accelerating voltage and 10,000X magnification.

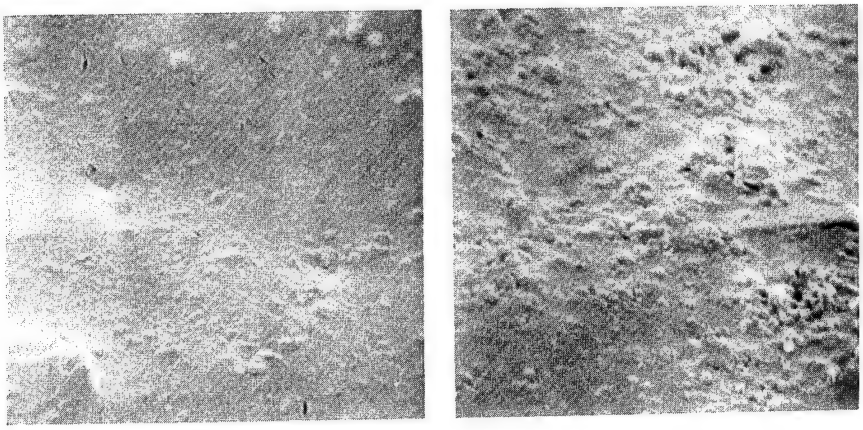

(a) (b)

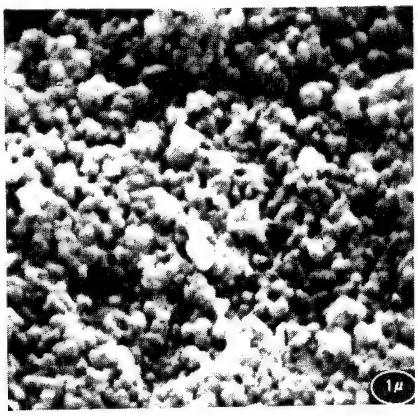

(c)

FIG. 1. Surface structure of different house paint formulations, based on Rhoplex AC-35, exposed in Newtown, Penna.: (a) after 7.5 months, not chalking; (b) after 16.5 months, not chalking; (c) after 5 years, chalking.

RESULTS AND DISCUSSION

Examination of Flat House Paint Formulation

Initially, three paint panels with Rhoplex AC-35 (Rhoplex is a registered trademark of the Rohm and Haas Company) as the binder in the formulation were examined. These panels had been exposed at Newtown, Pennsylvania, for 7.5 months, 16.5 months, and 5 years, respectively. SEM photomicrographs of representative areas of these three paints are shown in Figure 1. There is a definite increase in pigment detail discernable on the surface with increasing exposure. This observation led to the conclusion that chalking occurred when the binder eroded, so that the pigment and/or extender particles were no longer covered. The micrographs increased the confidence that it is possible to use the SEM for determining relative weatherability if known points are available.

A weathering program was developed to determine whether SEM could be used to detect durability earlier than conventional chalking measurements. The paint films examined were both high durability (T-88-1) and low durability (fast fail) formulations with 4 different acrylic binders. Some specifics of the high durability paints are given in Table I. The low durability formulation contained twice the TiO_2 concentration of the high durability formulation. The samples were weathered (a) in the Xenon Arc Weather-Ometer, with chips collected after every 200 hr exposure; (b) outdoors at Newtown, Pennsylvania, with chips collected every 3 months.

The unexposed low durability formulations based on all 4 binders showed many exposed pigment and extender particles on the surface when examined with SEM. Representative micrographs are shown in Figure 2. After 200 hr exposure in the Xenon Arc Weather-Ometer the binder is no longer visible on the surface in any of these formulations. This led to the conclusion that the initial pigment level of these low durability formulations was too high, and that none

TABLE I

Paint Formulation for Flat House Paint Series
(High Durability (T-88-1) Formulation)

$TiO_2/CaCO_3$/Cal Ink 8600 Phthalo Green*	39.5/58.9/1.6 wt.%
Coalescent	2.5% on binder solids
Pigment volume concentration	40%
Volume solids	41%
Initial viscosity	75 ± 1 K U
Initial pH	9.0

*Colorant added to enhance visual evaluation of chalking

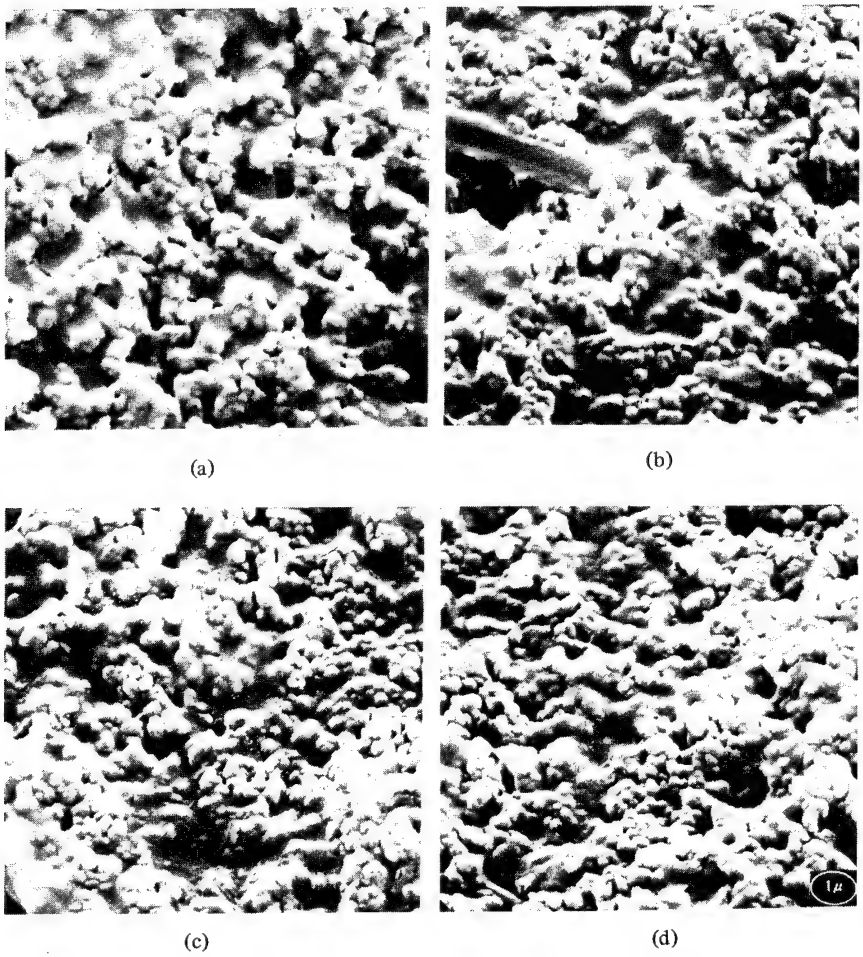

FIG. 2. Surface structure of unexposed fast fail house paint formulations: (a) based on Rhoplex AC-22; (b) based on Rhoplex AC-388; (c) based on EXP 1; (d) based on EXP 2.

of the binders is capable of binding the pigment. This conclusion is supported by chalking data as obtained with a Jacobson Chalk Tester. They show moderate to heavy chalking after 200 hr exposure with no differentiation among the 4 binders.

When the high durability formulations were examined, they were found to be essentially smooth. Only a few pigment particles could be detected on the surface. Representative micrographs are shown in Figures 3-6. The fine cracks in some of the images are probably artifacts, due to excessive amounts of gold coating used on the specimens. The paint surfaces themselves are most likely very smooth. Examination of micrographs taken after 400 hr Xenon Arc Weather-Ometer exposure shows that the paint based on Rhoplex AC-22 can clearly be differentiated from the others as having weathered the most severely. After 800 hr, the correct durability order, determined from the SEM data, was

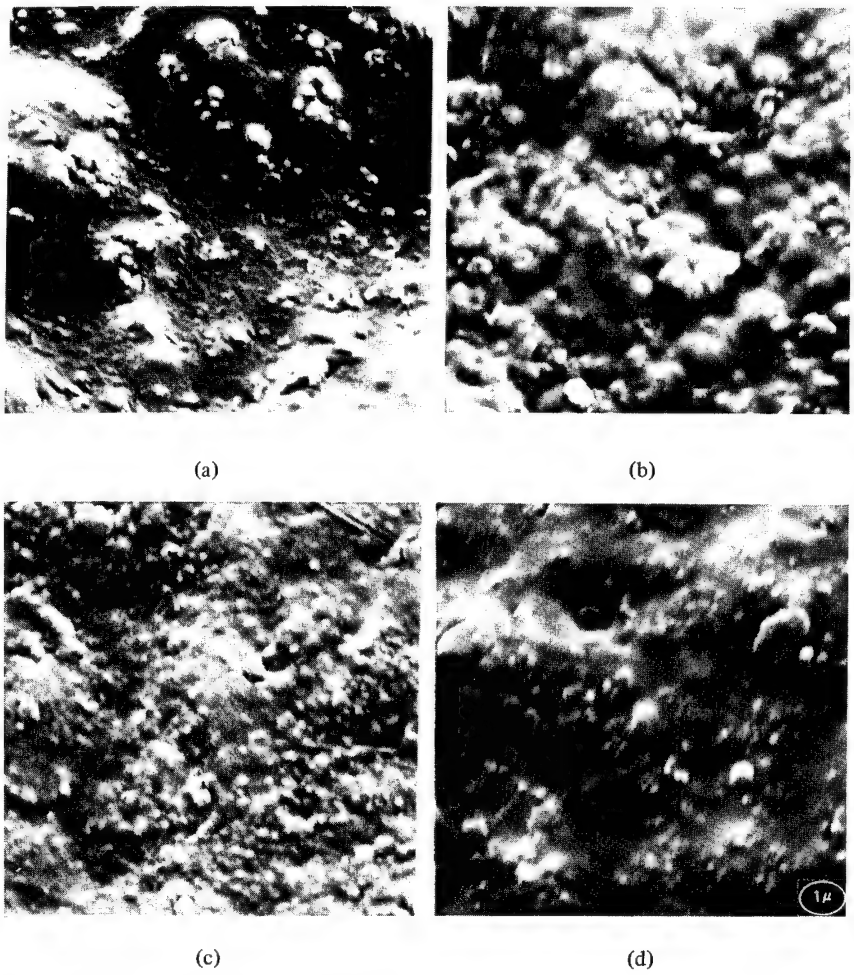

FIG. 3. Surface structure of a standard flat house paint formulation (T-88-1), based on Rhoplex AC-388: (a) unexposed control; (b) 400 hr in Weather-Ometer; (c) 800 hr in Weather-Ometer; (d) 3 months outdoor south 45° exposure at Newtown, Penna., series 71BM.

as follows: Rhoplex AC-388 is more durable than EXP 1 and EXP 2, which in turn are more durable than Rhoplex AC-22. The same order of durability was found after 1400 hr exposure. These findings agree with data taken by the standard chalking test. The ability to predict relative weatherability from the SEM data occurs at most 200 to 400 hr before the chalking data are conclusive. The same formulations described above are on exposure at Newtown, Pennsylvania. Only 3-month old samples have been examined so far. The high durability formulations show no evidence of binder erosion on the surface after this exposure, as can be seen in Figures 3-6. Longer weathering will be required before relative durability can be predicted from SEM and chalking data for exterior exposure.

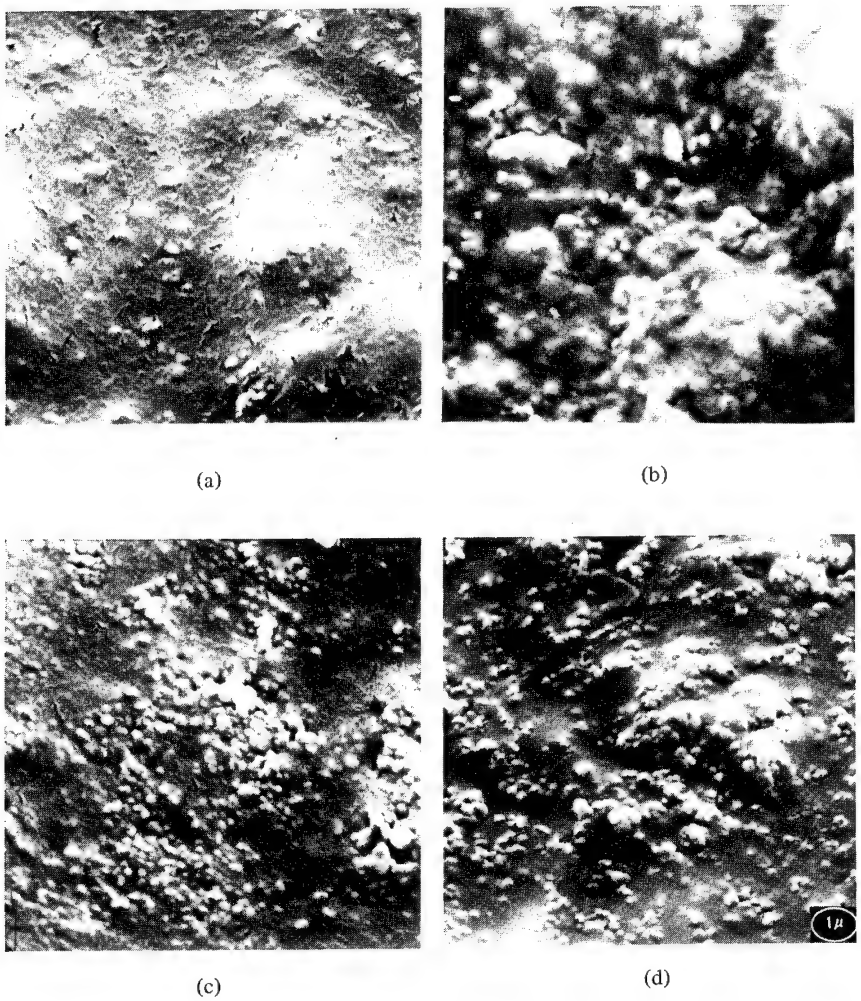

(a) (b)

(c) (d)

FIG. 4. Surface structure of a standard flat house paint formulation (T-88-1), based on EXP 1: (a) unexposed control; (b) 400 hr in Weather-Ometer; (c) 800 hr in Weather-Ometer; (d) 3 months Newtown, Penna., series 71BM.

Examination of Gloss Paint Formulations

The surface structures of three gloss paint formulations were characterized by SEM upon exposure in a modified Carbon Arc Weather-Ometer. This unit was a Dew Cycle Weather-Ometer with a carbon arc light source with the filters in place, but with a modified operating procedure: The black panel temperature is cycled from 145°F to room temperature, and the spray time is extended to 1 hr, followed by 2 hr of light only. The temperature was cycled with the water spray to obtain a hot/dry and cold/wet sequence. A fair correlation was found to exist between surface roughness and 60° gloss readings for these formulations, as can be seen from Figure 7. Smoother samples had higher gloss readings. There were, however, no indications from which to predict the future loss in gloss from the

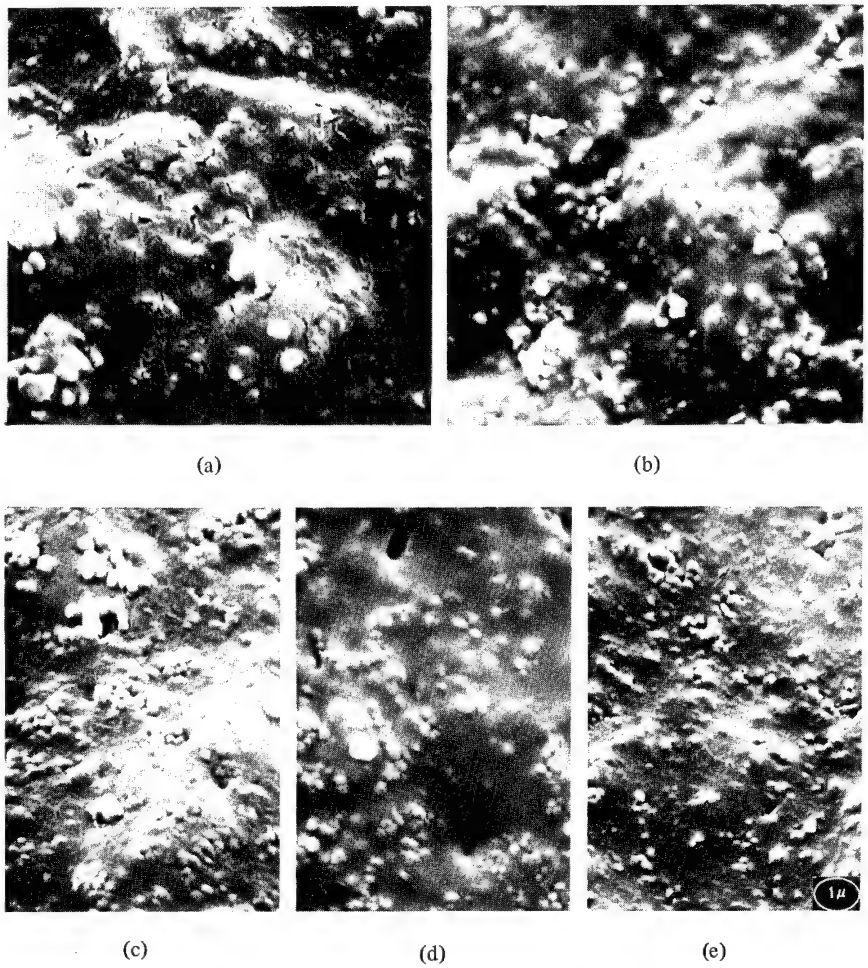

FIG. 5. Surface structure of a standard flat house paint formulation (T-88-1), based on EXP 2: (a) unexposed control; (b) 400 hr in Weather-Ometer; (c) 800 hr in Weather-Ometer; (d) 3 months Newtown, Penna., series 71BM; (e) 3 months Newtown, Penna., series 71CV.

surface structure. It was concluded that SEM offers no advantage over gloss measurements in following degradation of gloss paints on accelerated weathering.

The surface structures of ten gloss paint formulations exposed outdoors for 6 months in a south 45° direction were characterized by SEM. These paints varied in pigment volume concentration (PVC), types of TiO_2 and binders used. A summary of the gloss and SEM evaluations is shown in Table II. Included in these 10 samples were duplicates of the 3 paints examined after Weather-Ometer exposure. The outdoor exposed samples showed more TiO_2 protrusion than was seen in the Weather-Ometer samples after 800 hr exposure. Previous exposures had shown that Weather-Ometer and outdoor exposure durability data did not correlate. This indicates that the paints were not weathering by the same

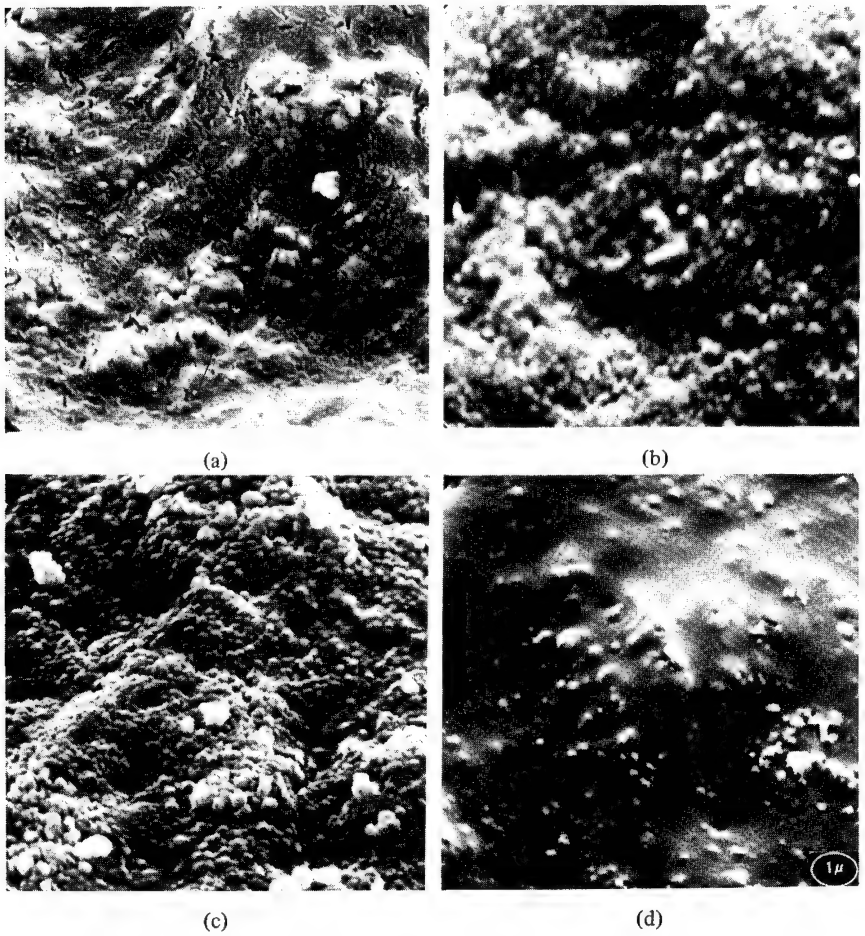

FIG. 6. Surface structure of a standard flat house paint formulation (T-88-1), based on Rhoplex AC-22: (a) unexposed control; (b) 400 hr in Weather-Ometer; (c) 800 hr in Weather-Ometer, (d) 3 months Newtown, Penna., series 71CV.

TABLE II

Summary of SEM and Gloss Data After Six Months S-45° Exposure at Newtown, Penna.

Sample Number	Paint Description				60° Gloss Data				SEM Evaluation 6 Month Grouping
	PVC	TiO_2	Binder	Coalescent	Unexp.	6 Months	Δ	% Ret.	
1	20	Titanox CLNC	1	Yes	55.0	38.0	16.4	70.2	2*
2	23	Titanox CLNC	1	Yes	47.8	35.4	12.4	74.2	2
3	25	Titanox CLNC	1	Yes	48.9	34.0	14.9	69.5	2
4	20	Tipure R-900	1	Yes	71.2	45.3	25.9	63.6	1
5	23	Tipure R-900	1	Yes	72.8	44.5	28.3	61.2	1
6	25	Tipure R-900	1	Yes	59.1	39.9	19.2	67.5	3
7	23	Tipure R-900	2	Yes	69.8	39.4	30.4	56.4	3
8	23	Tipure R-900	3	Yes	63.0	34.6	28.4	55.0	3
9	23	Tipure R-900	4	Yes	67.5	19.8	47.6	29.4	4
10	23	Tipure R-900	4	No	57.3	22.6	34.7	39.4	4

*Rating of 1 is most like unexposed film; 4 has most change.

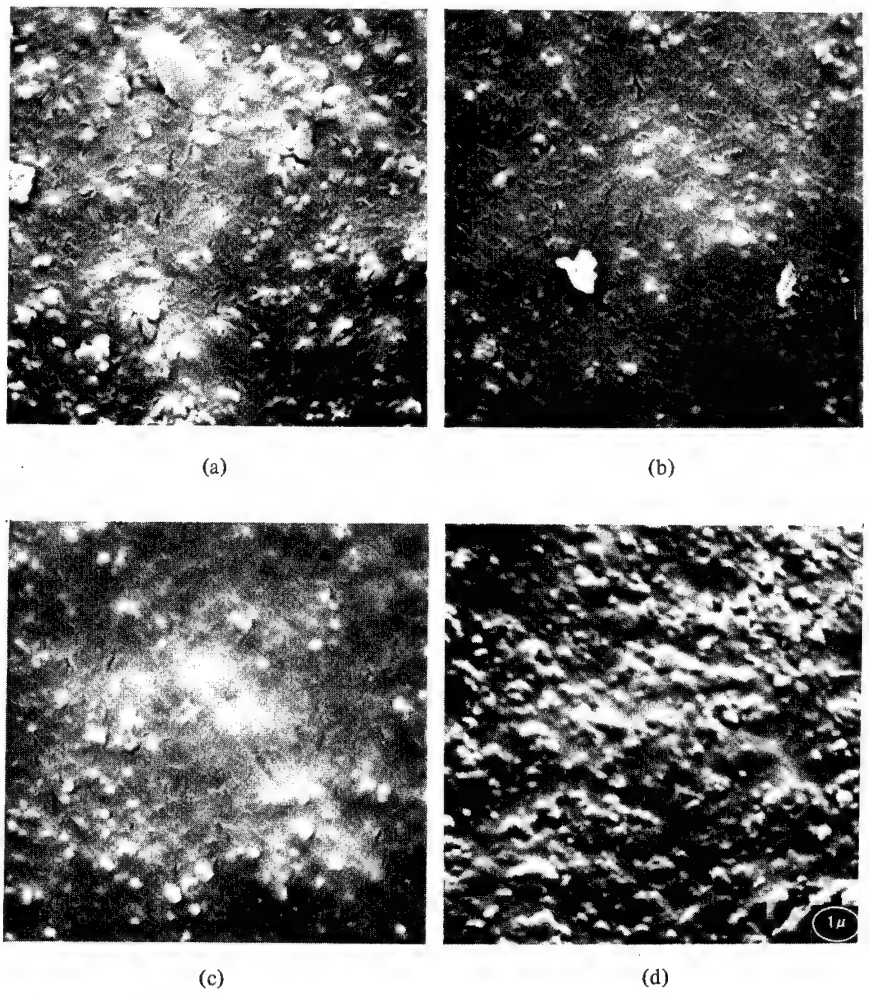

FIG. 7. Surface structure of a standard gloss paint formulation, based on Rhoplex AC-507: (a) unexposed control, 60° gloss = 71%; (b) 220 hr in Weather-Ometer, 60° gloss = 73%; (c) 805 hr in Weather-Ometer, 60° gloss = 69%; (d) 6 months Newtown, Penna., 60° gloss = 45%.

pathway in the Weather-Ometer and outdoors. Further studies will be required to determine the exact cause of the variation. Cold flow seems to occur in the Weather-Ometer, but to date we have been unsuccessful in isolating the exact conditions responsible.

The data in Table II shows that SEM is capable of distinguishing the worst samples (9 and 10) and the ones with the highest gloss (4 and 5), in agreement with the gloss readings. There is no apparent correlation between SEM groupings 2 and 3 and the gloss data for these 6 samples.

TABLE III

Chalking of Rhoplex 388 Paints after 2000 hr Weather-Ometer Exposure as Function of the Type of Extender Used

Extender	Degree of Chalking
Clay (Icecap K)	Severe
$CaCO_3$ (Snowflake)	Slight
Silica (Silver Bond B)	None

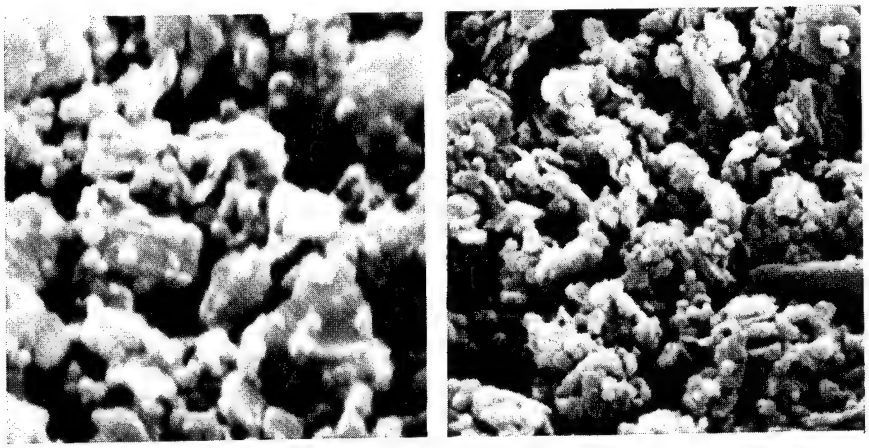

(a) (b)

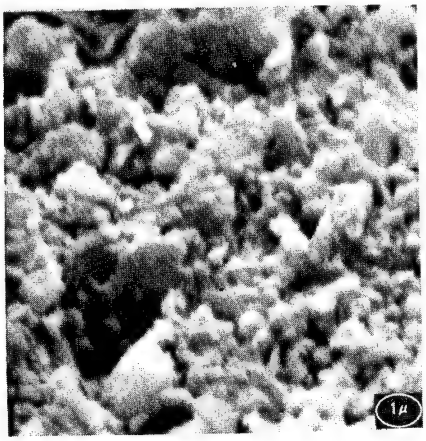

(c)

FIG. 8. Surface structure of Rhoplex AC-388 paint, extended with clay (Icecap K), before and after 2,000 hr in Weather-Ometer: (a) before weathering; (b) after weathering; (c) after weathering and washing.

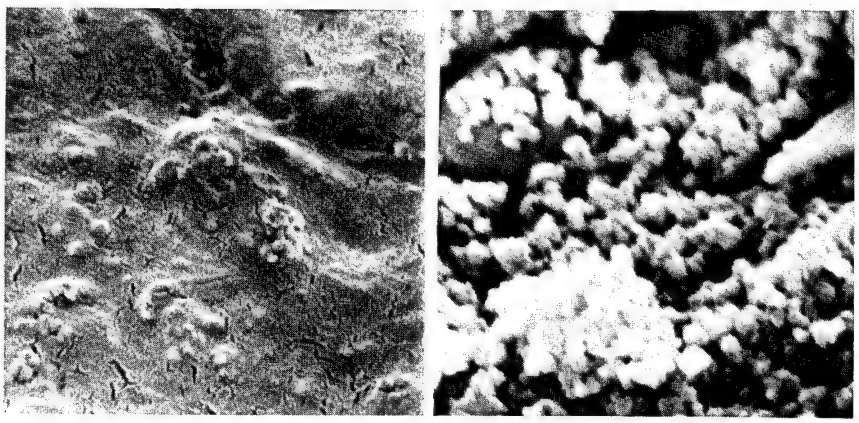

(a) (b)

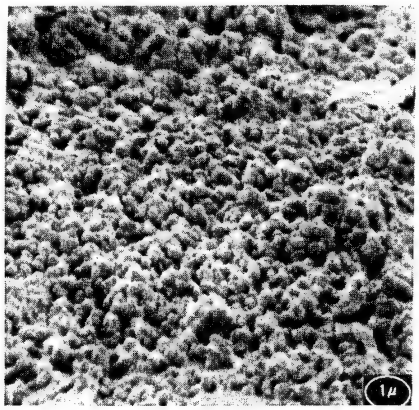

(c)

FIG. 9. Surface structure of Rhoplex AC-388 paint, extended with $CaCO_3$ (Snowflake), before and after 2,000 hr in Weather-Ometer: (a) before weathering; (b) after weathering; (c) after weathering and washing.

Effect of Various Extenders

Xenon Arc Weather-Ometer exposure of three paints with Rhoplex AC-388 as the binder and different extenders gave a wide range of chalking results, as shown in Table III. The SEM data also demonstrate this result. The paint containing clay did not form a tight film initially (Fig. 8). After weathering, all binder had been removed from the surface, so that the paint chalked severely. The paints with $CaCO_3$ and silica formed good films initially (Figures 9 and 10). After weathering, however, all evidence of binder on the surface is gone for the paint with $CaCO_3$, but for the silica-extended paint the binder can still be seen, and there is no chalking. The upper powdery layer can be removed by washing the paint surface, and the micrographs of such washed surfaces show films with sufficient binder to hold the pigment together.

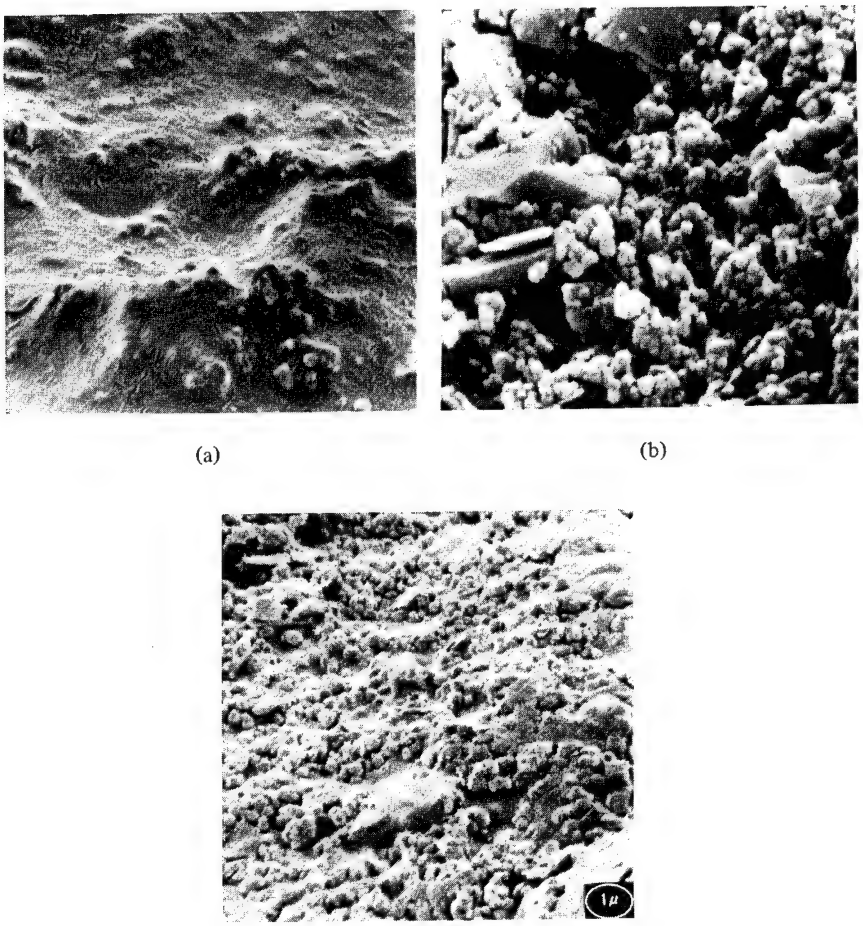

(a) (b)

(c)

FIG. 10. Surface structure of Rhoplex AC-388 paint, extended with silica (Silver Bond B), before and after 2,000 hr in Weather-Ometer: (a) before weathering; (b) after weathering; (c) after weathering and washing.

CONCLUSIONS

Scanning electron microscopy can be used to predict the weatherability of flat acrylic house paint formulations. The results correlate well with standard chalking tests, but time is not saved sufficiently to recommend routine usage. It is only an additional technique to compliment other established methods. SEM cannot compete with gloss readings as a routine measure of weatherability of gloss paints, because gloss measurements are more economical and offer a quantitative measure rather than a qualitative rating. SEM is useful for suggesting which parameters are most influential when Weather-Ometer data do not correlate with outdoor exposure data.

REFERENCES

[1] P. R. Sperry and A. Mercurio, "Exterior Durability of TiO_2 Pigmented Acrylic Coatings," presented at the Joint ACS-CIC Meeting, Toronto, Ontario, May 1970; *Organic Coatings and Plastics Chemistry Preprints, 30*(1), 400 (1970).

[2] J. A. Lavelle and E. E. Wormser, "The Use of the Scanning Electron Microscope in Coatings Applications," presented at the Chemical Specialty Manufacturers Association Meeting, May 1972.

[3] H. Lee, M. L. Swartz and D. G. Stoffey, *Appl. Polym. Symp., 16* (1971).

MONITORING COATINGS PERFORMANCE UPON EXTERIOR EXPOSURE

L. H. PRINCEN, F. L. BAKER, and J. A. STOLP

Northern Regional Research Laboratory, U.S. Department of Agriculture, Peoria, Illinois 61604

SYNOPSIS

The behavior of 19 commercial and experimental paints exposed on red cedar has been monitored with a scanning electron microscope. Included were acrylic, vinyl, linseed oil, alkyds, polyurethane, epoxy, chalking and nonchalking formulations, whites and tint-base paints, and glossy and flat finishes. Samples were taken biweekly and studied at 100X, 500X, and 2,000X. Occasionally, the samples were washed gently with soap and water before examination. Visual observations included chalking, dirt collection, whiteness, and gloss. Microwrinkling of the top surface was seen in coatings containing linseed oil and certain alkyds; it disappeared after as little as 2 weeks exposure. Dirt collection was initially strongest on solvent-base paints; latex paints without added alkyds stayed the cleanest. Within 4 to 5 months this behavior reversed: The chalking solvent-base paints appeared whiter and cleaner than the nonchalking latex paints. Chalking appears to be a function not only of pigmentation, but also of vehicle composition. Trim and tint-base paints deteriorated faster than expected. Small ring structures observed in the surface of the 2-component epoxy coating have been described, and a mechanism has been postulated for their formation. Some observations on the mechanism of chalking have been made.

INTRODUCTION

Traditionally, coatings producers have always examined their products rigorously and extensively on test fences and actual buildings for such properties as tint retention, mildew resistance, chalking, blistering, cracking, and gloss. The coating is applied to a standard substrate, the nature of which depends upon the intended end use of the product, and the resulting panel is exposed outdoors. Conditions can be predetermined with the location and its climate, direction of exposure, angle of panel, and by placing the panel either in open sun and rain or protecting it from these direct attacks. During the lifetime of the panels, they are periodically inspected and tested for changes in appearance and physical properties. Although appearance is generally checked with the naked eye, many workers have used optical microscopy [1, 2] and transmission electron microscopy [3-7]. Optical miscroscopy has definite limitations due to the opacity of pigmented films to light and due to the limited degree of magnification and depth of focus attainable [8]. Transmission electron microscopy has the disadvantage that the opacity of pigmented films to the electron beam requires the making of replicas, a tedious and difficult technique to say the least [9-11]. The scanning electron

Applied Polymer Symposium No. 23, 27-40 (1974)

microscope (SEM) has already been used successfully to monitor coatings performance in exposure studies [12, 13]. This instrument has the advantages of high resolution and great depth of field, and there is no difficulty in sample preparation [14, 15].

Our study was initiated to acquire more knowledge on the differences in exposure performance that seem to exist between the many different binder systems available these days. An extensive unpublished study, conducted by the National Flaxseed Processors Association (NFPA), pitted the best paints available made from linseed oil against the leading latex binders; after 4 years' exposure, the oil paints in white and all major tints protected as well as the latex paints and looked at least as good. However during the first year of exposure, when the homeowner is most critical about how his house looks, the latex paints appeared to be better looking than the solvent-base linseed oil coatings. This observation was the main reason for probing short-term effects of exterior exposure on paint films containing many different kinds of binders and binder blends. Both commercial and experimental formulations have now been tested for 72 weeks.

CHOICE OF COATINGS AND PANEL PREPARATION

The bulk of the paints for this kind of study should be commercial products, to be sure that their performance is acceptable. For this reason, 12 paints were purchased locally, and these included samples of vegetable oil, alkyd resin, nonmodified and alkyd-modified acrylic and vinyl, polyurethane, and epoxy paints; some were tint-base, others were strictly white. Also, six experimental paints made with nonmodified and alkyd-modified acrylic and vinyl acetate binders were tested, as was a TTP 00102C Class A, solvent-base paint with linseed alkyd as binder. Formulations of the 19 paints are given in Table I. Commercial designations of the paints have been omitted. Paints 13 through 18 are experimental formulations.

Panel preparation was carried out as follows by two professional painters: Preselected 36 in. × 6 in. western red cedar beveled siding (E. C. Miller Cedar Lumber Co.,* P.O. Box 750, Aberdeen, Wash. 98520) was painted with one coat of Dutch Boy 010 oil-base primer over the left two-thirds of each panel. The right third of each panel received one coat of the test paint. After several days of drying, the left third of each panel was given one coat of Sherwin-Williams SW-471 oil-base exterior paint as a reference, and the rest of the panel was given one coat of the same test paint that was used for the first coat on the right third of the panel. Consequently, each panel contained on the left a reference paint over primer; in the center, a test paint over primer; and on the right, the same test paint self-primed. The reference paint was identical to paint No. 11 in the

*Mention of firm names or trade products does not imply that they are endorsed or recommended by the Department of Agriculture over other firms or similar products not mentioned.

TABLE I

Formulations of 19 Paints Tested for Exterior Exposure, in Weight Percent

Number	Description	Oil	Alkyd	Vinyl	Acrylic	TiO_2	ZnO	Silicate	$CaCO_3$	ZnS	Solvent	Water
1	Acrylic	–	–	–	22.1	22.9	–	6.2	4.1	–	–	44.6
2	Acrylic, alkyd-modified	–	4.8	–	12.9	20.1	4.2	13.0	–	–	2.3	42.5
3	Soy alkyd	–	32.9	–	–	27.9	0.7	–	–	–	37.5	–
4	Linseed oil + alkyd	22.0	19.0	–	–	27.0	5.0	–	–	–	24.0	–
5	Safflower-soy alkyd	–	34.5	–	–	17.1	–	5.1	1.5	–	41.2	–
6	Linseed tint-base	30.5	–	–	–	14.8	20.0	14.8	7.4	–	10.3	–
7	Vinyl, alkyd-modified	–	6.2	22.4	–	22.5	–	2.7	4.3	–	–	41.9
8	Vinyl, alkyd-modified	–	6.4	13.7	–	23.4	–	–	15.6	–	–	40.7
9	Polyurethane	–	31.2[a]	–	–	25.7	–	–	–	2.6	40.5	–
10	Epoxy	–	29.0[a]	–	–	42.2	–	–	–	–	28.6	–
11	Standard linseed oil	30.5	–	–	–	14.8	18.2	24.0	–	–	10.3	–
12	Soy-tall alkyd	–	34.5	–	–	34.0	–	–	–	–	30.2	–
13	Acrylic	–	–	–	18.0	21.4	–	12.6	–	–	–	48.0
14	Acrylic, alkyd-modified	–	4.9	–	13.6	20.3	4.3	14.4	–	–	–	42.5
15	Vinyl acetate	–	–	19.1	–	26.3	–	10.2	–	–	–	44.4
16	Vinyl acetate, alkyd-modified	–	4.9	16.0	–	27.1	–	11.6	–	–	–	40.4
17	Acrylic, alkyd-modified	–	4.9	–	13.6	20.3	4.3	14.4	–	–	–	42.5
18	Acrylic, alkyd-modified[b]	–	5.6	–	20.3	21.0	–	5.1	–	–	–	44.1
19	TTP 00102C Class A	–	31.6	–	–	25.6	9.9	15.8	–	–	15.8	–

[a]Special binder, should not be considered to be true alkyd.
[b]Contained 3.9% organic yellow pigment.

series. The panels were dried indoors for 1 week and on November 15, 1971, were placed on a test fence in a vertical position for southern exposure.

SAMPLING FOR SEM

Before the panels were brought to the test fence, samples with a surface area of approximately 5 X 5 mm were cut with a scalpel from both the primed and self-primed areas of the test paints and from one of the reference paint areas. The exposed wood was touched up with some primer; and after drying for a few hours, all cut areas were painted over once more with SW-471. Sampling was repeated every 2 weeks. During one sampling time, only samples from the primed areas were taken; whereas the next time the samples were taken from the self-primed areas. These wood and paint chips were mounted on standard SEM studs and coated with approximately 200 Å of gold-palladium before being viewed in the SEM. Images were photographed at 100X, 500X, and 2,000X. The low magnification was taken at 100X to demonstrate that the image at 2,000X displayed a typical surface area. The intermediate magnification was photographed to show the best detail for the rougher features, such as dirt collection and effects of wood grain and brush marks on paint performance; whereas high magnification revealed such characteristics as chalking, mildew, distribution of pigment and extenders through the matrix, and wrinkling and pitting of the vehicle.

On several occasions, a small section of each area to be sampled was washed gently with some water and soap to remove dirt and chalk so that an estimate could be made of the condition of the paint film underneath. Such washing was carried out after 18, 24, 38, and 50 weeks for all panels; but after 14 weeks, a washed and an unwashed sample were taken from the reference paint areas every sampling day.

RESULTS

No perceptible differences could be seen microscopically or macroscopically between primed and self-primed panels during the study period of 72 weeks. Typical, but necessarily abbreviated, results are exemplified in Figures 1 and 2, which show the performance of two paints at 6 weeks intervals and at high magnification. Figure 1 shows that the acrylic paint (No. 1 from Table I) appears to weather slowly. The micrographs show no appreciable deterioration of the surface texture. However, intermediate magnification shows that dirt and grime collect rather easily on its rough-textured surface. The standard linseed oil solvent-base paint (No. 11) collected dirt early, but the free chalking, as evidenced in the micrographs after only 8 weeks, produced a clean, white surface. Chalking in this paint started after 8 weeks and was already pronounced after 14 weeks of exposure. Such macroscopic observations as gloss, cleanness,

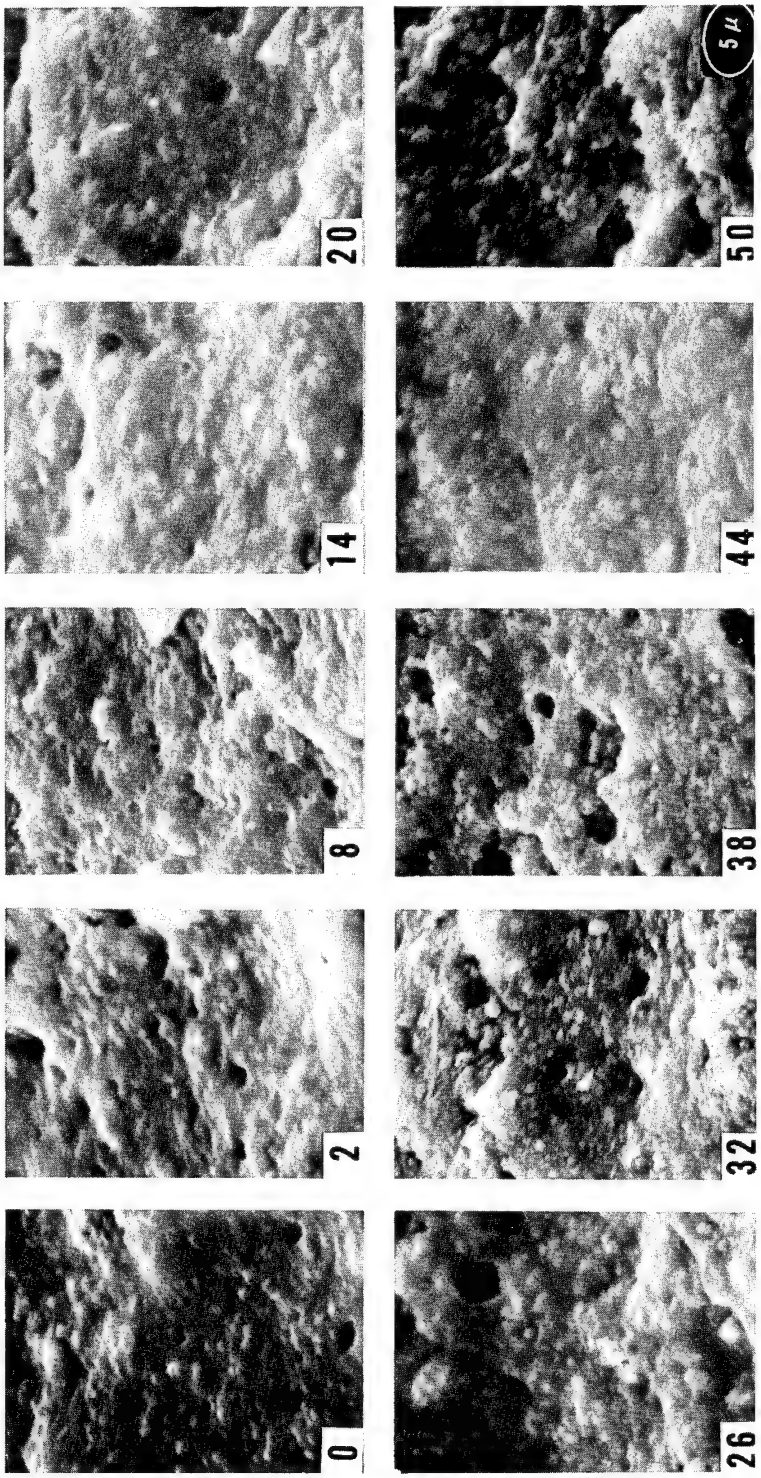

FIG. 1. Sections of acrylic paint specimens (No. 1 from Table I) photographed at 2,000X with a scanning electron microscope (SEM) at different ages. Age of each section is indicated in weeks in left corner. This paint shows little change with time. Specimen at 38 weeks was cleaned with soap and water.

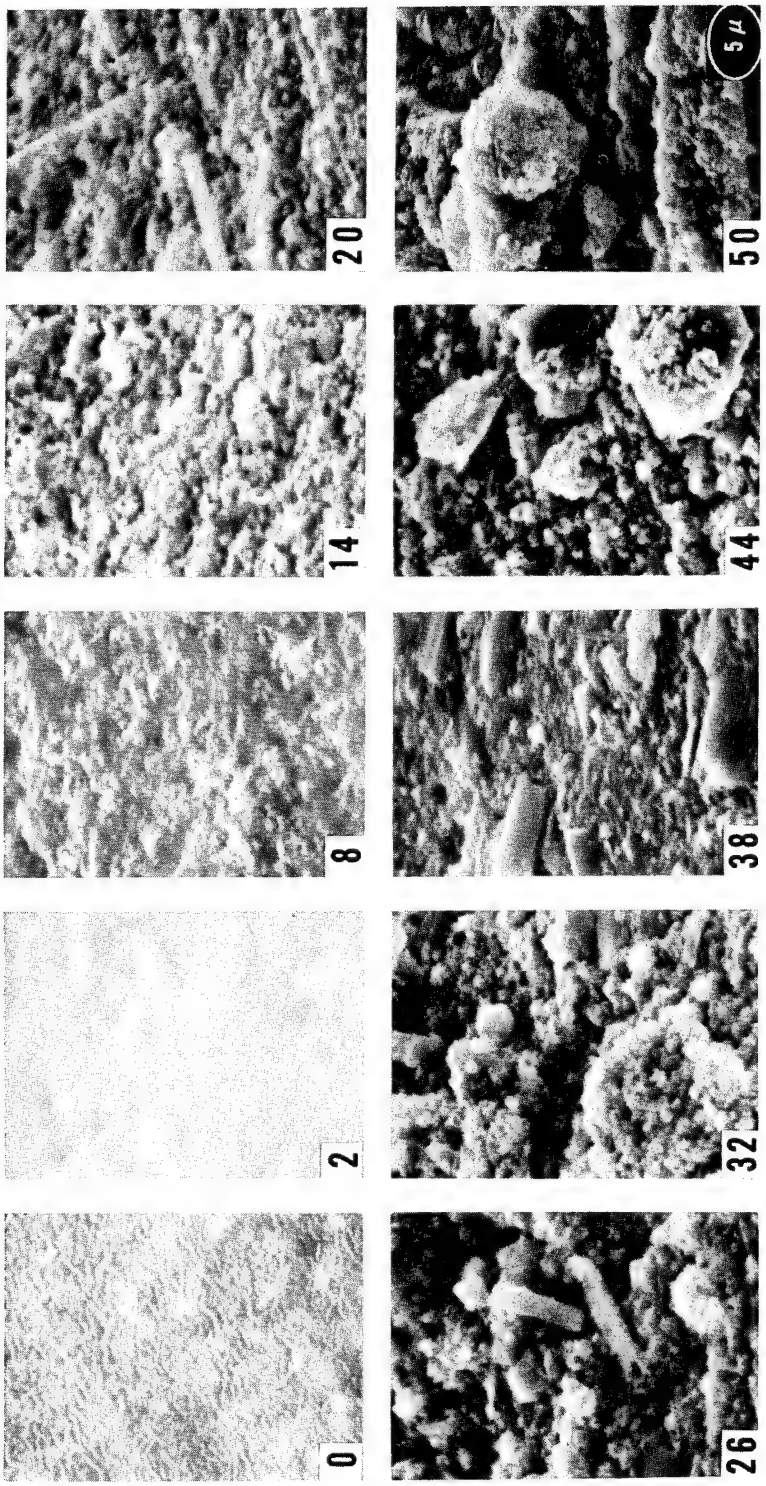

FIG. 2. Sections of standard linseed oil paint (No. 11 from Table I) at 2,000X. Chalking started at 8 weeks. Note microwrinkling at 0 time. Specimen at 38 weeks was cleaned with soap and water.

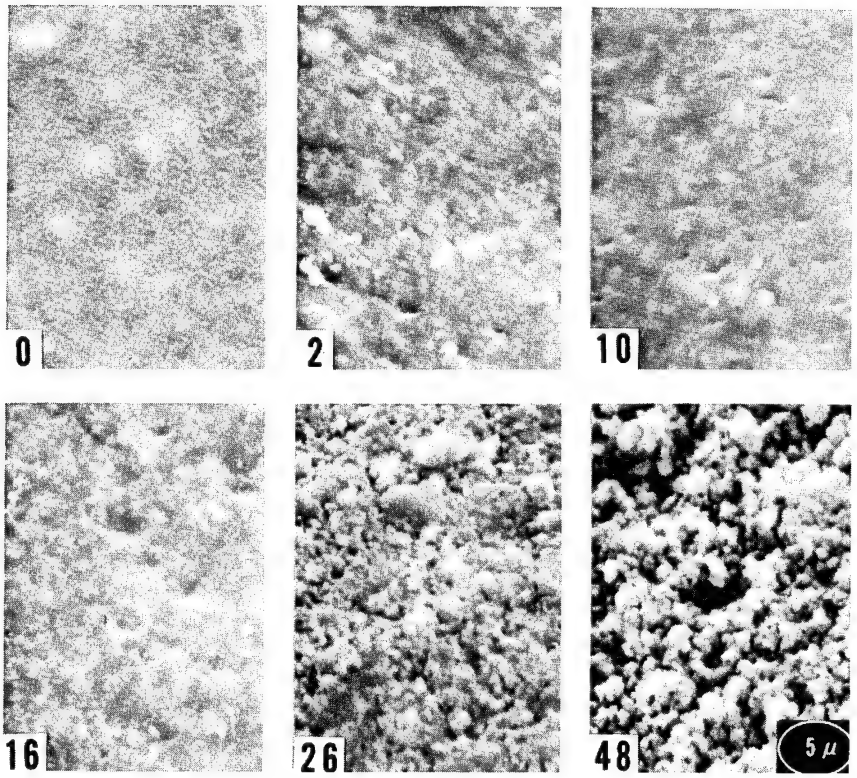

FIG. 3. Paint no. 4, glossy trim and tint-base. Sections of 2,000X micrographs at 0, 2, 10, 16, 26, and 48 weeks of age. Chalking started at 16 weeks; note microwrinkling at 0 time.

chalking, and whiteness at various intervals are presented for all paints in Table II. The observations were made outdoors and subjectively without the aid of any instrumentation, just as they would be made by the homeowner inspecting his house.

Figure 3 shows paint 4, a glossy trim and tint-base coating, at several stages of weathering. Chalking started at 16 weeks, and the glossy appearance was lost rapidly thereafter. Figures 4 through 7 depict the initial, 6-month, and 1-year conditions of the different types of paints at 2,000X. Included are alkyd-modified acrylic, alkyd-modified vinyl, linseed oil tint-base, linseed plus alkyd, safflower-soy alkyd, soy-tall alkyd, polyurethane, and epoxy coatings. The other nine paints, not shown in the figures, showed results similar to those in the same class or category.

INTERPRETATIONS AND CONCLUSIONS

Those paints containing linseed oil, linseed oil alkyd, or tall oil alkyd were the only ones with microwrinkling on the top surface after the films dried. This

TABLE II

Some Observations on Panels of 19 Paints Described in Table I

Number	Description	Gloss		Cleanness			Chalking				Whiteness		
		0 weeks	46 weeks	12 weeks	46 weeks	72 weeks	24 weeks	36 weeks	46 weeks	72 weeks	24 weeks	46 weeks	72 weeks
1	Acrylic	Flat	Flat	E[a]	P	P-F	–	–	–	–	F-G	P	P-F
2	Acrylic, alkyd-modified	Flat	Flat	E	P	P	–	–	–	–	G-E	F	P
3	Soy Alkyd	Glossy	Semi	F	F	F	–	S	S	+	P	F	F
4	Linseed oil + alkyd	Glossy	Flat	F	E	E	S	++	++	++	G	G	G
5	Safflower-soy alkyd	Glossy	Semi	P	F	G	–	S	S	S	F	F	F
6	Linseed tint-base	Glossy	Flat	P	E	F	+	++	++	++	F	F	G
7	Vinyl, alkyd-modified	Flat	Flat	G	P	P-F	–	–	–	S	F-G	P	P-F
8	Vinyl, alkyd-modified	Flat	Flat	G	P	P-F	–	–	S	S	F	P	P-F
9	Polyurethane	Glossy	Semi	P	F	F	–	–	S	S	P	F	F
10	Epoxy	Glossy	Glossy	P	F	F	–	S	+	+	P	F	F
11	Standard linseed oil	Glossy	Flat	P	E	E	++	++	++	++	E	E	E
12	Soy-tall alkyd	Glossy	Semi	P	F	F	–	S	+	++	P	P	G
13	Acrylic	Flat	Flat	G	F	P-F	–	–	–	–	G	P	P-F
14	Acrylic, alkyd-modified	Flat	Flat	G	E	G	S	+	++	++	G-E	G-E	G
15	Vinyl acetate	Flat	Flat	E	F	F	S	S	S	+	G	F	F
16	Vinyl acetate, alkyd-modified	Flat	Flat	G	F	G	S	S	S	+	G	F	G
17	Acrylic, alkyd-modified	Flat	Flat	E	E	E	S	+	++	++	F-G	F	G
18	Acrylic, alkyd-modified	Flat	Flat	G	P	P-F	–	–	–	–	Not applicable		
19	TTP 00102C Class A	Semi	Flat	P	E	E	++	++	++	++	E	E	E

[a]E = excellent, P = poor, F = fair, G = good, S = some chalk, – = no chalk, + = chalk, ++ = heavy chalk.

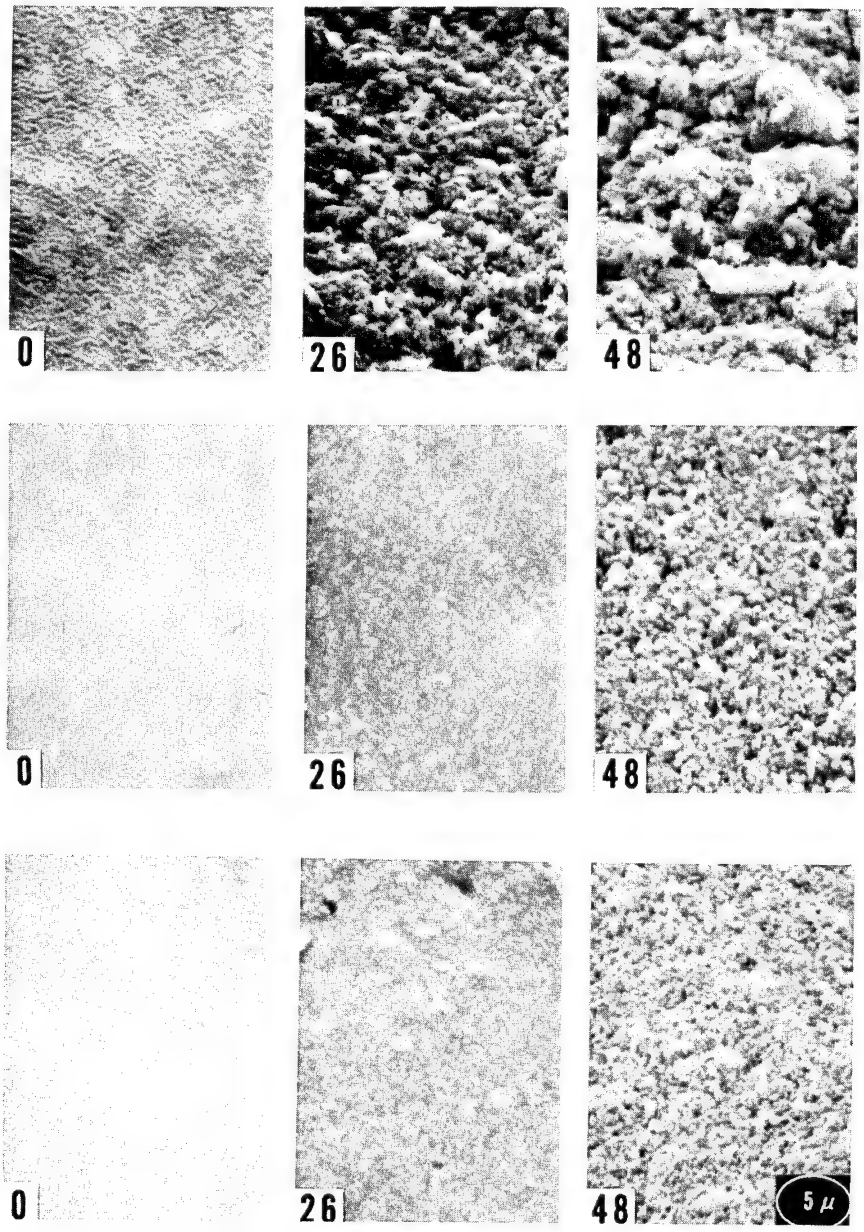

FIG. 4. Sections of paint specimens taken with SEM at 2,000X after 0, 26, and 48 weeks of aging. Top, no. 6 linseed oil trim paint. Chalking started at 12 weeks; microwrinkles at 0 time. Middle, no. 5 safflower-soy alkyd enamel. Chalking started at 32 weeks. Bottom, no. 12 soy-tall alkyd (high-priced). Chalking started at 30 weeks; note microwrinkles at 0 time.

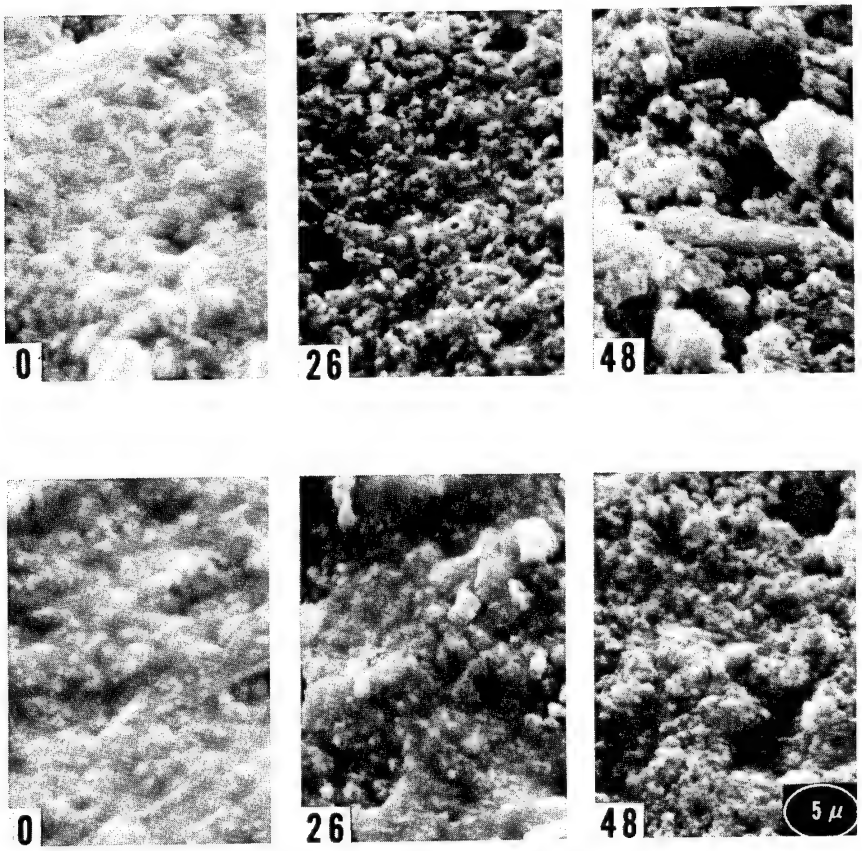

FIG. 5. Sections of alkyd-modified latex paints at 2,000X after 0, 26, and 48 weeks of aging. Top, no. 17 alkyd-modified acrylic; chalking started at 20 weeks. Bottom, no. 7 alkyd-modified vinyl; chalking started at 32 weeks.

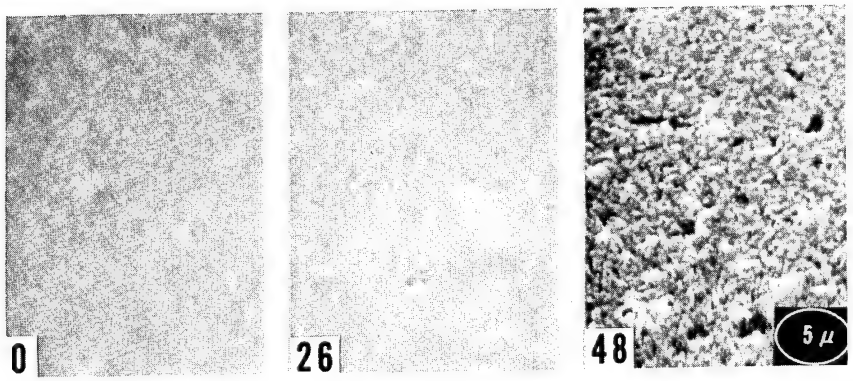

FIG. 6. No. 9 polyurethane at 2,000X after 0, 26, and 48 weeks of age. Chalking started at 40 weeks.

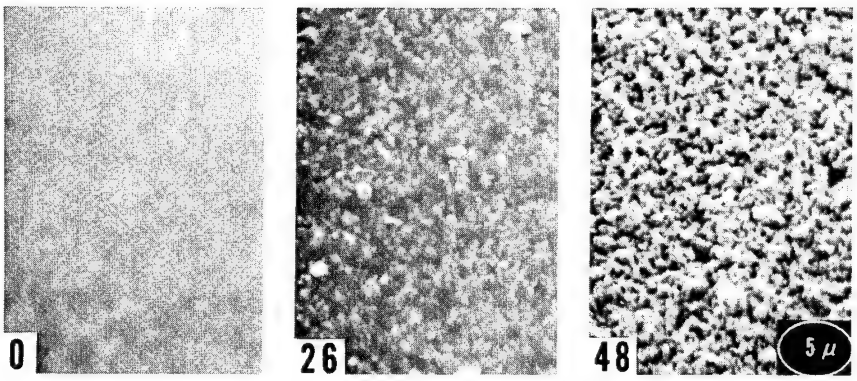

FIG. 7. No. 10 epoxy paint at 2,000X after 0, 26, and 48 weeks of age. Chalking started at 30 weeks.

microwrinkling was observed earlier for nonpigmented films of linseed oil [16]. Upon only 2 weeks of exposure, these wrinkles disappeared completely, and either the films became completely smooth and flat, or they had some small pits ($< 0.5\ \mu$) in the surface.

Dirt collection was also an early and rapid phenomenon. Solvent-base paints collected dirt more rapidly than water-base paints; those water-base paints with added vegetable oil-derived vehicles appeared to collect more dirt than those paints with only latex vehicles.

The most surprising behavior was the rate with which chalking developed, especially in the solvent-base trim and tint-base paints. In some paints, the pigment appeared to come to the surface and begin to break through after only 4 to 6 weeks. Although initially the solvent-base paints rated fair to poor in dirt collection and some also in whiteness, the rating changed drastically as soon as chalking became appreciable. The surfaces became exceedingly clean and white after less than 6 months. Off-white appearance was mainly due to dirt collection, except in a few paints; namely 3, 9, 10, and 12, which contained essentially only TiO_2 as pigment. When TiO_2 was used alone, the films showed a blue-grayish cast.

Tint-base and trim paints are not expected to chalk either quickly or heavily, because colors would fade and general appearance would be reduced. However, both paints in this category (4 and 6) started chalking and losing glossiness within the first 6 months of exposure. After only 9 months, they chalked as heavily as paints 11 and 19. Although this behavior increased surface cleanliness, it did not improve their whiteness much, so these paints performed in a completely unexpected fashion.

No blistering, cracking, or mildew attacks were seen, and no staining from the red cedar panels was observed. Even the apparently porous latex paints that were self-primed were not stained; this lack of staining may indicate that the surface porosity as shown in low-power micrographs (Fig. 8a) is not a true porosity, but rather ruptured air bubbles. The appearance of a typical rupture (Fig. 8b) seems to bear out this reasoning.

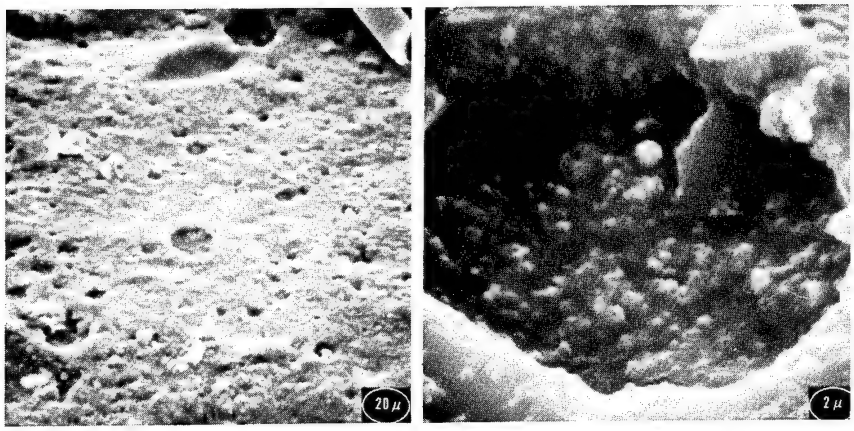

FIG. 8. Porous structure of paint no. 7 at (a) 500X and (b) close up at 5,000X.

Low magnification micrographs of the surface of the epoxy coating showed many peculiar and contrasty rings (Fig. 9a). They are not visible to the naked eye, but their size ranged from 30 to 500 μ in diameter. Closer examination indicates that the ring itself had a width of 5 to 10 μ, was slightly raised from the remainder of the surface, and was rather low in pigment concentration. There seemed to be more pigment inside the ring than outside, as if the pigment in the ring periphery retracted toward the center. Figures 9b and 9c show the ring at 1,000X and 10,000X, at high and low angle, respectively. The lack of pigment in the narrow band of the ring itself is obvious, as is the separation of pigment from the binder; i.e., chalking, which is also shown in Figure 10 at 20,000X. One possible explanation for the presence of these rings is poor mixing

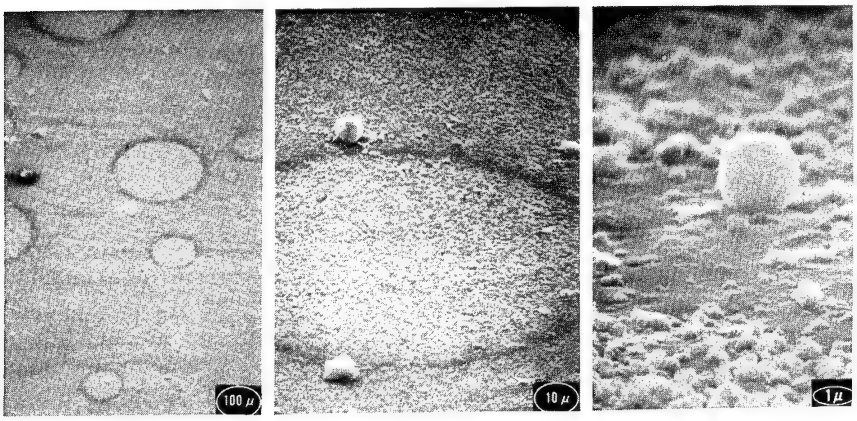

FIG. 9. Typical rings found on surface of paint no. 10 at (a) 100X, (b) 1,000X, and (c) 10,000X and low angle.

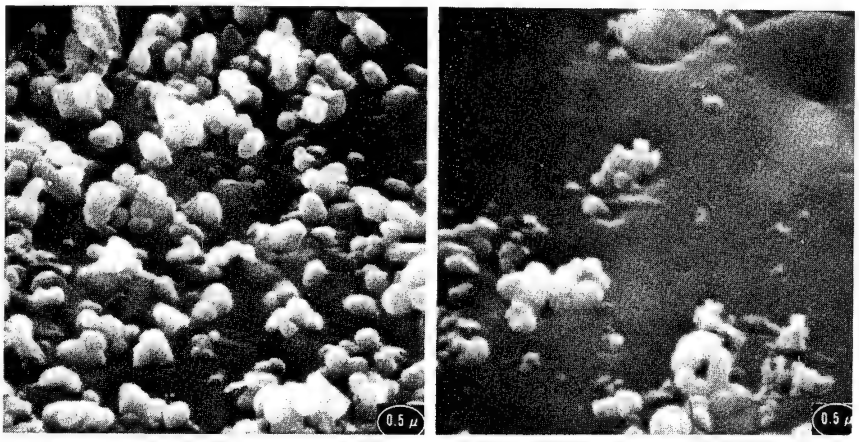

FIG. 10. Titanium dioxide particles chalking out of surface of paint no. 10 at 20,000X; (a) represents general surface area, (b) raised ring with low pigment density.

of the two paint components before application of the film. Whenever a tiny pocket of one component comes to the surface, it forms a ring, and surface forces may pull the pigment particles inward from the interface. When two such pockets meet each other at the surface, they behave like soap bubbles, and the pigment-poor outlines appear as two partial circles with a straight line between them. None of the one-component paints exhibited rings of this nature.

Detailed texture in high-magnification micrographs of chalking surfaces is often obscured by the presence of large particles of extender pigment. If the chalking paint contains only small-sized pigment particles, the image of the pigment-binder interface is better. The epoxy paint in our study was such a coating. At 34 weeks of age, its interface showed (Fig. 10) that the binder stayed smooth and uniform throughout the chalking process, and that the particles squeezed out of the surface after partial exposure. The binder then appeared to heal itself by flowing together again. Otherwise, holes from removed pigment particles would have remained, and the texture of the binder surface would have been much rougher.

Paint 18 had a flat yellow appearance, did not chalk, and looked rather dirty after 6 months' or more exterior exposure. A gentle rinse with some soap and water brought back the bright yellow color, something that was not possible with the trim and tint-base paints described earlier. After 1 year of exposure, this yellow paint did not respond so well to such cleaning action.

Apparently, acrylic and vinyl paints are less sensitive to climatic attack than vegetable oil-derived vehicles, with the acrylics being the least sensitive. However, with the lesser degree of chalking comes an increase in dirt collection, which makes for off-white appearance and dirty colors. Alkyd-modification and variation in pigment contents allow the degree of chalking to be controlled. On the other hand, coatings containing vegetable oil can also be formulated with low rates of chalking either by chemical modification of the vehicle or by

varying the rutile-anatase ratio in the pigmentation. Although vegetable oil solvent-base paints may have looked slightly inferior to latex paints at first, they improved rapidly with age and looked at least as good as, and often better than, the water-base coatings we bought for this study. Also, the change did not require a year, as indicated earlier by the NFPA, but took place within 4 to 5 months.

Unquestionably, the SEM is the instrument indicated for a study of coatings performance. SEM images of either rough- or smooth-surfaced, opaque paint films are easily interpreted. The initial development of chalking, dirt collection, and other properties can be recognized many weeks before traditional fence testing make them known, especially if SEM examination is done at briefer intervals than the usual 3-months, 6-months, or yearly panel examinations that are common in the coatings industry.

REFERENCES

[1] U. Zorll, *Deut. Farben Z., 15,* 334 (1961).
[2] W. C. McCrone, *Off. Dig. Fed. Soc. Paint Technol., 33,* 40 (1961).
[3] S. Wilska, *J. Oil Colour Chem. Assoc., 50,* 911 (1967).
[4] S. B. Twiss, D. M. Teague, and W. L. Weeks, *Off. Dig. Fed. Soc. Paint Technol., 28,* 93 (1956).
[5] E. Fischer and K. Hamann, *Farbe Lack, 63,* 209 (1957).
[6] S. B. Twiss, W. L. Weeks, and D. M. Teague, *Off. Dig. Fed. Soc. Paint Technol., 30,* 36 (1958).
[7] J. D. Nye and J. S. Mackie, *Off. Dig. Fed. Soc. Paint Technol., 34,* 716 (1962).
[8] J. Marriott, *J. Oil Colour Chem. Assoc., 41,* 363 (1958).
[9] S. H. Bell, *J. Oil Colour Chem. Assoc., 43,* 466 (1960).
[10] U. Zorrl, *Paint Technol., 27*(3), 32 (1963).
[11] R. Qyarendon, *Paint Mfr., 23,* 111 (1953).
[12] J. H. Bishop and S. R. Silva, *J. Oil Colour Chem. Assoc., 52,* 201 (1969).
[13] J. B. Zicherman and R. J. Thomas, *J. Paint Technol., 44,* 88 (1972).
[14] L. E. Brooks, P. Sennett, and H. H. Morris, *J. Paint Technol., 39,* 472 (1967).
[15] L. H. Princen and F. L. Baker, *Paint Varn Prod., 61*(12), 21 (1971).
[16] L. H. Princen, *Appl. Polym. Symp., 16,* 209 (1971).

THE FILLER–BINDER INTERFACE IN PAINT FILMS

R. L. EISSLER, F. L. BAKER, and J. A. STOLP

Northern Regional Research Laboratory, Agricultural Research Service, U.S. Department of Agriculture, Peoria, Illinois 61604

SYNOPSIS

A previously described, quantitative method for use with a scanning electron microscope (SEM) to study adhesion between filler particles and solidified vehicle matrix has been applied to four linseed oil film-pigment systems. Water sensitivity was compared of films from a bodied oil and an unbodied oil containing zinc oxide pigments with and without an organic phosphate treatment. SEM photomicrographs were taken, and the number of particles appearing in surfaces formed by tensile fracture of films were counted. After holding parameters related to the SEM and photographic exposure constant, appearance of only a relatively few pigment particles in photographs of fracture surfaces presumably meant good particle-binder adhesion. A three-way analysis of variance on geometric means of particle concentration indicated that adhesion improved in films from bodied oil and treated pigment when these films were tested dry before or after water exposure. Any similar improvement in films from unbodied oils was apparently obscured by the weak mechanicl strength of the vehicle. It seems possible to modify our method so that data can be taken directly and tabulated electronically from SEM images.

INTRODUCTION

Tensile, swelling, and blistering tests on linseed oil paint have been of considerable value in investigating the water sensitivity of these coatings. None of these tests, however, directly point out the effect that vehicle-filler interface has on water sensitivity. A practical importance of this interface rests on its ability to be modified by filler-surface treatment. In previous work [1], we outlined and partially evaluated a quantitative method for using a scanning electron microscope (SEM) to study adhesion between filler particles and the solidified vehicle matrix in a coating film. The method involved determining either the distribution of apparent particle diameters or the concentration of exposed particles of regular shape in surfaces formed by cross-sectional fracture of free films. Number and size of exposed particles were evaluated by counting and measuring them in photographs of fracture surfaces. Data for films before and after water treatment were evaluated and compared by a statistical test.

Our present work involves this same general method as applied to four sets of films. These experiments permit evaluation of effects of linseed oil, pigment surface treatment, and water exposure on filler-vehicle adhesion in a film. It appears impossible to gain these data directly by any other method. Since filler-vehicle adhesion is important, such data are of practical value in paint formulation.

Applied Polymer Symposium No. 23, 41-48 (1974)

Counting or measuring particles in photographs is tedious, time consuming, and subject to error. It should be possible to determine particles in fracture faces directly from the SEM image and then to tabulate their quantity electronically. To make results from our experiment more nearly like those from electronic counting, we considered a filler particle to be present when a spot lighter than its immediate background occurred in the photographic image of a fracture surface. This criterion is not the same as that employed earlier [1] where the human eye sees an image of a particle. The modification should help determine the ability of our method to be adapted to an electronic method for particle counting directly from the SEM image.

EXPERIMENTAL

Our experiment was designed to compare properties of films made up from each of two pigments in each of two linseed oils. The second pigment was prepared by treating the first one so as to give it a hydrophobic surface [2]. One linseed oil had been bodied to an M37 viscosity. The other was an alkali-refined, unbodied oil.

Films were prepared from formulations calculated to give a 30% pigment volume concentration in the final film. Vehicles for the formulations were made up by adding required amounts of lead and cobalt naphthenate driers to the appropriate linseed oils. Pigments were dispersed in vehicles with a high-speed mixer after which the blend was diluted to proper consistency with mineral spirits. All mixtures tested to better than 7 on a fineness of grind gauge immediately before films were prepared. To obtain unsupported films, pigmented mixtures were applied to Teflon* substrates with a drawdown bar and dried. Details of film preparation are given elsewhere [3].

Film A was prepared from an M37 linseed oil and an American-processed zinc oxide, described by its manufacturer as nodular, with an average particle diameter of 0.25 μ. SEM examinaion, however, revealed a number of acicular particles in this pigment. Film B contained this same zinc oxide but the unbodied linseed oil. Film C was prepared from M37 oil and a filler formed by surface treating the pigment used in films A and B. Film D was made up from surface-treated pigment and unbodied oil.

Surfaces for study with the SEM were prepared by tensile fracture of dumbbell-shaped specimens [4]. Water sensitivity was determined by comparing fracture surfaces from (a) films aged for 6 weeks in laboratory atmosphere, (b) films immersed in distilled water for 6 weeks and tested wet, or (c) films immersed in water for 4 weeks and dried in the laboratory for 2 weeks. Following treatment, specimens were fractured in tension at a crosshead travel

*Mention of firm names or trade products does not imply that they are endorsed or recommended by the Department of Agriculture over other firms or similar products not mentioned.

rate of 2 cm/min on an Instron tester. Opposing fracture faces were mounted on studs, side by side, for viewing with a Cambridge Stereoscan Mark IIa SEM. Mounted specimens were coated with a thin film of aluminum before viewing. Photographs were taken with the SEM of areas having a representative morphology for each fracture face. Magnification was 5000X on each photograph. To get consistently good images, it was necessary to direct the electron beam of the instrument at 5° from the normal to the fracture face in a direction that would be vertical on the specimen. Effect of a slight area distortion caused by this 5° difference was later removed by calculation. The electron gun accelerating potential was 20 kv for all photographs.

To determine the number of particles exposed in the fracture face, 3X enlargements of SEM photographs were used. Total magnification in the final enlargement was, therefore, 15,000X. Each enlarged photograph was ruled to give between 30 and 36 squares. Squares were 20.25 cm^2 in area and represented slightly more than 9 μ^2 on the original fracture face. The number of particles exposed in each square was determined by counting the number of relatively brighter areas showing in a photograph.

Tabulating squares according to count estimated a distribution of particle number density across the fracture face. Two photographs giving a total of from 60 to 72 squares were used to estimate each face.

EXPERIMENTAL RESULTS

Examples of ruled photographs of fracture surfaces are given in Figures 1 and 2. When particle counts on the two photographs of each fracture face were compared, a chi square test [5] indicated for each pair at the 5% level of significance that there was no difference between distributions. For this reason, data from the two photographs were combined to determine differences between fracture faces. Table I lists the arithmetic mean and range for the number of pigment particles counted per 4.5 cm X 4.5 cm square on enlarged photographs of fracture surfaces.

DATA ANALYSIS

A three-way analysis of variance [6] was computed for both the arithmetic and geometric means of particle number density on each of our fracture surfaces. Although both analyses told essentially the same story, geometric means are more suitable for establishing statistical significance for our data. The relative importance of the geometric mean stems from the proportionality, visible in Table I, between the range and the arithmetic average of particle number density over a given fracture surface.

Our raw data consisted of a tabulation of the number of particles (bright spots) found in several 4.5 cm X 4.5 cm areas on enlargements of each of two

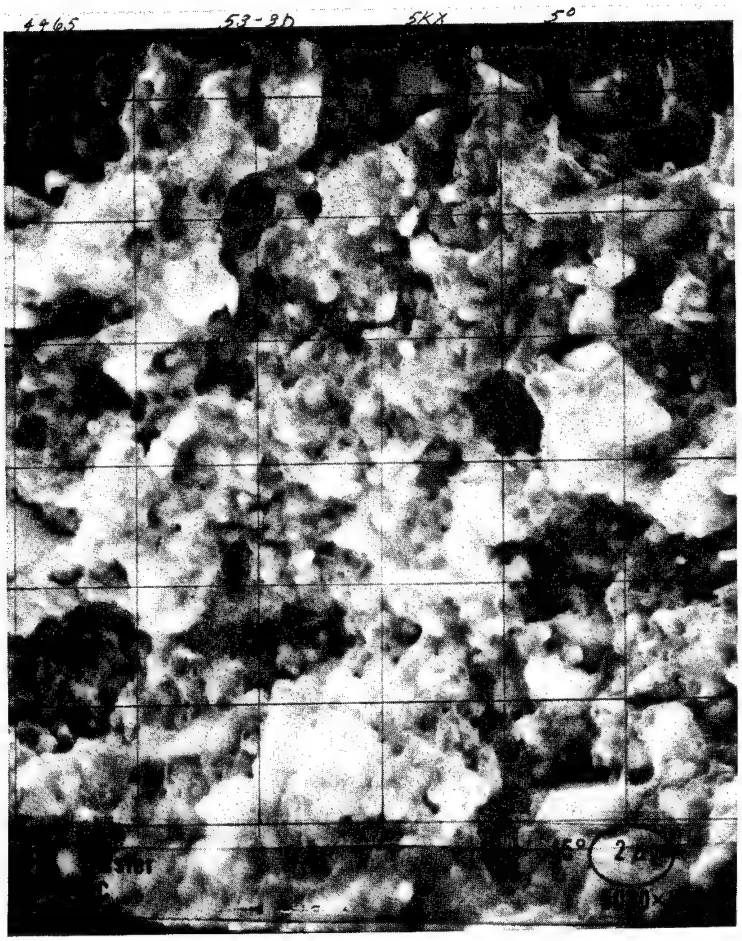

FIG. 1. Ruled photograph of fracture surface from a water-soaked film of M37 linseed oil.

5000X photographs of surfaces formed by tensile fracture of each film. Similarity of distributions from each of the two photographs allowed the data for each fracture to be combined. For all except one specimen, 36 squares were counted per enlargement. Geometry of photographs was such that areas were arranged in a six-row, six-column configuration. Raw data for these 11 specimens were subjected to an analysis of variance searching for significant row, column, or photographic effects. Column-row, column-photographic, and row-photographic interaction effects were also tested for significance.

DISCUSSION

Geometric means for particle number densities in fracture surfaces of our films are given in Table II. Averages for each film when aged, water-soaked, or

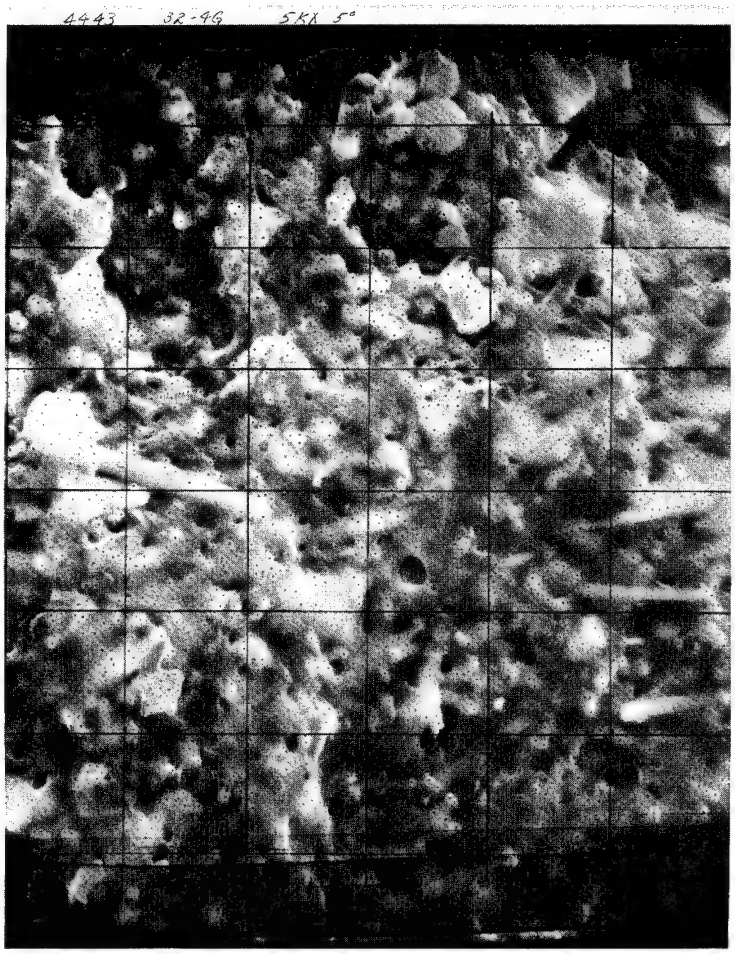

FIG. 2. Ruled photograph of fracture surface from a water-soaked/dried film of unbodied linseed oil.

water-soaked and dried are listed in the table. An analysis of variance on geometric means indicates that the three-way interaction is significant, and therefore only comparisons between individual pairs of means are valid. The least significant ratio between means in Table II at the 5% significance level was computed to be 1.096. On the basis of this criterion, the data show that under all conditions of comparison, films of unbodied linseed oil averaged fewer pigment particles in fracture surfaces than films of M37 oil. This result may well be brought about because the unbodied oil forms a mechanically weaker vehicle.

The vehicle could also account for a lack of difference when effects of the two pigments on fracture surfaces of water-soaked and water-soaked/dried films of unbodied oil are compared. Films from M37 linseed oil and treated pigment have a lower average occurrence of particles in fracture surfaces when aged and when water-soaked/dried than corresponding films from the same oil and regular

TABLE I

Arithmetic Mean and Range for Pigment Particles Counted Per Square in Fracture Surfaces

Conditions	Film of M37 linseed oil		Film of unbodied linseed oil	
	Particles per square			
	Mean	Range	Mean	Range
Untreated zinc oxide				
Aged	71.4	45	31.2	37
Water-soaked	97.6	95	44.8	37
Water-soaked/dried	100.6	53	58.3	65
Treated zinc oxide				
Aged	62.9	52	48.9	43
Water-soaked	93.5	77	41.1	25
Water-soaked/dried	79.9	67	57.1	53

TABLE II

Geometric Mean Particle Number Densities of Pigments in Fracture Surfaces*

Conditions	Particles/μ^2	
	Film of M37 oil	Film of unbodied oil
Untreated zinc oxide		
Aged	8.01	3.35
Water-soaked	10.60	4.85
Water-soaked/dried	11.04	6.28
Treated zinc oxide		
Aged	6.88	5.31
Water-soaked	10.22	4.53
Water-soaked/dried	8.74	6.21

*Least significant ratio between means at 5% level of significance 1.096.

zinc oxide. The last films are of relatively high-tensile strength and are quite brittle even when water-soaked [3]. When dried after soaking, films from bodied oil and untreated zinc oxide remain brittle but often vary in tensile breaking strength. Films from M37 oil and surface-treated zinc oxide appear as strong and no more extensible than those from the same oil and the untreated pigment. Lower particle numbers in fracture surfaces of films from bodied oil and treated pigments compared to similar films from untreated ones appear to be caused by greater adhesion at the pigment-vehicle interface. This conclusion is supported by the strength and lack of extensibility of zinc oxide pigmented films of bodied oil.

Films from bodied oil and untreated zinc oxide swell considerably more in water than films from the surface-treated pigment. The variable breaking strength of films from these same materials has been tentatively ascribed to the presence of small cracks formed when water-soaked films of this composition are dried [3]. If small cracks are the cause of variable breaking strength, then the relatively high number of pigment particles found in fracture surfaces of water-soaked and dried films from M37 oil and untreated zinc oxide probably means that these cracks occur at or close to the pigment-vehicle interface.

Results from analysis of our raw data for column, row, and photographic effects do not alter statements or conclusions given in previous paragraphs; however, only the column-photograph interaction failed to give some effects that were statistically significant. From total of 66 possible effects or interactions, 23 appeared statistically significant. Computed on a purely random basis, only about six of these effects or interactions should appear so. Because of specimen orientation in the SEM, row effects could be accounted for by pigment settling during initial drying of the film [7]. Photograph and row-photograph interaction effects might occur because of variation in photographic exposure. The possibility of accounting for column and column-row interaction effects is not so straightforward, however. Such effects might be accounted for by observer bias, by specimen orientation, or even by a systematic variation in intensity of the SEM electron beam with its position on the specimen.

Statistical analysis indicated also that we could have achieved the same relative standard deviation per mean as that actually attained by counting particles in only 16 squares on each of three different areas on a specimen. Had this been done, we would have eliminated about one-fourth of the work involved in the most tedious part of our experiment.

Along with film properties, parameters related to the SEM itself may also affect the number of filler particles found in a surface. Among such parameters are the conductive coating applied to specimens and the depth from which electrons are emitted below the conducting surface. Our method of counting particles is quite tedious and probably subject to some bias. Counting electronically directly from the SEM image would be faster and less subject to error. To make results from our experiment more nearly like that from electronic counting, we judged a filler particle to be in the surface when a spot lighter than the immediate background occurred in the photographic image. These spots vary in size and usually occur because a particle is located in or close

to the surface. Edges of small, sharp wrinkles on the vehicle surface can also give light spots in a photograph. In the rare circumstances when it did not appear that these spots could be distinguished from the filler particles by electronic analysis of the image, we also counted the spots as caused by particles.

CONCLUSIONS

Our method appears to give information that can be gained in no other way. It also seems possible to modify the method so that data can be taken directly and tabulated electronically from the SEM image. In general, films from unbodied linseed oil averaged fewer particles per μ^2 in their fracture surfaces than films from the bodied oil. This result was probably caused by the mechanically weaker vehicle matrix from unbodied oil. The weaker matrix also tends to obscure any possible differences caused by our pigments in films from this same oil. Dry films from M37 bodied linseed oil and surface-treated zinc oxide have a lower average occurrence of pigment particles in fracture surfaces than corresponding films from untreated zinc oxide. When this information is combined with tensile and swelling data, it appears to indicate a greater pigment-vehicle adhesion in films of bodied oil containing treated zinc oxide than in those from untreated material. Further analysis of our raw data indicates several minor effects that might be traced to method or instrument. We feel that further study of film fracture surfaces is worthwhile and that combining SEM observations with other tests will yield information of great value in formulating and improving paint.

The authors are grateful to Dr. W. F. Kwolek, Biometrician, Biometrical Services, U.S. Department of Agriculture, stationed at the Northern Laboratory, for suggestions and much of the statistical analysis of our data.

REFERENCES

[1] R. L. Eissler and L. H. Princen, *J. Electroanal. Chem.*, **37**, 327 (1972).
[2] R. L. Eissler, R. Zgol, and J. A. Stolp, *J. Paint Technol.*, **42**, 483 (1970).
[3] R. L. Eissler and L. H. Princen, *J. Paint Technol.*, **40**, 105 (1968).
[4] ASTM D412-62T, "Tentative method of tension testing of vulcanized rubber," Amer. Soc. Testing Mater., Philadelphia, Pa.
[5] G. W. Snedecor and W. G. Cochran, *Statistical Methods* 6th ed., The Iowa State University Press, Ames, 1968, p. 228.
[6] Ibid., p. 361.
[7] R. L. Eissler and F. L. Baker, *Appl. Polym. Symp.*, **16**, 209 (1971).

APPLICATIONS OF ENERGY-DISPERSIVE X-RAY SPECTROSCOPY IN INTERFACIAL COATING FAILURES

A. QUACH

Research and Development Center, Coatings and Resins Division, PPG Industries, Inc., Springdale, Pennsylvania 15144

SYNOPSIS

Among the more troublesome coating failures is the loss of adhesion of paint films, which often is caused by contamination of the substrate prior to the application of the coating. The application of a scanning electron microscope with an energy-dispersive x-ray spectrometer attachment for identification of the contaminants and their origin is discussed. Spherical particles are common contaminants observed. However, their origin may vary from welding spatter to pulverized-fuel boiler fly ash, and a chemical analysis is necessary to form a reasonable conjecture as to how and where these contaminants originated. Reaction of SO_2 pollutant with the pigment system in an old paint film may cause them to aggregate on the top surface, resulting in adhesion failure when a new paint is applied. The instrument was also used to determine the cause of discoloration failure (blackening of the Ag coating) of mirrors. X-ray spectroscopy indicated that the failure was induced by HCl vapor that attacked the Ag through unprotected edges of the mirrors.

INTRODUCTION

There are many causes of coating failures, and they have been well documented by Hess et al. [1]. Among the more troublesome failures is the adhesion failure of paint which often is caused by contamination of the substrate surface prior to the application of the coating. An applied film may also loose adhesion if it contracts or expands due to drying, temperature variation, water absorption, etc. In any event, the cause of the interfacial defect must be determined so that proper action can be taken. In this paper we wish to report the use of the scanning electron microscope (SEM) and its x-ray spectroscopic accessory for the identification of contaminants in several cases of paint failure. Other applications of the technique in the field of coatings are also discussed.

X-RAY SPECTROSCOPY

Since the commercialization of the SEM in the mid 1960's, applications of the instrument in the coatings industry have been increasing [2-8]. The Proceedings of the Annual SEM Symposia, published by IIT Research Institute, Chicago, Illinois, provide an excellent source of references to the theory, as well

Applied Polymer Symposium No. 23, 49-59 (1974)

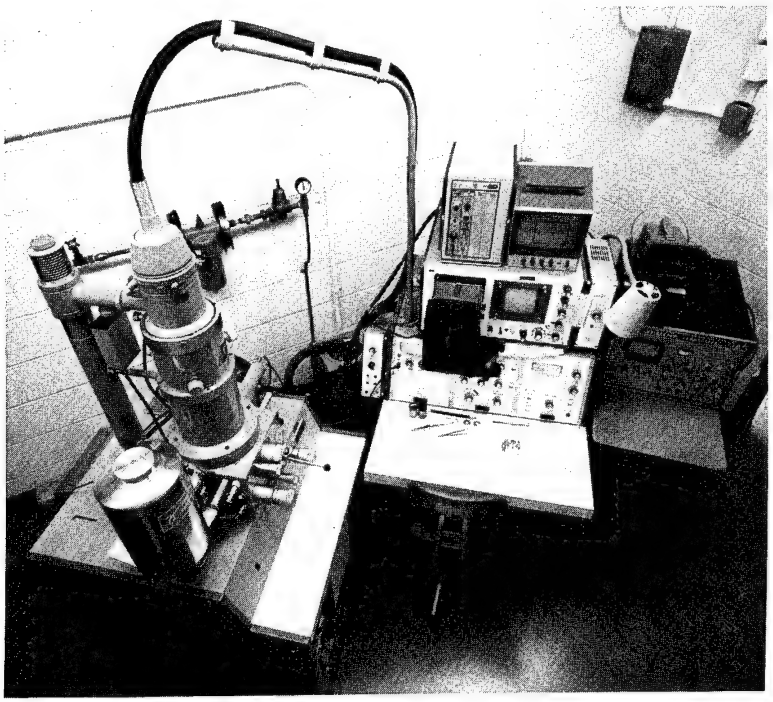

FIG. 1. Scanning electron microscope with ED x-ray spectrometer.

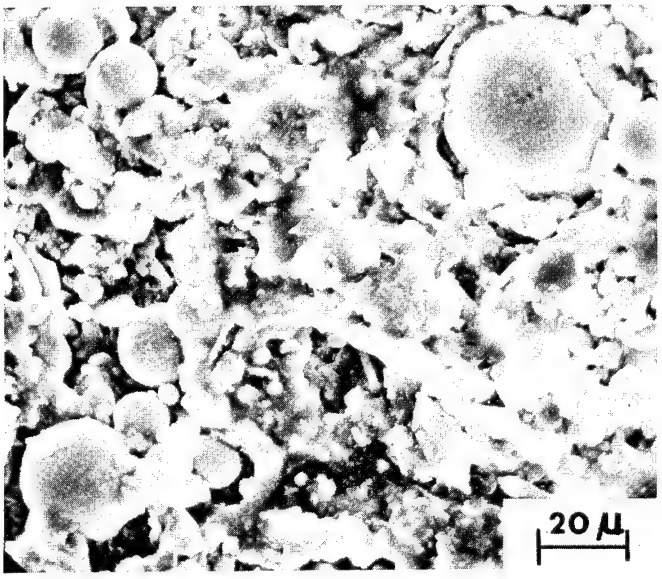

FIG. 2. SEM micrograph of underside of a paint chip peeled from a steel building chord. Spherical particles are iron welding spatter.

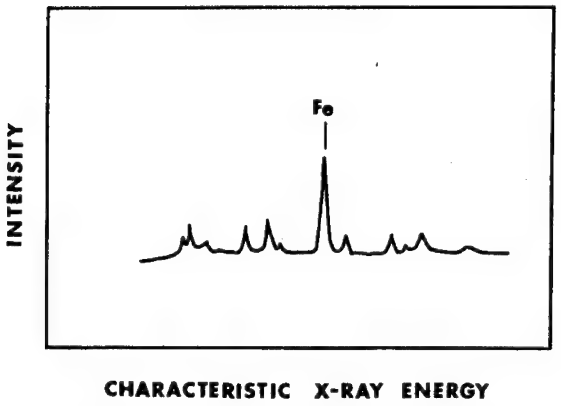

FIG. 3. ED x-ray spectrum of same area of Figure 2.

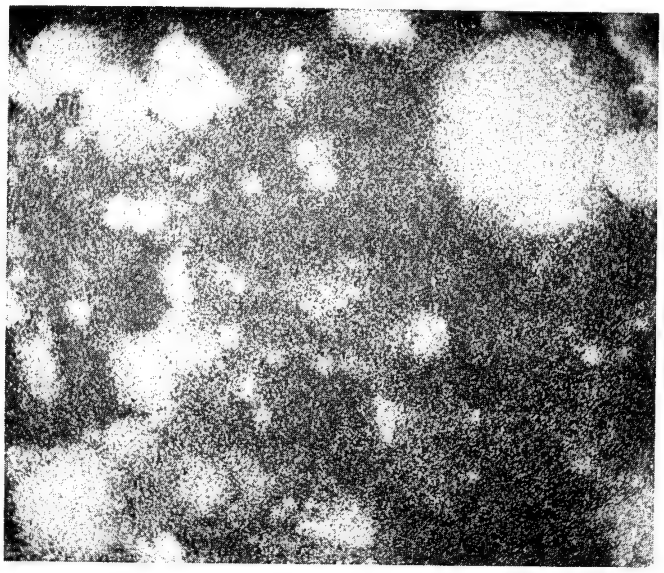

FIG. 4. Fe-distribution micrograph of same area of Figure 2.

as to applications in various research disciplines [9]. Holm [10] and Johari [11] have summarized the different operational modes of the SEM for characterization and analysis of surfaces. Particularly, the x-ray mode used for composition analysis was emphasized. When the SEM is operated in this x-ray mode, it works as an electron probe microanalyzer, and the term "x-ray spectroscopy" is used to describe this mode of operation. Detailed descriptions of the principles can be found in the above-mentioned references. Therefore, it suffices to say here that x-rays characteristic of each element present in the sample are emitted upon bombardment within the SEM column by the electron beam; the emitted x-rays are then analyzed according to either their wavelength

or their energy. The latter method is the most common today, and is generally known as non-dispersive spectroscopy, although energy-dispersive (ED) spectroscopy is a more proper term.

In general, analysis of either a spot, a line, or a surface can be performed. Most of the instruments available now have facilities for imaging and photographing the distribution of any selected element, provided that it is within the resolution power of the instrument. Our instrument is a JEOL Model JSM-2 scanning electron microscope, interfaced with a Princeton Gamma-Tech ED x-ray spectrometer, as shown in Figure 1. The SEM coupled with the ED x-ray spectrometer is unique in that observation of the size, shape, and structure of the object, and analysis of its composition can be made at the same time. This feature can greatly enhance the results, as well as facilitate the interpretation of a SEM study.

RESULTS AND DISCUSSION

Contamination by Welding Spatter

Figure 2 is a SEM micrograph of the underside of a paint chip that peeled from a steel building chord. Note the presence of spherical particles. An ED x-ray spectrum of this area is shown in Figure 3. The abscissa is the x-ray energy characteristic of the elements present. The intensity of a peak is related to the amount of each element present. It can be seen that Fe is the dominant element. An Fe-distribution photograph is shown in Figure 4, where the bright spots

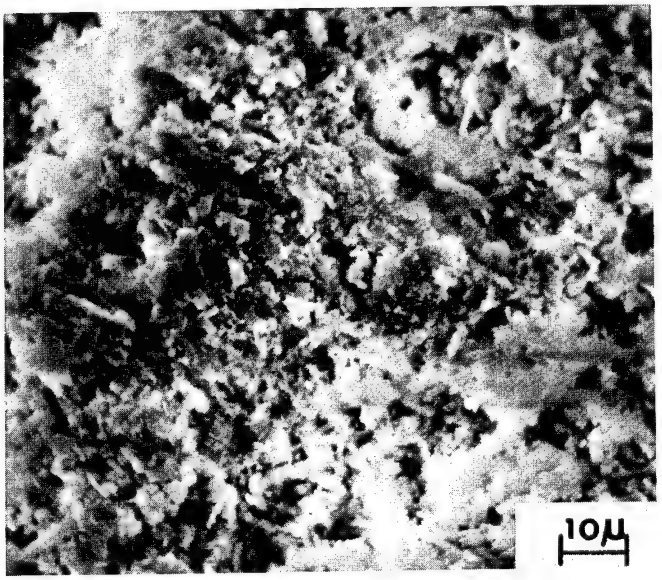

FIG. 5. SEM micrograph of plaster on the underside of a paint chip.

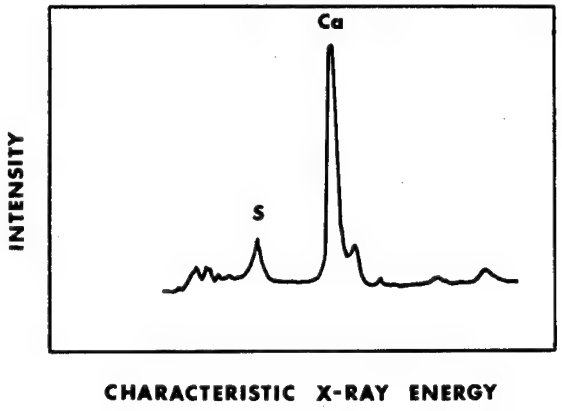

FIG. 6. ED x-ray spectrum of same area of Figure 5.

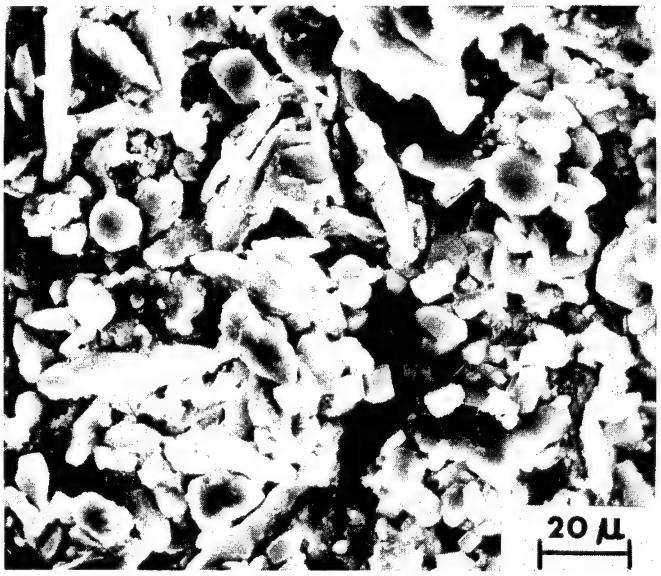

FIG. 7. SEM micrograph of underside of a paint chip peeled from an old paint surface Spherical particles are fly ash, others are pigments.

represent Fe-rich areas. These areas correspond to the spherical particles seen in Figure 2. Spot analysis of individual particles indeed confirms that they are iron particles. Such spherical iron particles are abundant on the underside of the paint chips. The spherical shape suggests that they were formed at high temperature; most probably they are the welding spatter that was not removed prior to the application of the coating. Spherical iron particles can also come from pulverized-fuel boiler fly ash in industrial areas (see below). However, the source of the contamination under discussion is not fly ash, since the paint film fails only near the welding regions.

Contamination from Plaster

Because of the extensive use of plaster and gypsum in the construction industry, dust from these materials is a common contaminant that causes poor adhesion of paint films on metal or primed substrates. Although this contaminant can easily be recognized by its appearance, a chemical analysis is sometimes required to confirm its existence. Figure 5 is a SEM micrograph of a white powdery deposit on the underside of a paint chip that peeled from a

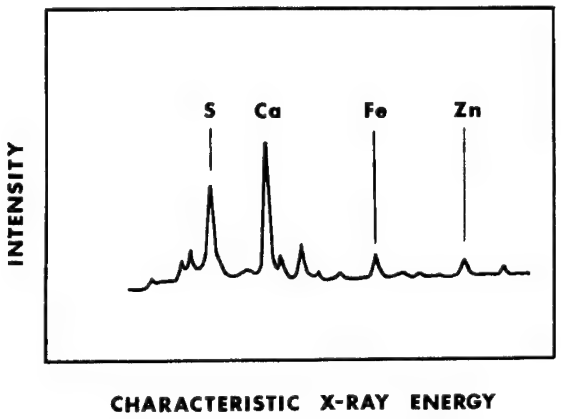

FIG. 8. ED x-ray spectrum of area of Figure 7.

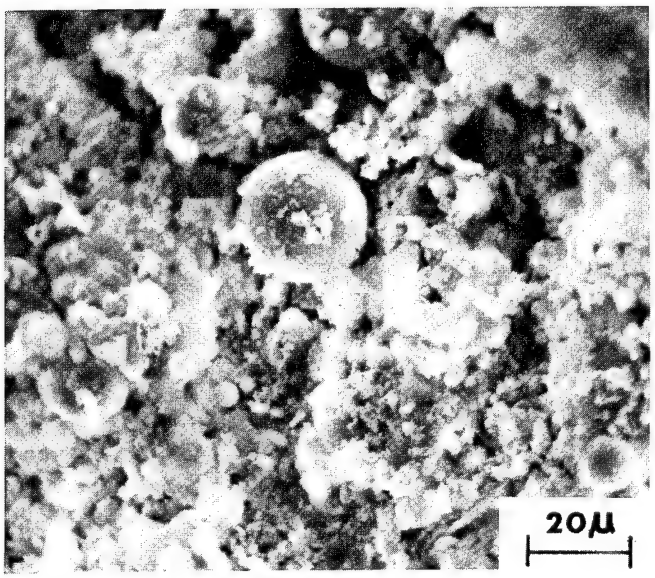

FIG. 9. SEM micrograph of underside of a paint chip peeled from a concrete surface, showing cement particulates.

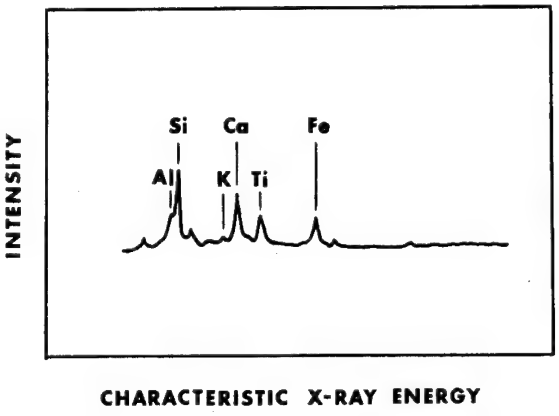

FIG. 10. ED x-ray spectrum of area of Figure 9.

primed surface. An ED x-ray analysis (Figure 6) indeed shows the presence of S and Ca, and therefore, confirms the existence of plaster or gypsum dust. Hess et al. [1] give an excellent account of plaster-related paint film defects.

Contamination by Fly Ash and Pigment from Old Paint

Fly ash is one of the culprits contributing to poor adhesion of paint films in industrial areas. Figure 7 is a SEM micrograph of the underside of a house paint chip that peeled from an old paint surface. Spherical particles again are observed, and ED x-ray analysis shows that they are again iron particles. These particles come from iron minerals in coal and are fused into dull black to steel-gray spheres of magnetite (Fe_3O_4). They are common in pulverized-fuel boiler fly ash [12]. The fly ash deposited on the old paint surface and was not properly removed before the new paint was applied.

An ED x-ray spectrum of Figure 7 is shown in Figure 8. Note the existence of the sulfur peak. A sulfur distribution map shows that the elongated particles in figure 7 correspond to S-rich areas. Since neither the coating nor the pigment systems of both the old and new paints contain sulfur compounds, the sulfur must have come from an outside source. Because ZnO pigment is present in the old paint, it is possible that the pigment has been attacked by SO_2 pollutant from the atmosphere of industrial areas. It has been reported [13] that ZnO is highly prone to attack by SO_2, with the formation of soluble compounds that are either washed away by water or remain on the surface in the form of large crystal aggregates with such composition as $ZnSO_4 \cdot 4H_2O$. An ED x-ray analysis indicates that these elongated particles also contain Zn. The Ca peak in the spectrum may come from either $CaCO_3$ extender pigment or from $CaSO_4$. The latter may have formed by reaction of $CaCO_3$ with SO_2 and moisture. These particles, together with fly ash, are the major causes of adhesion failure of new paint films.

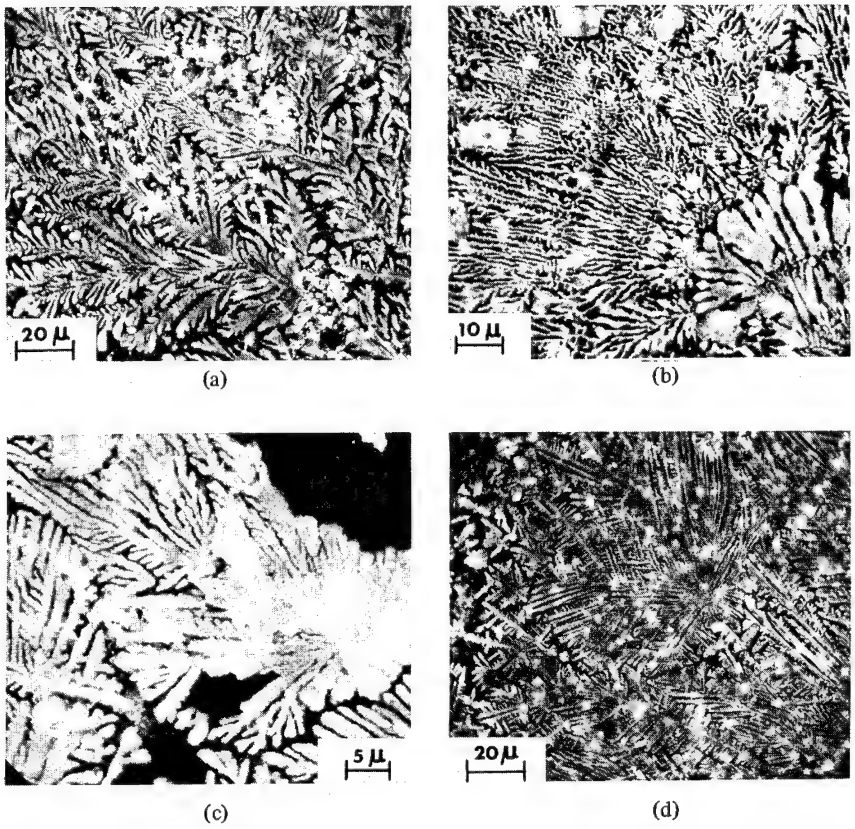

FIG. 11. SEM micrographs of the discolored area of a mirror. Dendritic structures are the Ag coating attacked by Cl-containing chemicals.

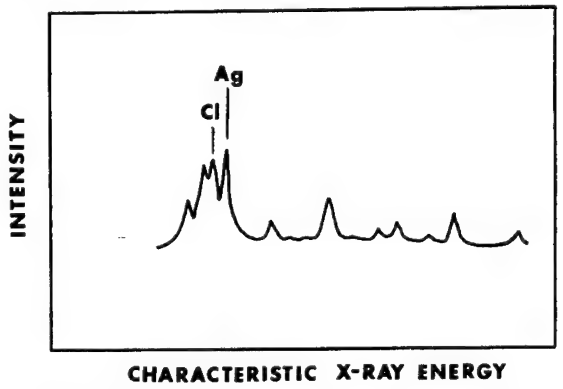

FIG. 12. ED x-ray spectrum of area of Figure 11.

Contamination by Cement Particles

Figure 9 is a SEM micrograph of the underside of a paint chip. The coating was applied to concrete beams and columns, and had been failing badly. It can be seen that spherical as well as odd-shaped particles are spread all over the

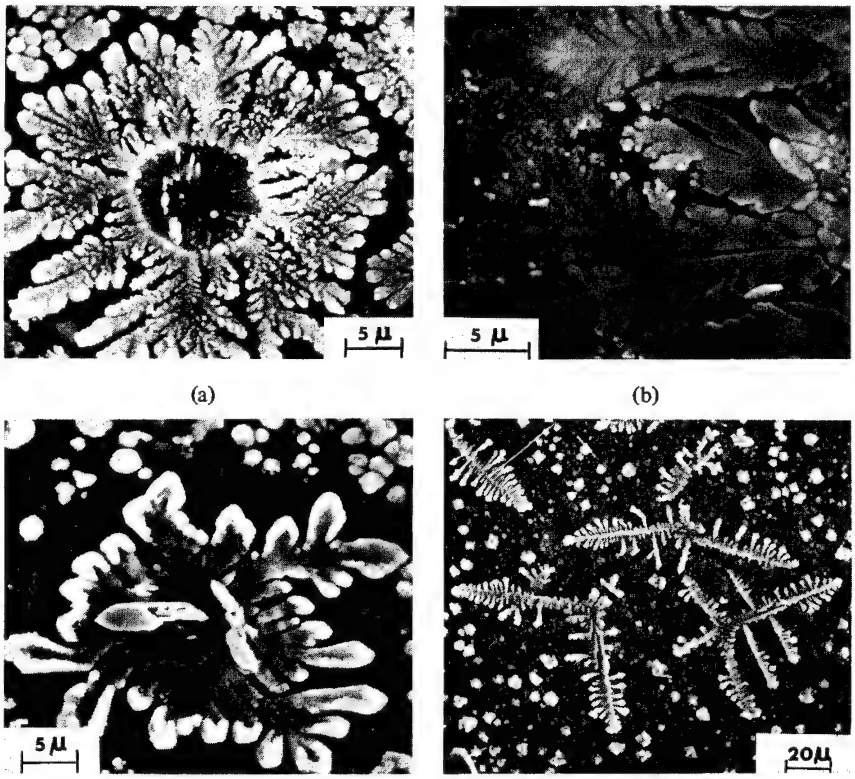

FIG. 13. SEM micrographs of the laboratory-induced discolored areas of a mirror by exposure to HCl vapor: (a) through (c) exposed for 116 hr using 0.1N HCl solution; (d) exposed for 20 hr using 1N HCl solution.

underside of the chips. An ED x-ray spectrum of the surface is shown in Figure 10. Aside from Ti from the TiO_2 pigment in the coating, the spectrum shows the presence of Al, Si, K, Ca, and Fe. These elements are the major constituents of a typical cement. Analysis of individual particles, including the spherical ones, indicate that they contain the same elements as the overall surface. The spherical cement particles must have formed at high temperature during the kilning process. These particles probably were pulled away from the concrete body, and they are the major cause of the adhesion failure. Observations of the paint film show cracks and fissures penetrating through the film. Entry of water through these openings could also assist in flaking the paint film.

Discoloration Failure of Mirror by Chemical Attack

So far we have discussed four cases of contamination that caused adhesion failure of coatings. We will now discuss a different kind of coating interfacial defect, namely the discoloration or black undercutting failure of the silver

coating on the back of mirrors. The blackening of the Ag coating took place at the polished or cut edges of mirrors installed in an apartment complex under construction. Figure 11 shows SEM micrographs of different areas of the failing regions. It can be observed that dendritic structures are typical of the failing areas. An ED x-ray analysis of these structures reveals, in addition to Ag and other elements characteristic of the mirror-backing coating, the presence of chlorine (Figure 12). The presence of Cl raises the question of possible attack of the Ag by Cl-containing chemicals through the edges of the mirror. A potential culprit is muriatic acid (dilute HCl solution), used in cleaning floors, pipes, etc., during construction.

To see if similar failure can be induced by HCl vapor, two good mirror samples were exposed to the vapor phase of 1N and 0.1N HCl solutions, respectively. The exposure time was 20 hr for the former, and 116 hr for the latter, while the temperature was controlled at 50°C. Results show that similar discoloration failure indeed can be observed in these exposed samples. SEM micrographs of laboratory-induced failing areas are shown in Figure 13. Dendritic structures are again observed, and ED x-ray spectra, similar to those of the construction site samples have also been obtained. These findings suggest that HCl vapor is in fact the chemical that attacked the silver of the mirrors. The attack started preferentially from the edges of the mirror, because due to polishing and cutting the edges were no longer protected by the mirror-backing coating.

CONCLUSIONS

We have demonstrated the power of the SEM when used in conjunction with an ED x-ray spectrometer. With these tools, elemental analysis can be completed in a very short time, and observation of the structure can also be obtained at the same time. The elemental analysis is certainly very helpful in interpreting SEM results, and in the case of coating interfacial defects, also in pointing out the source of contamination. The element distribution micrograph is especially useful in differentiating particles of different composition.

It has been shown that spherical particles are quite common in contaminants. However, care must always be exercized in concluding their possible origin. The possibility of chemical attack on the pigment system in a coating, or even on the coating itself, by foreign matter should also be considered.

Other applications of the technique in the field of coatings are numerous. For example, the technique has been used successfully to identify various pigments and extenders in unknown samples. In one case, we were able to determine the nature and the location of pigment particles in a void-containing microcapsule.

With the development of better detectors, electronics, and computerized systems, semi-quantitative work can be handled with ease. The combination of the SEM and the ED x-ray spectrometer should become a powerful tool for analysis and characterization of coatings and resins.

The author wishes to express his appreciation to Dr. P. E. Pierce for valuable and stimulating discussions, and to Mrs. K. Hilbeck for assistance in various aspects of this work.

REFERENCES

[1] M. Hess et al., *Paint Film Defects*, 2nd ed., Reinhold, N.Y., 1965.
[2] L. E. Brooks, P. Sennett, and H. H. Morris, *J. Paint Technol., 39,* 511, 472 (1967).
[3] P. Sennett, R. J. Drexel, Jr., and H. H. Morris, *Tappi, 50*(11), 560 (1967).
[4] P. Sennett, R. J. Drexel, Jr., and H. H. Morris, *Tappi, 51*(12), 567 (1968).
[5] G. D. Cheever and J. J. Wojtkowiak, *J. Paint Technol., 42*, 546, 409 (1970).
[6] L. A. Smith and W. A. Cote, *J. Paint Technol., 44*, 564, 71 (1972).
[7] J. B. Zicherman and R. J. Thomas, *J. Paint Technol, 44,* 570, 88 (1972).
[8] L. H. Princen, Ed., *Scanning Electron Microscopy of Polymers and Coatings (Appl. Polym. Symp. No. 16)*, Interscience, New York, 1971.
[9] *Proc. Annu. Scanning Electron Microscope Symp.* I-VI, IIT Research Institute, Chicago, Ill., 1968-1973.
[10] R. Holm, *Angew. Chem. Int. Ed. 10*(9), 591(1971).
[11] O. Johari, Res./Develop., *22*(7), 12 (1971).
[12] W. C. McCrone, R. G. Draftz, and J. G. Delly, *The Particle Atlas*, Ann Arbor Science Publ., Ann Arbor, Mich., 1967.
[13] S. Torlaschi et al., *11th FATIPEC Congress,* 207 (1972).

CHARACTERIZATION OF COATINGS BY ELECTRON MICROPROBE ANALYSIS

S. S. LABANA and M. WHEELER

Ford Motor Company–Scientific Research Staff
Dearborn, Michigan 48121

SYNOPSIS

This paper describes the electron microprobe instrument and the theory of its operation. Its use in the analysis of coatings is described in detail. Examples included are characterization of pigment dispersion in powder coatings, distribution of flattening agents in low gloss paints, identification of pigments, composition of a crater, and identification of a source of paint contamination. Also the use of the electron microprobe for the study of corrosion under paint on iron phosphated, zinc phosphated, and galvanized steel, and of corrosion in electroplated plastic is discussed. The limitation of electron microprobe analysis for qualitative and quantitative studies, the use of back scattered electrons for surface topography, and the preparation of specimens are also described.

INTRODUCTION

The electron microprobe has been extensively used for analysis of micron size areas for investigation of structures of alloys, diffusion in metals, solubility limits, inclusions, grain boundary migrations, phase equilibria, ore analysis, and other metallurgical problems [1-4]. The use of the electron microprobe has also been described in a few cases for the study of corrosion films [5, 6], and in biological systems for the study of calcification patterns [7, 8]. The technique is powerful for mapping out elemental composition of heterogeneous systems, for which the analysis was previously possible only on an average basis or by indirect methods.

Use of the electron microprobe for the study of ion diffusion through polymers, and for characterization of polymer composites has been described [9, 10], but application of the technique to polymers and coatings has been very limited. This paper describes the use of the electron microprobe for problems related to coatings.

THEORY OF OPERATION

The electron microprobe was developed by Castaing in the early 1950's. The technique involves bombarding a specimen with a narrow beam of electrons, and analyzing the emitted x-rays to establish the chemical composition at the point of irradiation. When an electron beam hits a specimen, a number of events take place, among which are: (a) x-ray emission; (b) reflection or back scattering of

Applied Polymer Symposium No. 23, 61-72 (1974)

electrons; (c) electron absorption by the specimen; (d) emission of secondary electrons.

Each element emits characteristic x-rays when excited by electrons of sufficient energy [11]. Analysis of the x-ray emission according to wavelength or energy distribution, therefore, identifies all the elements present at the point of irradiation [12]. Most instruments can detect elements with an atomic number as low as boron. The intensity of x-ray emission corresponding to a particular element is proportional to the amount of that element irradiated. Intensity measurements of x-rays of a particular wavelength, therefore, lead to quantitative determination of the element present [13]. Through intensity measurement of all the characteristic x-rays, the total chemical composition of a specimen can be determined. Although the qualitative analysis or detection of an element in the specimen is simple and quick, a quantitative analysis is more time consuming and subject to a number of errors. Generally, correction factors are needed to account for x-ray absorption, x-ray fluorescence effects, and complications due to the presence of elements of different atomic numbers [14]. A computer is needed to handle data, apply corrections, and calculate the chemical composition of a specimen.

The back scattered electrons can be used to modulate the brightness of a cathode ray tube to provide video pictures. The number of back scattered electrons reaching the detector depends both on the chemical composition and the surface topography of a specimen; the pictures obtained thus contain contrast due both to surface relief and variation in composition. Although it is not a common practice, the contrast information from topographical effects can be separated from that due to compositional variation by using two detectors placed 180° from each other. The intensity of absorbed electrons, also known as sample current, can also be used to produce video pictures, showing contrast due to changes in chemical composition of the surface area scanned.

The electron microprobe is useful for determining compositional variations in the specimen, since the electron beam can be scanned over an area of the specimen surface, and the intensity of the x-rays corresponding to a particular element can be synchronously followed. The video pictures thus produced give a distribution map of various elements. If only three elements are of interest, separate primary colors can be used for each, and a composite color picture can be made showing the distribution of the three elements in one picture.

EQUIPMENT

The equipment used in electron microprobe analysis is shown schematically in Figure 1. It consists of three basic components: (a) an electron optics system, to focus a beam of electrons on the specimen surface; (b) x-ray optics, to analyze the emitted x-rays according to wavelength and intensity; and (c) a viewing system, to aid in the selection of the exact area to be analyzed.

The electron optics system is similar to that used in the scanning electron microscope, except that the beam intensity is much higher, in order to generate

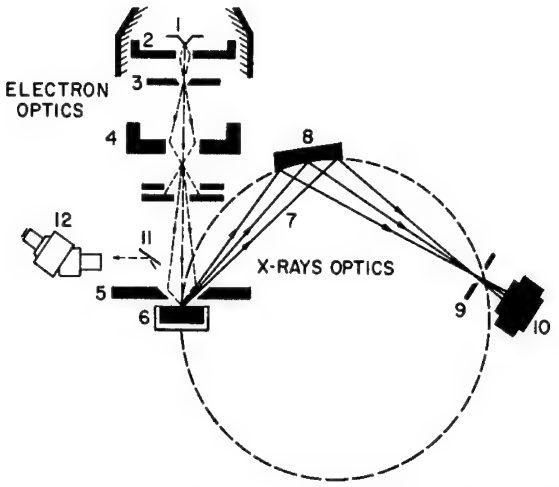

FIG. 1. Schematic diagram of an electron microprobe analyzer with (1) filament, (2) grid, (3) anodic plate, (4) condensor lens, (5) objective lens, (6) specimen stage, (7) characteristic x-rays, (8) diffracting crystals, (9) aperture, (10) x-ray detector, (11) mirror, (12) microscope.

a reasonable level of x-ray count rates [15]. Commonly, a scanned beam of 10 to 30 kV and of approximately 2,000 Å in diameter is used. The x-ray analyzer consists of a diffracting crystal of suitable d spacing, to separate the x-rays according to their wavelength. Some instruments are also fitted with energy dispersive x-ray analyzers. The x-rays in a wavelength analyzer are generally detected and their intensity measured by the use of a proportional counter, either of the flow or sealed type. The x-ray optics can be used to record the x-ray spectra, i.e. to measure all wavelengths of x-rays generated from a point in the specimen. Such an arrangement identifies all elements present at that site. Generally, an elemental analysis can be carried out quickly with energy dispersive techniques before doing quantitative analysis. The crystal and the counter can also be fixed in relation to the specimen to measure x-rays of a given wavelength as the electron beam scans an area to yield the distribution of an element in the specimen surface.

Even though the diameter of the electron beam used in the microprobe is about 2,000 Å, the x-ray resolution is only about 1 μm. The lower resolution stems from the x-rays being emitted in all directions and from electron diffusion or scattering effects. The resolution can be improved by using a lower accelerating potential for the electron beam, but because of the lower x-ray intensity then produced, the detection sensitivity of the instrument is reduced. For elements present in very low concentrations, slower scan rates or multiple scans may be needed [13]. The depth of electron penetration depends on the beam voltage and the specimen density. A 25 kV electron beam will penetrate to about 2 μm in iron, and about 8 μm in pigmented organic coatings. For analysis of thin coatings, care should be taken so that the beam does not penetrate beyond the coating being analyzed.

SPECIMEN PREPARATION

The surface of the specimen under study should be as smooth as possible, to avoid surface relief effects. The surface of most paint films can be analyzed without polishing. To study the cross section of a coating, the specimen should be embedded in cold setting epoxy or methacrylate resin and polished. In certain cases, microtome sectioning techniques, commonly used in transmission electron microscopy, may be employed. If the specimen is a poor electrical conductor, a thin layer of about 100 Å of carbon or aluminum is deposited on the specimen surface, to prevent charge build-up. This treatment minimizes beam reflection and dissipates energy, to reduce temperature rise in the specimen.

DATA PRESENTATION

Electron microprobe data can be presented in a variety of ways. Video pictures are obtained by the use of back scattered electrons, secondary electrons, or sample current. Intensity of characteristic x-rays is used to produce photographs of the distribution of an element in the area scanned. In such pictures, the brightest areas correspond to the highest concentration of the element. A line scan can also be used to follow the variations in the concentration of an element along a line. Quantitative data as percentage of an element present are generally obtained as point by point analysis, and they are presented normally in the form of tables. The examples used in this paper illustrate these modes of data presentation.

EXAMPLES

The electron microprobe has been used in determining the concentration of metal ions in electrodeposited coatings. During the anodic electrodeposition of paint films on steel, galvanized steel, or aluminum, the substrate undergoes dissolution and the metal ions are incorporated in the coating. The amount and nature of these metal ions effect the curing rate and color stability of the coating. Table I shows the concentration of iron along the section of such a coating deposited over mild steel. Near the paint-metal interface, the concentration of iron is about 1%. Moving away from the metal surface, the concentration of iron steadily decreases to about 0.3% near the top surface of the paint.

Table II gives similar data for electrodeposition of a clear coating on phosphated steel. In this case, a section of the coating was analyzed by electron microprobe for both iron and phosphorus. Phosphorus is no longer detectable at a distance of 4 μm from the metal surface, but iron is present throughout the thickness of the coating. It must be concluded from these data that during electrodeposition of paint on phosphated steel, iron phosphate remains in its place, but the metal underneath it undergoes dissolution and the metal ions

TABLE I

Concentration of Iron Along a Section of Electrodeposited Coating Over Steel

Distance from Metal Surface, μm	Iron, %
1	1.72
2	0.92
3	0.70
4	0.65
5	0.60
6	0.63
7	0.63
8	0.57
9	0.50
10	0.53
11	0.47
12	0.33
13	0.33

diffuse throughout the bulk of the coating. Again the concentration of iron is higher in the coating near the substrate and decreases towards the outer paint surface. Similar analysis shows that electrodeposited clear coatings on galvanized steel contain 0.78% zinc near the metal surface and 0.18% near the outer surface. Also, when deposited on an aluminum panel, the aluminum content of the film is 0.84% near the metal and 0.31% near the surface of the coating. In each case, the concentration of metal ions decreases away from the metal substrate. This result is contrary to the findings of May and Smith [16]. They established that the metal ion concentration is uniform throughout the coating thickness. The reason for this difference is not clear. The coatings examined by May and Smith ranged in thickness from 20 to 48 μm, whereas the coatings in this study were only 10 to 15 μm thick. It is possible that the metal ions have different diffusion coefficients in different electrodeposition materials, and that more uniform metal ion distribution is associated with higher diffusion coefficients.

Qualitative analysis for pigments present in a paint film is shown in Figure 2, where the spectra of characteristic x-rays emitted clearly indicate the presence of barium (from barium sulfate), titanium (TiO_2), iron (iron oxide), and zinc in the

TABLE II

Concentrations of Iron and Phosphorus in Coating over Phosphated Steel

Distance from Metal, μm	Iron, %	Phosphorus, %
1	1.40	5.32
2	0.92	1.81
3	0.76	0.54
4	0.65	0.00
5	0.63	0.00
6	0.56	0.00
7	0.47	0.00
8	0.42	0.00
9	0.36	0.00
10	0.31	0.00
11	0.25	0.00
12	0.23	0.00
13	0.19	0.00
14	0.14	0.00

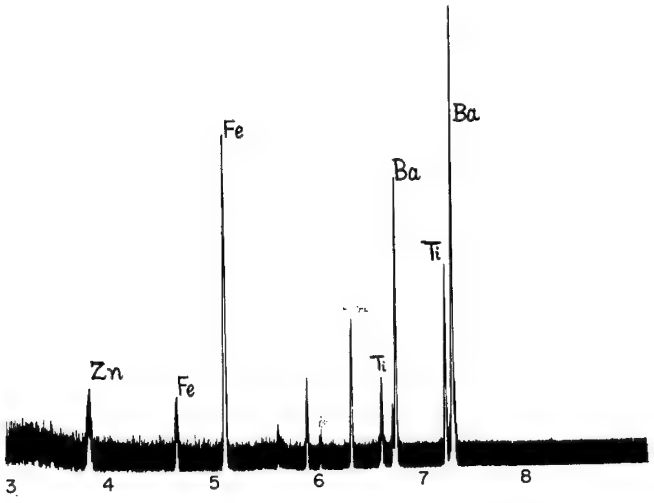

FIG. 2. Spectra of x-rays emitted from a paint film.

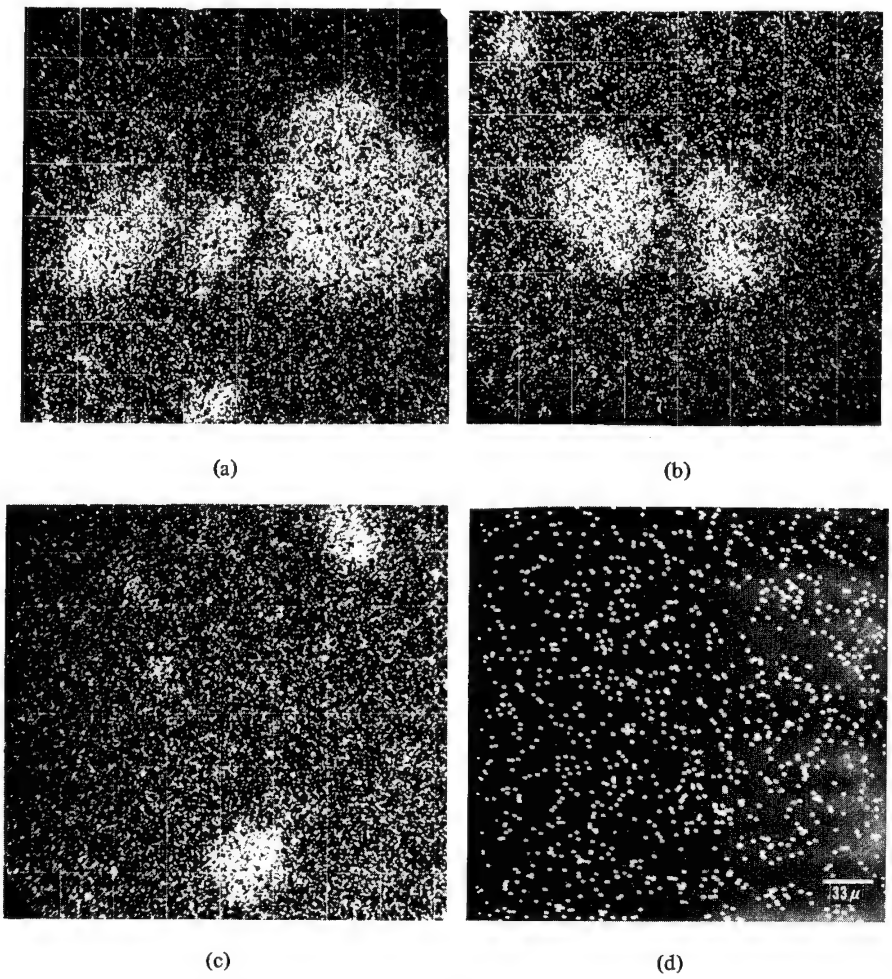

FIG. 3. Effect of mill rolling time on pigment dispersion in a powder coating; mill rolling time of (a) 1 min; (b) 4 min; (c) 6 min; (d) TiO_2 dispersion in a solvent-base paint for comparison.

paint. Such an analysis can be carried out in a few minutes on a very small sample of paint. This type of electron microprobe analysis can be used for identification of paint and in checking for paint contamination.

The electron microprobe can also be used to determine the degree of pigment dispersion in powder coatings. The usual techniques, such as the Hegmann gauge for pigment dispersion in liquid paints, are not applicable to powder coatings. Although a microscope can be useful to look at the state of pigment dispersion in powder coatings, the electron microprobe can be of greater value when a mixture of pigments is used. Figure 3 shows the effect of continued mill rolling on the dispersion of titanium dioxide. After short mill rolling time, large agglomerates of TiO_2 are represented by large white areas (Fig. 3a). With increasing milling time, a better dispersion of TiO_2 is obtained

(Figs. 3b and 3c). Figure 3d shows the dispersion of TiO_2 in a solvent-base automotive enamel. It appears that, in the coating produced from the solvent-base paint, the TiO_2 particles interact with each other to form a network structure. Otherwise the distribution of TiO_2 particle is quite uniform, without the presence of undispersed agglomerates.

The electron microprobe is also useful for corrosion studies, i.e. to locate corrosion sites, to identify the ions involved in corrosion, and to determine the composition of corrosion products. Figures 4a and 4b show iron and phosphorus images of the metal-coating interface of painted phosphated steel. The intense white area in Figure 4a is the metal panel. In Figure 4b a thin phosphorus-rich layer can be seen at the surface of the metal. Figure 4c shows the electron back scatter image of the metal-coating interface. A gap between the coating and the metal, produced by corrosion underneath the coating is observed. In Figure 4d, the phosphorus image in the corroded area shows the presence of small amounts of phosphorus in steel, but the phosphorus-rich area at the interface is absent. Because of the low concentration and thinness of the iron phosphate layer, it is difficult to draw conclusions from these pictures. For this situation, quantitative

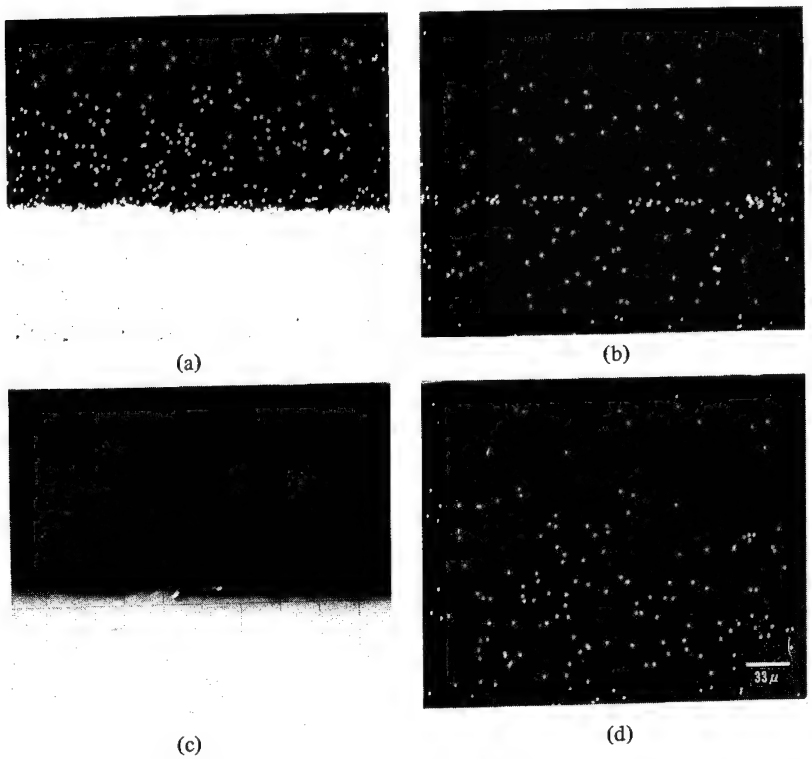

FIG. 4. Micrographs of a cross section of painted phosphated steel: (a) Iron image in uncorroded section; (b) phosphorus image in uncorroded section; (c) electron back scatter image in corroded area; (d) phosphorus image in corroded area.

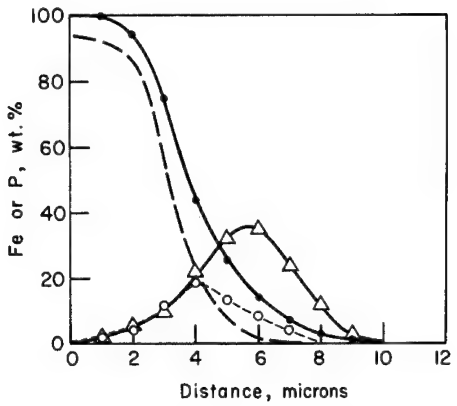

FIG. 5. Weight percent of iron and phosphorus along the cross section of painted phosphated steel as function of distance from the steel surface: (-●-) iron in uncorroded section, (-△-) phosphorus in uncorroded section, (-○-) phosphorus in corroded section, (- - -) iron in corroded area.

electron microprobe analysis is more useful. Figure 5 shows the concentration of iron and phosphorus in the noncorroded and corroded cross sections. In the noncorroded part, the maximum phosphorus concentration is approximately 36%. In the corroded part, the maximum phosphorus concentration is 18%, indicating that half of the phosphate is lost during corrosion. Moreover, it can be seen that the outer layers of the phosphate are lost, while the phosphate adjacent to the steel is still intact. Looking at the curve for iron concentration, it can be seen that the corroded area has a reduced iron concentration below the iron-iron phosphate interface, suggesting the formation of an iron hydroxide layer of several microns thick under the diminished phosphate layer.

Figure 6 illustrates the use of the electron microprobe to study the corrosion of galvanized steel. Iron and zinc images in an uncorroded cross section are shown in Figures 6a and 6b. Figures 6c and 6d show the same elements in a corroded cross section. It is quite clear from Figure 6d that the zinc layer is undergoing corrosion. At this stage, a thin layer of zinc on steel is still present, and the steel itself has not undergone any corrosion.

COMPARISON WITH OTHER TECHNIQUES

A number of other methods are also available for the analysis of a specimen. A comparison of electron microprobe analysis with two related methods, Auger electron spectroscopy and photoelectron spectroscopy, will be made. In Auger electron spectroscopy, the sample is irradiated with a beam of electrons with energies of up to 3 kV. At these relatively low energies a large number of excited atoms lose their excess energy through the emission of characteristic Auger electrons rather than through emission of characteristic x-rays. This phenomenon was first experimentally observed by the French physicist Auger in 1923. The energy of Auger electrons is characteristic of a given atom undergoing

irradiation. Various elements present at a surface can therefore be identified by their Auger electron spectra.

In Auger spectroscopy, the resolution is lower, the depth of the analyzed layer is very shallow, and the sample must be subjected to a much higher vacuum than in electron microprobe analysis. The utility of the Auger method has been described recently by Gjostein and Chavka [17] for the analysis of films of a few Angstroms thickness on metals, glass, ceramics, etc. Since the chemical environment of an atom causes shifts in the energies of Auger electrons produced, some information on the bonding state of the element can also be obtained by this method [18].

Photoelectron spectroscopy, also known as electron spectroscopy for chemical analysis (ESCA) or x-ray photoelectron spectroscopy, is based on the behavior of materials upon irradiation by x-rays [19]. In this type of spectroscopy, a sample is bombarded by monoenergetic x-rays of known energy, and the kinetic energy of the ejected electrons (photo-electrons) is measured. The kinetic energies of the photoelectrons produced are equal to the x-ray energy minus the binding energy of core electrons, and they are a function of (a) the element in the sample being irradiated, and (b) the chemical environment or

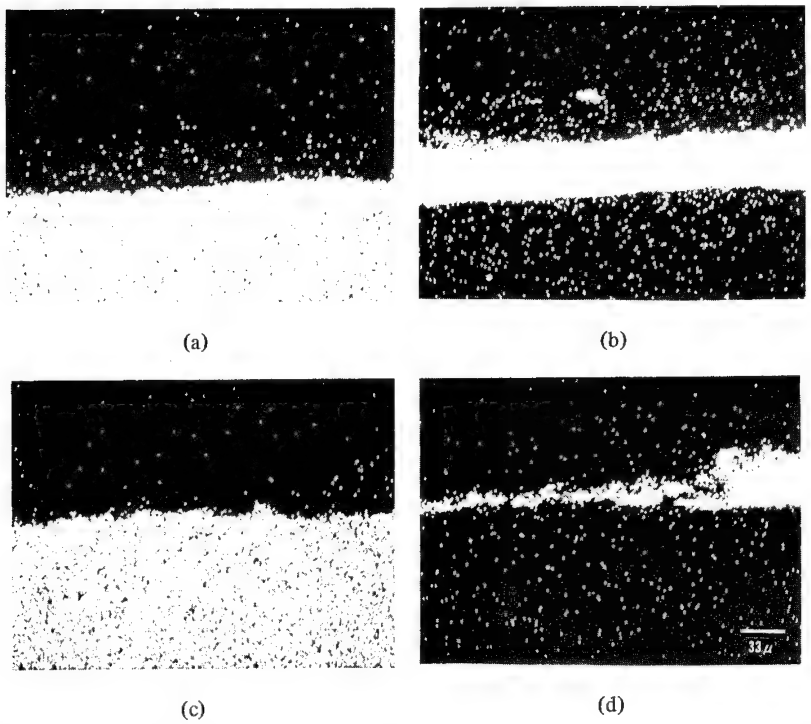

FIG. 6. Micrographs of original and corroded cross sections of painted galvanized steel: (a) iron in uncorroded section, (b) zinc in uncorroded section, (c) iron in corroded section, (d) zinc in corroded section.

TABLE III

Comparison of Electron Microprobe, Auger Spectroscopy, and ESCA

	Electron Microprobe	Auger Spectroscopy	ESCA
Principle	Electron bombardment/ x-ray analysis	Electron bombardment/ Auger electron analysis	X-ray bombardment/ electron analysis
Maximum sensitivity, g	10^{-14}	10^{-14}	10^{-11}
Time per sample, min	10-120	20	20-120
Surface survey capability	yes	yes (course)	no
Minimum volume, cc	10^{-12}	10^{-10}	10^{-4}
Depth of analysis, μm	1	10^{-3}	10^{-3}
Resolution, μm	1	20	-
Required vacuum, torr	10^{-5}	10^{-8}	10^{-6}
Instrument cost, $	90,000-150,000	30,000-100,000	40,000-100,000

oxidation state of the element [20, 21]. ESCA, like Auger analysis, is also useful for the analysis of layers of up to 50 Å thickness. The reliability of quantitative analysis by ESCA is not good at this time [22, 24]. A large area of the sample is irradiated, and therefore the technique is not suitable for mapping out the distribution of an element in the specimen surface, as can be done with the electron microprobe. Also, the maximum sensitivity of ESCA is somewhat lower than that of Auger spectroscopy and electron microprobe. Table III summarizes the comparison between the three methods of analysis.

The authors are grateful to G. Strosberg for electrocoated panels and to C. Melvin for reviewing the manuscript.

REFERENCES

[1] L. S. Birks, *Electron Probe Microanalysis,* Interscience, New York, 1963.
[2] E. Eichen, F. Kunz, and J. Tabok, ASTM Publ. STP 480, Amer. Soc. Testing Mater., Philadelphia, Pa.
[3] T. D. McKinley, K. F. J. Heinrich, and D. B. Wittry, *The Electron Microprobe,* Wiley, New York, 1966.
[4] K. F. J. Heinrich, ASTM Publ. STP 349, Amer. Soc. Testing Mater., Philadelphia, Pa., 163 (1964).
[5] H. H. von Strehblow and K. J. Vetter, *Ber. Bunsenges. Physik. Chem., 75,* 822 (1971).
[6] R. W. Merchant, "Electron microprobe analysis of thin corrosion films," General Electric Co. Rep., *KAPL-3482* (1969).
[7] I. Adler, ASTM Publ. STP 349, Amer. Soc. Testing Mater., Philadelphia, Pa., 183 (1964).
[8] T. A. Hall, A. J. Hale, and V. R. Switsur, in *The Electron Microprobe,* T. D. McKinley, Ed., Wiley, New York, 1966, p. 805.
[9] Abd-El-Bary, J. A. Manson, and J. I. Goldstein, *J. Mater., Sci., 5,* 898 (1970).
[10] S. S. Labana, H. K. Plummer, and W. J. Burlant, *Polym. Eng. Sci., 12,* 34 (1972).

[11] A. H. Compton and S. K. Allison, *X-Rays in Practice and Experiment,* van Nostrand, New York, 1935.
[12] H. A. Liebhafsky, *X-Ray Absorption and Emission and Analytical Chemistry; Spectrochemical Analysis with X-rays,* Wiley, New York, 1960.
[13] R. H. Heidel, *Anal. Chem., 43,* 1907 (1971).
[14] J. Philibert and R. Tixier, *Brit. J. Appl. Phys., 19,* 685 (1968).
[15] P. R. Thorton, *Scanning Electron Microscopy: Application to Materials and Device Science,* Chapman and Hall, London, 1968.
[16] C. A. May and G. Smith, *J. Paint Technol., 40,* 494 (1968).
[17] N. A. Gjostein and N. G. Chavka, *J. Test. Eval.,* 1, 183 (1973).
[18] R. F. Willis, B. Filton, and D. K. Skinner, *J. Appl. Phys., 43,* 4412 (1972).
[19] K. Siegbahn, *ESCA, Atomic, Molecular and Solid State Structure Studies by Means of Electron Spectroscopy,* Almquist and Wilsells, Uppsala, 1967.
[20] J. J. Jack and D. M. Hercules, *Anal. Chem., 43,* 729 (1971).
[21] W. E. Swartz and D. M. Hercules, *Anal. Chem., 43,* 1774 (1971).
[22] C. D. Wagner, *Anal. Chem., 44,* 1050 (1972).
[23] P. E. Larson, *Anal. Chem., 44,* 1678 (1972).
[24] J. S. Brinen and J. E. McClure, *Anal. Lett., 5,* 737 (1972).

ELECTRON SENSITIVE POLYMERS AS HIGH RESOLUTION RESISTS

M. HATZAKIS

IBM Thomas J. Watson Research Center,
Yorktown Heights, New York 10598

SYNOPSIS

This paper describes the use of pure polymers as electron sensitive resists of extremely high resolution for semiconductor and other device fabrication. Emphasis is placed on poly(methyl-methacrylate), (PMMA), which was found to be most suitable for its hardness, resistance to chemical etching, and adhesion to substrates. The process combines electron beam induced degradation of the polymer with subsequent "in situ" fractionation according to molecular weight changes. Consequently, areas of the resist exposed to the electron beam are removed upon development in a weak solvent of the original polymer, so that PMMA can be considered a positive resist. Design considerations such as choice of initial molecular weight of the polymer, dispersion, and choice of developer are also discussed in this paper. Exposure charge density can be varied from 5×10^{-6} to 5×10^{-4} C/cm^2, depending on the application and development process. A process is presented which allows metal or other material deposition through an exposed and developed PMMA resist mask onto the substrate by evaporation, sputtering, or plating. Specific applications of the resist system to device fabrication are presented, and the limitations and areas requiring improvement are discussed.

INTRODUCTION

Since the mid-1960's when the use of polymers as electron sensitive resists was first reported (1), a great deal of interest has been shown in the process and its application to microfabrication. This interest can be justified if one considers the present trend for miniaturization of electronic circuits, generated by the need for higher packing densities in the semiconductor and computer industries and by the desire to explore and make use of higher frequency bands for communication and guidance systems in the microwaves industry. This trend has already brought the size of the smallest circuit element down to one micron (10^{-6} m) or less, where resolution requirements make it very difficult if not impossible to use UV radiation for defining the image on photoresist. Most electronic circuits are still made by the planar process where the circuit pattern must be defined on the surface of a flat silicon wafer or other substrate through the exposure of a light sensitive temporary layer or resist. Exposure is made by contact printing or by projection of the image from a master mask. This process requires that the area of resist, either exposed or not exposed to UV, be removed upon development. The first case refers to positive resist, and the second to negative resist. In both cases the resolution of the process is limited by the wavelength of light. This type of exposure produces interference effects on the resist and makes it very difficult to define a line narrower than 1 μm.

Applied Polymer Symposium No. 23, 73-86 (1974)

Electron beam exposure represents a great inherent improvement in resolution over UV exposure, since beams of 100 Å diameter or less can be easily achieved with an associated wavelength of only tenths on an Ångstrom unit. However, in order to produce an economically feasible microfabrication system for devices of the size that is beyond the capability of UV exposure, a resist material must be used that requires very little charge for proper exposure. It also must maintain the resolution capabilities of the exposing beam without very significant deterioration after development. Experience has shown so far that these two requirements, sensitivity and resolution, are in constant conflict.

The purpose of this paper is to present a survey of materials that have been used so far as electron sensitive resists, with emphasis on poly-(methyl methacrylate), (PMMA), which is still preferred by most workers in the field. The various types of materials are summarized in Table I.

ELECTRON SENSITIVE MATERIALS

When a polymer is exposed to ionizing radiation, such as UV, electron beams, or other fast moving particles, both crosslinking and scission of the molecular chains can take place within the material. As a result the physical and chemical properties will undergo changes. If the number of crosslinks formed is larger than the number of breaks, the average molecular weight of the polymer increases, and its solubility in a given solvent will decrease. If on the other hand the number of scissions is larger, the polymer degrades, its average molecular weight decreases, and its solubility increases. Polymers with increased

TABLE I

Comparison of Properties of Some Negative and Positive Electron Resist Materials

Material	Type	Typical Sensitivity, C/cm^2	Resolution, μm (Minimum Line Width)	Compatibility with Semiconductor Fabrication	Authors	Reference
KTFR-KMER-KPR	Negative	5×10^{-6}	1	Good	Thornley-Sun	4
					Matta	5
					Broyde	9
Silicones	"	10^{-5}	0.5	Fair	Roberts	6
					Yatsui-Nakata-Umehara	7
Epoxidized Polybutadiene	"	5×10^{-8}	?	Fair	Hirai-Hatano-Nonogaki	8
AZ-1350 (Shipley)	Positive	5×10^{-5}	1	Good	Matta	5
					Hatzakis	10
Poly-(α-Methyl Styrene)	"	10^{-4}	?	Poor	Haller-Hatzakis-Srinivasan	1
Poly-(Methyl Methacrylate)	"	5×10^{-5} *	0.1	Good	Haller-Hatzakis-Srinivasan	1
		2×10^{-6} **			Ku-Scala	3
					Hatzakis	10
					Wolf et al	11
					Herzog et al	12
					Harris	13
					Ting	14

crosslinking can be used as negative resists, and those with increased scission as positive resists. The behavior of a polymer during irradiation can often be predicted from the structure of the monomer unit in the polymer, according to data collected by Shapiro [2]. The general rule is that if the carbon atoms in the main chain of the polymer carry at least one hydrogen atom, the polymer will crosslink upon irradiation. If a tetrasubstituted carbon atom is present in the monomer unit, the polymer tends to degrade.

Crosslinking Polymers

For a polymer of the crosslinking (negative) type to become insoluble, the irradiation dosage must be large enough to create a three dimensional network, and the polymer must reach the point of gel formation. Ku and Scala [3] have shown that the charge density of the exposing electron beam required for gelation is inversely proportional to the weight average molecular weight, $\bar{M}_w$, of the original polymer. This is reasonable, since for higher molecular weight polymers fewer crosslinks would be required for the formation of an infinite network structure. The expression derived by Ku and Scala is

$$Q = \frac{50\ qdA}{E\ G\ \bar{M}_w} \tag{1}$$

where Q = the charge density in C/cm^2, q = the electronic charge, d = the density of the polymer, A = Avogadro's number, E = the energy absorbed per unit area of the polymer film, and G = the radiation chemical yield, which is defined as the number of crosslinks effected per 100 eV of energy absorbed by the polymer.

Commercial photoresists, such as KOR, KPR, and KTFR from Kodak, can also be used as negative electron resists, but so can many other polymers. Thornley and Sun [4] have investigated the exposure characteristics of these resists, and they found that for KTFR a dose of 5×10^{-6} C/cm^2 is adequate at 14 kV to cause complete polymerization. Ku and Scala investigated some other polymers of the crosslinking type, such as polystyrene, polyacrylamide, and poly-(vinyl chloride). They were able to correlate the experimental results of sensitivity with the values obtained by using eq. (1), thus verifying the dependence of sensitivity on the initial molecular weight. They also observed, that the edge resolution of the high molecular weight polystyrene with $\bar{M}_w$ = 230,000 and $Q = 2.5 \times 10^{-5}$ C/cm^2 is not as good as the low molecular weight material of $\bar{M}_w$ = 20,000 and $Q = 3 \times 10^{-4}$ C/cm^2. This points out that resolution is inversely related to the sensitivity of the sample.

Matta [5] exposed KTFR at various beam accelerating potentials and charge densities, and found that there is an optimum charge density for each potential, being 10^{-5} C/cm^2 at 15 kV. He was also able to obtain a minimum line width of 1 μm for all beam voltages between 7.5 and 30 kV.

Other materials that have been used as resists include silicone compounds, such as the solid polymers obtained by hydrolysis and condensation of

methyltrichloro-silane [6] and others [7]. After exposure to the electron beam and subsequent development, these resists can be used either for chemical etching of SiO_2 or directly as a diffusion barrier on silicon substrates. Recently, a very sensitive negative electron resist was reported by Hirai et al. [8], that can be exposed and developed at charge densities of 5×10^{-8} C/cm^2 or less. These are epoxide-containing polymers, and the most promising one is epoxidized polybutadiene. These materials are prepared by epoxidizing the original polymer dissolved in toluene with peracetic acid solution. Epoxidation was found to increase the sensitivity of the original polymer to electron beam exposure by a factor of 30. Unfortunately, no data on resolution have been supplied to date.

Degrading Polymers

The use of polymers of the degrading type as positive electron beam resists was first investigated by Haller et al. [1], who established that of all classes of polymers tried the most promising one was poly-(methyl methacrylate), mainly because of its physical properties and resistance to acidic and alkaline etch solutions. This polymer has been investigated extensively by me [10] and many other workers, and it is used today as an electron resist by most people involved in electron beam fabrication. Other polymers investigated by Haller et al. include poly-(α-methyl styrene) and cellulose acetate, but these were ruled out because of their incompatibility with semiconductor fabrication processes, such as resistance to chemical etching, adhesion to the substrate, etc.

Shipley AZ-1350, a commercially available photoresist of the degrading type, has been evaluated as an electron resist by Matta [5] and me [10], and was found to develop correctly only within a very narrow range of exposure between 5 and 7×10^{-5} C/cm^2 at 15 kV. For this reason, and because it cannot tolerate alkaline etch solutions and does not offer the resolution capabilities of PMMA, it has found only limited use as an electron resist.

PMMA as Electron Resist

The PMMA polymer evaluated earlier [10] was polymerized from the monomer with azo-bis-isobutyronitrile as catalyst. The viscosity of 10% solution and the solubility rate of baked coatings indicate that the polymer thus produced is of relatively low molecular weight as compared with the commercially available Elvasite 2041 from Dupont [11]. The polymer was dissolved in methyl-isobutyl-ketone and was spin-coated on oxidized silicon wafers for electron beam exposure and development. A 10% solution at a spinning speed of 5000 rpm results in a dried resist thickness of 5000 Å. Development of the irradiated resist area is accomplished by immersion in a solution composed either of a weak solvent or of a combination of a good solvent and a nonsolvent of the original polymer. Ku and Scala [3] and Herzog et al. [12] used pure ethanol as a developer, whereas Haller et al. [1] used a 3:1 mixture of isopropyl alcohol (nonsolvent) and methyl isobutyl ketone (solvent). The mixture has the advantage that it provides for adjusting the developing time

for a given exposure by varying the mixture proportions. In all the early experiments with PMMA it was assumed that it was necessary to use a developer that does not dissolve any appreciable amount of unexposed resist in the time required to develop the exposed areas. That condition resulted in the use of the 3:1 mixture for developer. It was also found necessary to prebake the resist-coated samples at a temperature well above the glass transition temperature T_g of the polymer, in order to improve adhesion to the substrate and to decrease the solubility of the unexposed film in the developer. Since T_g for PMMA polymers is in the order of 120°C, a prebake of 160-170°C was used for periods of 15 min to 1 hr in air. According to Harris [13], considerable degrading of the polymer takes place above this temperature range. Prebaking at 160°C allows the molecules to rearrange, thereby removing the strains introduced in the film by the drying process. It also drives off any remaining solvent.

The sensitivity of PMMA resist depends on many variables, and therefore can only be defined for a particular set of conditions. Some of these variables are: (a) Choice of solvent or solvent/nonsolvent combination for the developing solution; (b) developer temperature; (c) resist layer thickness; (d) nature of the substrate; (e) electron beam accelerating voltage; (f) developing time. In order to obtain sensitivity data, PMMA resist was coated on silicon wafers oxidized with 5000 Å of SiO_2, and baked at 160°C for 1 hr. The resist thickness was measured after baking by interferometry. The wafers were exposed in an electron beam system that was adjusted to scan an area of 250 X 250 μm, so that a relatively uniform exposure was maintained in that area. The beam accelerating voltage was varied from 6 to 25 kV.

The samples were developed in the standard 3:1 solution at 23°C for 2 min. The results are presented in Figure 1. The minimum charge density required to

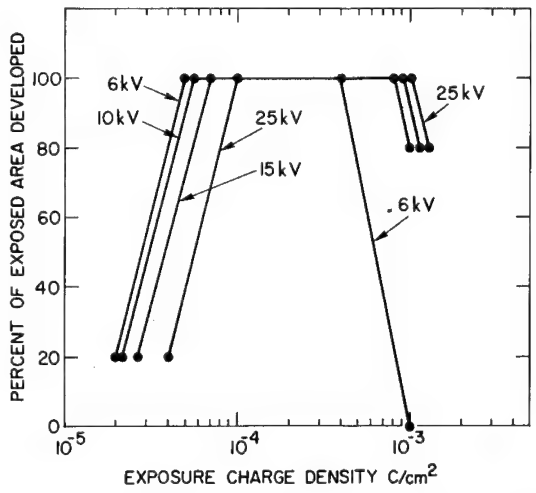

FIG. 1. Exposure characteristics of PMMA resist. Layer thickness = 8000 Å. Development was carried out in 3:1 isopropyl alcohol-methyl isobutyl ketone for 2 min at 23°C.

fully develop the exposed area is represented by the left inflection point of the curves. The right hand inflection represents over-exposure, beyond which crosslinking dominates. The resist reverses to the negative type past this point. Note that twice as much charge density is required at 25 kV as at 6 kV, indicating that for this resist thickness twice as much energy is transferred to the resist layer by the incident beam at 6 kV than at 25 kV, due to the shorter penetration range at lower voltage. Beam penetration profiles can be obtained with PMMA by exposing single lines with a focussed electron beam at various accelerating potentials on a resist layer that is much thicker than the penetration range of the beam. After development, the sample is fractured over an edge in a direction perpendicular to the direction of the lines, and the profiles can be studied in the scanning electron microscope (SEM). A composite SEM micrograph of line profiles, exposed at 10, 15, and 25 kV, is shown in Figure 2. These profiles show that the penetration range is approximately 3 μm at 10 kV, 5 μm at 15 kV, and 7 μm at 25 kV. The figure also shows that the energy dissipation reaches a peak at about 0.6 of the maximum penetration range. So, if a thin resist layer, such as 5000 Å, is exposed at 15 kV, less than 10% of the incident energy is absorbed by the resist, and the rest enters the substrate. These profiles present the best known experimental method of measuring penetration range and spacial energy dissipation of electron beams in solids. Also, the sensitivity advantage of exposing thin resist layers at 10 kV, and the resolution advantage at 25 kV become obvious from these profiles. These profiles have been discussed in more detail elsewhere [10-12, 15].

Exposure of Thin PMMA Resist Films

In the fabrication of microcircuits and devices it is always necessary to expose a thin layer of resist that is coated on the workpiece, in order to define a pattern by etching or other means after resist development. The required resist

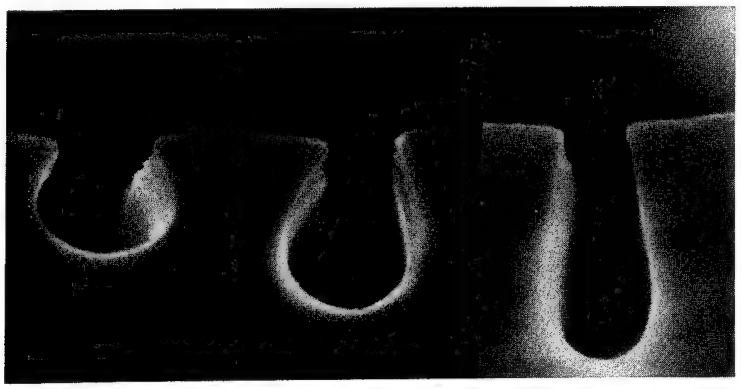

(a) (b) (c)

FIG. 2. Electron beam penetration profiles in PMMA resist at (a) 10 kV, (b) 15 kV, and (c) 25 kV. Exposure $Q = 2 \times 10^{-4}$ C/cm^2.

thickness depends on the type of process, and ultimately on the minimum line width to be exposed on the resist. It has been found that in general a ratio of resist thickness to minimum line width in excess of unity can be obtained easily with PMMA and a beam of 15 kV or higher.

The minimum spacing between lines in relatively thick resist layers ($> 0.5\ \mu m$) is limited by electron spreading in the resist. Such spreading is due to electron collisions with the resist molecules, rather than from back scattering from the silicon substrate. This is illustrated in Figure 3, which shows the cross section of a $1\ \mu m$ wide line exposed in $1.2\ \mu m$ thick PMMA resist at 10 kV. Comparison of this photo with the 10 kV profile of Figure 2 shows that the two cross-sections are identical in shape down to the interface with the substrate in Figure 3. Therefore, the silicon substrate has no effect on the shape of the resist profile. The same is true for the cross-section obtained at 25 kV in $2.5\ \mu m$ thick resist, shown in Figure 4, when it is compared with the 25 kV profile in Figure 2. For very thin resist layers ($<0.4\ \mu m$) beam spreading in the resist is minimized, and the effects of electron back scattering off the substrate become significant. This is shown in Figure 5, where lines were fabricated by exposure of a very thin layer (1500 Å) of PMMA resist with a 25 kV beam which was focussed to a spot of less than 100 Å in diameter. The lines were fabricated on a silicon substrate covered with a 1500 Å silicon nitride (Si_3N_4) layer. The silicon was etched completely in selected areas by a back etch, as described by Sedgwick et al. [16], leaving only the thin silicon nitride layer. The effect of substrate removal can be easily seen in this photo, where the line width above the substrate is 1000 Å, and above the nitride (dark area) only 500 to 600 Å. It can be concluded that for thick resist layer exposure an accelerating voltage of

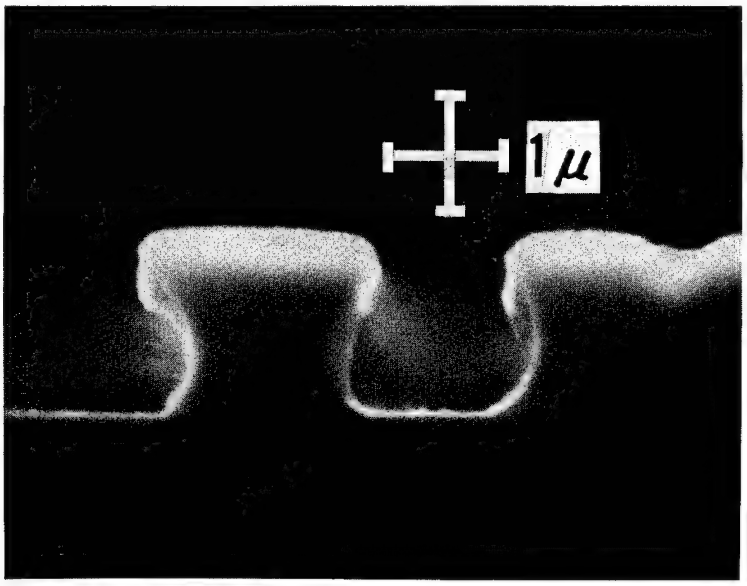

FIG. 3. Cross sections of lines exposed in $1.2\ \mu m$ thick PMMA resist over silicon substrate at 10 kV.

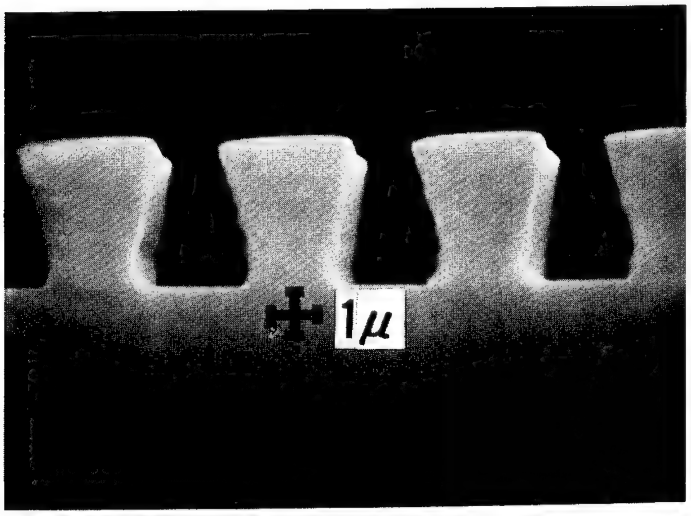

FIG. 4. Cross sections of lines exposed at 25 kV in 2.5 μm thick PMMA resist.

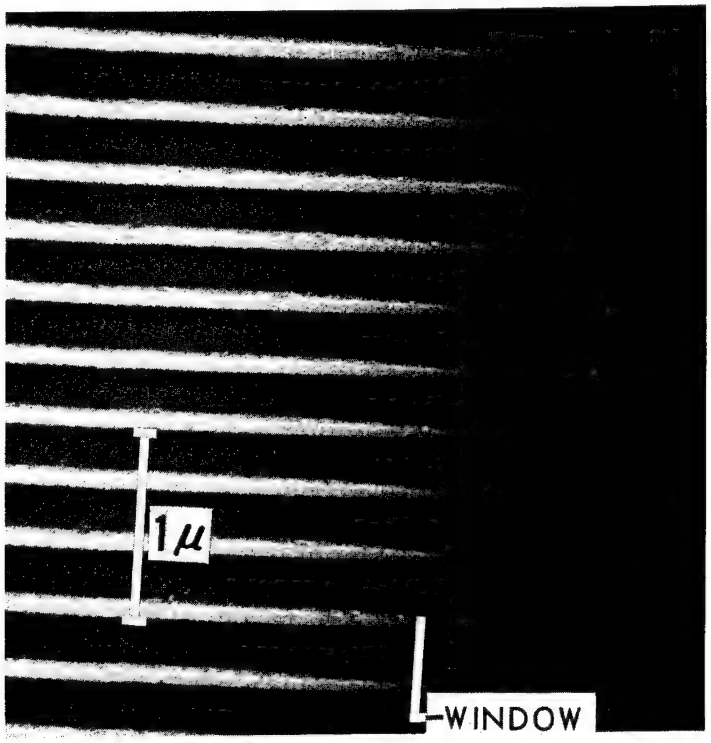

FIG. 5. SEM micrograph of extremely narrow metal lines fabricated with the lift-off technique with PMMA resist exposed at 25 kV. The effect of substrate removal on linewidth can be seen in the dark area at the right of the photograph.

25 kV or more should be used for minimum line width, whereas for thin layers on thick substrates lower voltages are preferred. The area from which back scattered electrons emerge decreases with decreasing accelerating voltage.

PMMA resist can be used after exposure and development as a mask for forming metallic structures, either by evaporation of the metal or other material through the resist mask (lift-off technique), or by plating or RF sputter deposition. This method has been described in detail [10, 17, 18] and is based on the fact that the undercut obtained in the developed resist provides a discontinuity between metal evaporated on the resist and that evaporated onto the substrate through the resist mask. This discontinuity makes it possible to remove the unexposed resist after metal deposition, without tearing between the metal on the resist and the metal on the substrate, as long as the metal thickness does not exceed 70% of the resist thickness. The concept itself and a cross-section of an actual metallized line before resist removal are illustrated in Figure 6. Examples of very thick metal lines and very narrow lines, obtained through the lift-off technique with evaporated aluminum, are shown in Figures 7 and 5, respectively. The types of devices and circuits that have been fabricated so far by using PMMA for etching or metallization with the lift-off technique are presented elsewhere [10, 11, 17-19]. An example of plating is shown in Figure 8, which is a SEM micrograph of a magnetic bubble circuit with 3000 Å wide and 1500 Å thick permalloy lines, plated through a PMMA resist mask exposed on a garnet film with a 15 kV beam.

Resist Sensitivity Improvement

All initial PMMA resist evaluation experiments were carried out with a resist developing solution which does not dissolve any of the unexposed part of the

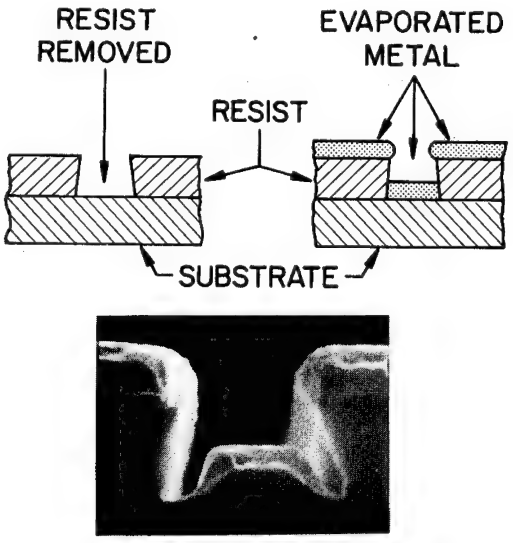

FIG. 6. Schematic of the lift-off technique before and after metal evaporation and actual SEM micrograph of the cross section of a line after metal evaporation.

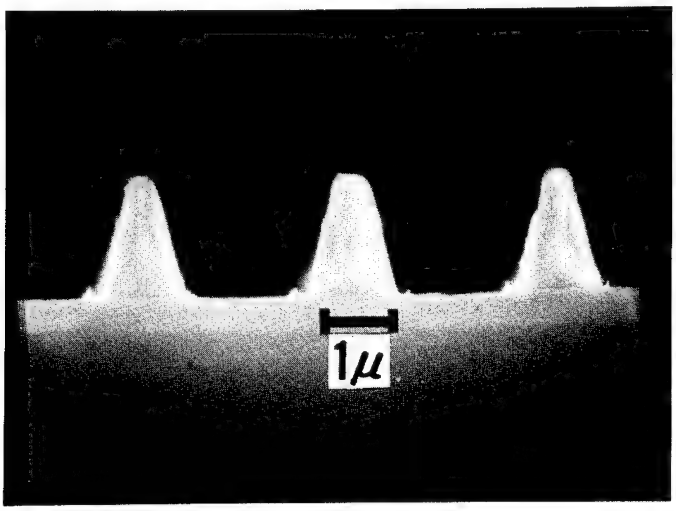

FIG. 7. Cross section of very thick (2.5 μm) aluminum lines fabricated with the lift-off technique with PMMA resist exposed at 25 kV.

resist layer in the time required to fully develop the exposed part. This limitation led to the use of the 3:1 mixture described earlier. It was also necessary to bake the resist layer above the glass transition temperature prior to exposure for improved adhesion to the substrate. In the course of resist solubility studies it was found that a resist layer, deposited from methyl isobutyl ketone and dried for hours without baking, could be redissolved in that

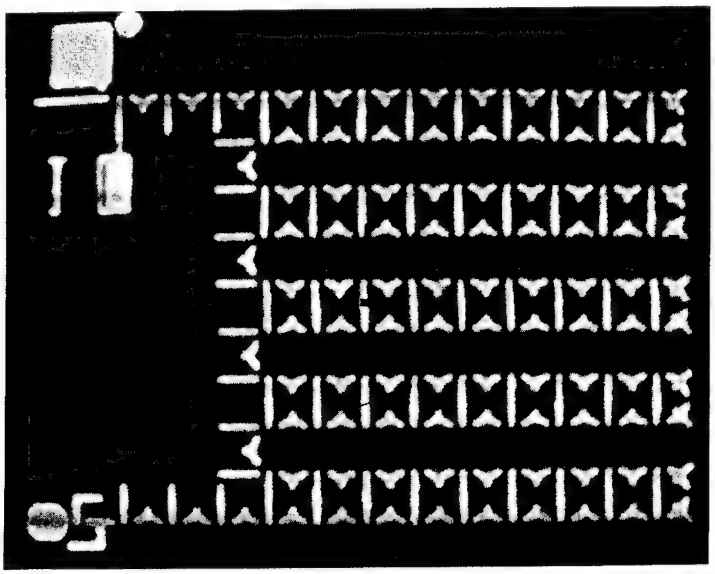

FIG. 8. Permalloy pattern fabricated by electroplating through PMMA resist. Metal thickness = 1500 Å, linewidth = 3000 Å.

solvent in a matter of seconds. However, after baking for 1 hr or more at 160°C, the same thickness layer cannot be completely removed, even after prolonged soaking in the solvent. This phenomenon can only be explained, if before baking some solvent remains in the resist and makes the layer porous and susceptible to solvent attack. This explanation is supported by Harris [13], who found no chemical change in the polymer upon prolonged baking at 170°C. This observation led to the use of undiluted methyl- isobutyl- ketone as a developer, although it will remove some of the unexposed resist during development. The amount removed is a function of the development time and of the exposure charge density. A graph of left-over resist thickness after complete development of the exposed area, and development time versus exposure charge density is shown in Figure 9. It can be seen that at an exposure charge density of 5×10^{-6} C/cm^2, compared to 10^{-4} C/cm^2 used earlier, the resist left-over thickness is 2300 Å from the original thickness of 6000 Å. The resolution of PMMA resist is not affected by this modified development process, as shown in Figure 10, where the pattern was exposed at 5×10^{-6} C/cm^2 at 12 kV with a minimum line width of 2000 Å. The solubility of PMMA resist in methyl- isobutyl- ketone has also been investigated by Ting [14], who has shown that once the development time as a function of exposure charge density has been determined for a thick film, the required time for thinner films can be obtained directly from the thickness versus time curves shown in Figure 11. He has also shown that the solubility rate of the exposed resist is not a linear function of thickness, but that it increases with distance from the surface. This result is consistent with the exposure profiles of Figure 2. The resist sensitivity is one of the most important properties, and requires further investigation. To make any electron beam fabrication system economically feasible, the exposure time per circuit element must be very short. The exposure time is given by the relation

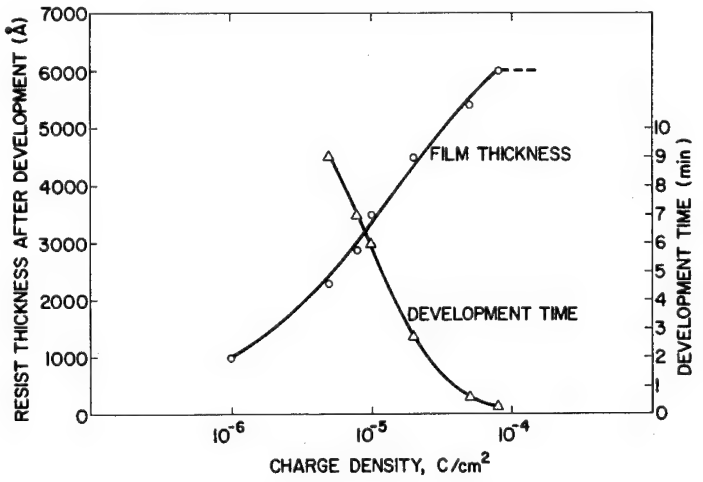

FIG. 9. Exposure sensitivity of PMMA resist versus final resist thickness and development time. Development carried out in methyl isobutyl ketone at 24°C. Initial resist thickness = 6000 Å; beam voltage = 12 kV.

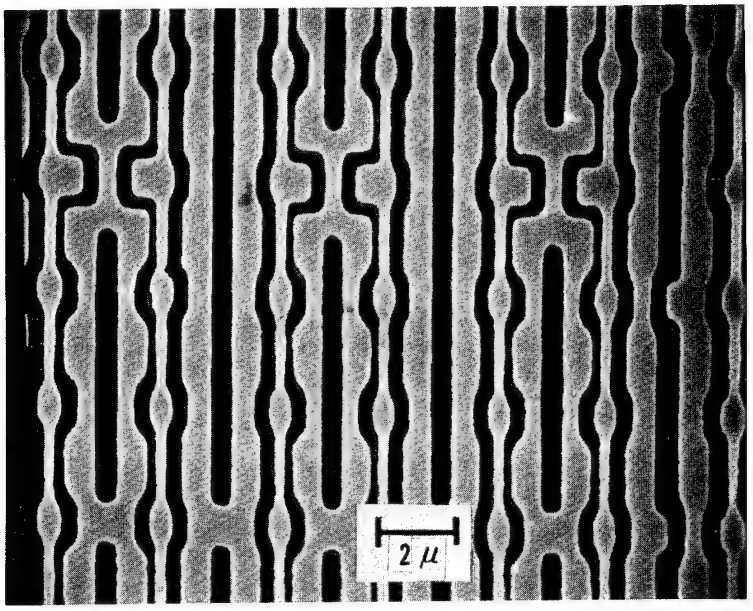

FIG. 10. High resolution pattern fabricated with the lift-off technique with PMMA resist exposed at 5×10^{-6} C/cm^2 and developed in methyl isobutyl ketone.

$$t = \frac{Q\,A}{I} \tag{2}$$

where Q = the exposure charge density in C/cm^2, A = the exposed area in cm^2, and I = the beam current in A. For example, a very bright beam of 10^{-6} A with a diameter of 1 μm would require a time of 650 sec to expose one square inch of resist area at 10^{-4} C/cm^2 charge density. These numbers make obvious the need for resist sensitivity improvement.

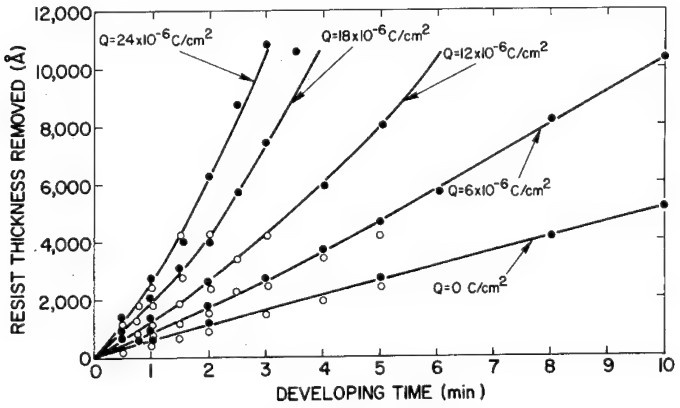

FIG. 11. Solubility characteristics of PMMA resist in methyl isobutyl ketone at various exposure charge densities.

Other considerations in selecting a degrading type polymer as a positive electron resist are the molecular weight and the dispersity of the polymer. Harris determined the solubilities of various polymer fractions, and came to the conclusion, as did Haller et al., that the ideal polymer would be monodisperse, since a small reduction in the average molecular weight would be sufficient to produce a change in the solubility that can be easily differentiated in the proper developing solution. Since monodisperse polymers are not easily obtained, Harris proposed that a desirable molecular weight distribution for PMMA resist should have sharp cut-offs at 50,000 and 600,000, so that there are very few molecules with sizes below and above these weights. It will ensure that no large molecule chains remain in the exposed area, resulting in incomplete development. It also will minimize the chance for pinhole formation in the unexposed areas. The choice of average molecular weight is arbitrary. Ku and Scala [3] have shown that the sensitivity of any degrading type polymer to electron beam exposure is independent of the initial molecular weight of the polymer, especially if the exposure charge density is large.

CONCLUSIONS

The two basic requirements for any electron resist material are sensitivity and resolution. Of all the resists tried so far of both negative and positive types, the most promising one is PMMA, since it has demonstrated the highest resolution. One area that requires further investigation is resist sensitivity improvement, either by modification of PMMA or by introduction of new and more electron sensitive materials.

REFERENCES

[1] I. Haller, M. Hatzakis, and R. Srinivasan, *IBM J. Res. Develop.*, **12**, 251 (1968).
[2] A. Shapiro, *Radiation Chemistry of Polymeric Systems*, Interscience, New York, 1962.
[3] H. Y. Ku and L. C. Scala, *J. Electrochem. Soc.*, **116**, 980 (1969).
[4] R. F. Thornley and T. Sun, *J. Electrochem. Soc.*, **112**, 1151 (1965).
[5] R. K. Matta, *Electrochem. Technol.*, **5**, 382 (1967).
[6] E. D. Roberts, *Proc. 3rd Int. Conf. Electron, Ion Beam Sci. Technol.*, Electrochem. Soc., New York, 1968, p. 571.
[7] Y. Yatsui, T. Nakata, and K. Umehara, *J. Electrochem. Soc.*, **116**, 94 (1969).
[8] T. Hirai, Y. Hatano, and S. Nonogaki, *J. Electrochem. Soc.*, **118**, 669 (1971).
[9] B. Broyde, *J. Electrochem. Soc.*, **116**, 1241 (1969).
[10] M. Hatzakis, *J. Electrochem. Soc.*, **116**, 1033 (1969).
[11] E. D. Wolf, F. S. Ozdemir, W. E. Perkins, and P. J. Coane, *Rec. 11th Symp. Electron, Ion, Laser Beam Technol.*, San Francisco Press, San Francisco, 1971, p. 331.
[12] R. Herzog, J. Greeneich, T. Everhart, and T. Van Duzer, *IEEE Trans. Electron Devices*, **ED-19**, 635 (1972).
[13] R. A. Harris, *J. Electrochem. Soc.*, **120**, 270 (1973).
[14] C. H. Ting, *Rec. 11th Symp. Electron, Ion, Laser Beam Technol.*, San Francisco Press, San Francisco, 1971, p. 345.

[15] M. Hatzakis, *Appl. Phys. Lett.*, 18, 7 (1971).
[16] T. O. Sedgwick, A. N. Broers, and B. J. Agule, *J. Electrochem. Soc.*, 119, 1769 (1972).
[17] M. Hatzakis and A. N. Broers, Record 11th Symp. Electron, Ion, Laser Beam Technol., San Francisco Press, San Francisco, 1971, p. 337.
[18] A. N. Broers and M. Hatzakis, *Sci. Amer.*, 227, 5, 34 (1972).
[19] R. F. M. Thornley, M. Hatzakis, and V. A. Dhaka, *IEEE Trans. Electron Devices*, ED-17, 961 (1970).

A MODIFIED METHACRYLATE POSITIVE ELECTRON RESIST

E. D. ROBERTS

Mullard Research Laboratories,
Redhill, Surrey, England

SYNOPSIS

A positive resist is described comprising polymethacrylate chains, crosslinked by carboxylic acid anhydride bridges, which are formed *in situ* on the substrate. The crosslinked film is insoluble, but upon irradiation with electrons the anhydride bridges are broken, restoring the straight chain structure and rendering the material soluble again. As the unirradiated film remains insoluble, it is possible to use an active solvent as developer. This feature can lead to some increase in sensitivity over standard poly-(methyl methacrylate) resists and permits much greater latitude in development conditions, which is particularly useful when patterns with submicron details are to be made. Variations in resist composition and treatment are possible, enabling the sensitivity and film properties to be changed to suit particular requirements. Patterns in the resists have been made by electron exposure between 8 and 40 $\times 10^{-6}$ C/cm^2. Evidence is presented to show the superior heat and solvent resistance of the resists, and the vertical or slightly undercut edges in patterns. Infrared spectra confirm that the anhydride bridges are destroyed by electron irradiation. Submicron patterns of metal have been produced by the "lift-off" technique with these resists.

INTRODUCTION

When organic chemicals are subjected to the action of ionizing radiation, two types of net reaction may be observed. Molecules may be either linked together to form larger molecules, or they may be broken down to smaller ones. Both types of reactions occur simultaneously, but one always predominates. Usually it is the former reaction. This kind of behavior is also observed in film-forming polymeric materials. Polymers in which the molecules become linked together, i.e. crosslinked, become insoluble after irradiation. Thus, if the film supported on a substrate is irradiated by a pattern of electrons, those areas of the film corresponding to the irradiation pattern are rendered insoluble. Rinsing the substrate in a solvent removes unirradiated material, leaving behind a pattern of crosslinked film corresponding to the irradiation pattern. Such crosslinking polymers form the basis of negative-working resists used in electron beam technology. Conversely, if the polymer suffers predominantly main chain scission upon irradiation, which leads to a decrease in average molecular weight, the irradiated material becomes more easily soluble than the unirradiated polymer, and can be selectively removed. This type of polymer forms the basis of positive-working electron resists. The number of irradiation-degradable

Applied Polymer Symposium No. 23, 87-98 (1974)

polymers suitable as positive electron resists is relatively small, and the only material of this type that has been used to any extent is poly-(methyl methacrylate), PMMA [1, 2]. This substance is a satisfactory etch resist, and it has also been employed in a very elegant "lift-off" technique for producing fine patterns of metal [3]. This process can be accomplished successfully by virtue of the slight undercutting of the resist that occurs after development of electron beam-defined patterns [3].

In developing irradiation patterns in PMMA films, one tries to dissolve selectively regions of lower molecular weight from regions of higher molecular weight material of similar straight-chain structure, relying upon the difference in rate of dissolution of the two regions in the developer. At high electron exposures this difference can be substantial, but at low exposures it may be relatively small. Then the unirradiated material may also dissolve appreciably in the time required to dissolve all irradiated material. One is always trying to distinguish and differentiate between soluble and less soluble regions. PMMA has definite restrictions in its use as a resist material: (a) The sensitivity of the resist is limited by the relatively small change in dissolution rate after irradiation at low exposures; (b) it is rather difficult to control the development of very fine patterns; (c) the developed film pattern is thermoplastic and can be deformed easily, particularly in applying the "lift-off" technique, if the film becomes heated during processing.

This paper describes an experimental positive-working resist system in which the unirradiated film is crosslinked, and therefore insoluble. Irradiation destroys the crosslinks, restoring the straight chain form which is readily soluble. The development process is thus required to distinguish only between soluble (irradiated) and insoluble (unirradiated) regions, and therefore will need less critical control. More active developing solvents may be used than are permissible with PMMA, leading to possible increases in sensitivity. The developed film pattern, being crosslinked, is more resistant to thermal deformation than standard PMMA patterns are.

PREPARATION AND PROPERTIES OF CROSSLINKED FILMS

Theory

The chemical bond joining the carboxyl group to the α carbon atom in carboxylic acids is relatively sensitive to rupture by ionizing radiation [4]. It seemed likely that this property would also be present in carboxylic acid anhydrides. If then polymer chains could be crosslinked through anhydride groups, as shown below, the polymer should be rendered insoluble:

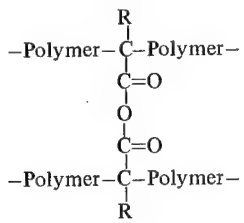

The effect of ionizing radiation should be to break the crosslinks between the anhydride group and the polymer chain carbon atom, thus restoring its thermoplastic nature and rendering it soluble and developable. When necessary in the course of a fabrication process, the crosslinked resist itself may be removed by soaking in a mixture of acetone and concentrated ammonia solution. The latter breaks the crosslinks, producing an amide group on each chain, and the separated chains will dissolve in the acetone:

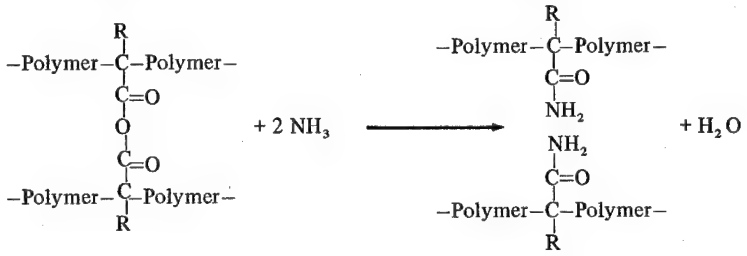

Other reagents, such as fuming nitric acid, may be used to destroy the polymer completely if other considerations allow this.

Preliminary Experiments

Our first experiments involved attempts to copolymerize methyl methacrylate with methacrylic anhydride directly on a silicon slice by using initiators to produce polymerization at room temperature. There was great difficulty in producing satisfactory thin films. When the mixture of monomers was applied to a silicon slice while fluid enough to spin to a uniform coating, the monomers evaporated before polymerization was complete, leaving only a very thin film of crosslinked polymer. However, if one waited until the polymerization had proceeded far enough for the material to be no longer volatile, the gel point was reached before it was possible to apply the mixture and spin to give a uniform layer. One usable film was prepared by spreading the mixture at its gel point over the slice with a spatula and spinning it as rapidly thereafter as possible. The resulting film was rather thick and not very uniform, but it was irradiated with a finely focussed electron beam and developed by soaking in acetone for 3 min. The pattern obtained is shown in Figure 1a. The pattern is not significantly altered by immersion in acetone for a further 30 min, as can be seen from Figure 1b. The exposure was rather high at 1.5×10^{-4} C/cm^2, but its choice was arbitrary, and the experiment demonstrated that the principles involved were valid. A similar experiment was performed successfully with ethylene glycol dimethacrylate to form the crosslinks.

The electron beam machines used in this work have been described earlier [5, 6]. The accelerating voltage in most experiments was 10 kV, although energies up to 30 kV have been used in making submicron patterns.

Preparation of Uniform Crosslinked Films

The difficulties of preparing crosslinked films on silicon slices by polymerization *in situ* have been mentioned. The best spun films are usually obtained from

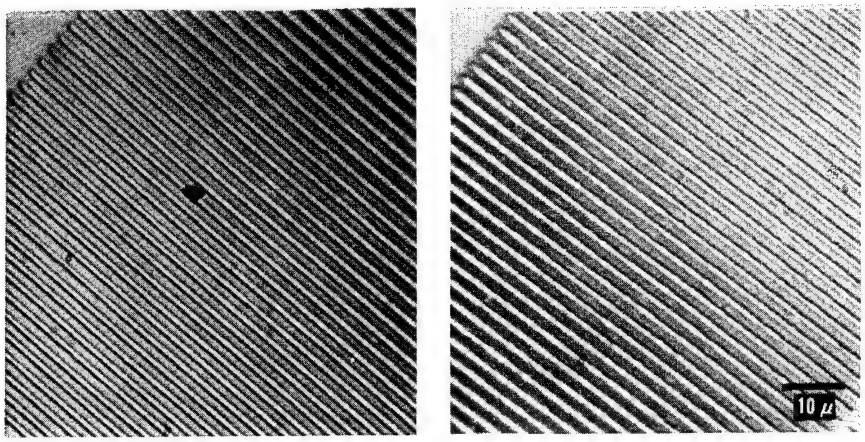

(a) (b)

FIG. 1. Fine lines in methyl methacrylate/methacrylic anhydride film, polymerized *in situ*. Exposure was 1.5×10^{-4} C/cm^2: (a) Developed for 3 min in acetone; (b) 30 min immersion in acetone. 930X.

solutions of solid polymers in solvents which are not too volatile. It was found that satisfactory films could be made from suitable copolymers, which are prepared by conducting the polymerization in a conventional way in glass apparatus. The crosslinking was then carried out *in situ* on the silicon slice after spinning a uniform film of the copolymers.

One method of preparing acid anhydrides is to react an acid chloride with a carboxylic acid:

$$RCOCl + HOOCR' \longrightarrow RCO{\cdot}O{\cdot}OCR' + HCl$$

This method was adapted to suit the proposed resist system. Two copolymer solutions were prepared, one containing methyl methacrylate and methacrylic acid, the other methyl methacrylate and methacryloyl chloride. The solutions were mixed in the proportions required to provide equivalent quantities of methacrylic acid and methacryloyl chloride, and films were spun from the mixed solutions. Upon drying the films were up to 1.5 μm thick. The spun films are still soluble, and crosslinking is effected by subsequent heat treatment, when the following reaction occurs:

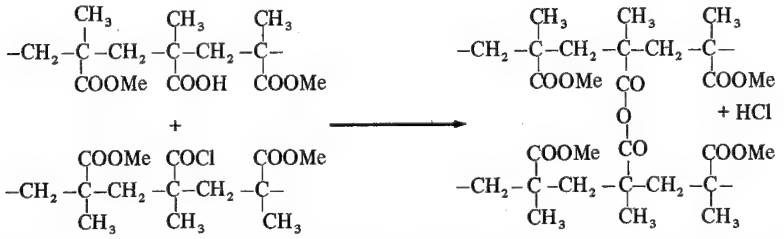

The degree of crosslinking may be controlled by the proportions of acid and acid chloride in the copolymers and by the heat treatment applied to the spun films. The effects are shown in Table I.

Irradiation of Crosslinked PMMA Films

The sensitivity of crosslinked films to the effects of electron bombardment decreases as the degree of crosslinking increases, as can be seen from columns 1-3 of Table I. Films of the resist have been tested by exposing them to a broad beam of electrons [6]. A simple pattern was produced by placing a fine copper grid in loose contact with the resist film to act as a shadow mask. Figure 2 shows scanning electron micrographs of small portions of such patterns. Satisfactory patterns have been obtained at exposures between 8 and 40 $\times 10^{-6}$ C/cm^2, depending upon the degree of crosslinking in the films. Development was carried out in methyl isobutyl ketone (MIBK). The micrographs in Figure 2 are of grid patterns made under a variety of conditions. All appear to have the vertical or slightly undercut edges necessary for successful application of the "lift-off" metallization technique. Figure 3 is an electron micrograph of some fine lines produced in the resist.

TABLE I

Properties of Crosslinked Methacrylate Films

Mol% Crosslinking Groups in Copolymers	Heat Treatment in dry N_2 to effect crosslinking, min/°C	Minimum Exposure for 1 min development in MIBK,* 10^{-6} C/cm^2	% of Film Dissolved After 1 min	
			Acetone	MIBK*
0 (Standard PMMA)	(15/200)	-	90	6
1	15/200	15	20	0
3	30/115	-	85	7
	15/130	12	45	0
	15/150	20	9	0
	15/200	20	0	0
	15/200**	20	10	1
10	30/115	6-8	25	0
	15/130	20	2.5	0
	15/150	35	0	0
	15/200	35	0	0
	15/200**	35	0	0

*Methyl isobutyl ketone.
**Heated in air.

Greater sensitivity is obtained if the developing time is extended. For example, grid patterns exposed in 10% crosslinked films heated for 15 min at 200°C require an exposure of only 20 to 25 $\times 10^{-6}$ C/cm^2 if the development time is extended to 2 min. A 3% crosslinked film requires only about 10 $\times 10^{-6}$ C/cm^2 under those conditions.

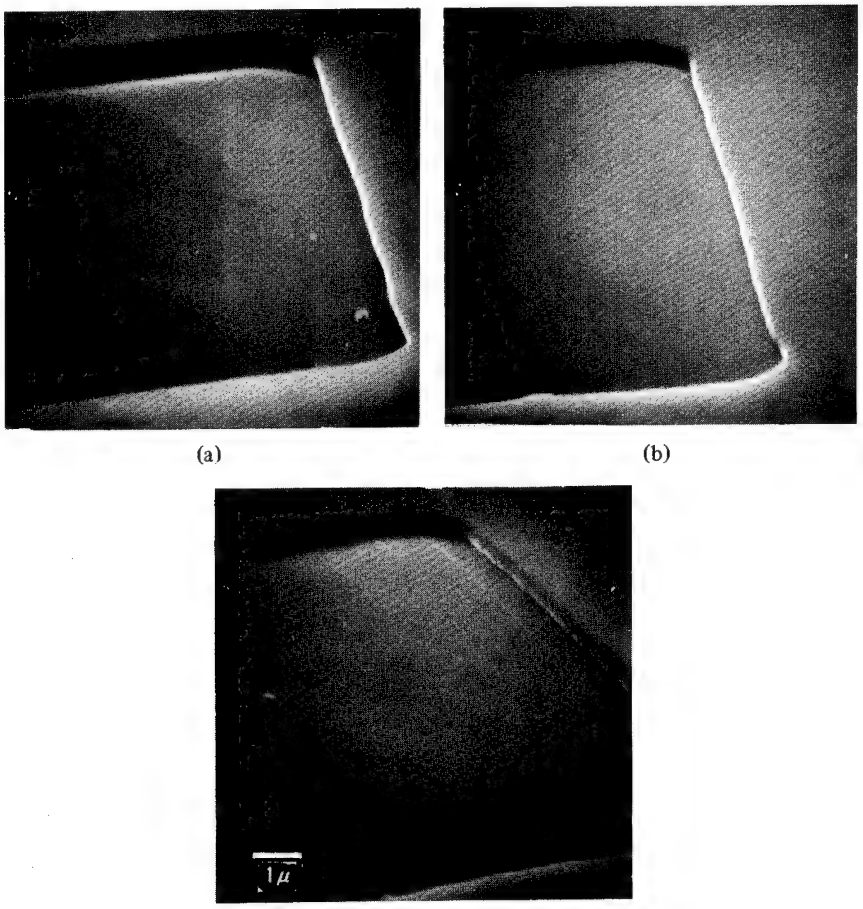

(a) (b)

(c)

FIG. 2. SEM micrograph of crosslinked PMMA pattern: (a) 3% copolymers, crosslinked for 15 min at 200°C, exposed at 2.5×10^{-5} C/cm², and developed for 2 min in MIBK; (b) 10% copolymers, crosslinked for 15 min at 115°C, exposed at 1×10^{-5} C/cm², and developed for 1 min in MIBK; (c) 10% copolymers, crosslinked for 15 min at 200°C, exposed at 4×10^{-5} C/cm², and developed for 1 min in MIBK. 7000X and 65°.

Heat and Solvent Resistance of the Films

The superior heat resistance of the crosslinked material is demonstrated in Figures 4 and 5, which show patterns in standard PMMA exposed at 5×10^{-5} C/cm² and in crosslinked PMMA exposed at 4×10^{-5} C/cm², respectively. Both developed patterns have been heated for 15 min at 130°C after development. The standard PMMA pattern has flowed considerably and would be unsuitable for use in the "lift-off" metallization technique, while the crosslinked pattern is unchanged.

Films of the crosslinked materials were immersed in MIBK and acetone for various periods of time to see if any weight loss could be detected. The films

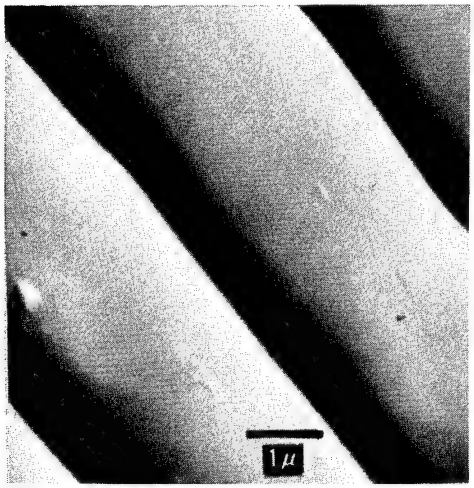

FIG. 3. SEM micrograph of fine lines in crosslinked PMMA pattern: 10% copolymers, crosslinked for 15 min at 200°C, and developed for 2 min in MIBK. 10,000X and 45°.

were 1 to 1.5 μm thick and weighed from 1000 to 1500 μg. The results are presented in columns 4 and 5 of Table I. Films from copolymers containing either 3 or 10 mol % of crosslinkable groups, heated at 200°C for 15 min in dry nitrogen to produce crosslinking, were completely insoluble in acetone and MIBK. These films remain insoluble even after 15 min immersion or after immersion for 5 min in boiling acetone. It has been found that usually any soluble material in the films is removed during the first minute of immersion in

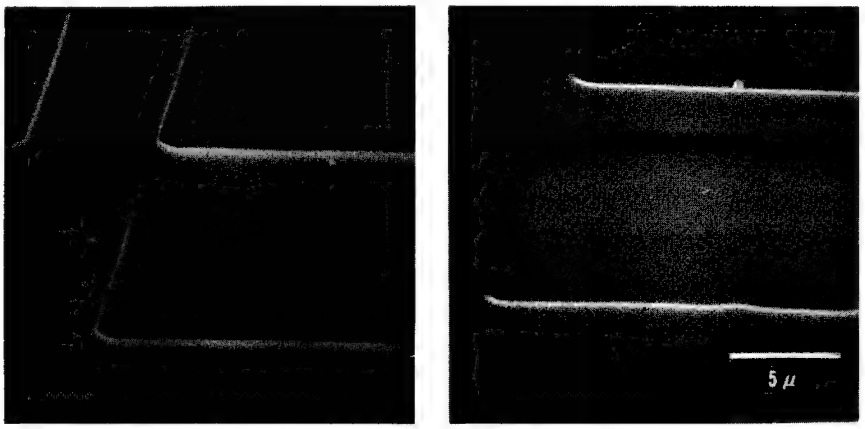

(a) (b)

FIG. 4. Standard PMMA grid patterns, dried 15 min at 200°C, exposed at 5×10^{-5} C/cm², and developed for 1 min in isopropyl alcohol/water (95/5): (a) developed pattern; (b) same after heating for 15 min at 130°C. 3300X and 65°.

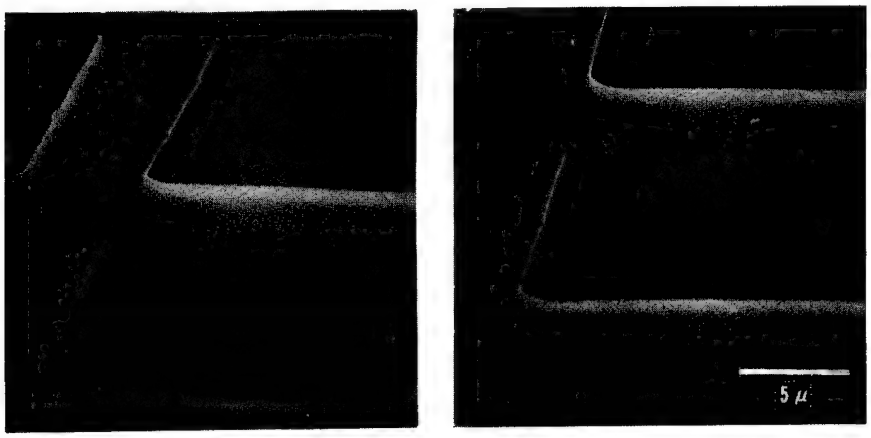

(a) (b)

FIG. 5. Crosslinked PMMA grid patterns. 10% copolymers, crosslinked for 15 min at 200°C, exposed at 4×10^{-5} C/cm^2, and developed for 1 min in MIBK: (a) developed pattern; (b) same after heating for 15 min at 130°C. 3300X and 65°.

cold acetone. Thereafter little, if any, further dissolution occurs. These results are in contrast to standard PMMA which dissolves slowly but completely in MIBK and rapidly in acetone. A PMMA film 1.5 μm thick dissolved almost completely in cold acetone in less than 1 min of immersion.

Films containing only 3% crosslinkable groups dissolve slightly if the crosslinking is performed in ambient atmosphere. A possible reason for this solubility is that acid chloride groups near the surface may be hydrolyzed by the available moisture to form carboxyl groups. These are not able to react with other carboxyl groups to form anhydride bridges. Thus a thin film of acid copolymer which is still soluble remains on the surface of the resist film. In dry atmosphere this hydrolysis cannot occur and the true crosslinking reaction is not suppressed.

Infrared Absorption Spectra

A portion of the infrared spectrum of a crosslinked film, prepared from copolymers with 10 mol% of methacrylic acid and methacryloyl chloride is shown in Figure 6a. The same portion of the spectrum of the same film after irradiation at 4×10^{-5} C/cm^2 but before development is shown in Figure 6b. The absorption peak at 1730 cm^{-1} is probably due to unreacted acid and chloride groups, and that at 1810 cm^{-1} is one of the peaks due to anhydride groups [7]. Anhydride can give rise to two peaks in this region, but one is probably obscured by the large peak at 1730 cm^{-1}. In the spectrum of the irradiated sample, the peak at 1810 cm^{-1} has disappeared completely, indicating that the irradiation process has destroyed the anhydride crosslinks. The disappearance of this peak upon irradiation has been observed in every case

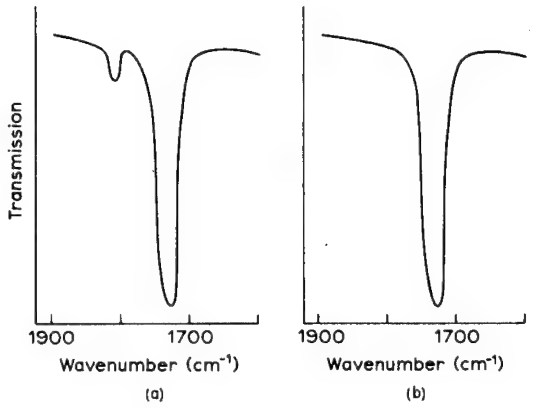

FIG. 6. Infrared spectra of crosslinked PMMA resist (10% copolymers): (a) before irradiation; (b) after 4×10^{-5} C/cm^2 exposure.

examined, irrespective of the degree of crosslinking in the film, provided that the exposure has been high enough to convert it to the soluble condition. The remainders of both spectra between 2.5 and 25 μm are identical with each other and with that of PMMA.

Crosslinked PMMA in "Lift-off" Metallization

The crosslinked methacrylate systems described above have been used to apply the "lift-off" technique of metallization [3]. The patterns of dimensions slightly below the micron level were prepared by scanning a focussed beam nominally 0.25 μm in diameter over silicon or oxidized silicon slices coated with crosslinked methacrylate. The patterns were developed by immersing in MIBK. It was found that submicron patterns required a longer time for development than the 16 μm squares produced by the shadow mask method described earlier. Therefore, the fine patterns were developed for 2 min. It was also found beneficial to finish the development by immersion in fresh developer with gentle ultrasonic agitation to ensure that no residue remained in the developed grooves. Metal was then evaporated over the resist which was subsequently removed. Patterns of aluminum made in this way on silicon substrates with 3% crosslinked methacrylate resist are shown in Figure 7. The resist has been removed by dissolution in a mixture of 3 volumes acetone and 1 volume ammonia solution (S.G. = 0.88). While this process can be conducted in open vessels, it has been found advantageous to carry it out in a sealed container, so that higher temperatures may be employed to accelerate the dissolution of the resist. Patterns of gold (upon a thin layer of nichrome to assist adhesion) on both silicon and oxidized silicon substrates were prepared by a similar method and are shown in Figures 8 and 9, respectively.

The patterns shown in Figures 7 through 9 were made with a beam of electrons of 30 kV energy and 8×10^{-9} C/cm. Patterns can be made at lower energies, with values down to 10 kV having been employed. Variations in the size

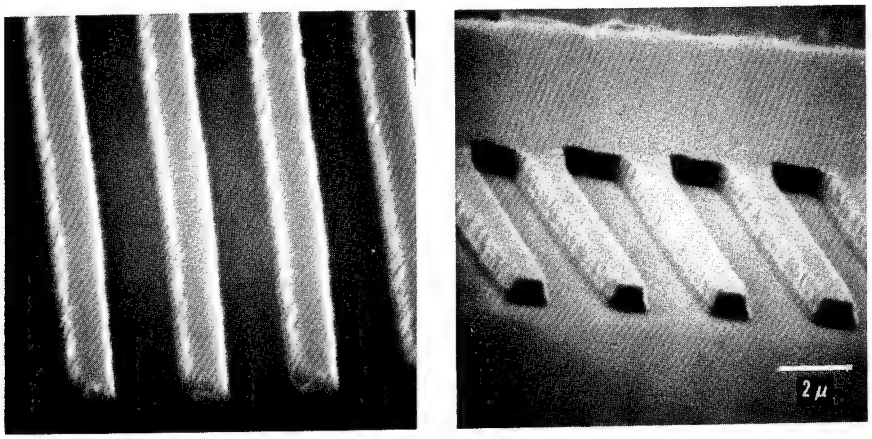

(a) (b)

FIG. 7. Aluminum patterns on silicon produced by "lift-off" technique with 3% crosslinked PMMA resist: (a) 6300X and 45°; (b) 5600X and 80°.

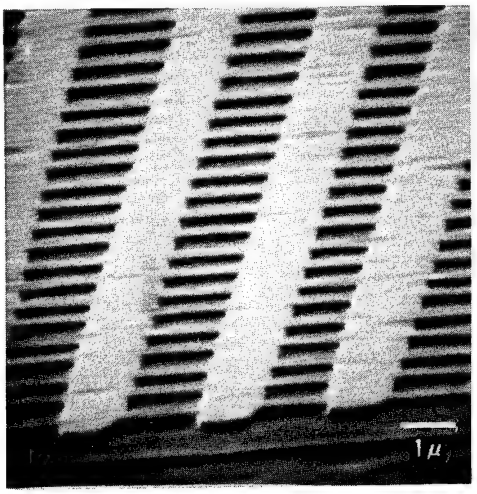

FIG. 8. Gold patterns on silicon produced by "lift-off" technique with 3% crosslinked PMMA resist. 7000X and 80°.

of patterns produced in crosslinked methacrylate films when the exposure and/or electron energy are changed show the same trends as those observed in standard PMMA [8].

DISCUSSION

The main mechanism by which the described resist system operates is clearly by scission of the anhydride crosslinks. It is possible that upon irradiation these groups are eliminated as carbon oxides. Likely there is also some scission of the

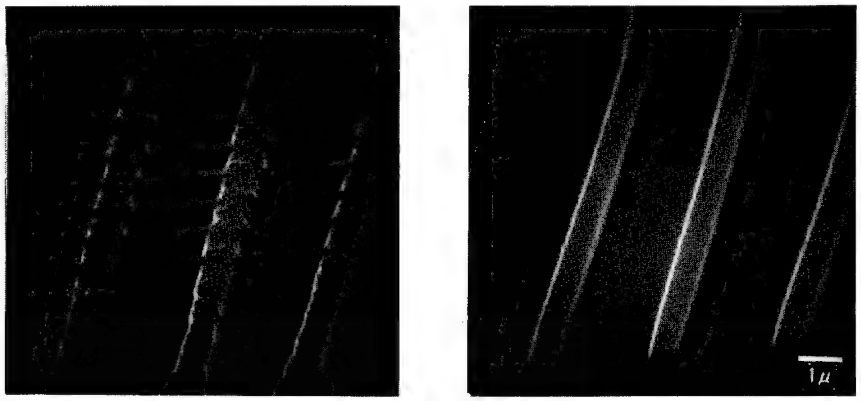

(a) (b)

FIG. 9. Gold patterns on oxidized silicon produced by "lift-off" technique with 3% crosslinked PMMA resist: (a) 7000X and 65°; (b) 7000X and 45°.

main methacrylate chains as in PMMA itself. Experiments with various developer compositions allow detection of main chain scission, at least in those systems with exposures in the region of 5×10^{-5} C/cm^2. However, this mechanism is not crucial to this new system as it is to PMMA.

A wide range of variations of the system is possible, since the degree of crosslinking can be controlled through the copolymer compositions and by the heat treatment to which the mixed copolymer film is subjected before irradiation. As is often the situation, some compromise may be necessary between the requirements of sensitivity and of heat and solvent resistance of the film, but even the most sensitive of the systems we have tried so far has been sufficiently insoluble to allow great latitude in the development time. Some care is needed in the selection of the developing solvent to avoid the possibility of swelling the crosslinked resist, which could lead to degradation of image quality. However, the developer can be chosen to avoid this danger even in the most sensitive, lightly crosslinked systems.

CONCLUSIONS

A positive-working electron resist system has been described in which a crosslinked insoluble film may be converted by electron irradiation to a soluble form. The system can produce resists with sensitivities from slightly less than 1×10^{-5} C/cm^2 upwards, and has a great latitude in developing conditions. The resists may be used in the "lift-off" technique for metallization. It is believed that this is the first study of insoluble films in positive-working systems.

The author thanks the Directors of Mullard Research Laboratories for permission to publish this paper. He also appreciates helpful discussions with Mr. H. N. G. King, Dr. T. R. Neill, and Mr. H. Davies. He thanks Mr. M. R. Burgess, Mr. K. Jones, Mr. G. L. Macdonald, and Mrs. J. Ryan for the electron micrographs, Miss A. M. Cole for the infrared spectra, and Mr. R. C. Barclay for the submicron patterns.

REFERENCES

[1] I. Haller, M. Hatzakis, and R. Srinivasan, *IBM J. Res. Develop.*, **12**, 251 (1968).

[2] H. Y. Ku and L. C. Scala, *J. Electrochem. Soc*, **116**, 980 (1969).

[3] M. Hatzakis, *J. Electrochem. Soc*, **116**, 1033 (1969).

[4] A. J. Swallow, *Radiation Chemistry of Organic Compounds*, Pergamon Press, England, 1960, p. 111.

[5] R. A. Ford, H. N. G. King, and J. M. S. Schofield, *Proc. 3rd Int. Conf. Electron, Ion Beam Sci. Technol.*, Electrochem. Soc., New York, 1968, p. 561.

[6] E. D. Roberts, *Proc. 3rd Int. Conf. Electron, Ion Beam Sci. Technol.*, Electrochem. Soc., New York, 1968, p. 571.

[7] N. B. Colthup, *J. Opt. Soc. Amer.*, **40**, 397 (1950).

[8] E. D. Wolf, F. S. Ozdemir, W. E. Perkins, and P. J. Coane, *Rec. 11th Symp. Electron, Ion, Laser Beam Technol.*, San Francisco Press, San Francisco, 1971, p. 331.

POLY(BUTENE-1 SULFONE) AS A POSITIVE ELECTRON RESIST

M. J. BOWDEN and L. F. THOMPSON

Bell Telephone Laboratories,
Murray Hill, New Jersey 07974

SYNOPSIS

Poly(butene-1 sulfone) behaves as a highly sensitive positive electron resist. It has been shown to serve as a mask both in high resolution etching of SiO_2 and tungsten and for Al/Au vapor evaporation (lift-off). It is at least an order of magnitude more sensitive than any known positive electron resist, with a nominal value for sensitivity of 2×10^{-6} C/cm^2. Resolution for both etching systems as well as for the lift-off technique is well below 6000 Å. At doses above 10^{-4} C/cm^2, the resist can be patterned and developed without using any solvent development or "wet" step. This phenomenon, termed vapor development, results from depolymerization of the irradiated polymer. This process is temperature dependent, and enhanced sensitivity to 5×10^{-6} C/cm^2 results from exposure at elevated temperatures.

INTRODUCTION

This paper describes the evaluation of poly(butene-1 sulfone), PBS, as a positive electron beam resist. Brown and O'Donnell [1] have recently investigated the effect of γ-irradiation on PBS. They reported that the material degraded rapidly under γ-irradiation, with a G(scission) = 11. G(scission) is defined as the number of main chain fractures per 100 eV of energy absorbed [2], and is therefore a direct measure of degradation sensitivity. A value of 11 is greater than that of most other degrading polymers, as can be seen from Table I. For example, poly(methyl methacrylate) or PMMA, a widely used positive electron beam resist, has a value of only 2 [3]. No other studies on the effects of high energy irradiation on aliphatic polysulfones have been reported.

At the present state of the art, engineering and economic considerations for direct electron beam fabrication require a sensitivity of $\sim 1 \times 10^{-6}$ C/cm^2 or better. Sensitivities of this order of magnitude have been achieved for materials currently under investigation, but such materials all function as negative resists. PMMA is the only positive resist of any significance reported to date [4,5]. The sensitivity of PMMA is generally considered to be 5×10^{-5} C/cm^2, although greater sensitivity has been reported [6]. Processing at lower critical doses generally has proven to be unsatisfactory [7].

A series of poly(olefin sulfones) was evaluated earlier, of which PBS appeared most promising [8]. A detailed investigation of the sensitivity and resolution of PBS has now been completed. The results include exposure characteristics of the resist and its subsequent use in the lift-off mode and as a mask in high resolution etching of SiO_2 and tungsten.

Applied Polymer Symposium, No. 23, 99-106 (1974)

TABLE I

G(scission) at 20°C for Degrading Polymers under Irradiation[a]

Type of Polymer	G(scission)
Poly(isobutene)	4
Poly(methyl methacrylate)	2
Poly(α-methyl cellulose)	16
Cellulose	11
Poly(α-methyl styrene)	0.3

[a]Data from J. H. O'Donnell and D. F. Sangster [2].

EXPERIMENTAL

Poly(butene-1 sulfone) was prepared by UV irradiation of an approximately equimolar proportion of butene-1 (14 g) and sulfur dioxide (7 g). The monomers were condensed at -80°C on a vacuum line and sealed under vacuum. The reaction tube was then irradiated for 6 hr at 0°C with light from a Hanovia medium pressure Hg lamp. The tube was rotated several times during irradiation to prevent build-up of precipitated polymer on the walls of the tube. After irradiation, the tube was again cooled to -80°C, subsequently cracked open and allowed to warm to room temperature where excess monomer evaporated. The remaining polymer was dissolved in methyl ethyl ketone, MEK, precipitated into methanol, and dried in a vacuum oven for 24 hr at 40°C.

The substrates were spin-coated with the polymer from a filtered solution by using a Headway Research Model EC-101 spinner. A 5% solution of PBS of $\overline{M}_v = 1.6 \times 10^6$, dissolved in 40% MEK/60% cyclohexanone, deposited a 4000 Å film when spun at 2000 rpm. The films were prebaked for 0.5 hr at 110°C.

The resist was exposed to electron irradiation in a modified Cambridge Mark II Stereoscan scanning electron microscope equipped with a beam programmer. After exposure the image was developed by spraying for 15 sec with a developer consisting of 85% MEK and 15% 2-propanol. The resist was then post-baked for 0.5 hr at 110°C. Two substrate materials, SiO_2 and W, were used for this evaluation. The SiO_2 was thermally grown in a steam furnace, and etched with a buffered HF solution. The W was deposited from WF_6 by a chemical vapor deposition technique, and etched with a standard tungsten etch solution. The remaining resist could be stripped from the substrate by spraying with MEK.

The resolution was evaluated in three modes: (a) as an etching mask for SiO_2; (b) as an etching mask for W; (c) as a vapor evaporation mask for Al/Au vapor evaporation. For a positive resist we define resolution as the narrowest line which can be etched or vapor deposited by using the resist as a mask. The sensitivity data (critical dose) reported in this paper were obtained as follows: A resist film was spun on a SiO_2 substrate; a series of pads of known area were exposed at various electron doses, developed, and post-baked; the SiO_2 was

etched in buffered HF, and the remaining resist stripped in MEK. The critical dose was taken as the least dose required to obtain a clearly etched window in SiO_2. The effects of both excessive dose (over-exposure) and accelerating voltage were evaluated. The dose was varied by varying the line scan time in single line scan mode pattern at constant magnification and current.

RESULTS AND DISCUSSION

Physical and Chemical Characteristics of PBS as a Resist

PBS gave uniform, pinhole-free films, as examined by optical microscopy, when spun from MEK/cyclohexanone solutions. It adhered well to the substrates examined, and it was not affected by excessive baking times as long as the temperature was below 120°C. In general, the aliphatic polysulfones are relatively unstable to heat, (PBS has been reported to decompose at 230°C with a rate constant of 2.0×10^{-3} min^{-1}, resulting in 12% decomposition after 1 hr [9]). However, thermal instability presents no problem at the temperatures utilized in this study. PBS was found to be a chemically inert etching mask for both acidic and alkaline etching systems. The aliphatic polysulfones are known to be stable to acids, but they are degraded by strongly alkaline solutions [10]. No degradation was observed during the reported etch times in the recommended etching solutions.

Evaluation as an Electron Resist

Solvent Development: The first step in the quantitative evaluation of this resist was to determine an optimum developing system. Sensitivities were obtained with a number of solvent systems of different solubility parameters. The results are presented in Table II. It can be seen that a developing solvent containing 85% MEK and 15% 2-propanol results in the highest sensitivity. Therefore, this solvent system was used in all subsequent measurements.

The sensitivity increased as the accelerating voltage was decreased. Figure 1 shows this trend, which is similar to other electron resists. The nominal sensitivity at 5 kV was 2×10^{-6} C/cm^2. The increase in sensitivity with

TABLE II
Sensitivity Dependence of PBS on Nature of Solvent Developing System

Solvent System	δ, $(cal/cc)^{1/2}$	Sensitivity, C/cm^2
Methanol	14.5	3×10^{-4}
MIBK/2-propanol	8.4-11.5	8×10^{-6}
MEK/2-propanol	9.3-11.5	1.3×10^{-6}
Amyl Acetate	8.5	6×10^{-6}

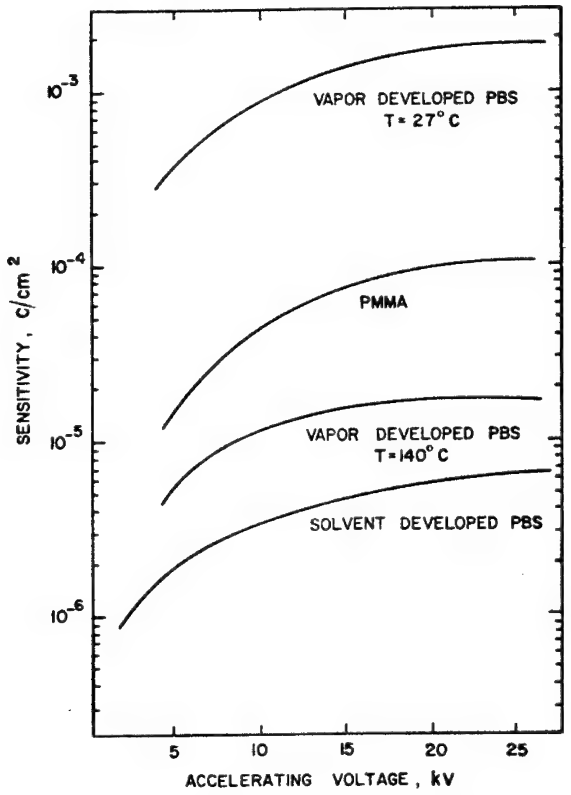

FIG. 1. The effect of accelerating voltage on sensitivity of several electron resists.

decreasing voltage may be attributed to more efficient energy absorption at lower voltage. Film thickness determines the lowest voltage that can be used.

The resolution for both etching systems as well as with the lift-off technique was below 6000 Å. Figure 2 shows some typical etched SiO_2 patterns. Figure 2a is a bar pattern, written with a bar/space ratio of unity, and it shows 7000 Å bars on 1.4 μm. spacing. This indicates that the chip was not overetched. Figure 2b is a typical pattern with 4000 Å etched grooves.

Figure 3 shows typical micrographs of etched tungsten films. Figure 3a represents 1 μm tungsten bars with 1 μm spacing. One important feature about both the SiO_2 and the W etching is that large areas ($\sim$75 μm X 75 μm) can be exposed with no detectable defects. Figure 3b is again a typical grid pattern.

Figure 4 shows a SEM micrograph of 1000 Å thick gold pads which were vapor deposited through a PBS mask. These pictures clearly demonstrate that PBS serves as a mask in the lift-off mode. Lines with widths of less than 4000 Å are easily obtained. However, no evaluation was made of closely spaced, high resolution, interdigital type structures from this mode.

Figure 5 is a plot of maximum etched line width, obtained by exposing the resist until no further increase is observed, as a function of accelerating voltage for PBS and a negative resist. It can be seen that the line widths obtained from PBS do not exhibit strong voltage dependence. This behavior is typical of most positive resists but contrary to that of negative resists.

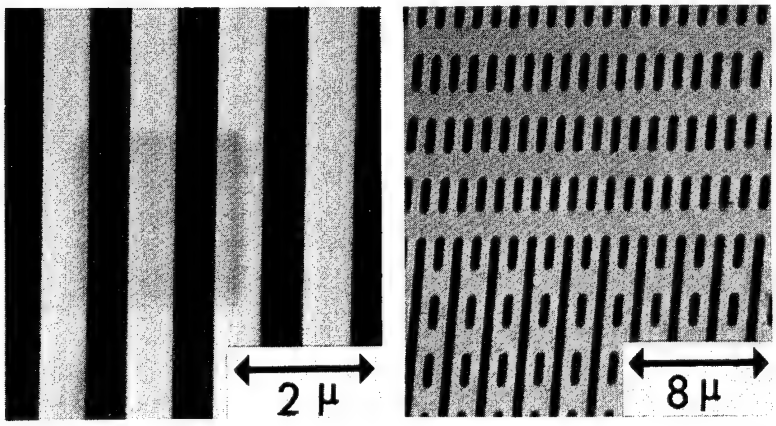

FIG. 2. Patterns etched in 2000 Å of SiO_2 with PBS as a mask.

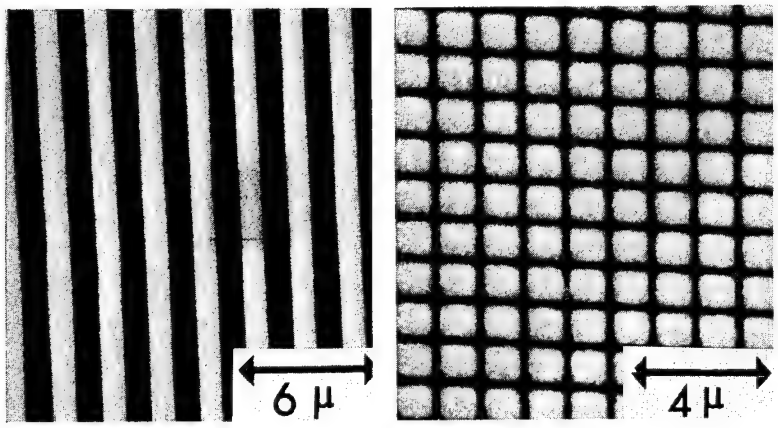

FIG. 3. Patterns etched in 1000 Å of CVD tungsten with PBS as a mask.

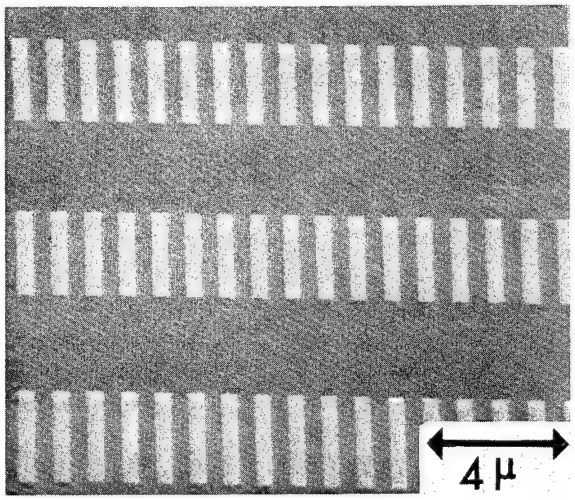

FIG. 4. Gold pattern produced with PBS as a "lift-off" or evaporation mask.

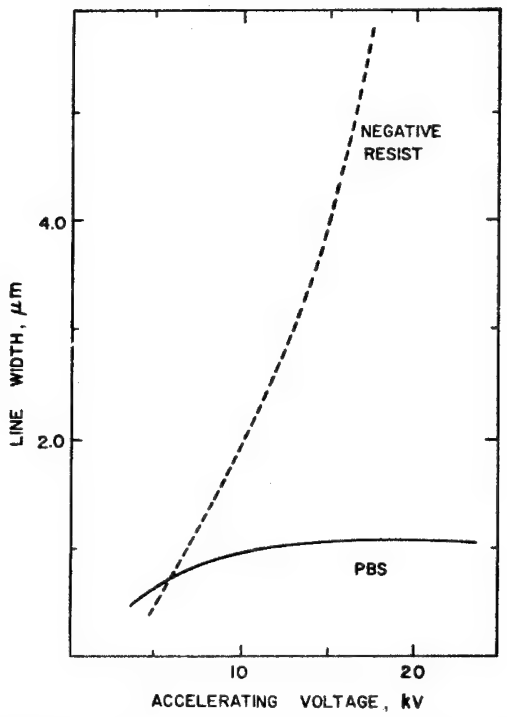

FIG. 5. Maximum etched linewidth as a function of accelerating voltage for PBS and a typical negative resist.

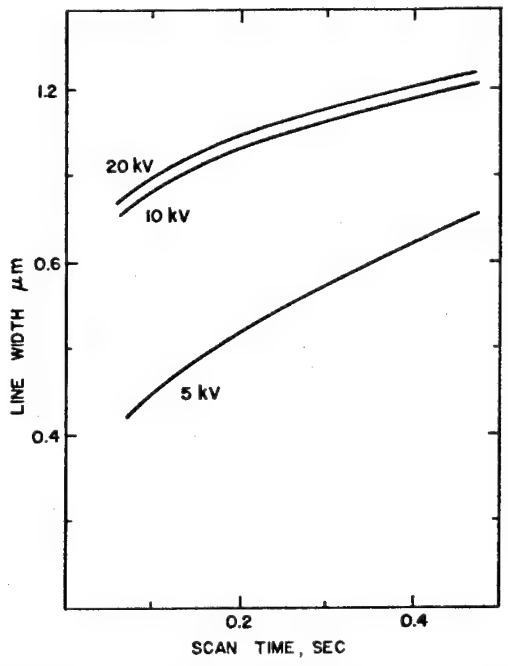

FIG. 6. Etched linewidth as a function of dose for PBS.

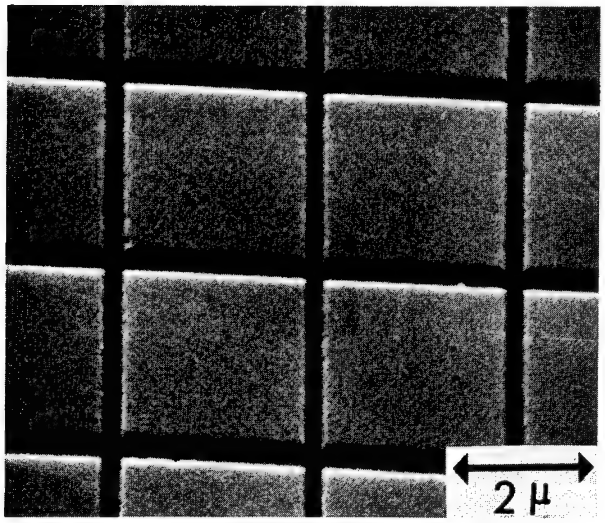

FIG. 7. Pattern etched in 2000 Å of SiO_2 with a vapor developed PBS mask.

Figure 6 shows the line width dependence on total exposure dose for three voltages. It is essentially a representation of the effect of over-exposure. The curves have been corrected for beam diameter at the currents and voltages used. They demonstrate that the resist must be correctly exposed in order to maximize resolution.

Vapor Development: One aspect of this resist is that at doses above 10^{-4} C/cm^2, it can be patterned and developed without any solvent developing or "wet" step. Some typical micrographs of patterns etched through a vapor developed PBS mask are shown in Figure 7. It can be seen that factors such as edge acuity are greatly improved. Elimination of a solvent development process requires that the degraded fragments of the irradiated polymer depolymerize at the irradiation temperature. The product gases are removed by the vacuum system of the electron beam column, hence we have termed this process vapor development. Factors determining the tendency of this material to vapor develop have been discussed recently [11]. The rate of vapor development, which determines the sensitivity, depends mainly on the rate of depropagation and on the rate of chain termination. The sensitivity depends markedly on

TABLE III
Vapor Development Sensitivity at 5 kV as Function of Temperature

Irradiation Temperature, °C	Sensitivity, C/cm^2
21	3×10^{-4}
58	2.1×10^{-4}
140	6×10^{-6}

irradiation temperature. Some preliminary results are listed in Table III, where it is shown that raising the temperature from 20 to 140°C increased the sensitivity of a 1500 Å film from 3×10^{-4} to 6×10^{-6} C/cm^2.

CONCLUSIONS

Poly(butene-1 sulfone) is a good positive electron beam resist, which is at least an order of magnitude more sensitive than PMMA. At the expense of sensitivity, edge definition can be enhanced and solvent development eliminated by resorting to the vapor development mode. Sensitivity may be enhanced by irradiation at elevated temperature.

The authors wish to thank R. D. Heidenreich and E. D. Feit for helpful comments concerning this work.

REFERENCES

[1] J. R. Brown and J. H. O'Donnell, *Macromolecules, 5,* 109 (1972).
[2] J. H. O'Donnell and D. F. Sangster, *Principles of Radiation Chemistry,* Arnold, London, 1970, p. 25.
[3] A. Charlesby, *Atomic Radiation and Polymer,* Pergamon, Oxford, England, 1960, p. 338.
[4] I. Haller, M. Hatzakis, and R. Srinivasan, *IBM J. Res. Develop., 12,* 251 (1968).
[5] M. Hatzakis, *J. Electrochem. Soc., 116,* 1033 (1969).
[6] M. Hatzakis, this issue, p. 73.
[7] R. F. W. Pease, private communication.
[8] L. F. Thompson and M. J. Bowden, *J. Electrochem. Soc., 120,* 1722 (1973).
[9] M. A. Naylor and A. W. Anderson, *J. Amer. Chem. Soc., 76,* 3962 (1954).
[10] E. M. Fettes and F. O. David, *High Polymers,* vol. 13, Interscience, New York, 1962.
[11] M. J. Bowden and L. F. Thompson, *J. Appl. Polym. Sci., 17,* 3211 (1973).

PROPERTIES OF SOME ELECTRON SENSITIVE SILOXANE RESISTS

M. GAZARD, J. C. DUBOIS, and C. DUCHESNE

Thomson-CSF, Laboratoire Central de Recherches, Domaine de Corbeville, 91-Orsay, France

SYNOPSIS

Three negative siloxane resists were synthesized: polymethylsiloxane (PMS), polyvinylsiloxane (PVS), and polyphenylsiloxane (PPS). Properties such as molecular weight, refractive index, and stability were determined. PMS and PVS must be dissolved in 2-propanol because solutions are more stable than the dry products. The resists were coated on silicon wafers and irradiated in a scanning electron microscope. PMS and PPS need a charge dose density in the order of 10^{-4} to 10^{-3} C/cm^2 to be completely crosslinked. PVS needs only 5×10^{-6} C/cm^2, and therefore is the more interesting and promising resist. Through heating at 800°C the crosslinked resists can be converted into silica. The dielectric properties of the formed silica were measured: the resistivity was 10^{12} Ωcm, the dielectric constant was between 4 and 8, and the dielectric strength was 10^6 V/cm. These resists are suitable for the fabrication of microelectronic devices and integrated optics.

INTRODUCTION

Integrated circuit manufacturing requires the use of resists to control etching operations. Very attractive resists for this purpose are electron sensitive polymers, since better resolution can be obtained with electron beams than by other means. Recently such polymers have also been used to fabricate optical waveguides for integrated optics [1, 2]. The behavior of polymers under electron beam irradiation has already been studied for a long time. Two types of materials can be recognized [3]: crosslinking polymers, such as polyacrylates, polyamides, and polysiloxanes, and degrading polymers, such as polymethyl methacrylates. Silicone resists are very interesting, because the composition of their primary chain is close to that of silica. Silicones may be utilized as insulating films between metal layers [4] or as diffusion barriers [5]. Recently their use as passivating layers has been proposed [6].

A study was undertaken to examine the possibility of using electron sensitive siloxane resists in microelectronics. A previous paper [7] describes some properties of a highly sensitive polyvinylsiloxane. Two other siloxanes were studied, and the purpose of this paper is to present the results of work done in the field of silicone electron beam resists for microelectronics. Some preliminary experiments were conducted to evaluate the materials for integrated optics, in etching optical waveguides in a suitable glass, and in fabricating waveguides in the electron resist material itself. The results of these experiments are also presented.

Applied Polymer Symposium No. 23, 107-116 (1974)

MATERIALS

Three siloxane resists were synthesized from methyl-, vinyl-, and phenyltrichlorosilane. The methyl- and vinylsilane were hydrolyzed in ethyl ether, and the hydrolyzate was polymerized with ammonium hydroxide. The phenylsilane was hydrolyzed in toluene, and polymerized with potassium hydroxide. PMS and PVS molecular weights were determined with a vapor pressure osmometer; PPS molecular weight was determined through viscosimetry. Table I gives the molecular weights and the refractive indexes of the three siloxanes.

Due to their low molecular weight, PMS and PVS are soluble in many organic solvents, such as ethers, ketones, and alcohols. The most suitable solvent for handling these two products was found to be 2-propanol. PPS is soluble in aromatic solvents and tetrahydrofuran. Coating solutions were prepared by dissolving PPS in benzene.

PVS and PMS are greatly affected by moisture in the ambient atmosphere, and they become insoluble in organic solvents very readily upon exposure to moisture. They must therefore be kept over sulfuric acid in a vacuum. However, solutions of PMS and PVS in 2-propanol are stable if prepared immediately after synthesis.

Crosslinking occurs between 65 and 70°C for PMS, and at 75°C for PVS. PPS is a more stable product, and it has to be heated above 400°C to undergo transformation.

ELECTRON BEAM IRRADIATION

Clean silicon wafers were spin-coated with siloxane after ultrafiltration of the solutions. Concentrations of the solutions and spinning speeds were chosen so that the thickness of the resist layers was in the range of 0.2 to 1.0 μm. Thickness measurements were made by means of interferometry.

Electron beam exposures were made in a Cambridge Mark II Stereoscan scanning electron microscope. Areas of 4×10^{-4} cm^2 were irradiated with an electron beam current of 10^{-12} to 10^{-8} A, a scanning time of 40 sec, and an accelerating voltage of 20 kV. The line frequency was chosen so that the lines

TABLE I

Molecular Weights and Refractive Indices of Siloxane Resists

Resist	Molecular Weight	Refractive Index
PMS	1100	1.428
PVS	1345	1.442
PPS	10,000	1.563

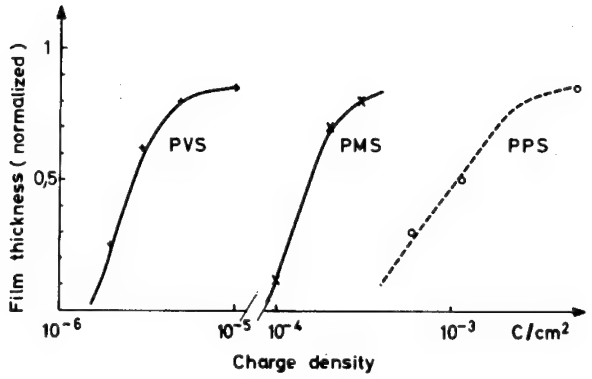

FIG. 1. Exposure characteristics of siloxane resists polyvinylsiloxane (PVS), polymethylsiloxane (PMS), and polyphenylsiloxane (PPS).

were not resolved. Immediately after exposure the samples were developed by soaking for a few seconds in acetone for PMS and PVS, and in benzene for PPS resists. The wafers were then dried by blowing dust-free nitrogen over them, and the remaining thickness of the resists was evaluated. Exposure characteristics are presented in Figure 1. The minimum charge densities necessary for resist crosslinking are listed in Table II. PVS has the highest sensitivity; only 5×10^{-6} C/cm^2 is necessary to crosslink the resist completely. PPS shows the lowest sensitivity. Similar results were found by Yatsuo Yatsui with other silicone resists [8].

In order to determine resolution, separate lines were exposed in silicone layers, and Figure 2 is a micrograph with lines of 0.5 μm wide in PVS. These lines were obtained in a 0.4 μm thick layer with an exposure charge density of 5×10^{-10} C/cm at 20 kV. The beam diameter was 0.1 μm. The greater the scan speed, the thinner the line width, if the charge density is maintained constant. Lines of 0.5 μm have also been obtained in PMS and PPS layers.

The crosslinked resists present good resistance to chemical etching agents, except to hydrofluoric acid. They dissolve slowly in sulfuric acid.

TABLE II

Minimum Charge Density for Siloxane Resists

Resist	Minimum Charge Density, C/cm^2
PVS	8×10^{-7}
PMS	8×10^{-5}
PPS	3×10^{-4}

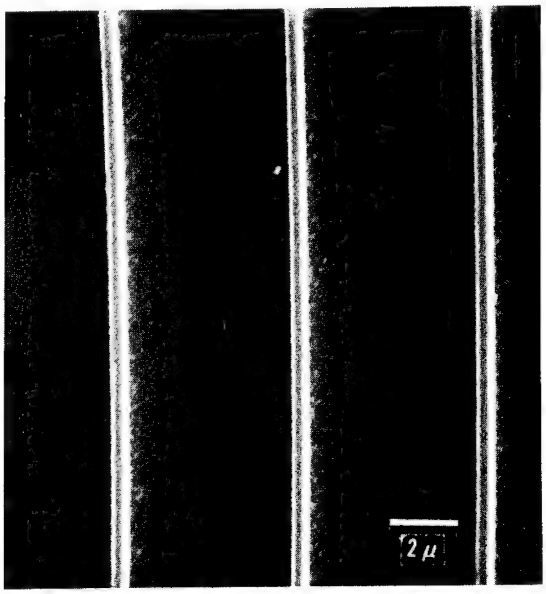

FIG. 2. SEM image of lines exposed at 20 kV in PVS; 4400X.

THERMAL TRANSFORMATION OF CROSSLINKED RESISTS

Application in Microelectronics

The behavior of crosslinked PMS and PVS during heating has been investigated. The parameters studied are temperature and the nature of the atmosphere, which may or may not be oxidizing. The silicon wafers with crosslinked siloxane layers were baked in an argon atmosphere for 3 hr at different temperatures. Thermal analysis showed that weight loss occurred above 400°C. The thickness of the film decreased and reached about 50% of the initial thickness at 800°C, where it became stable. Infrared absorption by C-H and Si-C bonds decreased, with the final product being a polymer with only Si-O bonds, as shown in Figure 3. Thus carbon and hydrogen are removed, and the polymer remaining appears to be silica. The degradation was more rapid under an argon-oxygen (1:1) atmosphere. These experiments show that PMS and PVS can thus be converted into silica during the post-baking process. This property is very interesting because these results allow rapid fabrication of silica patterns through a procedure outlined in Figure 4.

To follow the transformation and to determine the dielectric properties of the silica formed, dielectric measurements were made on silicon-PVS-aluminum structures as a function of heating conditions. The resistivity of the silica was evaluated by measurement of the voltage necessary to obtain a current of 1 nA. The dielectric constant was measured with a capacitance bridge at 1 MHz. The results are presented in Table III.

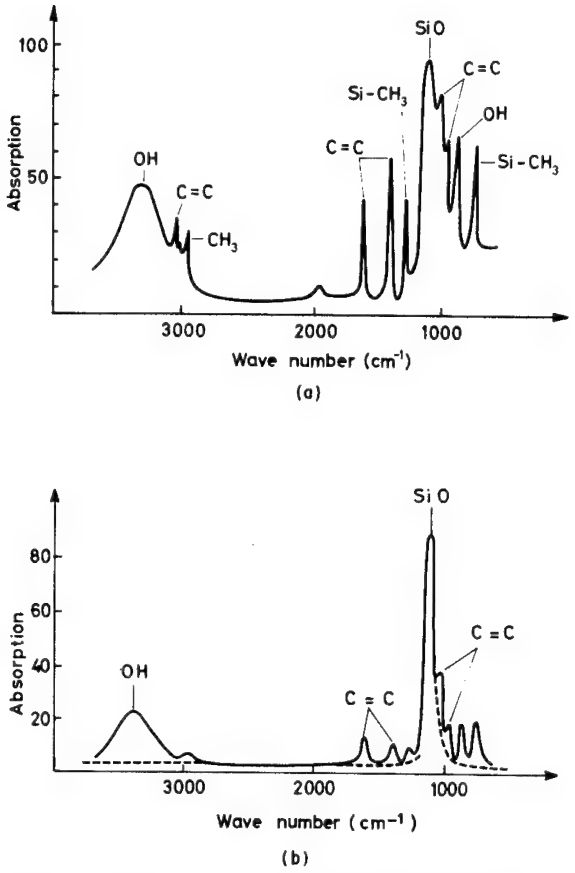

FIG. 3. Infrared spectra of PVS; (a) before exposure; (b) after exposure, (——) before post-baking,(- - - -) after post-baking at 800°C for 3 hr.

TABLE III

Dielectric Properties of Heated Crosslinked PVS vs Conditions of Heating

Property	Argon/Oxygen (1:1)		Argon	
	500°C	800°C	650°C	800°C
Resistivity, Ωcm	1-4 x 10^{11}	10^{12}	4 x 10^{12}	10^{12}
Dielect. Constant	7-8	4-6	10	4-8
Dielect. Strength, V/cm	10^{6}	10^{6}	4 x 10^{6}	10^{6}

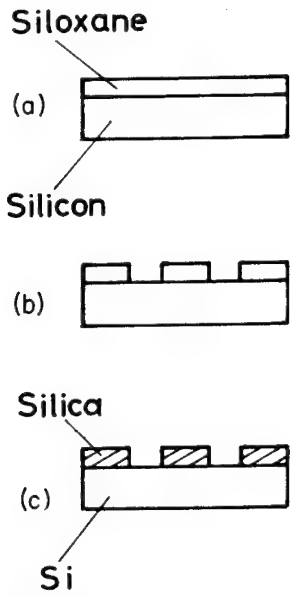

FIG. 4. Procedure of manufacturing silica patterns: (a) siloxane coating; (b) irradiation and development; (c) heating.

Similar results have been obtained with PMS resists. Table III shows that the dielectric constant changes very rapidly when temperature increases. The change occurs more rapidly in an oxidizing atmosphere. Resistivity and dielectric strength do not undergo important modification. Above 800°C no further changes take place in dielectric properties and in the infrared spectra. Final dielectric properties are somewhat inferior to those of thermal silica. The high dielectric constant is near that of SiO, whereas the refractive index of 1.5 is near that of SiO_2. Thus, the compound probably has a composition between that of SiO and SiO_2. Perhaps some carbon still remains in the polymer, although it cannot be detected in the infra-red spectrum.

To test the masking properties of silica, some diodes were made through diffusion and implantation of dopants in silicon wafers. For ion implantation the blocking thickness is comparable to that of thermal silica. To examine the profile of implantation or diffusion, the junction was revealed with a copper stain. Two examples are shown in Figure 5.

Siloxane Resists for Integrated Optics

Two ways of producing optical wave guides were considered and tried. In the first one, the resist was irradiated according to the desired pattern, and after development the pattern was used to sputter etch in a suitable substrate. The procedure is outlined in Figure 6. The guide consisted of a 5000 Å thick layer of glass ($n = 1.566$) on a substrate of $n = 1.515$. A 200 Å layer of gold was

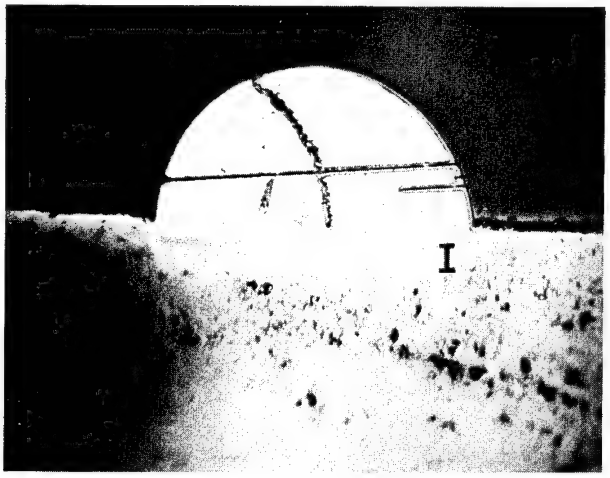

(a)

(b)

FIG. 5. Profiles of n-p junctions: (a) implantation of P in p-silicon with junction thickness of 0.65 μm; (b) diffusion of P in p-silicon with junction thickness of 0.3 μm. The junctions are indicated by bars.

evaporated, and a 8500 Å thick film of PVS was spin-coated. After irradiation and development, the wafers were baked at 600°C to harden the resist and to obtain a uniform etching. With an argon pressure of 2×10^{-4} torr, a current density of 0.8 mA/cm^2, and an ion energy of 1 keV, the etch rate is about 750 Å/min. Figure 7 gives an example of a 10 μm wide light guide.

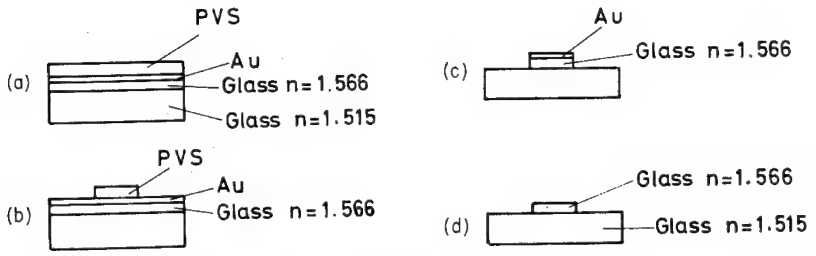

FIG. 6. Procedure for manufacturing optical waveguide in a glass of n = 1.566; (a) PVS coating; (b) irradiation and development; (c) ion sputter etching; (d) Au removal.

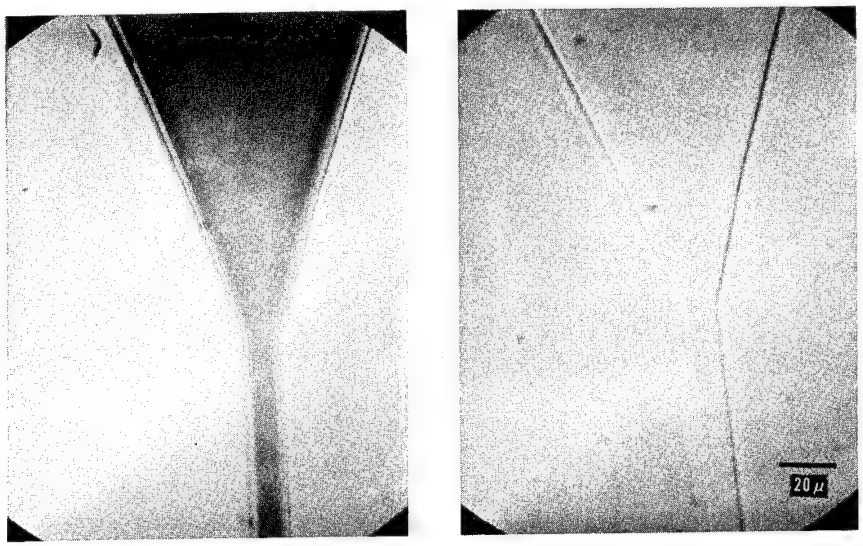

(a) (b)

FIG. 7. A 10-μm wide light guide in a glass of n = 1.566: (a) after exposure and heating of PVS; (b) after backsputtering.

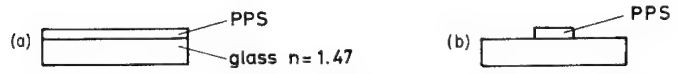

FIG. 8. Procedure of manufacturing an optical waveguide in a PPS film: (a) PPS coating; (b) after irradiation and development.

In the second way, the pattern written in the resist forms the guide according to the procedure outlined in Figure 8. The resist must have a higher refractive index than the substrate and low optical losses. PPS has a high refractive index, and it was interesting to test this material for making waveguides. The tests were decisive and conclusive; it was possible to propagate a

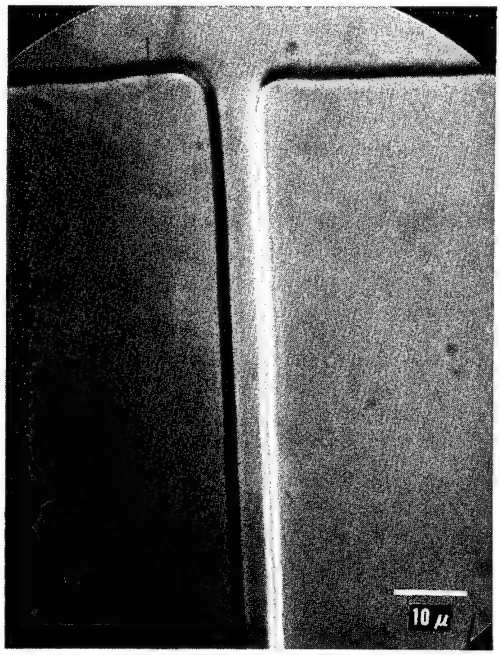

FIG. 9. A 5-μm wide light guide in PPS film; 1040X.

He-Ne laser beam in a 5 μm wide guide on a glass of n = 1.47. The structure of this guide is represented in Figure 9.

CONCLUSION

Siloxane resists are very interesting for microelectronics and integrated optics. Especially polyvinylsiloxane is promising, since it needs only 5×10^{-6} C/cm^2 of irradiation to be crosslinked. Polyvinyl- and polymethylsiloxane are transformed into silica when they are post-baked at 800°C. Although the resistivity and dielectric strength of this silica are less than that of thermal silica, it can be used as an insulating layer. It may also produce barriers for diffusion and ion implantation. The possibility of using polyphenylsiloxane to fabricate optical waveguides has been demonstrated. The three resists possess good resolution capabilities and permit fabrication of small geometric elements.

The authors wish to thank the "Délégation Générale à la Recherche Scientifique et Technique" and the "Direction des Recherches et Moyens d'Essais" who partially sponsored the research described here.

REFERENCES

[1] D. B. Ostrowsky and J. C. Dubois, "Digest of Technical Papers" (Meeting Integrated Optics, Guided Waves, Materials, and Devices, Las Vegas, Nevada, 1972). Optical Soc. Amer., Washington, D.C., paper MB7-1.

[2] J. E. Goell, "Digest of Technical Papers," (Meet. Integrated Optics, Guided Waves, Materials, and Devices, Las Vegas, Nevada, 1972), Optical Soc. Amer., Washington, D.C., paper MB8-1.

[3] A. Chapiro, *High Polymers*, vol. 15, Interscience, New York, 1962, p. 353.

[4] H. Aoe, Y. Yatsui, and T. Hayashida, *Microelectron. Rel., 9,* 267 (1970).

[5] E. D. Roberts, *Proc. 3rd Int. Conf. Electron, Ion Beam Sci. Technol.*, Electrochem. Soc., New York, 1968, p. 571.

[6] E. D. Roberts, *Proc. 5th Int. Conf. Electron Ion Beam Sci. Technol.*, R. Bakish, Ed., Electrochem. Soc., Princeton, N.J., 1972, p. 112.

[7] J. C. Dubois and M. Gazard, *Proc. 5th Int. Conf. Electron Ion Beam Sci. Technol.*, R. Bakish, Ed., Electrochem. Soc., Princeton, N.J., 1972, p. 102.

[8] Y. Yatsui, T. Nakata, and K. Umehara, *J. Electrochem. Soc., 116,* 94 (1969).

EPOXIDIZED CIS-1,4-POLYBUTADIENE, A HIGHLY SENSITIVE ELECTRON BEAM RESIST

S. NONOGAKI, H. MORISHITA, and N. SAITOU

Central Research Laboratory, Hitachi, Ltd.,
Tokyo 185, Japan

SYNOPSIS

Cis-1,4-polybutadiene was epoxidized with peracetic acid to produce a highly sensitive electron beam resist. The epoxidized polymer can be insolubilized with an electron beam irradiation of 5×10^{-8} C/cm² at 15 kV. In the range of 5 to 20 kV, the sensitivity increases with decreasing accelerating voltage and with increasing molecular weight of the polymer. The data on the relationship between sensitivity S and degree of epoxidation α were found to follow a theoretically derived correlation $S = S_0 + J\alpha/(1 - K\alpha)$, where S_0, J, and K are constants. The equation can be derived by assuming that the insolubilization process of the polymer involves a chain reaction. With this polymer and an electron beam drafting machine, finely patterned chromium masks have been obtained. The minimum width of the chromium lines thus obtained is 1.5 μm.

INTRODUCTION

It has been reported previously that some kinds of polymers containing epoxy groups are very sensitive to electron beams [1]. Epoxidized cis-1,4-polybutadiene, found to be the most sensitive of these polymers, has been investigated in more detail. We wish to present the latest results of this work.

EXPERIMENTAL

Cis-1,4-polybutadiene (JSR BRO1, Japan Synthetic Rubber Co., with intrinsic viscosity $[\eta] = 2.8$ in toluene) was epoxidized with peracetic acid in monochlorobenzene. Then, the solution was washed with water, neutralized with sodium bicarbonate, diluted with cyclohexane, and centrifuged to give a clear solution of the epoxidized polymer. In most instances, the polymer was then precipitated by adding cyclohexane or ethanol to the solution, dissolved again in monochlorobenzene, and stored.

The polymer is considered to have the structure

$$(-CH_2-\underset{\diagdown O \diagup}{CH}-CH-CH_2-)_m(-CH_2-CH=CH-CH_2-)_n$$

where m and n are the numbers of epoxidized and unepoxidized butadiene units,

Applied Polymer Symposium No. 23, 117-123 (1974)

respectively. The epoxy content of the polymer was determined by having a known quantity of the polymer react with a known quantity of hydrochloric acid in pyridine, and by back-titrating the remaining of acid to determine the consumption by the epoxy groups. The degree of epoxidation, $\alpha = m/(m+n)$, is readily obtained by simple calculation from the epoxy content thus determined.

The electron beam exposure characteristics of the polymer were obtained through the following procedure. The polymer solution was coated on oxidized silicon wafers, with polymer film thicknesses ranging from 0.15 to 0.35 μm, exposed to an electron beam with varied charge densities, and developed in methyl isobutyl ketone. In some cases, where the epoxy contents were relatively low, toluene was used as the developer. The thickness of the insolubilized film was measured with an interference microscope, normalized with its saturation value, and plotted as a function of the charge density.

RESULTS AND DISCUSSION

Sensitivity and Accelerating Voltage

Figure 1 exemplifies typical exposure characteristics of the epoxidized polymer at different accelerating voltages. In the voltage range shown in the figure, the sensitivity increases with decreasing voltage. The same tendency has been observed by Broyde [2] with the commercial photoresist KTFR from Kodak.

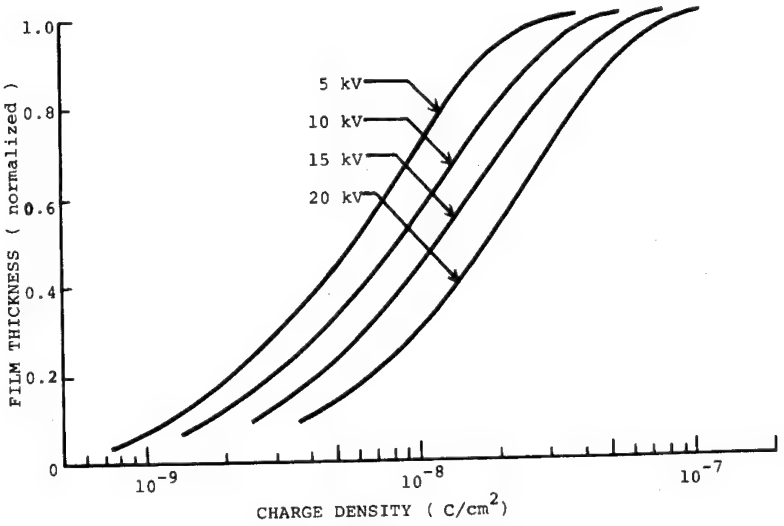

FIG. 1. Typical exposure characteristics of epoxidized cis-1,4-polybutadiene at different accelerating voltages.

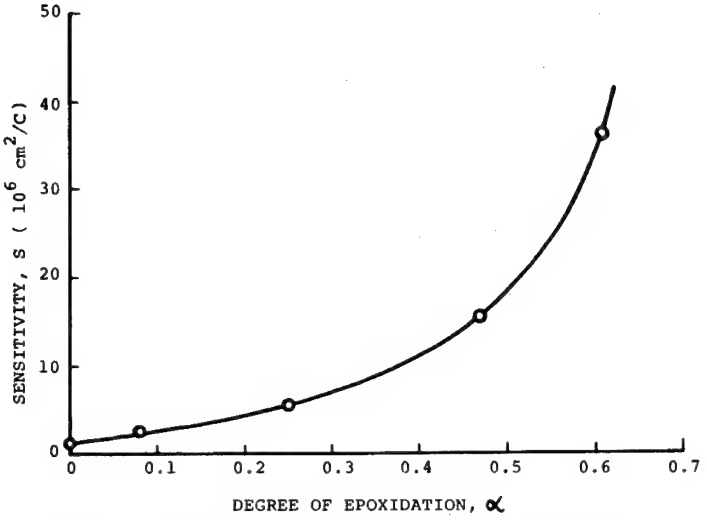

FIG. 2. Sensitivity as a function of the degree of epoxidation.

Sensitivity and the Degree of Epoxidation

A series of polymers with varying epoxy contents was prepared, and their exposure characteristics were measured at an accelerating voltage of 15 kV. The results are summarized in Figure 2. In this figure, the sensitivity S, defined as the reciprocal of the charge density with which the thickness of the insolubilized film reaches 80% of its saturated value, is plotted against the degree of epoxidation α.

It was previously ascertained that the epoxy groups are opened very efficiently by irradiation with an electron beam [1]. This finding implies that a chain reaction is involved in such a ring opening process. In the curing process of epoxy resins, it is believed that a catalytically opened epoxy group is capable of opening another epoxy group, so that the reaction may proceed through successive opening of a large number of epoxy groups. Therefore, it seems reasonable to assume that similar successive reactions take place in the materials tested here. With this assumption, and further considerations as shown below, we can derive an equation that accurately explains the observed relationship between S and α.

If the probability of an additional ring opening by an already opened epoxy group is p, then N epoxy groups which were initially opened by irradiation will result in the opening of $N(p + p^2 + p^3 + \ldots)$ epoxy groups. Consequently, the sensitivity S can be expressed as

$$S = S_0 + S_i + S_i(p + p^2 + p^3 + \ldots) = S_0 + \frac{S_i}{1 - p} \qquad (1)$$

where S_0 is the sensitivity in the absence of epoxy groups, and S_i is the sensitivity that would be exhibited if the radiation-induced ring openings were not followed by successive ring openings. If we assume that both S_i and p are proportional to α, then we can obtain the equation

$$S = S_0 + \frac{J\alpha}{1 - K\alpha} \tag{2}$$

where J and K are constants.

The observed correlation between S and α (Fig. 2) can be expressed accurately with this equation by choosing appropriate values for S_0, K, and J. If we express the sensitivity S in 10^6 C/cm^2, and we let $S_0 = 1.1$, $J = 11.8$, and $K = 1.3$, then the equation becomes

$$S = 1.1 + \frac{11.8\,\alpha}{1 - 1.3\alpha} \tag{3}$$

This is the relationship shown in Figure 2 by the solid curve. The curve is in good agreement with the observed data, and it supports the chain reaction mechanism, by which the high efficiency of epoxy ring opening, as well as the high sensitivity of the polymer, can be explained.

Sensitivity and Molecular Weight

Ku and Scala [3] have shown that the sensitivity of a negative electron resist is supposed to be proportional to the molecular weight of the resist polymer. In order to confirm this correlation for our resist material, we dissolved the polymer (α = 61%) in monochlorobenzene, and fractionally precipitated the polymer into six fractions with cyclohexane as a nonsolvent. As expected, the sensitivity was found to increase with an increase in molecular weight. Figure 3 shows the exposure characteristics of the initially precipitated (high molecular weight) fraction and the finally precipitated (low molecular weight) fraction, together with those of the unfractionated polymer. There is a difference in sensitivity between these two fractions by a factor of about 10. It can also be seen that the sensitivity of the high molecular weight fraction is about twice that of the unfractionated polymer.

Stabilization of the Polymer

When the epoxidized polymer was applied in electron beam microfabrication, we found that the polymer film becomes partially insoluble in the developing solvent, even in the absence of irradiation. We also discovered that after development a very thin film of the polymer is left on the unexposed area of the substrate. This phenomenon is an obstacle to accurate engraving of the substrate, and therefore, must be eliminated. Several methods, such as purification of the polymer, pretreatment of the substrate, and addition of

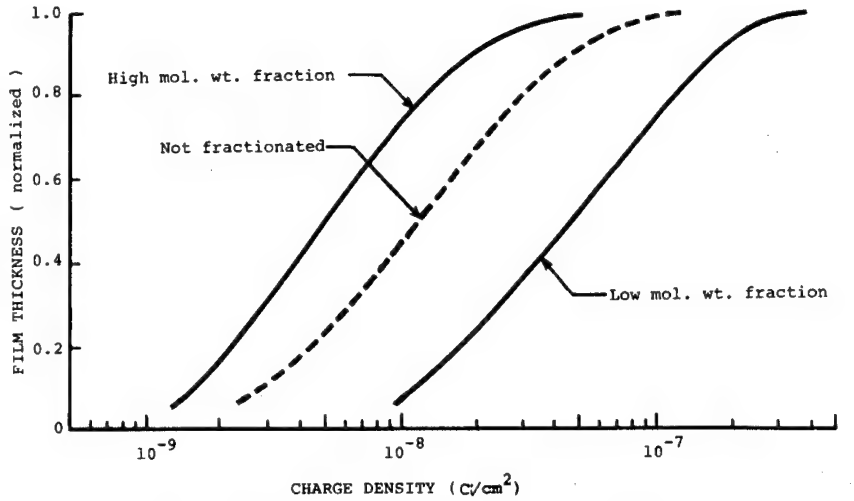

FIG. 3. Effect of the molecular weight on the sensitivity.

stabilizers, have been tried in order to prevent this spontaneous or "dark" insolubilization. Of these methods, the most effective was the use of stabilizers. Addition of 1% trimethyl lauryl ammonium chloride to the polymer was found to be sufficient to prevent "dark" insolubilization. Also some inorganic salts, such as potassium iodide, cesium iodide, or sodium carbonate were found to be effective. However, with these salts a solvent, such as cyclohexanone, that can dissolve them to some extent, must be used in place of monochlorobenzene.

Application

The epoxidized polymer has been used as an electron beam resist, mainly in electron beam chromium mask fabrication. In this application, the insolubilized resist film is post-baked at 140°C for 20 min in order to enhance both adhesion and chemical resistance of the polymer. By using this resist and an electron beam drafting machine, fine chromium gratings [4] and computer holograms [5, 6] have been fabricated.

Resolution Capability

In order to determine the resolution capability, a resist film on a chromium-clad glass plate was scanned with an electron beam with a diameter of about 0.05 μm, to obtain fine lines of insolubilized resist. With these lines as a mask, the chromium layer was etched chemically, and the resulting chromium lines were observed with a scanning electron microscope to determine the line width. Figure 4 shows a SEM micrograph of the chromium lines thus obtained. As shown in the figure, a line width of about 1.5 μm can be attained.

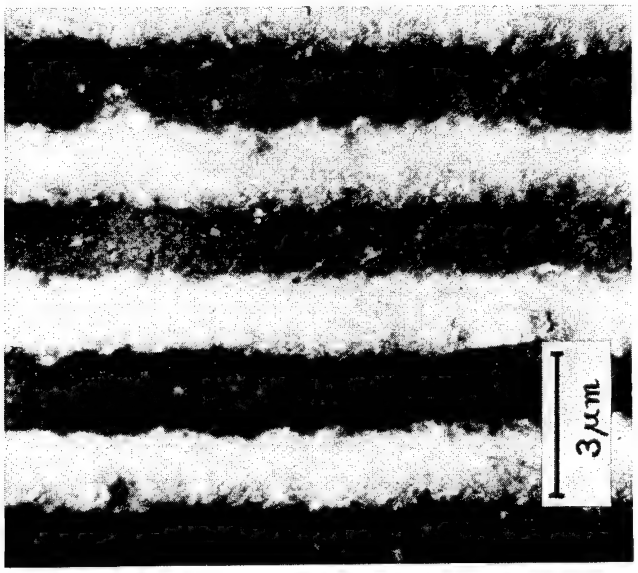

FIG. 4. SEM micrograph of chromium lines formed on a glass plate by electron beam microfabrication technique. The bright lines are the chromium layers.

Removal of the Resist Film

A convenient way to remove the resist film, either post-baked or not, from the substrate is to burn it off by heating the substrate in air above 480°C for 20 min. The resist film can also be removed conveniently with a plasma machine, if available. Insolubilized but not post-baked film is easily dissolved in acetic acid, containing a small quantity of potassium permanganate. However, post-baked resist is very stable, and it dissolves very slowly, even in a chromic acid cleaning mixture.

CONCLUSION

Epoxidized cis-1,4-polybutadiene insolubilizes very efficiently upon irradiation with electron beams. The relationship between the sensitivity and the degree of epoxidation of the polymer can be explained accurately by assuming that the insolubilization process of the polymer involves a chain reaction mechanism.

Thin films of the polymer insolubilize slowly, even in the absence of irradiation. However, this phenomenon can be eliminated by adding to the polymer a small quantity of some kind of stabilizer, such as trimethyl lauryl ammonium chloride.

The polymer can be used as a resist material in electron beam microfabrication systems. An electron beam exposure of 5×10^{-8} C/cm^2 is sufficient to insolubilize the polymer film on a substrate.

The authors are grateful to Mr. T. Otaka for his work with the scanning electron microscope, and to Mr. Y. Honda for his assistance in the electron beam exposure experiments.

REFERENCES

[1] T. Hirai, Y. Hatano, and S. Nonogaki, *J. Electrochem. Soc., 118,* 669 (1971).
[2] B. Broyde, *J. Electrochem. Soc., 116,* 1241 (1969).
[3] H. Y. Ku and L. C. Scala, *J. Electrochem. Soc., 116,* 980 (1969).
[4] A. Maekawa, C. Munakata, Y. Miura, Y. Honda, N. Siatou, and S. Nonogaki, *Jap. J. Appl. Phys., 10,* 810 (1971).
[5] S. Yonezawa, Y. Kando, S. Kasai, and A. Maekawa, *Jap. J. Appl. Phys., 10,* 1279 (1971).
[6] A. Maekawa, N. Saitou, Y. Honda, and Y. Miura, *Jap. J. Appl. Phys., 10,* 1658 (1971).

RADIATION CHEMISTRY OF EPOXIDIZED POLYBUTADIENES-NEGATIVE ELECTRON BEAM RESISTS

E. D. FEIT, R. D. HEIDENREICH, and L. F. THOMPSON

Bell Telephone Laboratories,
Murray Hill, New Jersey 07974

SYNOPSIS

Epoxidized polybutadienes are potential candidates as resists for electron beam lithography. They are very sensitive to low doses of radiation ($\sim 10^{-8}$ C/cm^2, $\sim$ 0.08 Mrad). At these low doses they crosslink and insolubilize by a very efficient chain process. At higher doses, the chain process for crosslinking becomes progressively more inhibited. The inhibition causes an unexpectedly slow rate of formation of crosslinked film. Changes in epoxy content (0.26-0.86 mole fraction) effect no major changes either in threshold dose for gel formation or in the rate of gel formation. Thin films were generally less sensitive to radiation than thick films.

INTRODUCTION

Electron lithography is expected to offer several advantages over photolithography in the fabrication of microcircuits. Increased miniaturization and resolution below the limits of photolithography is achieved by exposure with a scanned electron beam of small diameter ($\sim$ 100 Å). By programming the scan of the beam, a mask-free exposure is possible. Improved resist performance is achieved with electron lithography for two reasons. First, many more polymeric materials are available, since sensitivity to a narrow radiation energy window (3000-6000 Å) is not a prerequisite for their choice. Secondly, pure polymer systems can be used. High resolution pattern delineation has been reported at low voltage exposure of negative, crosslinking electron beam resists [1].

This paper discusses the radiation chemistry of epoxidized polybutadienes, a crosslinking polymeric material, with particular emphasis on those features that are lithographically important. A general theory of radiation effects on polymers has been developed, principally by Charlesby [2, 3]. Epoxidized polybutadienes were chosen for comparison to this theory, since they have been reported by Nonogaki to be extremely sensitive to electron radiation and serve as good electron resists [4].

EXPERIMENTAL PROCEDURES

1, 4-Polybutadiene (B. F. Goodrich Chemical Company, Ameripol CB221, 98% *cis*) was epoxidized by a method similar to that of Nonogaki [4]. A 5 to

Applied Polymer Symposium No. 23, 125-138 (1974)

10% excess of the calculated amount of a titrated solution of peroxyacetic acid in acetic acid [5, 6] was added in 0.5 hr at 45°C to a 3% solution of polybutadiene in toluene or toluene and chlorobenzene. One hour after addition was completed, the reaction mixture was washed with an equal volume of water. The aqueous layer was discarded, and the organic layer was dripped into at least 10 times its volume of chilled methanol. The polymer separated as a white, rubbery solid, and was purified by a second precipitation in methanol from a 5% dioxane solution. The material was then stored as a dioxane solution.

The polymer was spin coated from solution to the desired thickness on a 2000 Å layer of silica on a silicon wafer using standard techniques [7]. The resulting films were exposed with a 5 kV electron beam in a Cambridge Stereoscan Mark II scanning electron microscope. The dose was varied by adjusting either the current or time. The films were developed by dissolving the unexposed areas in a moderately effective solvent, such as dioxane-butanone or toluene-benzene in 3:1 ratios.

The area of developed film was measured by optical microscopy with a calibrated filar micrometer eyepiece. The exposure dose is reported in Coulombs per cm^2 (C/cm^2) as the product of the specimen current and the exposure time divided by the developed area. The developed area is not expected to differ greatly from the exposed area. The samples were then gilded with standard vacuum evaporation techniques, and the thickness of the polymer film was measured by polarization interferometry at 5890 Å [7]. A filar micrometer eyepiece was used to determine the fringe displacement relative to the fringe to fringe distance. The direction and order of the fringe displacement was seen using white light. The thickness of the film is reported as a normalized thickness that remains invariant with higher doses, rather than as a fraction of the initial thickness. The accuracy of the measurement on the same exposed area or an adjacent area was found to be ± 200 Å. Prolonged development (100 times longer than necessary) gave slightly lower thickness values, but the uncertainty was still within the range found for duplicate sets of exposures in which the developing rate was kept constant. A minimum set of ten exposures was made during each measurement. Frequently, a set of measurements was reinvestigated two or more times. Scatter in the data appears principally in comparing sets of exposures rather than in comparing exposures within a single set.

Calorimetric data were obtained with a Perkin-Elmer differential scanning calorimeter Model 1.

RESULTS

The epoxy content of the polymer was determined by quantitative nuclear magnetic resonance spectroscopy [8]. The fraction of epoxidized double bonds in the polymer was calculated by measuring the area of the olefinic proton absorbances (δ 5.2) and the area of the ring proton absorbances of the epoxy group (δ 2.4). The epoxy content is the ratio of the epoxy area to the sum of the epoxy and olefinic areas. This analysis slightly exaggerates the epoxy content since it neglects to record those units of the polymer that are neither vinyl nor epoxy groups. Such units are known to be present at about 5% from infrared

TABLE I

Epoxy Content and Elemental Analysis of Electron Resist Polymers

Polymer	Epoxy Content[a]	Calculated[b] Composition,%			Experimental[c]		
		C	H	O	C	H	O
CB221	0.00	88.82	11.18		88.55 88.72	11.59 11.40	
EPB-11	0.23						
EPB-7	0.50	78.70	9.91	11.41	74.33 74.75	9.63 9.63	15.36 15.57
EPB-9	0.54						
EPB-8	0.70	74.63	9.40	15.99	70.72 71.15	9.28 9.11	20.29 20.76
EPB-6	0.86	71.38	8.99	19.63	70.15 69.88	8.91 8.65	21.06 20.87

[a]Determined by NMR spectroscopy.
[b]Calculated from epoxy content.
[c]Determined by Midwest Microlab, Inc., Indianapolis, Indiana.

spectroscopy and elemental analysis. The additional units are hydroxyl and carbonyl groups resulting from ring opening of the epoxy groups, and/or from oxidation of the main chain. The epoxy content and the results of elemental analysis are given in Table I. The nmr technique is superior to titrometric methods [9], because the conditions required to give consistent and rapid analysis for epoxy groups do also crosslink and precipitate the polymer.

The molecular weights of the epoxidized polymers were determined by gel permeation chromatography. The values of $\overline{M}_n$ and $\overline{M}_w$ are given in Table II and

TABLE II

Molecular Weight and Dispersity

Material	$\overline{M}_n$	$\overline{M}_w$	$\overline{M}_w/\overline{M}_n$
CB221[a]	77,000	204,000	2.65
EPB-11	50,600	174,500	3.45
EPB-9	52,500	143,700	2.74
EPB-8	46,100	116,900	2.54
EPB-6	45,800	94,800	2.07

[a]Data supplied by B. F. Goodrich Chemical Company.

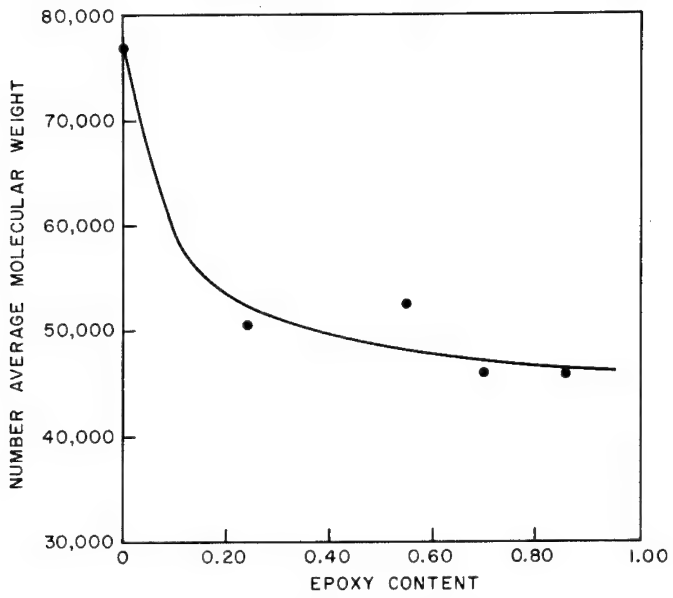

FIG. 1. Number average molecular weight as function of epoxy content.

shown in Figures 1 and 2. $\overline{M_n}$ initially decreased rapidly as the epoxy content increases, and then more slowly, indicating that rapid chain scission predominates in the early stages of epoxidation. $\overline{M_w}$, on the other hand, decreases almost linearly with epoxy content. The dispersivity $(\overline{M_w}/\overline{M_n})$ increases rapidly with low epoxy conversion, and then decreases toward a value of 2, as indicated in Table II. The latter value represents the dispersivity of a polymer that has undergone random scission [2, 10].

The glass transition temperature, melting point, and heat capacity of the cis-1, 4-polybutadiene (CB221) and the most highly epoxidized material (EPB-6) were determined. The results are compared in Table III. The conclusion is drawn from these two extreme cases that all the polymeric materials described in this paper were evaluated above their glass transition temperature.

Effect of Epoxy Content

The sensitivities of the five EPB's and of CB221 at 5 kV are shown in Figures 3a–f. Generally, the shapes of the curves are similar. At an initial film thickness of 4500 to 5000 Å all the resists, except EPB-8, began to gel at doses $\leqslant 5 \times 10^{-9}$ C/cm^2. EPB-8 became detectibly cross-linked and insoluble at $\sim 1.5 \times 10^{-8}$ C/cm^2. All the EPB's attain maximum thickness between 5×10^{-7} and 2×10^{-6} C/cm^2. The threshold dose (D_g^i), the final-thickness dose (D_g^o), the final thickness (z_i), and the slopes of the linear portions of the curves from 20 to 90% of the final thickness are given in Table IV. It is clear that

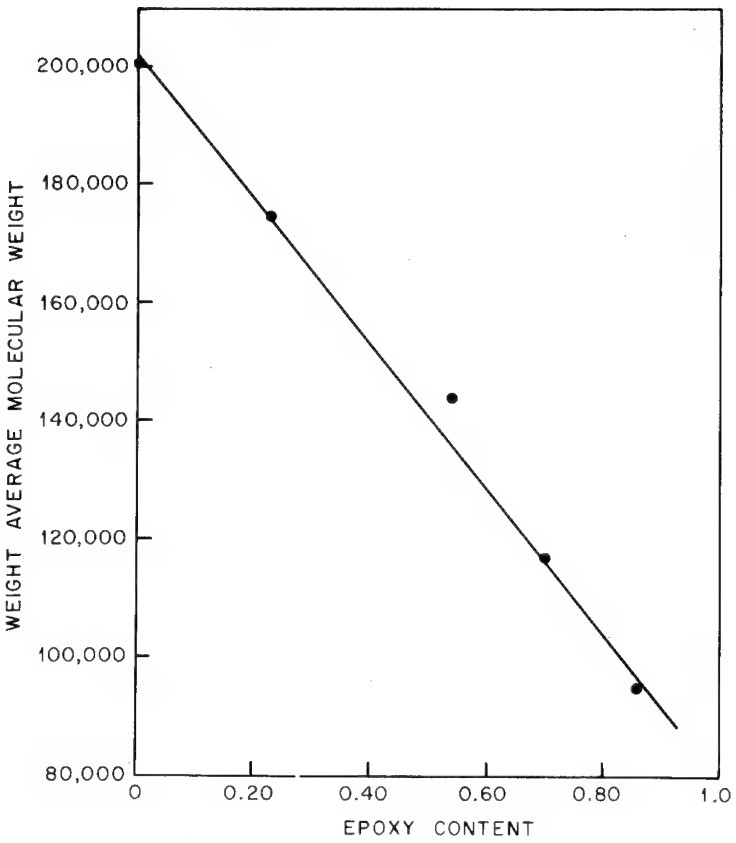

FIG. 2. Weight average molecular weight as function of epoxy content.

both D_g^i and D_g^o are independent of the degree of epoxidation. EPB-8 appears similar to the other materials, except that D_g^i is slightly displaced towards higher doses. However, none of the materials exhibit as low a final-thickness dose (D_g^o) as reported by Nonogaki et al. [4].

Effect of Initial Film Thickness

Two initial film thicknesses, 4500-5000 Å and 2000-2200 Å, were studied for several epoxy contents. A tendency toward lower sensitivity for the thinner film appears in all cases studied as indicated in Figures 3a, b, d, and f. EPB-6 is least sensitive to thickness, whereas EPB-11 and CB221 display pronounced shifts in sensitivity. This difference in sensitivity is further magnified when absolute film thickness is considered, rather than fractional thickness. For example, it requires an order of magnitude lower dose to obtain a final thickness of 2000 Å from a film of EPB-6 with an initial thickness of 5000 Å, than from a film with an initial thickness of 2000 Å.

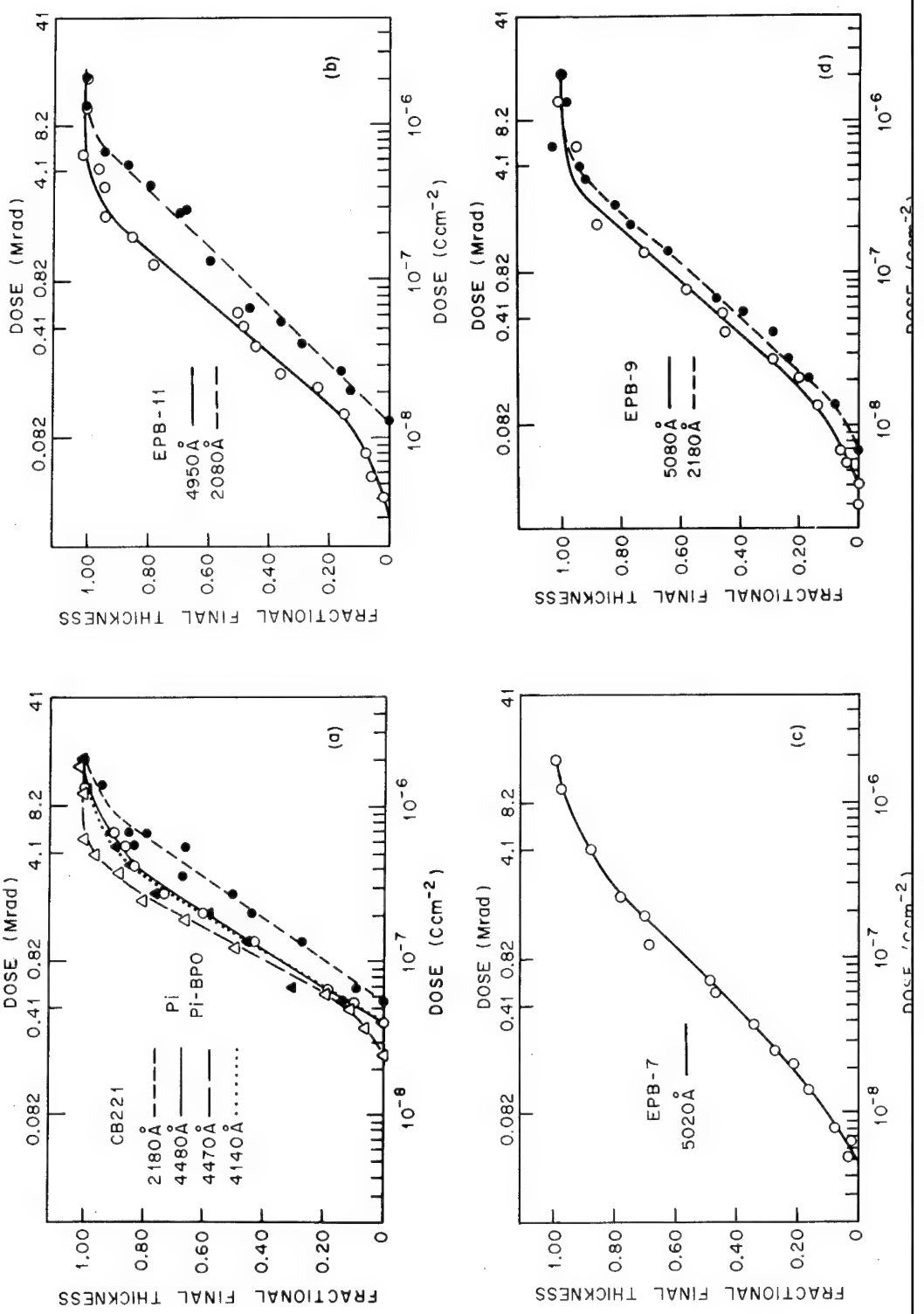
(a)
CB221
2180Å
4480Å
4470Å
4140Å
Pi
Pi-BPO
(b)
EPB-11
4950Å
2080Å
(c)
EPB-7
5020Å
(d)
EPB-9
5080Å
2180Å
DOSE (Mrad)
0.082
0.41
0.82
4.1
8.2
41
DOSE (Ccm⁻²)
10⁻⁸
10⁻⁷
10⁻⁶
FRACTIONAL FINAL THICKNESS
0
0.20
0.40
0.60
0.80
1.00

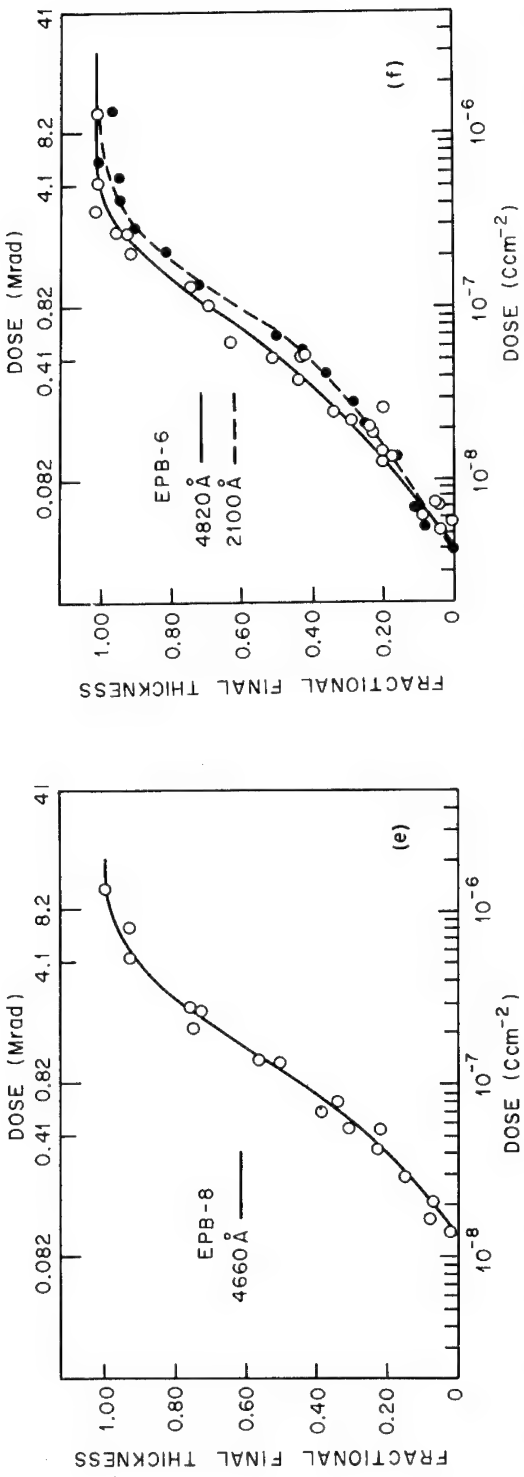

FIG. 3. Fractional final thickness of the polymers as a function of dose: (a) CB221, as received, precipitated (Pi), and precipitated and benzoyl peroxide added (Pi-BPO); (b) EPB-11; (c) EPB-7; (d) EPB-9; (e) EPB-8; (f) EPB-6. The order used is that of increasing epoxy content.

TABLE III

Calorimetric Data

Material	T_g(°C)	mp(°C)	C_p(cal/g°C)
CB221	-108	-10 to -5	0.100
EPB-6	- 20	+78	0.084

Effect of Additives

The effect of small amounts of added material on the sensitivity was examined in order to probe the mechanism of cross-linking and the importance of impurities in the polymer. Irganox 1010 (a commercial free-radical inhibitor) was used at 0.9 and 6.4% by weight, benzoyl peroxide (a free-radical initiator) at 1.1%, N-phenyl carbazole (an electron acceptor) at 1.0%, and chloranil (an electron acceptor) at 1.0%. The effect of these additives on the sensitivity of EPB-11 is shown in Figure 4. None of the additives effected a sensitivity differential large enough to give firm information about the mechanism of crosslinking. Generally, all the additives lower D_g^i to $< 2 \times 10^{-9}$ C/cm^2 and raised D_g^o to $\sim 1 \times 10^{-6}$ C/cm^2. This result can be explained by adhesion promotion and dilution effects.

Benzophenone was reported by B. Broyde [11] to affect the electron sensitivity of KTFR, a commercial photoresist, with a reduction of $D_g^o - D_g^i$ by a factor of 3.5. Benzophenone, added at 1.1%, did not produce a change in sensitivity of EPB-9.

The sensitivities of CB221 are shown in Figure 3a as received (with free-radical inhibitors and anti-oxidants), as precipitated once in alcohol, and with 1.2% benzoyl peroxide. It appears that the initial film thickness is more important than the history of the sample.

TABLE IV

Sensitivity Values and Radiation Yields

Material	Threshold Dose D_g^i, C/cm^2	Final Thickness Dose D_g^o, C/cm^2	Slope*	z_i, Å	E_g, eV/cm^3	E_M, eV/molecule
CB221	2.5×10^{-8}	6.0×10^{-7}	0.93	4480	1.1×10^{19}	1.4
EPB-11	3.5×10^{-9}	6.0×10^{-7}	0.61	4950	1.4×10^{18}	0.12
EPB-7	5.0×10^{-9}	1.9×10^{-6}	0.51	5020	1.9×10^{18}	0.16
EPB-9	4.0×10^{-9}	8.0×10^{-7}	0.58	5080	1.5×10^{18}	0.13
EPB-8	1.3×10^{-8}	1.3×10^{-6}	0.71	4660	5.5×10^{18}	0.42
EPB-6	4.0×10^{-9}	5.0×10^{-7}	0.62	4820	1.6×10^{18}	0.13

*Determined as Δthickness/Δlog (dose) in the linear portion of the plots.

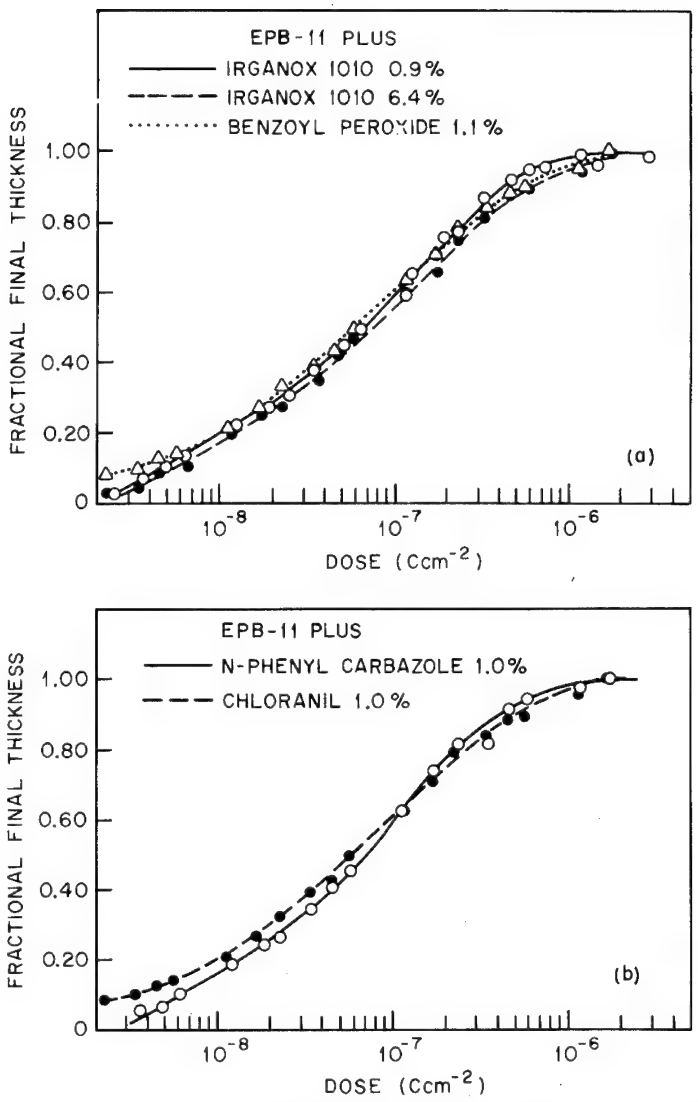

FIG. 4. Fractional final thickness of EPB-11 as a function of dose and of various kinds of additives.

DISCUSSION

Depth-Dose Function

Recently, Heidenreich et al. [12] developed a theory concerning the depth-dose response of polymeric films in relation to electron beam lithography. The depth-dose function for electrons is based on measurements of ionization as a function of beam penetration and of penetration of electrons as a function of

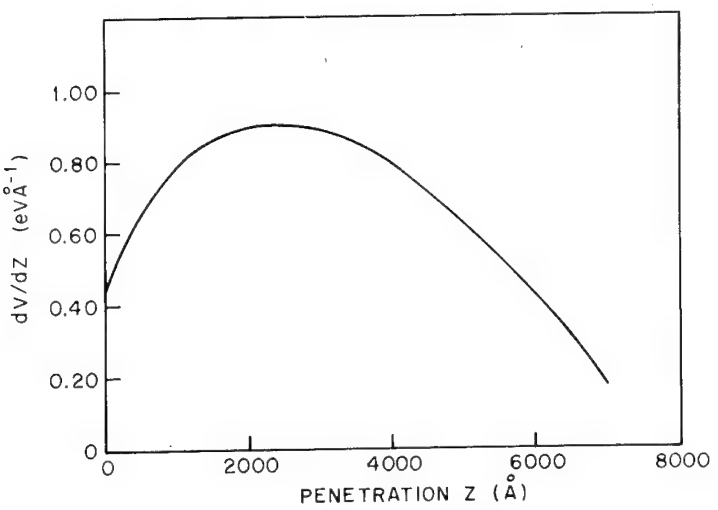

FIG. 5. Energy loss dV/dz as a function of penetration z.

accelerating potential. The specific energy loss (dV/dz) as a function of penetration (z) at 5 kV has been calculated from a normalized energy loss function and is shown in Figure 5. Heidenreich et al. described both a situation in which the total film thickness is less than the penetration distance for maximum energy loss and one in which the total film thickness is greater than the penetration distance for maximum energy loss. In the former case, the maximum energy density and the maximum initiation rate for crosslinking should occur at the film-substrate interface. In the latter case, maximum energy density and initiation of crosslinking occur in the body of the film, away from the interface. Experimental results showed that for these two cases, at constant epoxy content, the D_g^i value for the thick film is actually less than or equal to the value for thin films.

The energy loss function of 5 kV was integrated and is shown in Figure 6. When back scatter and secondary emission are neglected, the integrated function is almost linear to a film thickness of 5000 Å, with an absorption coefficient of 0.82 eV/Å. This coefficient has been used to determine the dose in Mrad (10^8 erg/g) as shown on the upper axis of several of the figures. For that purpose, the density of all polymers was assumed to be unity.

The Gel Point

The gel point is commonly defined as the point at which a crosslinked, insoluble network first occurs in the polymer [2, 3]. It is an important property for electron sensitive materials used in lithography [12]. In this paper the gel point is defined as the dose at which gel is first detected as a layer adhering to the substrate (D_g^i).

Two mechanisms for the formation of a crosslinked, insoluble network should be distinguished. In the first, each link in the network requires separate

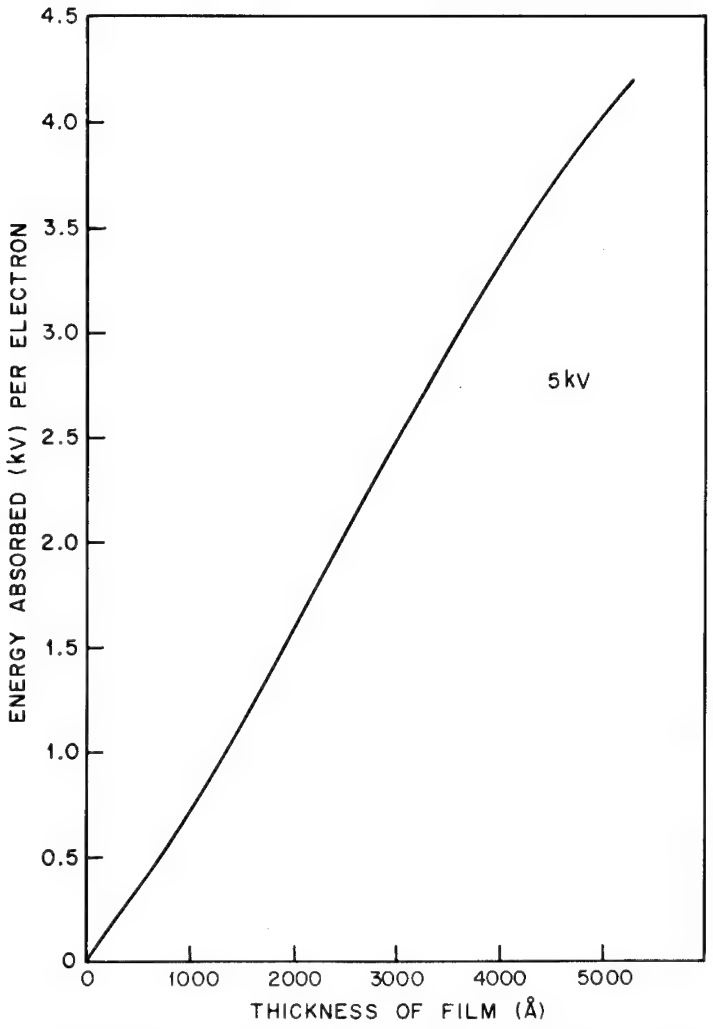

FIG. 6. Energy absorbed per electron as a function of film thickness.

activation by one or possibly two acts of ionization or excitation. In the other, a single ionization gives rise to a number of links via a chain reaction [2]. The gel energy can be calculated from radiation theory [12]:

$$E_M = E_g \frac{\overline{M_n}}{N \times d} = \frac{D_g{}^i}{e} \left(\frac{dV}{dz_i}\right) \frac{\overline{M_n}}{N \times d} \qquad (1)$$

where E_g is the gel energy in eV/cm^3, $\overline{M_n}$ is the number average molecular weight of the polymer, N is Avogadro's number, d is the density, e is the electronic charge, and dV/dz_i is the specific energy loss across the polymer thickness. Table IV shows that the value of E_M is normally less than 0.5

eV/molecule, which is characteristic for a radiation initiated chain polymerization, rather than a non-chain process [13].

Network formation in CB221 may also be a chain process, but the situation is not as clear as in the EPB's, since the radiation yield is not as high. Crosslinking efficiencies of about 10 have been reported for the free radical chain polymerization of *cis*-polybutadiene [14].

Chain Propagation of Network Formation

Charlesby investigated the radiation sensitivity of unsaturated polyesters as model systems for a theory on chain propagation of network formation [15]. The theory and the model are in good agreement and instructive when compared with results from the electron exposure of EPB's. The level of unsaturated acid in the polyesters ranged from 50 to 100%. The variation in sol fractions with exposure dose did not exceed 10% after the gel point was reached. Theory predicted such a slight dependence of sensitivity on the number of sites per molecule capable of forming a crosslink [2, 13]. A linear relation between the logarithm of the sol fraction and exposure dose was predicted [2, 13] and found in the polyesters [15].

The sensitivity of EPB's was invariant with the number of epoxy sites per molecule, just as the sensitivity of unsaturated polyesters is independent of the number of double bonds. Any small variation with epoxy content may be lost in the scatter of the data or compensated for by molecular weight changes. The EPB's, however, show a nearly linear dependence of gel fraction on the logarithm of the dose, as shown in Figures 3b-f. The fraction of the film remaining after exposure and development is practically equivalent to the gel fraction, since it remains almost unchanged in volume with prolonged extraction. Recently, Heidenreich [12] and Charlesby [13] predicted an exponential dependence on dose. Both theories agree that the rate of depletion of sol with dose is a function of remaining sol:

$$-\frac{d\,(sol)}{d\,D_g} \sim (sol) \times \text{Constant} \tag{2}$$

The observed dependence requires that the rate of formation of gel with dose is inversely proportional to the dose:

$$\frac{d\,(gel)}{d\,D_g} \sim \frac{\text{Constant}}{D_g} \tag{3}$$

Such a relationship is strongly self-inhibiting, whatever the details of the mechanism.

Radiation Induced Scission

Not all radiation initiated events lead to network formation. Radiation is known to degrade many polymers, even when the net reaction results in

crosslinking. Charlesby and Pinner [16, 17] have studied simultaneous crosslinking and degradation. When the ratio of degradation to crosslinking efficiencies exceeds 2, gel does not appear. The theory was developed for random crosslinking and random scission, and as expected, it does not describe the behavior of either the EPB's or CB221. Radiation induced scission, however, is believed to be important, because of the radiation chemistry of closely related materials.

The chemistry of the epoxy group is well understood [18]. The ionic polymerization of epoxy monomers is the chemical basis for commercially important poly(alkene oxides) and thermosetting epoxy resins [19, 20]. Free radical reactions on the other hand, lead to fragmentation and rearrangement but not to polymerization [18, 21]. The radiation polymerization of propylene oxide at low temperature has been described as both a cationic and an anionic process [22]. From model compounds it is inferred, therefore, that radiation crosslinking of EPB occurs through the epoxy groups by an ionic mechanism to form a network of 1, 2-diether links. Indeed, Nonogaki et al. observed the disappearance of epoxy and appearance of ether groups in the infrared spectra of EPB exposed to very high doses [4].

Polyethylene oxide can serve as a model for the 1, 2-diether links of the crosslinked network of irradiated EPB's. Salovey and Dammont reported that solid polyethylene oxide gels *in vacuo*, but the ratio of scission density to crosslink density remains very high, in the order of 0.6 [23]. The relatively large doses necessary to obtain high gel content in EPB's may arise from the efficiency with which crosslinks are cleaved by further radiation.

CONCLUSIONS

EPB's are very sensitive to low doses of radiation, $\sim 10^{-8}$ C/cm^2 or ~ 0.08 Mrad, which is almost a factor of 10 more sensitive than CB221. The threshold dose and the rate of gel formation do not increase with increasing epoxy content from 0.23 to 0.86. The original film thickness affects the sensitivity; thin films tend to be less sensitive than thick films. EPB's and CB221 cross-link and insolubilize by a very efficient chain mechanism at low doses. At higher doses chain crosslinking becomes progressively more inhibited; crosslinking in CB221 is less inhibited than that of the EPB's. The rate of formation of crosslinked film with dose was unexpectedly slow. The radiation-induced scission of the crosslinked network is proposed as a partial explanation for the slow rate of gel formation.

The authors thank J. L. Bartelt for independent sensitivity measurements on EPB-6 and EPB-11; F. J. Padden, Jr. for assistance in measuring volumes of the exposed films; E. P. Otocka for molecular weight determinations; and H. E. Bair for calorimetric data.

REFERENCES

[1] L. F. Thompson, E. D. Feit, C. M. Melliar-Smith, and R. D. Heidenreich, *J. Appl. Phys., 44,* 4048 (1973).

[2] A. Charlesby, *Atomic Radiation and Polymers,* Pergamon Press, Oxford, 1960.

[3] A. Chapiro, *Radiation Chemistry of Polymeric Systems,* Interscience, New York, 1962.

[4] T. Hirai, Y. Hatano, and S. Nonogaki, *J. Electrochem. Soc., 118,* 669 (1971).

[5] B. D. Scully and P. L. Williams, *Analyst, 87,* 653 (1962).

[6] T. W. Scully, D. Swern, and J. T. Scanlan, *J. Amer. Chem. Soc., 67,* 412 (1945); D. Swern, in *Organic Peroxides,* vol. 1, Interscience, New York, 1970, ch. 6.

[7] W. A. Pliskin and S. J. Zanin, *Handbook of Thin Film Technology,* McGraw-Hill, New York, 1970, ch. 11.

[8] A. J. Durbetaki and C. M. Miles, *Anal. Chem., 37,* 1231 (1965).

[9] H. Lee and K. Neville, *Handbook of Epoxy Resins,* McGraw-Hill, New York, 1967, pp. 4-14 to 4-18.

[10] P. J. Flory, *Principles of Polymer Chemistry,* Cornell University Press, Ithaca, N.Y., 1971, pp. 325–326.

[11] B. Broyde, *Bell Syst. Technol. J., 49,* 2095 (1970).

[12] R. D. Heidenreich, L. F. Thompson, E. D. Feit, and C. M. Melliar-Smith, *J. Appl. Phys., 44,* 4039 (1973).

[13] A. Charlesby, *Proc. Royal Soc. (London), A, 241,* 495 (1957).

[14] L. D. Loan, *Pure Appl. Chem., 30,* 173 (1972).

[15] A. Charlesby, V. Wycherley, and T. T. Grrenwood, *Proc. Royal Soc. (London), A, 244,* 54 (1957).

[16] A. Charlesby, *J. Polym. Sci., 11,* 513 (1953).

[17] A. Charlesby and S. H. Pinner, *Proc. Royal Soc. (London), A, 249,* 367 (1959).

[18] R. J. Gritter, *The Chemistry of the Ether Link,* S. Patai, Ed., Wiley-Interscience, New York, 1967, ch. 9.

[19] N. G. Gaylord, *Polyethers,* vol. I, Interscience, New York, 1963.

[20] H. Lee and K. Neville, *Handbook of Epoxy Resins,* McGraw-Hill, New York, 1967.

[21] A. Oku, M. Okano, and R. Osa, *Bull. Chem. Soc. Jap., 37,* 570 (1964).

[22] Y. Tabata, Y. Fujita, and K. Oshima, *J. Polym. Sci., B, 6,* 715 (1968).

[23] R. Salovey and F. R. Dammont, *J. Polym. Sci., A, 1,* 2155 (1963).

POLYDIALLYLORTHOPHTHALATE: A NEW HIGH SPEED THERMALLY STABLE ELECTRON RESIST

J. L. BARTELT

Bell Telephone Laboratories, Murray Hill, New Jersey 07974

SYNOPSIS

Electrons have been found to crosslink polydiallylorthophthalate (PDOP) with a sensitivity better than 10^{-6} C/cm^2. This sensitivity, together with PDOP's excellent adhesion to metals and SiO_2, has made it one of the most promising materials for electron-lithography. A complete electron-lithographic processing sequence for PDOP has been developed for this purpose, and some representative structures that have been patterned by electron-lithography and fabricated with PDOP as etching mask will be shown. The limiting resolution appears to be better than 500 lines/mm. Results of both DSC and TGA thermal analysis, used to determine the optimum temperature for postbaking and the region of thermal degradation, will be presented. PDOP shows only 15% weight loss at 275°C in air. Thus PDOP is especially useful in patterning processes requiring high thermal stability.

INTRODUCTION

Electrons have been found to crosslink polydiallylorthophthalate (PDOP) with a sensitivity of better than 10^{-6} C/cm^2. Electron resists with sensitivities this high allow the economic fabrication of microelectronics by direct electron beam exposure "on the wafer." Sensitivity alone, however, is not sufficient to make a good resist; resolution, defect density, adhesion, etch resistance, and processing must also be considered. Several epoxide-containing materials have been reported with high sensitivity to electrons [1], but PDOP has performed much more satisfactorily under actual device fabrication conditions.

PDOP is commercially available, and is usually prepared by homopolymerization of diallylorthophthalate at elevated temperatures and with ordinary peroxide catalysts. Because the monomer is bifunctional, the polymerization is extremely complex, and may result in soluble thermoplastic products or in insoluble thermosetting products. The soluble products, referred to as β-polymer or prepolymer, are isolated at low monomer conversions. They are believed to be composed of monomer units linked through one allyl radical per unit, with the other allyl radical left free. The numerous pendant allyl radicals are potential sites for crosslinking, and are probably responsible for the high electron sensitivity of the prepolymer. The prepolymer used in this study was specifically prepared for use as a resist material. A coating solution containing 15% by weight of the prepolymer in cyclohexanone was used for evaluation studies.

Applied Polymer Symposium No. 23, 139-145 (1974)

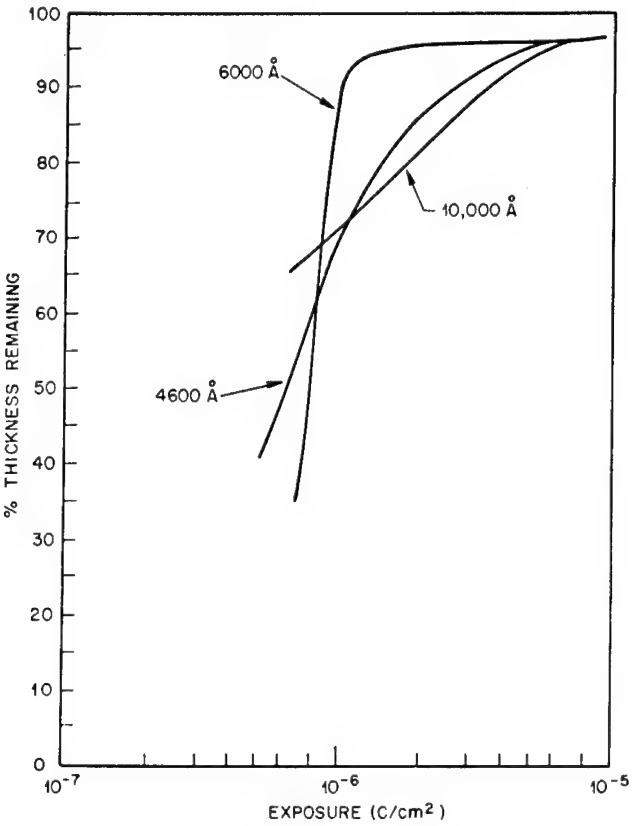

FIG. 1. Percent thickness remaining as a function of exposure of PDOP at 5 kV for different thicknesses.

EXPERIMENTAL

Coating and Film Thickness

The 15% PDOP solution yields films of excellent uniformity by spin coating, and if the solution is filtered and applied under clean conditions, the films are substantially free of defects. Films for this study were prepared by spin coating onto metallized or oxidized silicon wafers. A typical thickness of 0.6 μm was produced by spinning at 4000 rpm. Other thicknesses were produced by varying the spinning speed according to the formula:

$$T = 61.1\ S^{-0.557} \tag{1}$$

where T is the thickness in microns, and S is the spinning speed in rpm.

TABLE I

Linewidth in 0.6 μm Thick PDOP as Function of Voltage and Exposure, μm*

	Exposure, C/cm^2		
Voltage, kV	4×10^{-7}	8×10^{-7}	1.6×10^{-6}
5	2.94	3.54	4.26
7	2.64	3.70	4.08
10	2.34	3.06	3.66

*Nominal linewidth is 3.0 μm.

Exposure, Sensitivity, and Resolution

Exposure characteristics and patternability were determined for PDOP with a Cambridge Mark II Stereoscan scanning electron microscope, which was equipped with a digital pattern generator. The optimum dosage for PDOP has been found to depend on (a) initial thickness, (b) accelerating voltage, (c) substrate density, (d) development, and (e) resolution required for a given beam size and address structure of the pattern generator.

In Figure 1 the percent thickness remaining after exposure and development for a number of PDOP samples of different initial thicknesses are plotted as a function of exposure at 5 kV. Otherwise the samples were treated identically. Note that the general exposure range for crosslinking PDOP is 5×10^{-7} to 5×10^{-6} C/cm^2. Even more important is the result that as the initial resist thickness approaches the Bethe range for the electrons (0.66 μm at 5 kV in PDOP) the slope of the thickness vs. exposure curve increases. The steeper slopes are desirable since they present the system with higher contrast, sharper relief images, and better resolution.

For initial resist thicknesses in the order of 0.5 μm or more one observes an apparent increase in the sensitivity of PDOP as the accelerating voltage is decreased. This effect amounts to about 7×10^{-8} $C/cm^2/kV$ in the range from 5 to 10 kV. Two problems arise, however, in trying to take advantage of this sensitivity increase by arbitrarily decreasing voltage. First, the electron penetration range falls off with voltage, and at the desired thicknesses there is not enough penetration at voltages below 5 kV to obtain critical dosages at the substrate interface. The second limiting problem is that linewidth appears to be sensitive to accelerating voltage and exposure.

Table I shows a series of measurements on the variation of linewidth as a function of dosage and voltage in a 0.6 μm PDOP film on SiO_2. The exposures

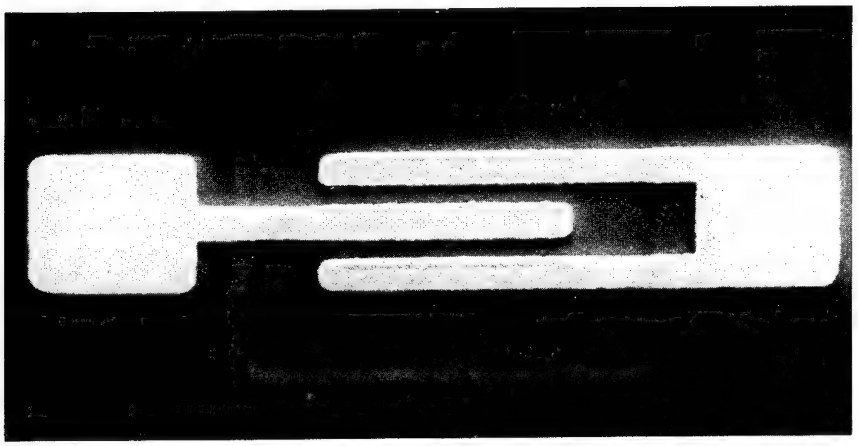

FIG. 2. An experimental transistor fabricated with PDOP, showing 2.5 μm stripes.

used for this determination were line and space patterns of nominally 3 μm wide. They were derived by blanking a raster scanned beam for 12 out of each 24 lines, while the pattern generator was set for 4 lines per micron. The data show that linewidth increases with decreasing voltage and with increasing exposure. The data have been fitted to empirical functions, and analysis shows that linewidth variations can be minimized with respect to exposure variations at constant thickness remaining, if an accelerating voltage of 6.9 kV is used. It is expected that this optimum voltage will be higher for thicker resist films. If exposures are made at 6.9 kV, the dosage required to produce lines and spaces of exactly 3 μm is 5×10^{-7} C/cm^2. This dosage results in 45% of the original thickness remaining. If the dosage is increased slightly at 8×10^{-7} C/cm^2, the lines will widen to 3.6 μm, and the thickness remaining will be 62%.

Finally, the effect of substrate density on exposure should be mentioned. Exposures on metallic substrates require a dose from 1/3 to 1/2 less than that required for exposures of comparable patterns on SiO_2. This reduction is required to correct for the increased back-scattering from the metal surface.

Solubility and Development

The solubility of PDOP has been studied in approximately twenty-five selected organic liquids. The range of solubility parameters of good solvents was 9.3 to 9.8, with a few minor deviations due to polarity and hydrogen bonding considerations. The solvents were typically nonhydrogen bonding and exhibited low fractional polarity.

On the basis of these solubility tests, developers and rinses were formulated for scum-free development and minimum swelling for good pattern definition. Effective developers were formulated by blending good solvents, such as 1, 2-dichloroethane, chlorobenzene, or diethylene glycol monoethyl ether, with diluents, such as the aliphatic acetate esters. Rinses which were compatible with these developers and had desirable evaporation rates were taken from the

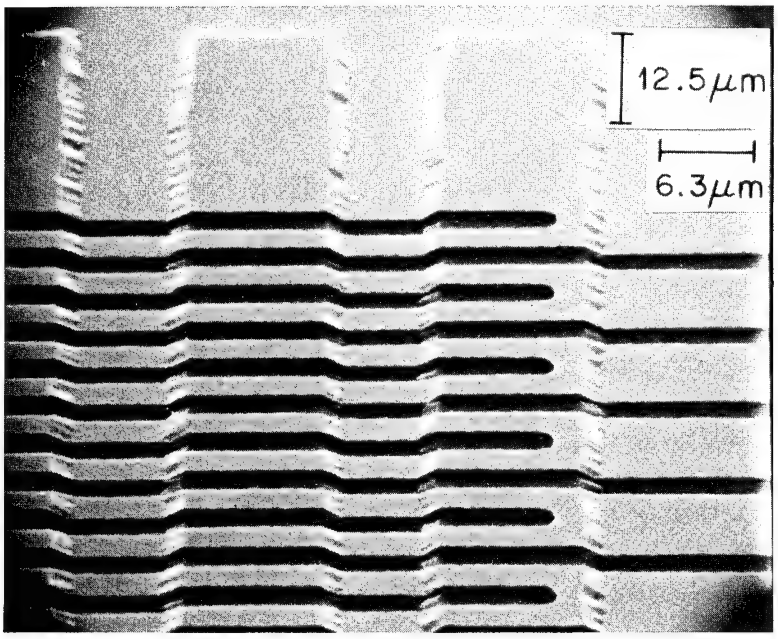

FIG. 3. Metal meander patterns over 0.6 μm oxide steps.

marginal and poor solvents, such as isopropyl alcohol or the aliphatic acetate esters. While PDOP can be tray developed or spray developed by hand with air brushes, automatic spray developers are capable of better uniformity and reproducibility; they were thus used in this study.

Baking, Crosslinking, and Thermal Stability

One of the most difficult tasks in establishing an optimum resist processing sequence is to find the best time-temperature cycle for baking. A new approach to this problem was taken with PDOP by using differential scanning calorimetry (DSC) and thermogravimetric analysis (TDA), to find the temperatures of solvent removal, crosslinking, and thermal degradation. DSC and TGA thermograms were run in air ambients at a heating rate of 10°C/min. The DSC thermogram clearly showed solvent removal up to about 130°C. Between 150°C and 170°C a small exotherm appears, which is believed to be due to crosslinking. A large exotherm, which begins at about 200°C and extends out to 350°C, is indicative of thermal degradation. On the basis of these results, the processing of PDOP as an electron resist includes pre-baking at 100–130°C to remove coating solvent, and a post-bake at 170–190°C after development to remove development solvents and to complete crosslinking of the polymer. While isothermal DSC analysis shows that crosslinking is complete at these temperatures within a few minutes, it has been found necessary to bake for at least 30 min to promote adhesion.

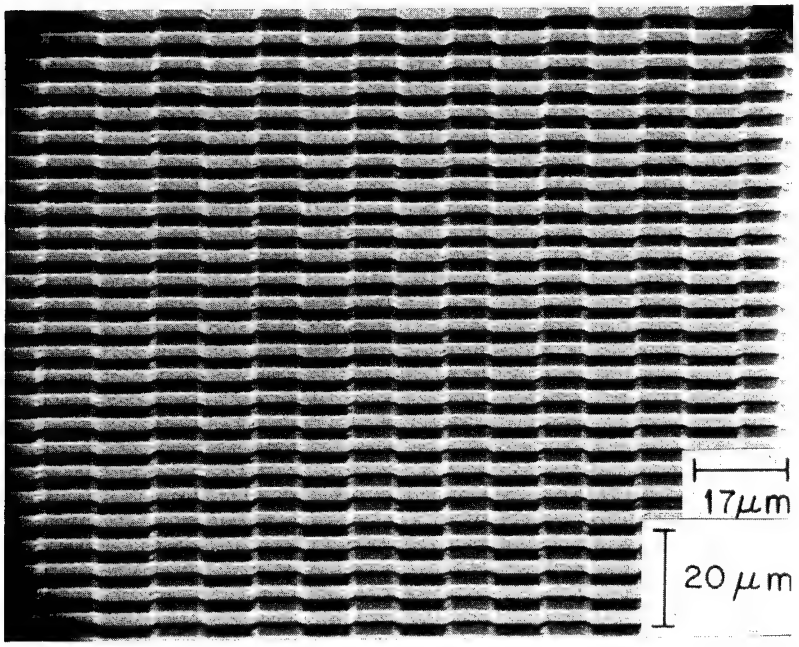

FIG. 4. Expanded view of Fig. 3.

The DSC curve suggests excellent thermal stability for PDOP, and that conclusion is confirmed by TGA. The TGA thermogram shows less than 15% weight loss up to 275°C. The onset of major weight loss does not occur until the range of 300–325°C is reached. This has many implications about new uses for PDOP in applications where thermal stability is required. For example, thermal stability plays a role in sputter etching or ion-milling. It is also possible to evaporate or sputter metals over PDOP patterns without fear of flow or degradation due to heating.

Stripping

The removal of PDOP, after patterns have been defined and etched, requires the use of an oxidizing agent. In particular, a dichromate-sulfuric acid cleaning solution (Allied Chemical RT-1 Photoresist Stripping Solution), warmed to 100–120°C, was used successfully. Other commercial proprietary strippers, such as A-20 or A-30 (Allied Chemical) and J-100 (Indust-Ri-Chem Co.), as well as oxygen plasma stripping or heating in ozone, may be used successfully where circumstances dictate.

CONCLUSIONS

Polydiallylorthophthalate (PDOP), when processed as described above, is one of the most promising negative electron resist materials available. Its primary

advantages are high speed, fine resolution, good adhesion to metals and SiO_2, good etch resistance, and thermal stability. PDOP and its processing have proven to be completely dependable with continuous usage in several device fabrication studies. For example, Figure 2 shows an experimental transistor with PDOP used for each oxide and metallization etching step. While the geometry is not submicron (center-to-center spacing of the metal stripes is 5.0 μm), working transistors were made in good yields, where the PDOP process proved to be highly reliable. Figures 3 and 4 show metal meander patterns over oxide steps as another example of process reliability. The patterns had lines which were 0.2-0.25 μm thick, 2.5 μm wide, and had an aggregate length of about 100 mm, with somewhat more than 11,000 steps over 0.6 μm thick oxide. Measurements showed these patterns to be electrically continuous, again proving the reliability of PDOP under very realistic test conditions.

The authors would like to thank P. W. Shackle and R. F. Helm for making their data and SEM photomicrographs of the transistor and meander pattern experiments available.

REFERENCES

[1] T. Hiari, Y. Hatano, and S. Nonogaki, *J. Electrochem. Soc., 118,* 669 (1971).

THE STUDY OF FIBER FRACTURE

J. W. S. HEARLE and B. LOMAS

University of Manchester Institute of Science and Technology, Manchester, M60 1QD, England

A. R. BUNSELL

School of Applied Sciences, University of Sussex, Falmar, Sussex, England

SYNOPSIS

The introduction of the scanning electron microscope has bridged the gap between optical and conventional transmission electron microscopy with regard to magnification range, depth of field, and specimen manipulation. It has made a close study of the fracture morphology of textile fibers possible. As a result the various forms of fiber fracture can now be classified. This paper presents brief summaries of the different classes of fracture, together with variants that have been encountered. Some explanations of the breaking behavior are given, although as yet many fracture modes are not fully understood. Mention is made of preparation and mounting techniques that were especially developed to handle textile fibers, the majority of which have diameters of only a few micrometers.

INTRODUCTION

The advent of scanning electron microscopy has opened up the subject of fiber fractography, because it is now possible to see the whole specimen in focus. In comparison, the optical microscope has a very limited depth of focus. The general features of a fiber fracture are clearly visible on SEM micrographs of low magnification, and much fine detail can be examined at higher magnification. Fiber fracture research is important for several reasons: (a) for its general scientific interest; (b) for the insight into mechanisms of failure in fibers, and thus as a guide to the possibility of improving of fiber properties by the producer; (c) for the insight into the causes of failure in use and processing, and thus as a guide to improvement in processing methods or into the construction of yarns, fabrics, and garments; (d) as a means of diagnosis for causes of failure.

The extensive amount of work on this subject at the Institute can be briefly summarized by a classification of the forms of fracture that have been observed. However, there are many variants and combinations of the basic fracture forms, and a full account of the studies on different modes of fracture of different fibers is, or will be, contained in other manuscripts.

Applied Polymer Symposium No. 23, 147-156 (1974)

SEM EXAMINATION

Every facet of the fracture surface of a fiber has to be examined, usually from more than one angle, to understand fully its morphology. Therefore, a fractured fiber must be mounted in such a manner that the break can be thoroughly examined without having to resort to remounting techniques. A specially adapted specimen stub has been developed, in which fractured fibers are held in an upright position [1]. This stub has a platform, a little thicker than the conventional stub, from which a step has been cut. The two parts of the stub are held together by a small screw. The hole in the step portion has an eliptical shape, to allow a millimeter or so of movement between the two parts of the stub.

The commonly used textile fibers have very small diameters compared with their length, and it would be impossible to mount them satisfactorily directly into the stub. To facilitate handling, the fibers are laid on the adhesive side of adhesive tape, so that the fractured ends project about 1 mm from the edge of the tape. The fibers are then sandwiched between the adhesive sides of the tape, and a strip containing the fibers is cut out and inserted into the split stub. The two parts of the stub are pushed together and screwed firmly in position. The fiber ends are now held in place in an upright position across the diameter of the stub. The assembly is ready for coating with silver or gold. Several fibers can be examined at a time, and it is simple to note their order in relation to the fold in the adhesive tape. The split stub can also be used for examining cross-sections of cloth, film, broken wire, and failed tungsten filaments.

It is important to note that the fiber ends should not project more than a millimeter or so from the edge of the tape, as there is a danger of fiber movement in the beam with greater lengths, particularly with fibers of very small diameters.

Sometimes it is necessary to examine a long split or crack in a fiber. In these instances it is more convenient to lay the fiber on the surface of a conventional stub. With wet adhesives it is very likely that such fine fibers will sink in, and a detail may be covered with glue. Therefore, other methods of mounting have to be used. Textile fibers are poor conductors of electricity, and to prevent charging they must have good contact with the stub, in addition to having to be coated with a suitable conducting material, such as gold or silver. In our experience, just adhering the ends of the fiber to the stub is not entirely satisfactory. A better method is to lay the fiber on a stub covered with a double side adhesive tape. However, such tape, like textile fibers, is a poor conductor and will exhibit localized charging in the SEM. This charging problem can be overcome by coating the tape with a conducting metal, e.g., gold or silver, before the specimen is mounted on it. The metal coating does not destroy the adhesive properties of the tape. A similar amount of metal as is normally used for sample coating is evaporated on the tape; the specimen is then mounted and the whole assembly recoated with metal. The fiber now has good contact with a conducting surface and has also received a conducting coating, both of which are

important requisites for good specimen preparation. This method of sample preparation is also used to good effect with textile fabrics.

Another type of adhesive tape is 3M's copper tape, which has one side coated with a conducting adhesive. If the copper tape is stuck to the stub with a conducting paint, so that the adhesive layer is upper-most, samples can then be laid directly onto the tape without prior metal coating. This method has worked satisfactorily with fabrics, and with aggregates of lead powder, where standard methods resulted in charging of the specimens. It has also been used successfully as a substitute for regular adhesive tape in preparing fractured fiber ends for mounting in the described split stub.

The procedures and stubs described all pertain to the Stereoscan SEM, made by Cambridge Scientific Instruments Ltd. Similar techniques and platforms can undoubtedly be designed for other SEM's.

CLASSIFICATION OF FIBER FRACTURE MORPHOLOGY

Studies of failure in both synthetic and natural fibers have revealed that a number of different fracture mechanisms exist for fibers, and that fiber fracture may be classified accordingly. A brief summary of each type of failure follows.

Brittle Elastic Failure

Glass fibers which are broken by a simple tensile pull behave as a classic Griffith material, with rapid failure following crack initiation at a surface fault. This mode of failure is typical of a brittle high modulus material. Highly extensible, elastomeric fibers probably fail in a similar manner.

Ductile Crack Growth

The failure of many synthetic fibers under simple tensile loadings involves crack growth of an inherently stable nature. Nylon, polyester, and some acrylic fibres fail from the surface, and during propagation the crack opens to a V-shape, due to plastic deformation ahead of the crack. Finally, catastrophic failure occurs, with the morphological result shown in Figure 1. Variants of the basic form are sometimes found.

This type of failure is not seen in other structures, and it has been shown to develop through several stages [2]. During the slow crack propagation stage, when drawing of the remaining material is occurring, it is necessary to increase the load continuously for further crack growth to result. A geometrically modified form of ductile crack growth occurs when nylon fibers are broken in torsion.

What appears to be a completely different fracture morphology occurs in the tensile fracture of light-degraded nylon, shown in Figure 2. However, this fracture is probably multiple ductile crack growth from internal voids.

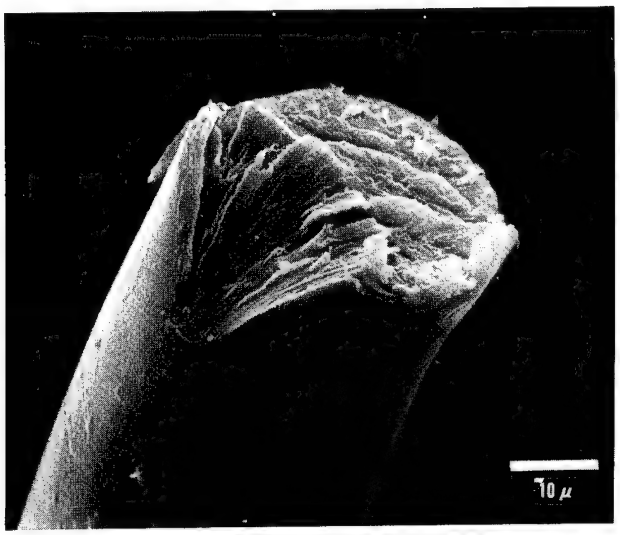

FIG. 1. Typical example of failure through ductile crack growth.

Axial Splitting

Some natural fibers, such as cotton, have a marked fibrillar composition, which give rise to splitting along their length [3]. Cotton consists of a fibrillar structure arranged in a helical spiral which reverses at intervals along its length. Failure is often associated with such reversal zones, although it rarely occurs

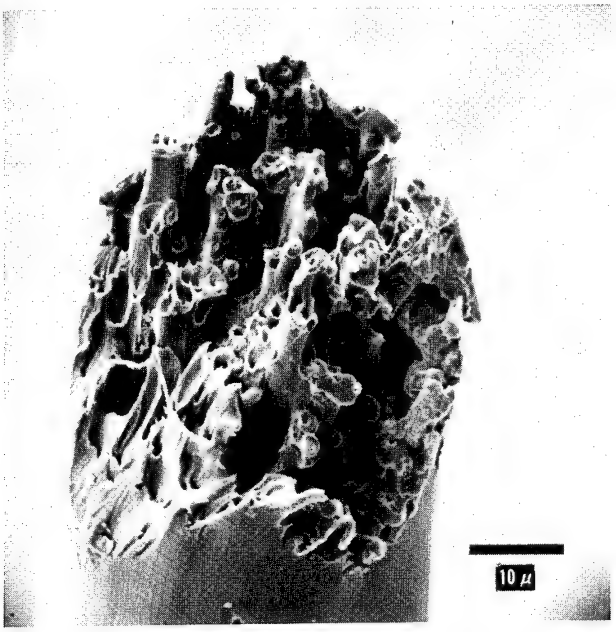

FIG. 2. Tensile fracture of light-degraded nylon.

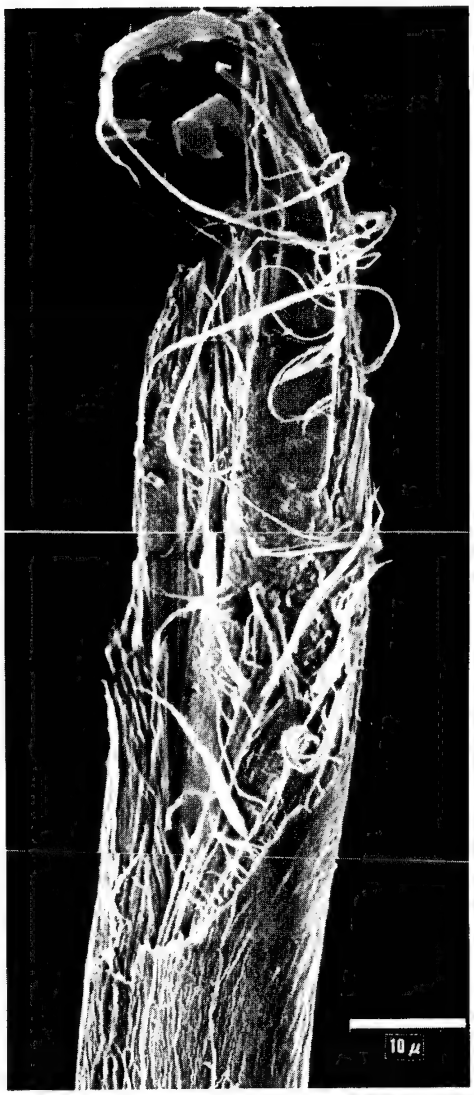

FIG. 3. Cotton fiber fractured after axial splitting.

exactly at a zone. Failure occurs after separation of the fibrillar structure and a final shear tear between ends of the split, as shown in Figure 3. Also in torsional fracture of some acrylic fibers, such splitting dominates.

Fracture Perpendicular to the Fiber Axis

Some acrylic fibers, such as Courtauld's Courtelle fiber, behave as though they are composed of bunches of fibrils, aligned along the fiber axis direction with poor cohesive bonds between them. In a simple tensile pull, Courtelle fiber

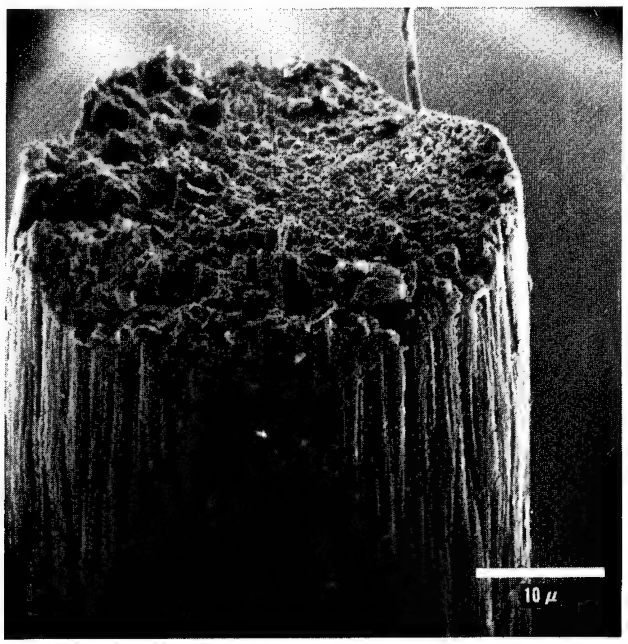

FIG. 4. Example of acrylic fracture perpendicular to the fiber axis.

is found to fail at the level of the constituent bunches of fibrils, and the crack may initiate internally at a particularly weak region. The surrounding fibrils then take up the load, and the fracture of subsequent bunches follows across a radial plane. Figure 4 is an example of such behavior, which is also similar to the fracture of reinforced materials but on a smaller scale.

Rayon, acrylic, wool, and crosslinked cotton fibers show breaks which run across the fiber, with no clear crack morphology and moderate roughness. In some instances separate perpendicular fractures are linked by an axial split.

Failure Along Kink Bands

When fibers of polyester are bent, lines at 45° to the axis may be observed on the inside of the bend, when viewed between crossed polars in the optical microscope. Such lines are known as kink bands. They are formed under compression and are regions of re-orientation due to shear forces. They can also be seen in nylon at elevated temperatures. Repeated flexing of such fibers leads to failure along these lines.

Axial Splitting Due to Tensile Fatigue

It has been demonstrated by Bunsell and Hearle [4] that fibers of nylon 66 can fail by a tensile fatigue mechanism, that results in a very distinctive fracture morphology. The fracture initiates at the surface, and then turns to run along

the fiber for several fiber diameters, until the load bearing cross-section is reduced sufficiently for tensile failure to occur, as exemplified in Figure 5. Fatigue failure occurs after about 10^5 cycles, and a necessary condition is that the cycling goes down to zero loading. If the cycling pattern is raised to a positive minimum load, but not so that the maximum load causes a tensile failure, the fiber will not suffer fatigue.

This type of behavior has also been found to occur with super-high tenacity nylon 66 fibers, which have undergone more drawing than those reported earlier. DuPont's aromatic polyamide fiber Nomex performs in a similar fashion.

Polyester fibers are found to fail by a similar mechanism, although the zero minimum load criterion has yet to be confirmed for these fibers. The angle of penetration of the fatigue fracture in polyester is smaller than in the polyamides, and a substantially longer longitudinal crack develops before failure.

Acrylic fibers examined for fatigue failure do not fail in the same manner, although they also split. The splitting may originate internally, and in this way it reduces the load-bearing cross-section until complete failure occurs. A precursor acrylic fiber used in manufacturing carbon fibers was found to fail under both cyclic and simple tensile loadings by splitting of its structure. The carbon fiber, however, was always found to fracture straight across a radial section.

Other Breaks and Fiber Ends

Examination of fiber ends can be used for diagnosis of the cause of failure. A nylon fiber cut with a razor blade has a different end than one cut with scissors, as shown in Figures 6 and 7. This type of information can be used to identify

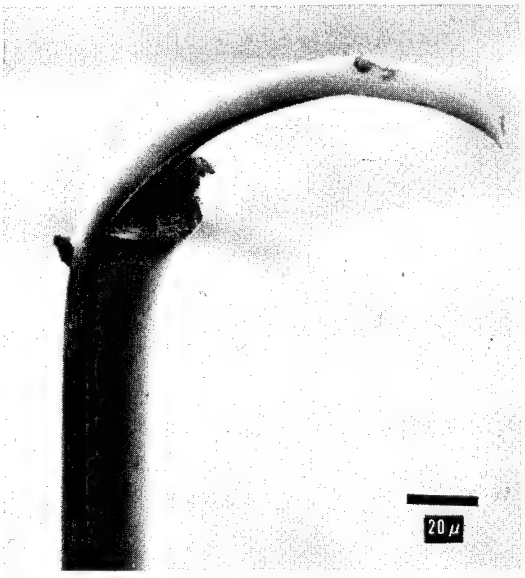

FIG. 5. Axial splitting due to tensile fatigue in nylon.

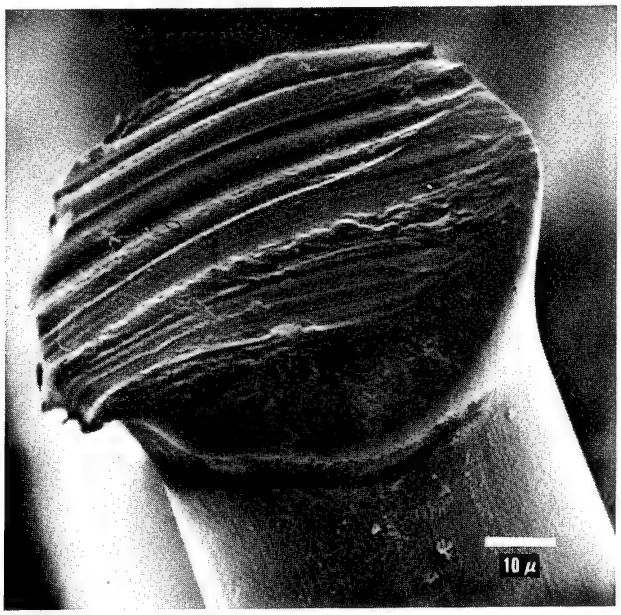

FIG. 6. Nylon fiber cut with razor blade.

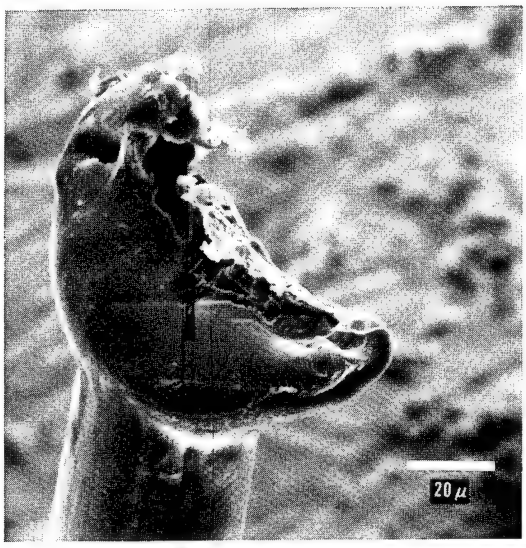

FIG. 7. Nylon fiber cut with scissors.

breaks occurring in the various manufacturing processes, such as stapling, singeing, and raising. It has also been observed that degradation of nylon fibers by chemical attack, heat, or light (see Fig. 2) can modify the normal tensile fracture pattern. This also applies to other fibers, as in the fracture morphology of raw and crosslinked cotton.

Breakdown of Fibers in Use

When fibers are subjected to normal "wear and tear," as in an article of clothing, they undergo various stresses and strains, such as bending, stretching, repeated flexing, and abrasion. They are also subjected to the effects of frequent laundering or dry cleaning. Therefore, the broken fibers present in a worn garment rarely result from a simple tensile pull. For instance, the hydrogen bonding in a cotton fiber is weakened by the presence of water. Figure 8 shows the effect of repeated laundering only on cotton sheets, whereas Figure 9 represents the type of damage present at the folds of collars and cuffs of a worn cotton shirt. The latter shows the combined results of frequent laundering, abrasion, and other stresses the fabric has suffered during use.

CONCLUSION

Scanning electron microscopy has made it possible to study fibers fracture morphology closely. This paper has demonstrated how fiber fractures can be separated into some basic types. Doubtless some additions and variations on the basic forms can be made, as other fibers and failure due to other types of stress are being investigated. However, the main features of the classification are probably now established.

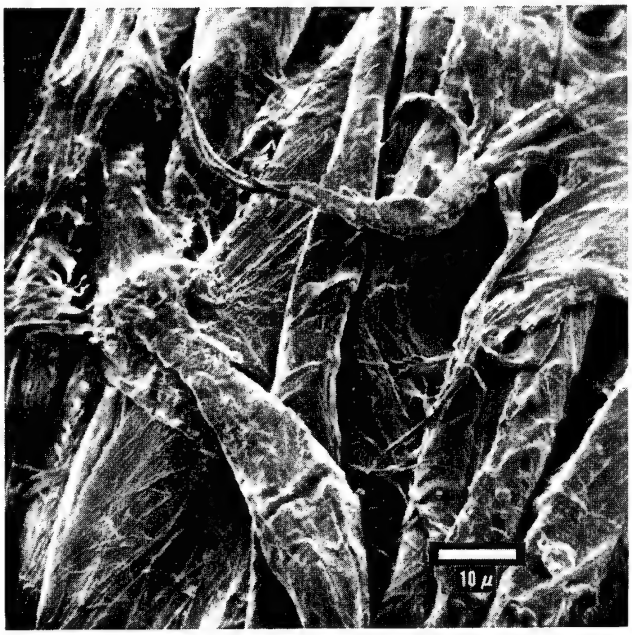

FIG. 8. Effect of repeated laundering only on cotton fabric.

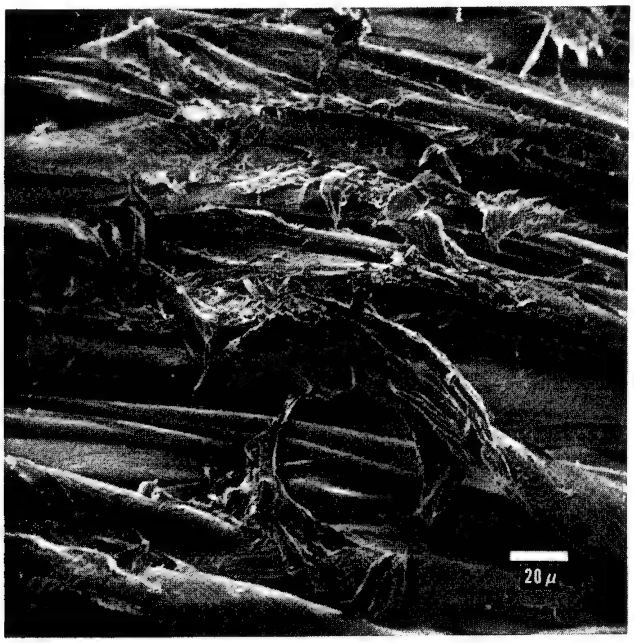

FIG. 9. Effect of laundering and wear in fold of collar of shirt.

There is now need for work on several other aspects of this subject matter. Apart from the classical brittle fracture of glass fibers, none of the fracture mechanics are understood, nor is the relation to fiber structure clear. In practical technology there is a need to study the influence of manufacturing conditions on fracture, and the forms of fracture which occur in typical conditions of use or processing.

The scanning electron microscope was made available through a grant from the Science Research Council, and parts of the work have been supported with grants from the Ministry of Defence and the International Institute for Cotton.

REFERENCES

[1] P. M. Cross, J. W. S. Hearle, B. Lomas, and J. T. Sparrow, *Proc. 3rd Annu. Scanning Electron Microscope Symp.*, IIT Research Inst., Chicago, 1970, p. 81.
[2] J. W. S. Hearle and P. M. Cross, *J. Mater. Sci., 5,* 507 (1970).
[3] J. W. S. Hearle and J. T. Sparrow, *Text. Res. J., 41,* 736 (1971).
[4] A. R. Bunsell and J. W. S. Hearle, *J. Mater. Sci., 6,* 1303 (1971).

STRUCTURE–PROPERTY RELATIONSHIPS OF POLYETHYLENE GRAFTED GLASS FIBER COMPOSITES

I. KAMEL, M. J. KOCZAK, and R. D. CORNELIUSSEN

Department of Metallurgical Engineering,
Drexel University,
Philadelphia, Pennsylvania 19104

SYNOPSIS

Radiation induced grafting of polyacrylic acid to the surface of glass fibers has been found very effective in enhancing the interfacial adhesion with polyethylene. Short length glass fibers, 390 μm long and 12 μm in diameter, were subjected to gamma radiation in the presence of acrylic acid vapor. The grafted polyacrylic acid did not exceed 1.0% of the fiber weight. Following grafting and molding, the polyethylene grafted fiber glass composites were fractured at 78°K and 300°K, and subsequently examined by scanning electron microscopy. The results indicate fracture morphology similar to that of commercially available composites which employ a silane treatment to the glass fibers. Both yield strength and elastic modulus were substantially improved for the grafted glass fiber composites. The microscopy results reveal a strong interfacial adhesion between the fibers and the polyethylene matrix. This adhesion was effective at liquid nitrogen temperature as well as at room temperature, and resulted in improved mechanical behavior.

INTRODUCTION

Glass fiber reinforcement provides an attractive means of enhancing the mechanical properties of organic polymer composites. However, a current limitation is the poor interfacial adhesion between the glass fiber and the polymer matrix. In order to alleviate this problem, commercial processes utilize silane coupling agents to improve interfacial bonding, thereby increasing composite strength. However, this method has some limitations: (a) it requires the selection of a proper coupling agent for each polymer, and this requires a tedious and lengthy study for each composite system; (b) the silane treatment increases the surface friction at the fiber surface, thus creating processing problems in the mixing of short glass fibers and polymer particles.

In this paper we present a new and improved method of enhancing the interfacial adhesion between the polymer matrix and the reinforcing glass fibers, resulting in an efficient load transfer at the interface and improved mechanical properties [1]. This method utilizes grafting of a polar monomer, acrylic acid (AA), to the surface of the glass fibers by γ-radiation. Subsequently, the poly(acrylic acid) (PAA) is crosslinked to the polymer matrix by heat, resulting in an effective interfacial bond between fiber and matrix. Such radiation

Applied Polymer Symposium No. 23, 157-165 (1974)

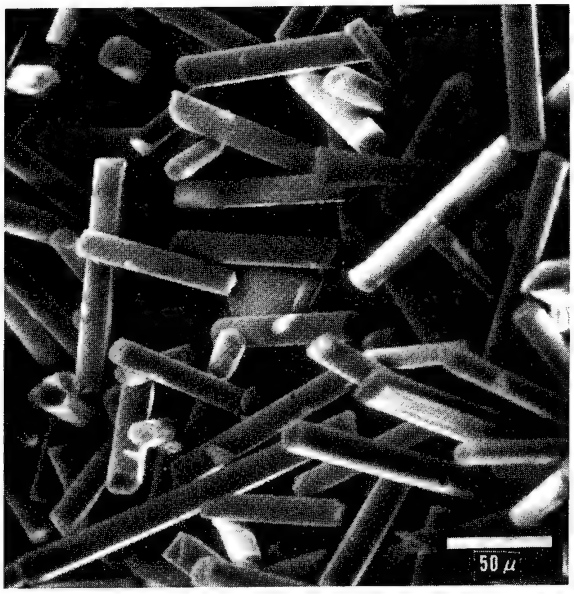

FIG. 1. Glass fibers as received; 300X.

processing appears to be applicable to a large variety of polymer matrices. In addition, the grafting of AA was found to have no effect on the flow and mixing characteristics of the composite, thus eliminating the processing problems attendant with silane treatments.

In a previous study, Kamel and Corneliussen reported on the improved tensile strength of high density polyethylene (PE)–glass fiber composites [1]. In

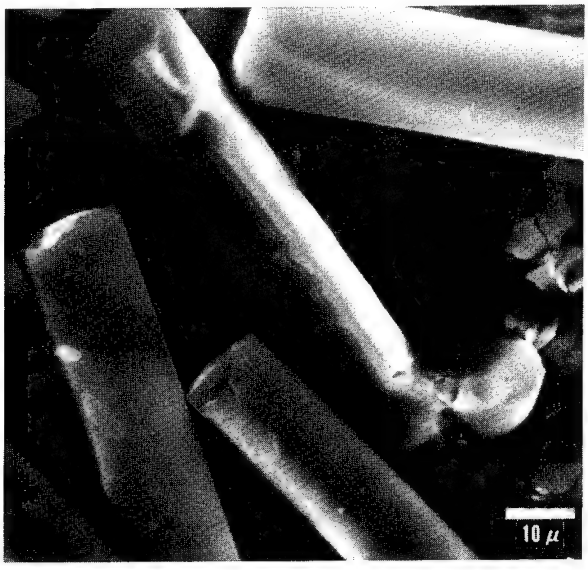

FIG. 2. Glass fibers, grafted with poly(acrylic acid); 1000X.

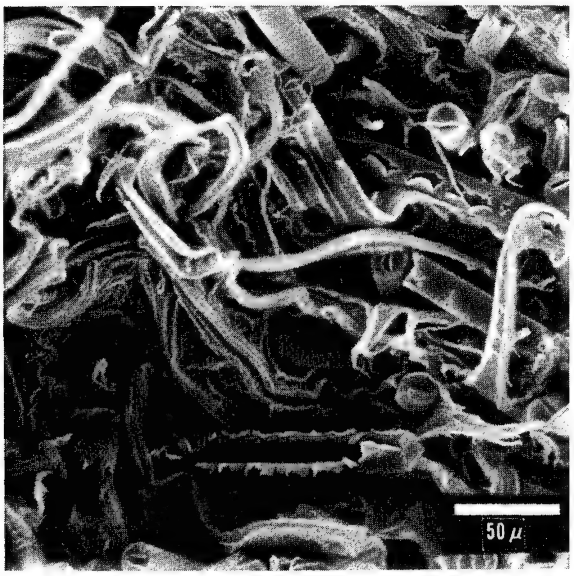

FIG. 3. Fracture surface of ungrafted composite at 300°K; 300X.

this paper we will examine the fiber/matrix interface by scanning electron microscopy, thus providing a structure/property correlation that may be related to the processing history.

EXPERIMENTAL

Materials

Untreated Vitro Strand G chopped glass fibers (Johns Manville Co.) with an average length of 390 μm and a diameter of 12 μm were used as the reinforcing phase (Fig. 1). The polymer matrix was a high density polyethylene, Fortiflex A60-900N (Celanese Co.), with a density of 0.960 g/cm^3 and a melt index of 9.0. A commercial PE-glass fiber composite (Liquid Nitrogen Processing Corporation) served as a standard for comparison.

Processing and Grafting Procedures

PE pellets were dissolved in boiling xylene and subsequently precipitated by cooling to room temperature. After evaporation of xylene and drying, the remaining fluffy powder was used for subsequent processing. The glass fibers were exposed to AA vapor in evacuated ampules. Evacuation is necessary in order to remove any trace of oxygen which may serve as an inhibitor for the polymerization reaction. Following evacuation and exposure to AA vapor, the ampules were irradiated in a γ-field to a dose of 0.1 Mrads at the γ-radiation facility of the National Bureau of Standards, Washington, D.C. After irradiation

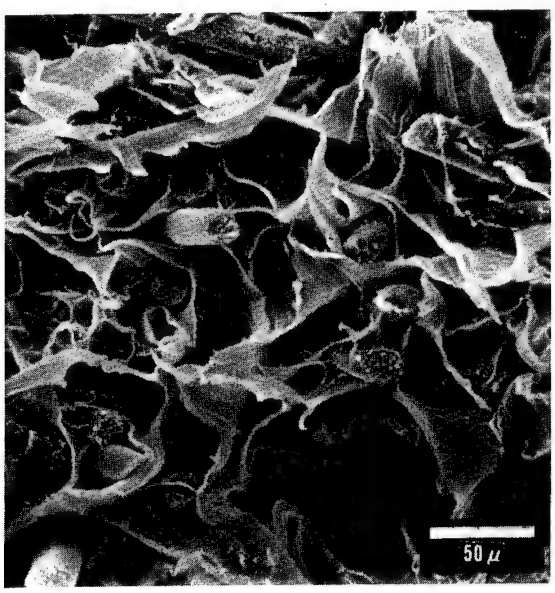

FIG. 4. Fracture surface of grafted composite at 300°K; 300X.

the fibers were dried in a vacuum oven in order to remove any traces of unreacted monomer. The PE powder and glass fibers were blended in a twin shell mixer, and subsequently compression molded at 177°C to form 1 mm thick sheets. Tensile specimens were cut from the sheets.

Sample preparation for scanning electron microscopy included vapor deposition of chromium onto rotating specimens. Although specimen rotation

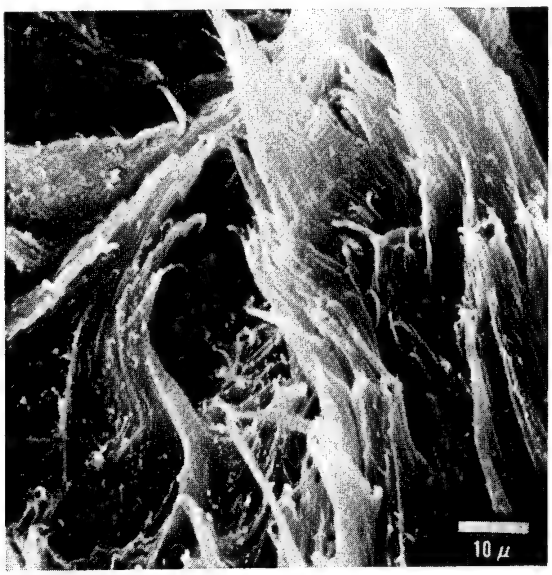

FIG. 5. Fracture surface of polyethylene without fibers at 300°K; 1000X.

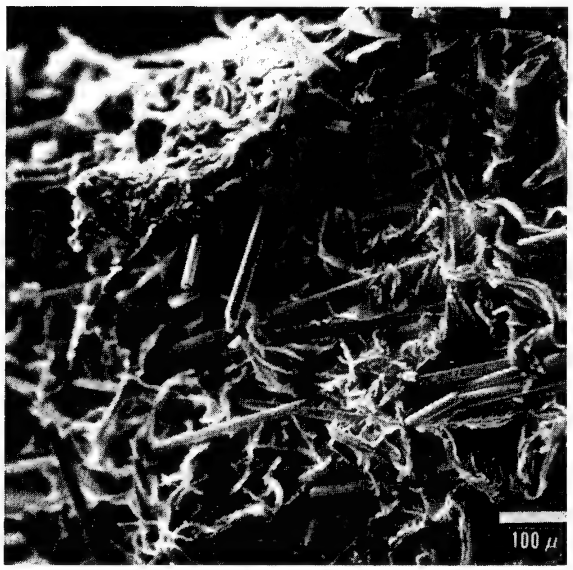

FIG. 6. Fracture surface of commercial composite at 300°K; 100X.

during deposition provided a reasonably conducting sample, some charging was noted, but lower condenser and beam currents appeared to minimize such surface charging effects. Acceptable results were obtained at 25 kV, small beam spot sizes, and low currents of the order of 10^{-10} A.

RESULTS AND DISCUSSION

The ungrafted and grafted fibers are shown in Figures 1 and 2, respectively. Less than 1% of weight of PAA was bonded to the fibers in all cases. The only noticeable change in the fiber appearance upon grafting is a slight opaqueness, as evidenced in Figure 2. After compression molding, the samples were fractured at 78°K and 300°K, and examined in the scanning electron microscope.

At 300°K, the tensile strength of the ungrafted glass fiber composites was inversely proportional to the volume fraction of glass fibers, indicating no load transfer between fiber and matrix. In contrast, the use of grafted fibers resulted in a considerable improvement in the composite strength; at 40 volume % fiber reinforcement, the composite strength was increased 150% over the unfilled PE matrix. Details of the fracture surfaces at 300°K for the ungrafted and grafted composites are shown in Figures 3 and 4, respectively. For comparison, an unfilled polyethylene fracture surface at 300°K is shown in Figure 5.

It is interesting to note that the grafted fibers become oriented, parallel to the tensile axis, whereas the ungrafted fibers are oriented randomly (Fig. 3 and 4). The reorientation may be attributable to the improved interfacial adhesion of the grafted fibers. The commercial composite, fractured in tension under similar conditions, exhibited very little fiber orientation (Fig. 6). This lack of

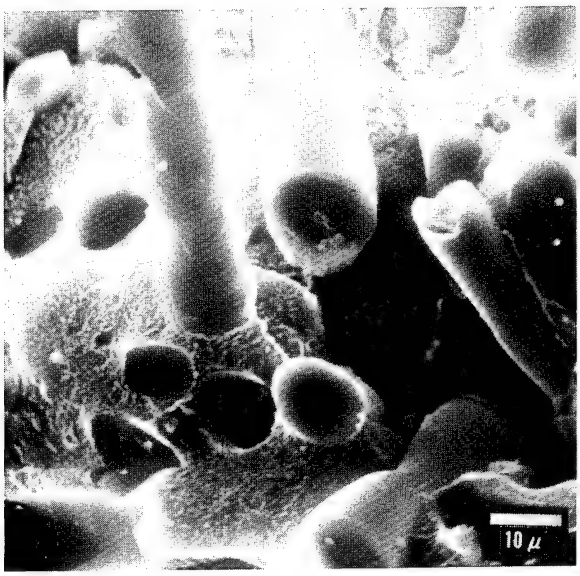

FIG. 7. Fracture surface of ungrafted composite at 78°K; 1000X.

orientation in the commercial product may result from the use of longer glass fibers, which may hinder their alignment during tensile loading.

Examination of composite fracture surfaces at 78°K provides further evidence for improved interfacial adhesion as a result of grafting. Figures 7 and 8 show the fracture surfaces of the ungrafted and grafted glass fiber–PE composites. The fracture surface of PE without glass fibers at 78°K is shown in

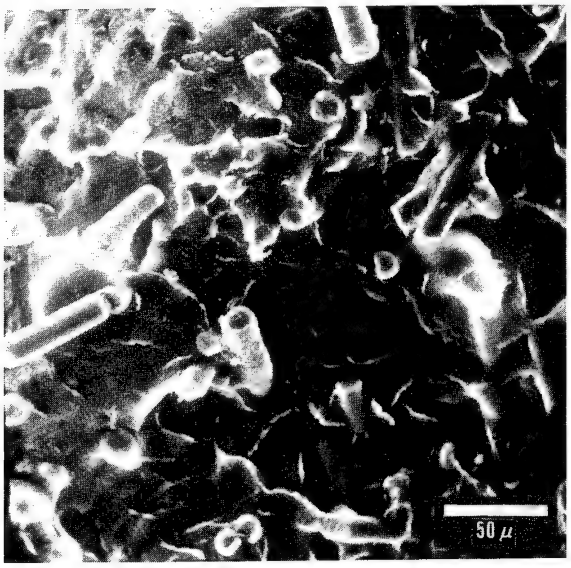

FIG. 8. Fracture surface of grafted composite at 78°K; 300X.

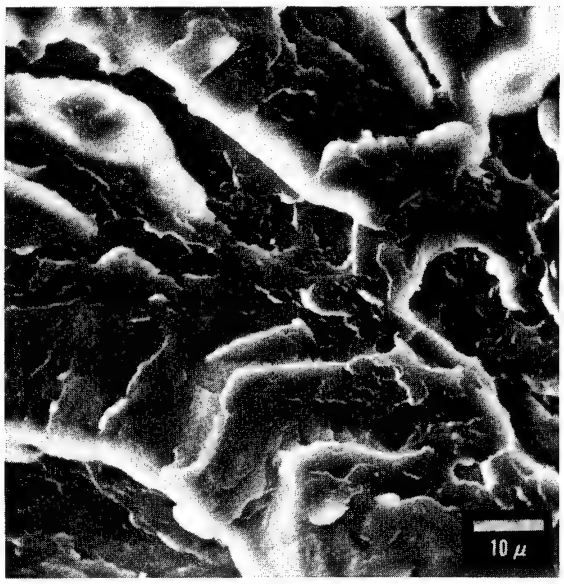

FIG. 9. Fracture surface of polyethylene without fibers at 78°K; 1000X.

Figure 9 for comparison. Poor adhesion is apparent in the ungrafted fiber composite of Figure 7, where fiber pull-out is prevalent. The grafted fiber composite of Figure 8 appears to have an improved interfacial bond, with fewer fiber pull-outs. The commercial composite, shown in Figure 10, exhibited no adhesion at 78°K, and tensile fracture resulted in excessive fiber extraction. Detailed examination of the grafted composite fracture surfaces clearly

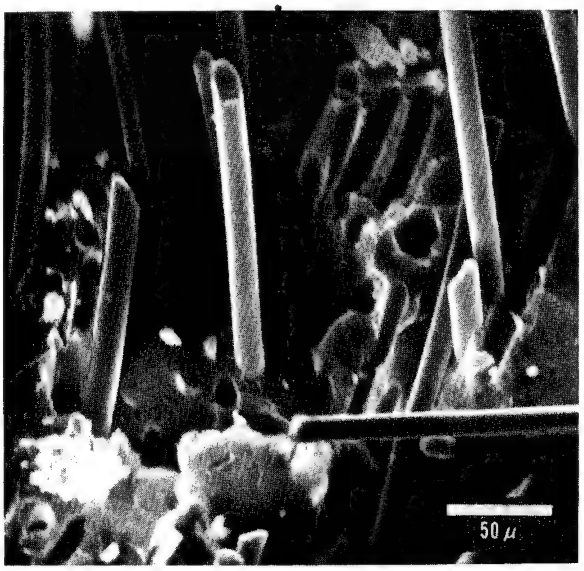

FIG. 10. Fracture surface of commercial composite at 78°K; 300X.

FIG. 11. Fracture surface of grafted composite at 78°K; 1000X.

demonstrates the improved polymer/fiber interfacial adhesion (Figs. 11 and 12).

CONCLUSIONS

The substantial improvement of tensile properties of grafted glass fiber composites can be related to the improved interfacial bonding between the

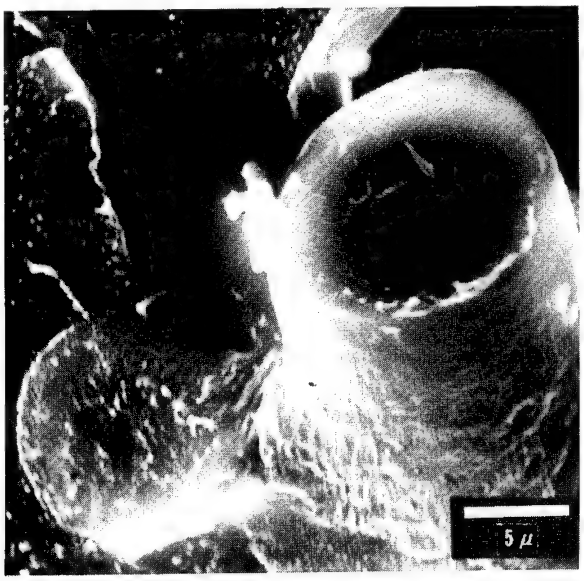

FIG. 12. Fracture surface of grafted composite at 78°K; 3000X.

glass fiber surface and the polymer matrix. The bonding may be explained by γ-radiation induced grafting of AA to the surface of the glass fibers, followed by bonding of the PAA to PE by heating during compression molding [2]. The improved interfacial adhesion has been confirmed in the present investigation by direct examination of fracture surfaces by scanning electron microscopy. In conclusion, the study demonstrated that the grafting treatment is superior to commercial silane fiber treatments, particularly at very low temperatures.

The authors gratefully acknowledge program support by the National Science Foundation Departmental Development Grant.

REFERENCES

[1] I. Kamel and R. D. Corneliussen, "Tensile properties of polyethylene/grafted glass fiber composites," presented at the 7th Middle Atlantic Regional Meeting of the Amer. Chem. Soc., Philadelphia, Pa., February 14–17, 1972.

[2] W. F. Busse and J. A. Boxler (assigned to DuPont Co.), U.S. Pat. 2,838,437 (June 10, 1958).

MICROSTRUCTURES AND PHYSICAL PROPERTIES OF SYNTHETIC AND MODIFIED PAPERS

L. H. LEE

Xerox Corporation,
Wilson Center For Technology,
Rochester, New York 14644

SYNOPSIS

Synthetic and modified papers presented new challenges to electrophotographic and printing technologists. Conventional thermal fusing used in xerography places additional requirements on synthetic papers. In lithography, printing requires special kinds of ink or special treatment of the synthetic paper surface. This study describes the microstructures of several synthetic papers, e.g. Tyvex (spun-bonded polyethylene), Papylon (polyvinyl alcohol), Acroart (high density polyethylene), Printel's (polystyrene), and poly(vinyl chloride) paper. Scanning electron micrographs were used for the detailed examinations. Two modified papers, Texoprint and Xerox Microspheres paper, are included in the investigation. Physical properties of both synthetic and modified papers are discussed, along with those of conventional paper. The advantages of using Xerox Microspheres paper for xerographic copying are enumerated in light of special requirements of thermal and mechanical properties.

INTRODUCTION

In the past several years, synthetic papers made from thermoplastics have become a technological success [1-5]. In such countries as Japan and England, where forestry products are scarce, the use of synthetic papers in printing and packaging may be the best answer to the shortage of conventional paper [3].

Although synthetic papers are not perfect substitutes for conventional papers made from natural fibers, they have better resistance to moisture, grease, mildew, and flexural fatigue [2, 3]. Synthetic papers are generally more durable than conventional paper, but they are not without problems. One of the problems is the behavior in printing. For art printing, adhesion and wetting of inks to synthetic papers require either surface treatment of the paper or special ink. None of the current synthetic papers are suitable for electrophotographic (xerographic) copying, which requires thermal fusing of toners on paper [4].

Our work was partly born from the search for a synthetic paper that can be used for xerographic copying. This preliminary study describes microstructures and physical properties of several synthetic papers. We also studied two modified papers; the modifications were mainly the addition of a polymer to cellulosic fibers as a coating or as a filler. Those papers modified by grafting [6] are not within the scope of this study.

Applied Polymer Symposium No. 23, 167-179 (1974)

METHODS OF MAKING SYNTHETIC AND MODIFIED PAPER

Two principal methods have been used to make synthetic paper [4]. They are: (a) Spun-bonding of fibers and incorporating of fibers into a polymer matrix; (b) paperizing of plastic film through surface roughening (sand blasting), embossing, laminating with paper, chemical or solvent etching, clay coating, or filling with inorganic matter.

This study includes two fibrous synthetic papers: Tyvex, a spun-bonded polyethylene by DuPont [7], and Papylon, manufactured by Sancho Company [8]. Papylon is a composite of Vinylon poly(vinyl alcohol) fiber and Fibribond, a slightly heat-treated poly(vinyl alcohol) fiber. Fibribond is an intermediate product of Vinylon, and it swells in cold water but dissolves in hot water. Therefore, when these two fibers are combined and processed through an ordinary papermaking machine, Fibribond swells in a web-forming process. The swollen Fibribond fibers give the webs the strength necessary to leave from the wire of the couch roll and proceed onto the blanket. Some Fibribond fibers are partially dissolved by the water in the web, when it is passed through the dryer. Consequently, the dissolved portion acts as a binder for the Vinylon fibers.

We have examined several synthetic papers that were filled with inorganic matter. They are: Acroart, a filled, high-density polyethylene by Mead Paper Corporation [9]; Bakelite, a rigid vinyl, poly(vinyl chloride) paper by Union Carbide Corporation [10]; and Printel's, a filled polystyrene by Sekisui Chemical Company [11].

One of the modified papers included in this study is Texoprint by Kimberley-Clark Corporation [12]. It is a low-density absorbent sheet from bleached kraft fiber, which is impregnated in a saturating mixture of latex and opacifying fillers. The impregnated sheet, which picks up 60% of its own weight in dry solids, is then coated on both sides with printing fillers (titanium dioxide and clay) and flexible latex binder. The basic weight varies between 80 and 190 lbs/ream for 25 in. x 28 in./500. The other modified paper included is Xerox Microspheres paper, which is a lightweight material, in contrast to Texoprint and conventional paper [13]. It is modified with Saran microspheres [14] and isobutane as a blowing agent. In the initial state, the average diameter of the microspheres is 5 to 8 μm; in the expanded state, after heating at 65°C to 95°C, the diameter increases to 25 to 40 μm. The paper contains 9% microspheres and some polymeric binders.

MICROSTRUCTURES OF SYNTHETIC AND MODIFIED PAPERS

Microstructures of the papers discussed in the above section were studied with the scanning electron microscope (SEM). The general techniques of the preparation of samples have been described by Fernquist and Short [15]. The papers were coated with a thin film of gold (500-1000 Å). The coating operation was carried out at 6 to 20 V for 1 to 3 sec. Caution was taken not to heat the polymer surface by the radiation. The conductive surface could

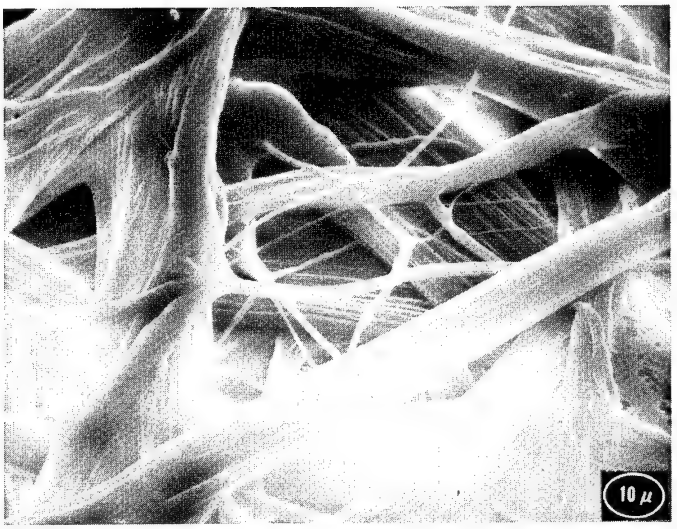

FIG. 1. SEM micrograph of Tyvex polyethylene spun-bonded paper; 1,000X.

then be viewed directly in the SEM at 20 kV with specimen currents of 10^{-9} to 10^{-10} A.

The structure of Tyvex resembles that of cellulosic fibers, as shown in Figure 1. Tyvex fibers are not porous, and do not absorb water or inks. The diameter of these fibers ranges from 2 to 20 μm. The small fibers are bonded together not by binders or sizes, but by heat and pressure. Therefore, the SEM does not reveal any particulate matter in the interstitial areas.

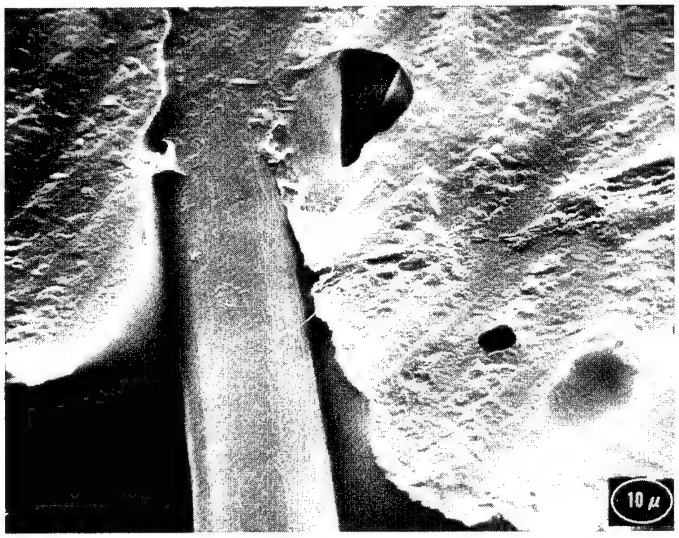

FIG. 2. SEM micrograph of Papylon poly(vinyl alcohol) paper; 1,000X.

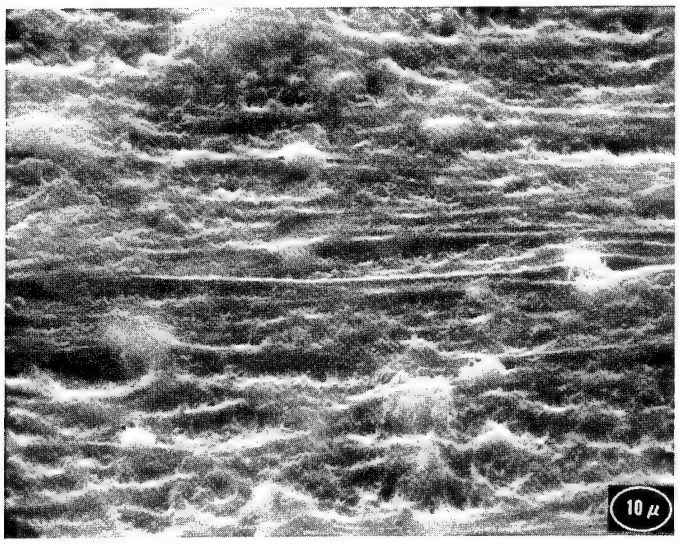

FIG. 3. SEM micrograph of Acroart polyethylene paper; 1,000X.

Papylon contains a binder derived from Fibribond and Vinylon fibers. In Figure 2 the SEM shows the two-phase structure, which is similar to that of a fiber-reinforced thermoplastic. Since the two components are of the same origin and have the same modulus, there is no reinforcement in physical properties.

The other three synthetic papers are film-like, and their microstructures are shown in Figures 3, 4, and 5. In Figure 3, Acroart high-density polyethylene film shows an uneven and nonporous surface, which is presumably specially treated. There are some particulate filler particles present. The Bakelite poly(vinyl chloride) paper in Figure 4 shows also an uneven and nonporous surface with some particulate filler in the matrix. The microstructure of Printel's is somewhat different, as seen from a comparison of Figure 5 with Figures 3 and 4. This paper could have been formed by compressing either finely cut polystyrene ribbons or a combination of polystyrene and a ribbon-like filler. The surface is more inhomogeneous than those of Acroart and poly(vinyl chloride) papers.

Modified papers, unlike synthetic papers, retain the basic cellulosic structure of conventional paper. In the case of Texoprint, the heavy latex coating tends to cover up the underlying cellulosic fibers, as shown in Figure 6. However, the coating is not uniform, and there are spots where fibers are barely visible in the micrograph.

In practice, all conventional papers can be considered as modified papers, because they contain binders, sizes, and fillers. Such additives are clearly visible in Figure 7. However, the new modified papers generally show significant changes in physical properties. For example, the density of Microspheres paper is substantially lower than that of conventional paper (Table I). Scanning electron micrographs show that Saran microspheres are embedded among the interstitial areas (Figs. 8 and 9). Most microspheres adhere very well to the binder. The hollow microspheres lower the density of the paper.

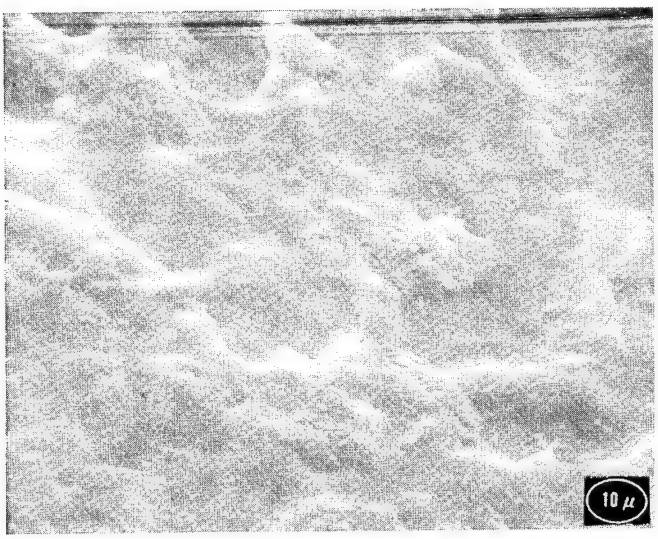

FIG. 4. SEM micrograph of Union Carbide's poly(vinyl chloride) paper; 1,000X.

PHYSICAL PROPERTIES OF SYNTHETIC AND MODIFIED PAPERS

Spun-bonded Fibers

Tyvex Type 10 is a stiff, paper-like material [7]. The high degree of packing of fine, interconnected fibers produces a smooth surface, good opacity, and a very high whiteness. In addition, the large number of bonds per unit volume gives a stable and abrasion-resistant surface. Typical properties of

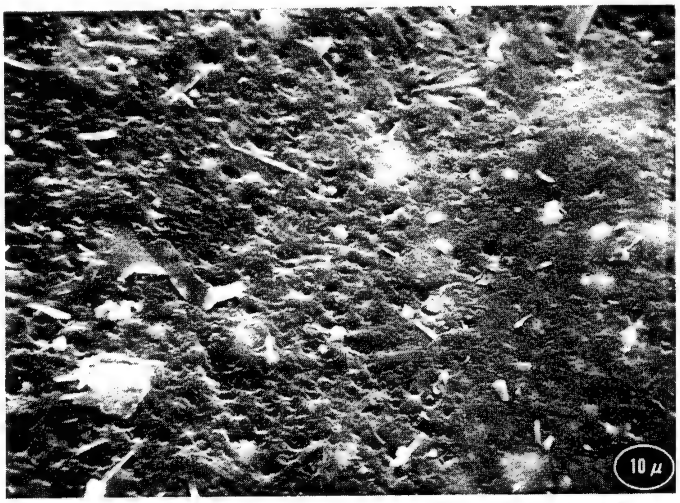

FIG. 5. SEM micrograph of Printel's polystyrene paper; 1,000X.

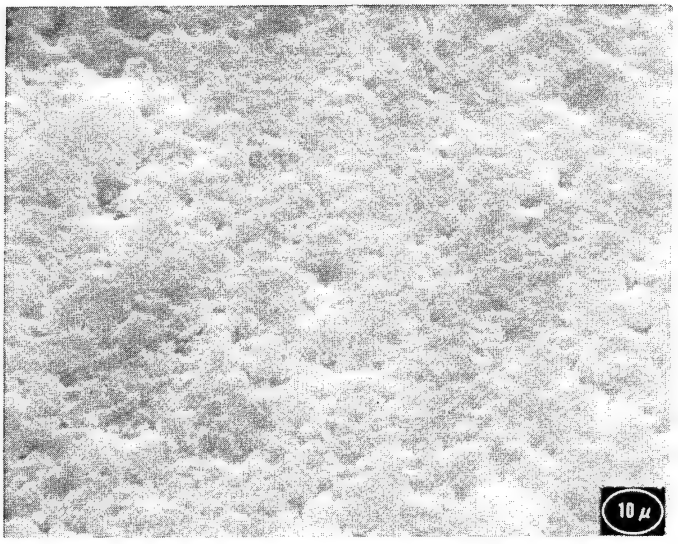

FIG. 6. Texoprint latex-modified natural paper; 1,000X.

Tyvex paper are shown in Table I. Owing to its hydrophobic nature, it is unaffected by relative humidity. The dimensional change is estimated to be less than 0.01% between 0 and 100% relative humidity at constant temperature. It is also resistant to water-borne soil, mildew, and most strong acids and alkali. Tyvex is relatively stable upon aging, but it is somewhat affected by ultraviolet irradiation. Tyvex is affected by hydrocarbon solvents, and swelling generally takes place in the presence of such solvents. It is also affected by heat; it begins

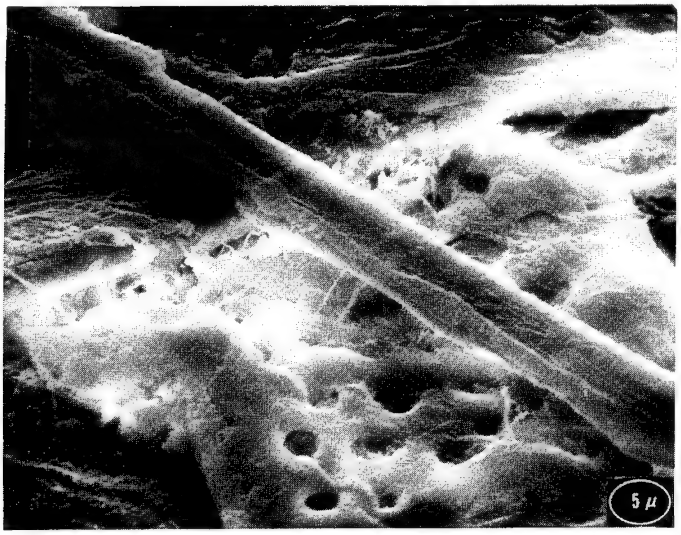

FIG. 7. Felt side of conventional paper; 2,000X.

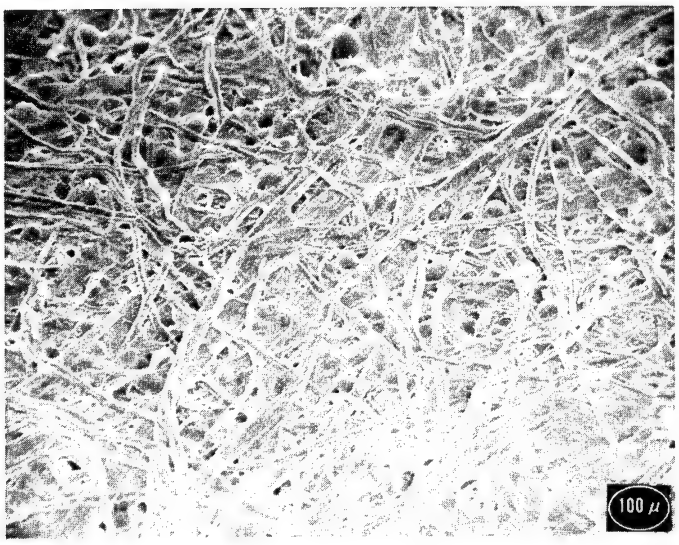

FIG. 8. Wire side of Xerox Microspheres paper; 100X.

to shrink at 118°C and softens at 135°C. Therefore, it is unsuitable for xerographic copying, which requires thermal fusing.

Unlike most hydrophobic synthetic papers, Papylon [8] contains hydrophilic fibers and is thus oil resistant. Papylon does not melt, but it softens and shrinks at high temperatures. At or around 180°C the shrinkage becomes noticeable.

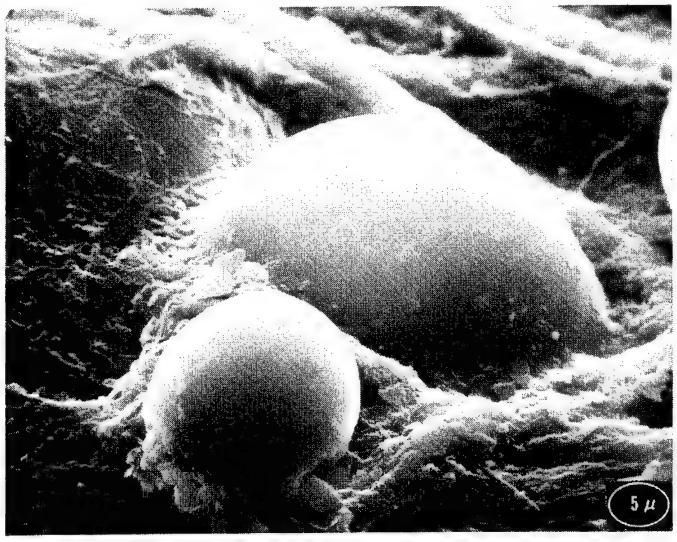

FIG. 9. Felt side of Xerox Microspheres paper; 2,000X.

TABLE I

Physical Properties of Conventional, Synthetic, and Modified Papers

Property	Direction	Art Paper	Xerox 1524 (13)	Tyvek (7)	Papylon (BFN 2) (8)	Acroart (9)	Printel's (11)	Micro-spheres (13)
Basis weight, g/m^2		130	75	97	25.6	190	-	47
Thickness, μm		119	105	205	113	170	-	106
Apparent density, g/ml		1.09	0.71	0.47	-	1.12	-	0.44
Brightness, %		82	82	88	-	82	90	83
Opacity, %		97	88	98	-	98	94	80
Tensile strength, kg	Machine	8.5	7.6	14.1	8.8	3.8	3.6	5.1
	Cross	6.4	3.5	12.1	4.1	3.8	3.6	2.9
Elongation, %	Machine	1.8	2.1	37	9.9	480	12	2.3
	Cross	4.5	3.0	34	8.3	570	18	6.1
Tear strength, g	Machine	60	56	290	51	210	-	31
	Cross	59	70	500	72	450	-	32
Burst strength, kg/cm^2		2.3	2.0	-	2.4	-	-	1.3

Paperized Films

Polymeric films generally have higher elongations and lower moduli than paper. The properties of unoriented and biaxially oriented films were compared with those of cellulosic paper [4]. It is noteworthy that the physical properties of cellulosic paper and spun-bonded fibers differ according to the direction in which the paper moves during processing, while those of paperized films do not to the same extent.

TABLE II

Some Physical Properties of Polymers Used in Making Synthetic Papers

Polymer	Critical Surface Tension, (dyn/cm)	Solubility Parameter	Glass Temperature, °C
Polypropylene	29	9.2	-20
Polyethylene	31	8.0	-36
Polystyrene	33-36	9.1	100
Polyvinyl chloride	39	9.5	81
Polyvinylidene chloride	40	12.2	-19
Polyvinyl alcohol	37	12.6	85

FIG. 10. Coalesced toner on the felt side of Xerox Microspheres paper; 1,000X.

The physical properties of Acroart and Printel's are also shown in Table I. Tensile strengths of both papers are lower than those of art paper or Xerox 1524 paper. However, the elongations of both papers are much larger than those for the conventional papers. High elongation, such as that of Acroart, is not desirable. The tear strengths of olefin papers, such as Tyvek and Acroart, are much higher than those of conventional papers (Table I). Furthermore, the tear strengths in the cross direction are approximately twice those in the machine

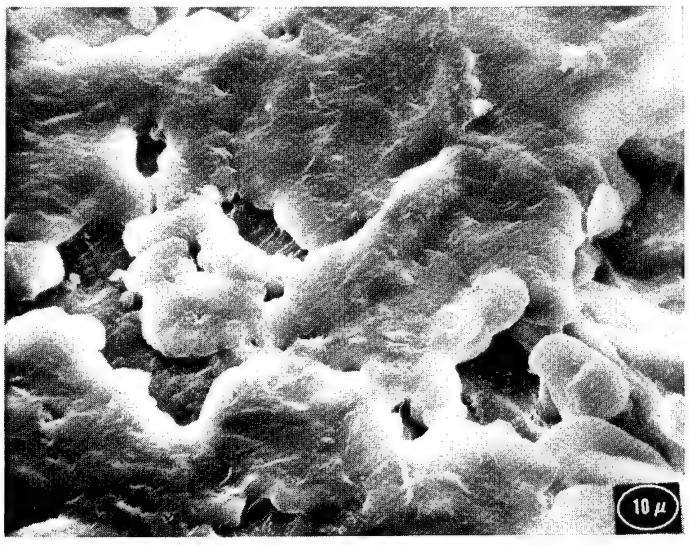

FIG. 11. Coalesced toner on the wire side of Xerox Microspheres paper; 1,000X.

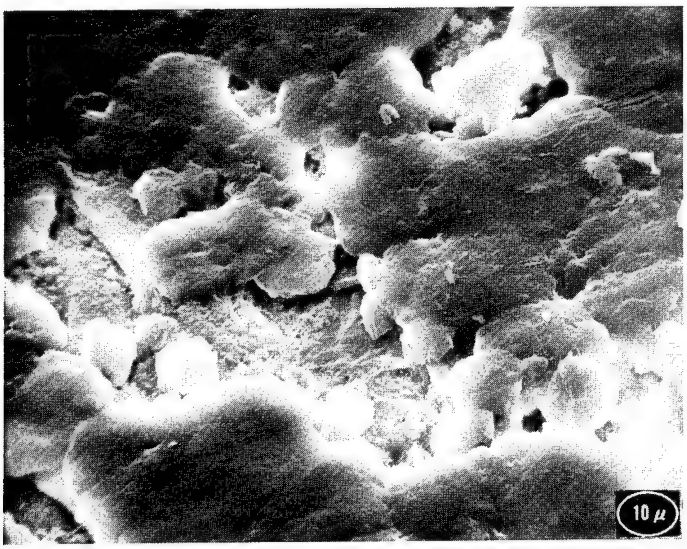

FIG. 12. Coalesced toner on the felt side of Xerox 1024 paper; 1,000X.

direction. High tear strength is a beneficial property for these two synthetic papers.

Microspheres Paper

Lightweight Microspheres paper has an interesting combination of physical properties (Table I). Besides being lightweight, this paper is suitable for use in unconventional copying machines. The tensile, tear and burst strengths of Microspheres paper are somewhat lower than those of conventional paper. It is rougher than conventional paper, and it has a Sheffield smoothness of 285 for the wire side, as compared to a value of 140 for conventional paper [13].

INHERENT PROBLEMS OF PRINTING AND COPYING ON SYNTHETIC PAPERS

Adhesion and Wetting of Ink

Successful printing requires a good ink-paper adhesion. Good adhesion calls for the spreading of ink on paper and subsequent penetration of the ink into the fibers. Spreading of ordinary lithographic inks on synthetic papers is hampered by the low surface wettability of most polymers used in making synthetic papers. Table II presents some pertinent data of such polymers [16]. One of the basic requirements for spontaneous spreading is that the surface energy of the substrate be greater than that of the liquid. Therefore, spontaneous spreading of ink on low surface energy material requires either the modification of the

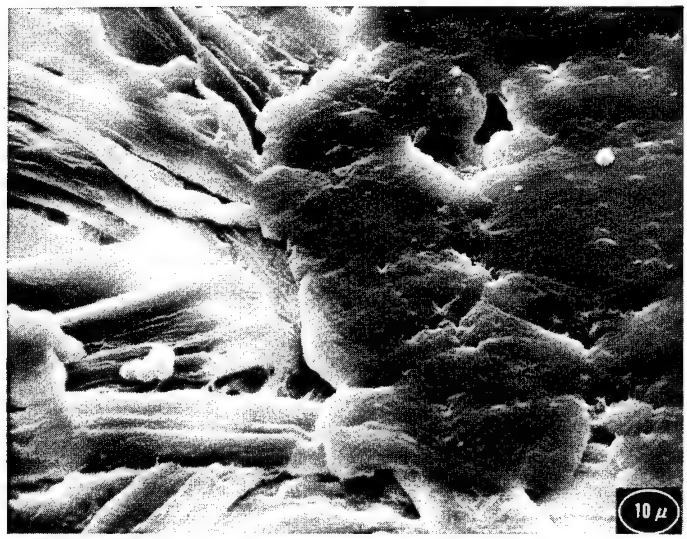

FIG. 13. Coalesced toner on the wire side of Xerox 1024 paper; 1,000X.

surface by corona discharge or controlled oxidation, or the use of special inks.

From the above study on microstructures, it becomes evident that penetration of lithographic inks into synthetic papers is almost impossible. Modification with special coatings and filler layers has met with a certain degree of success [4]. The induced porosity and the increase in surface energy help both penetration and spreading of lithographic inks that contain linseed oil or similar drying oils. For those inks, drying is usually a slow process. For unmodified surfaces, flexographic or gravure printing inks can be used. These inks dry faster upon evaporation of the solvent than lithographic inks. Furthermore, by matching the solubility parameters of the ink and the paper (Table II), a compatible system can be obtained to achieve minimum swelling of the paper surface by the ink vehicle. Swelling could facilitate diffusion and promote adhesion. Other methods have also been used to promote adhesion, such as special inks, chemical treatment, or mechanical roughening of the paper surface [4].

There appear to be no printing problems for modified papers, such as Texoprint and Microspheres paper. Lithographic inks can be used without special precaution or special treatment of the paper surface. The relatively high surface tension of microspheres (40 dyn/cm) should enhance ink-paper adhesion.

Static and Thermal Deformation

There are at least two problems associated with the use of synthetic papers for xerographic copying. The first problem is caused by the storage of static charges in synthetic paper [4], due to the high resistivity of these polymers (10^{15} - 10^{16} Ωcm vs 10^{12} Ωcm for natural paper). These static charges hinder automatic paper handling in a xerographic machine. Antistatic additives have

been used successfully in some printing, and the same type of treatment may solve the paper handling problem in copying machines.

The second problem, thermal deformation [4], is serious, and is the major obstacle in using synthetic papers for xerographic copying. Most of the currently available synthetic papers are made to compete with conventional paper in cost, and low-cost polymers have mostly low glass transition temperatures (Table II). Since glass transition is the phase change at which a glassy solid transforms gradually into a rubbery liquid-like material, heating of a synthetic paper above its glass temperature would naturally cause deformation. To prevent deformation at the fusing temperature of a xerographic toner, it may be necessary to introduce crosslinking in the paper by irradiation or filling by an inorganic material. Inorganic pigments can help increase the glass temperature of the polymer matrix.

Xerox Microspheres paper is not deformed by heat, and can fulfill most xerographic copying requirements. For optimum copying performance the paper should have a reasonably smooth surface for toner fusing, should not have scorching tendencies, and should have a high stiffness, a low level of curl, a controlled conductivity level, and a reasonably controlled moisture content [13]. Microspheres paper is closest to regular cellulosic paper in meeting these requirements. Fixing of xerographic images on the former (Figs. 10 and 11) is equivalent to that on the latter (Figs. 12 and 13). Actually, the rougher surface of the Microspheres paper enhances toner-paper adhesion.

CONCLUSIONS

Scanning electron micrographs of synthetic papers show the nonporous nature of the spun-bonded fibers and paperized films. The lack of porosity prevents inks from penetrating into the paper. Since most of the current synthetic papers are made of low surface energy polymers, the spreading of ink is also a problem. Therefore, in improving ink-paper adhesion, special surface treatment and flexographic type inks have been employed.

There are advantages in using synthetic papers, such as resistance to moisture, grease, and fatigue. However, static charge accumulation and thermal deformation have been major problems, especially in xerographic copying. The static problem may be solved by using antistatic additives, but the inherent thermal deformation problem of currently available synthetic papers requires major efforts in research.

Lightweight Microspheres paper can be used for xerographic copying and art printing. The full potential of this new, modified paper has not yet been defined. While there has not been a synthetic paper suitable for xerographic copying, this type of modified paper deserves some consideration.

The author is indebted to Mr. R. G. Fernquist and Mrs. J. Dulmage of Xerox Corporation for preparing the scanning electron micrographs.

REFERENCES

[1] O. A. Battista, *Synthetic Fibers in Papermaking,* Wiley, New York, 1964.
[2] O. A. Battista, *Pulp Pap. Int., 8*(2), 65 (1966).
[3] C. Benjamin and M. J. Viney, *Plast. Polym., 39,* 64 (1971).
[4] H. Lunk and K. Stange, *Angew. Chem. Int. Ed. Engl., 10*(5), 287 (1971).
[5] R. A. A. Hentschel, *Tappi, 55*(8), 1174 (1972).
[6] R. B. Phillips, J. Quere, G. Guiroy, and V. T. Stannett, *Tappi, 55*(6), 858 (1972).
[7] E. I. du Pont de Nemours and Co., "Properties and processing of Tyvek® spunbonded olefin," Technical Service Sect. Text. Fibers Dept., No. 135, December 1967.
[8] Sancho Co., "Papylon®," Tech. Bull.
[9] Mead Paper Co., "Acroart®," Tech. Bull.
[10] Union Carbide Corp., "Bakelite rigid vinyl for graphic arts," Tech. Bull.
[11] Sakisui Chemical Co., "Printel's" Tech. Bull. (in Japanese).
[12] Kimberley-Clark Corp., "Texoprint," Production Data.
[13] G. Trier, *Tappi, 55,* 769 (1972).
[14] D. L. Kanaga and R. M. Gooch, U.S. Pat., 3,293,114, December 20, (1966).
[15] R. G. Fernquist and J. M. Short, *Proc. 14th Annu. Conf. Soc. Vac. Coaters,* 1971, p. 26, Pub. by Vacuum Coaters Soc.
[16] L. H. Lee, *J. Appl. Polym. Sci., 12,* 719 (1968).

SCANNING ELECTRON MICROSCOPY OF HIGH SPEED FIBER IMPACT PHENOMENA

R. C. LAIBLE, F. FIGUCIA, and B. H. KIRKWOOD

U. S. Army Natick Laboratories,
Natick, Massachusetts 01760

SYNOPSIS

Visual observation of nylon impacted at very high speeds, including ballistic speeds, shows a large amount of plastic deformation and melting of the broken fiber ends. In attempts to produce fibers for special applications, manufacturers have produced organic fibers with moduli greater than that of glass, and with heat resistance values far greater than that of nylon. The initial products of this type showed a typically brittle fracture, because of their low ductility. They also showed a tendency to split longitudinally. The better products show this splitting to a more marked degree, to where it reaches a state best described as fibrillation. This process is thought to be of considerable importance, because (a) it tends to minimize premature brittle fracture, and (b) considerable energy is absorbed in creation of the many subsurfaces.

The potential for high strength in these new aromatic polymers is probably due to the extended polymer chains, which are broken more nearly in unison during extension. However, the realization of these high strengths with such low elongation fibers depends upon the process of fibrillation, to prevent premature catastrophic failure. The strength of the aromatic polyamide "Fiber B" is 23 g/d or 400,000 psi, as contrasted to 10 g/d or 150,000 psi for the strongest nylon tire cord previously available. The theoretical value of approximately 200 g/d or 4,000,000 psi can be calculated on the basis of all primary bonds breaking at once.

INTRODUCTION

The effect of high-speed impact upon fibrous materials has been the subject of numerous papers in the last forty years. A monograph by Lyons summarizes a good deal of that work [1]. The major objectives were: (a) to investigate the fundamental viscoelastic properties of polymeric fibrous materials, and (b) to predict the performance of fibrous materials under field conditions by laboratory procedures. Many devices were used in an attempt to simulate field conditions, such as the action of cords in auto and truck tires, the opening of a military parachute, high speed stitching, and ballistic impact. The devices included relatively low constant speed testers, such as the Instron, falling weight devices in which the testing speed is governed by the drop height, pendulums, rotating disk machines, pneumatic testers, and actual transverse impact in which a missile strikes a yarn perpendicular to the long fiber axis. The testing speeds covered the range from fractions of a millimeter per second to a thousand meters per second. The transverse impact test can be varied to include most velocities encountered in the field of ballistic protection, where the fibrous materials may

Applied Polymer Symposium No. 23, 181-191 (1974)

be destined for use in a vest, to provide protection against pistol fire or fragmenting munitions. These studies led to an understanding of the significant rate dependence exhibited by fibrous materials. The general trends of increasing breaking strength, modulus, and decreasing elongation at break with increasing rate of testing has been documented [1-6]. Many of these publications relate this behavior to the concept of relaxation times and/or the ability of molecular groupings to move in a given time frame [3-5].

A dramatic example of the inability of an important process to take place in a short testing time is furnished by undrawn nylon. This material possesses a huge capacity for work absorption when tested in tension at slow speeds in an Instron. Attempts to capitalize upon this property by using undrawn nylon for a ballistic vest have failed [1]. Obviously the process of drawing cannot occur in the time frame of interest in ballistic impact. This behavior of undrawn nylon has been shown more clearly with transverse impact experiments on yarns [7]. The researchers took a series of nylon 66 yarns, which differed systematically in mechanical properties, and subjected these yarns to static rates of straining as well as to ballistic rates of straining. The undrawn nylon specimens absorbed 260 J/g in a slow tensile test of 1.67%/sec, because of its large elongation at that rate of testing. However, they absorbed only 10 J/g under transverse impact at a high speed of 5000%/sec. More highly drawn yards exhibited a much more modest loss in breaking energy with an increase in straining rate. The study showed that an undrawn nylon should not be an effective energy absorber at the high rates of loading characteristic of those encountered in aerial delivery. Additional tests with undrawn nylon at even higher rates of loading confirmed experimentally the poor performance demonstrated in a ballistic vest.

In any failure process study it is useful to investigate the morphology of the material after fracture. Earlier, any investigation of fracture surfaces was necessarily limited to that possible with light microscopy, and later with the transmission electron microscope. In 1958 an extensive microscopic study was conducted of a multilayer nylon armor panel upon transverse impact with .22 caliber missiles, but the study was restricted to the use of light microscopy [8]. Some valuable information was obtained concerning the fusion of nylon fibers and the extreme localization of the effect of the impact. The information was obtained with difficulty through painstaking and tedious work, due to the small depth of focus attained in light microscopy.

Now, with the advent of the scanning electron microscope (SEM), it is possible to investigate more efficiently the morphology of fibrous materials degraded by high speed impact. Such a study has been conducted and is the subject of this paper. The materials considered have included not only nylon but also the new, high modulus aromatic polyamides.

EXPERIMENTAL

Tensile Tests

Tensile data were generated at two rates of straining, a conventional textile testing rate of 1.67%/sec, and the fastest rate available with a pneumatic tester,

5000%/sec. The latter rate of testing is still short of that characteristic of ballistic impacts, but it is the highest rate of testing for which transducers can give an accurate measure of load and deflection. This limitation is mainly due to wave effects.

The conventional tests were performed with a standard Instron Tensile Tester, operating at a constant extension rate of 2.1 mm/sec. The high speed tests were performed on the FRITS* Piston Tester, which is pneumatically driven by compressed nitrogen gas at approximately 6.42 m/sec. All tests at both strain rates were performed on specimen lengths of 128 mm (5 in.), with a pretension of approximately 12 g applied immediately before clamping. The specimens were individually weighted after test to establish the denier (linear density) in each case.

Scanning Electron Micrographs

The broken ends of the fractured yarns were mounted on specimen studs with silver paint and single-faced adhesive aluminum tape. The samples were coated in a vacuum evaporator at 3×10^{-5} torr with a thin layer of carbon, followed by a thin layer of gold. The carbon deposition allows better distribution of the subsequent gold coating. During the coating process the samples were rotated 360° and tilted 180° to obtain a uniform and complete coating. The fracture patterns of the coated samples were observed in an AMR Model 900 scanning electron microscope in the secondary electron mode.

RESULTS AND DISCUSSION

Scanning electron micrographs have greatly facilitated the investigation of fiber morphology after high-speed impact. The depth of focus available with the SEM makes it possible to observe many fibers at once. For example, Figure 1 shows fractured ends of nylon fibers resulting from impact with a small, 10 caliber cylinder, weighing 87 mg. Fusion is clearly indicated from the mushroom-like appearance at the end of almost every broken fiber. Although ballistic impact has been emphasized, it should be pointed out that such fusion and mushroom shaped ends have also been observed in fibers after longitudinal impact at only 30 m/sec, as well as in ballistic impact [8, 9].

In order to develop fibrous materials with a greater potential for high performance in industrial and military applications, such as tire cords, parachute suspension lines, and ballistic protective items, it is necessary to take into account one or more of the following factors: (a) Improved mechanical properties of yarns, especially strength, generally yield better candidates in fabric form for defeating fragments, whereas decreased creep can eliminate flat-spotting in tires; (b) raising the melting point and strength retention at high

*Fabric Research Impact Test System.

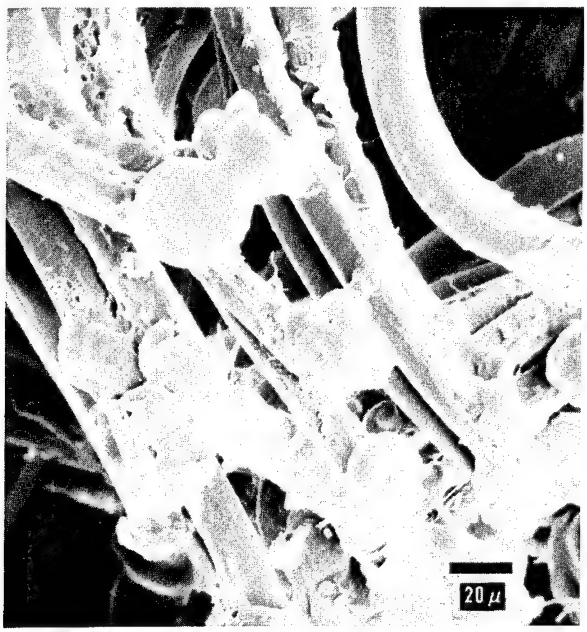

FIG. 1. Nylon fibers broken and fused from missile impact; 450X.

temperature of a fiber may yield better candidates for resistance to high speed impact; (c) a higher modulus to density ratio (specific modulus) would increase the fiber's ability to respond quickly to high speed impact, so that it would mitigate the extreme localization of the deformation previously noted by Susich [8].

The first of these factors, improvement in the mechanical properties of nylon 6 and nylon 66, has been studied by tire cord manufacturers. The results have been fairly negative, as the changes in molecular weight necessary to produce stronger fibers makes the polymers impossible to spin on a production basis. This is due to the fact that the intrinsic viscosity rises very fast with molecular weight, and the polymers are intractable, although they have super-strength potential [10, 11].

The second and third objectives, higher heat resistance and faster response to impact, could be addressed by the introduction of aromatic groups in the polymer backbone. It has been shown that both modulus and melting point could be raised significantly by the introduction of benzene rings in the main chain [12]. Properties of many aromatic and aromatic-aliphatic polyamides tend to verify this contention [13]. Poly (p-phenylene adipamide), the product of adipyl chloride and paraphenylene diamine, has a melting point of 340°C, as contrasted with the 255°C value characteristic of nylon 66, which has the same acid unit but is made with an aliphatic amine component [13, 14]. Polyterephthalamides, made by interfacial polymerization, exhibit generally high

melting points. For example, the product of tetramethylene diamine and terephthaloyl chloride, has a melting point of 436°C [15].

This rise in melting point when compared to nylon, is of course partially due to the reduction in the number of methylene groups in the diamine, but the major influence of the phenyl groups is apparent. This influence can be demonstrated with atomic models by contrasting the flexibility of polyethylene with that of either poly(p-phenylene) or the aromatic-aliphatic polymers described here. The stiffness of the aromatic polymers results in a lower change in entropy from the solid to the liquid, because of the restrictions in the number of configurations possible, as compared to an aliphatic polymer. The melting point of a material is inversely proportional to the entropy change upon melting, and must necessarily rise with increased stiffness.

Modulus is also related to stiffness. Poly(tetramethylene terephthalamide) exhibits a modulus of over 90 g/d or 1,500,000 psi, as contrasted with 40 g/d or 580,000 psi for all aliphatic nylon 66 [15]. A fairer comparison with nylon 66 would be the polymer prepared from hexamethylene diamine and terephthaloyl chloride, which has a modulus 50% greater than the aliphatic nylon. In any event, the potential for the preparation of fibers with increased heat resistance and larger moduli by the introduction of aromatic groups has been demonstrated clearly some years ago. Problems arise in the preparation of large quantities of these polymers and in the conversion of them into fibers. Only two processes were available for preparation, namely interfacial polymerization and low temperature solution polycondensation. The former method yields a product from diacid chloride and diamine, which is never really in solution. Then a method of spinning the fiber has to be found. Even the aliphatic-aromatic polyamides, such as polyhexamethylene terephthalate cannot be melted without decomposition. An all aromatic polymer would be even more likely to decompose upon melting. Even solution spinning, a less desirable process, is difficult, because of the insolubility of these aromatic polymers. Solvents such as concentrated sulfuric acid are generally required, which are not convenient for large scale production. These difficulties have in the past restricted the fiber preparation to laboratory quantities.

The first appearance of aromatic polyamide fibers in more substantial quantities was a family of fibers produced by Monsanto and designated as X-500. These fibers are reported to have an aromatic polyamide-hydrazide structure:

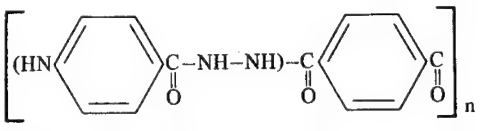

Black et al. have discussed these fibers in some detail [16, 17]. The X-500 yarns are quite temperature resistant with little weight loss up to 400°C. The temperature resistance is also obvious from the absence of fused fibers after ballistic impact, as shown in Figures 2 and 3. These micrographs also indicate the

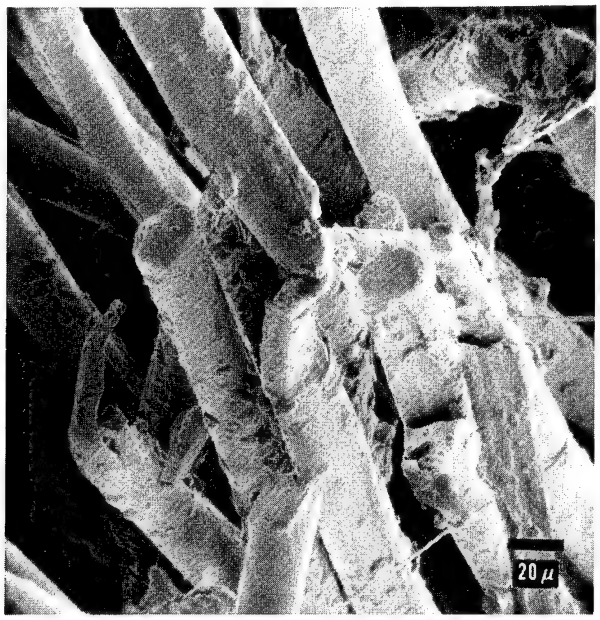

FIG. 2. X-500 fibers broken from ballistic impact; 400X.

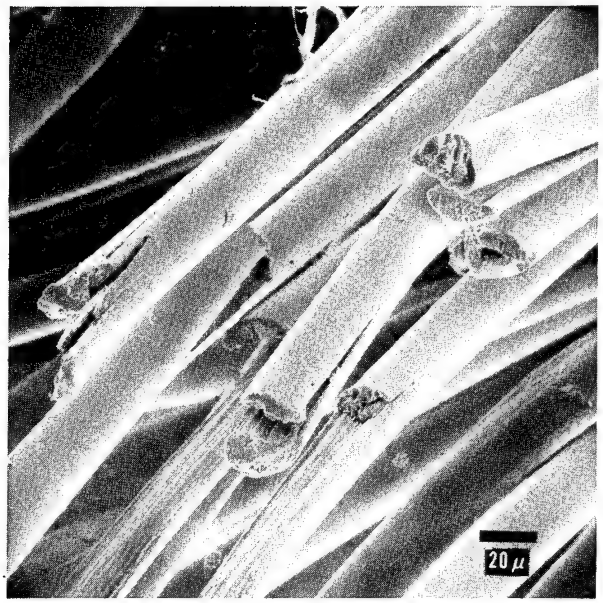

FIG. 3. X-500 fibers have the tendency to split longitudinally from impact; 410X.

predominance of brittle fracture, which might have been predicted from the stress-strain properties of the X-500 type yarns. These properties are compared in Figure 4 with those of nylon 66. The yarns were tested both at a static (1.67%/sec) and a dynamic (5000%/sec) rate of straining. The increased modulus is quite apparent from the curves, which also show the rather modest strength and work to rupture. One of the reasons for these modest strength values may be the intensional break-up of the order through the introduction of comonomers.

A more successful product has been marketed by DuPont under the designations PRD 49-IV and Fiber B. This material is reported [17, 18] to have a structure like:

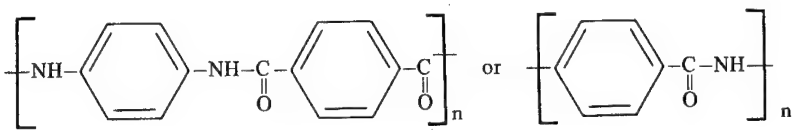

The first structure is analogous to nylon 66, whereas the second is similar to the repeat structure of nylon 6. This all-para aromatic polyamide possesses a strength of 23 g/d at slow rates of straining. The properties of Fiber B at slow strain rate of 1.67%/sec are given in Table I in units familiar to either engineers, textile technologists, or physical scientists. It is interesting to compare these values with those for nylon and other conventional fibers. The sound velocity value of 9400 m/sec is higher than the 2400-3400 m/sec for nylon or even the 4800-6000 m/sec for steel. This high value is due to the high modulus value, which is approximately equal to that of glass on a psi scale but vastly superior on a specific modulus or textile basis. It has been shown that moduli in the range of 10^{12} dyn/cm^2 can be estimated for poly(1, 4 benzamide) and poly(1, 4 phenylene terephthalamide) [18]. The calculations are based upon values for the force constants of the chemical bonds in the polymer chain as derived from vibration fequencies.

The strength values exhibited by PRD 49-IV are the highest exhibited by any fibrous material. They can be compared with the 10 g/d value of nylon tire cord, the strongest fiber cord used commercially. A simple calculation can be made to

TABLE I

Mechanical Properties of Fiber B at Strain Rate of 1.67%/sec

Property	English Units	Textile Units	Metric Units
Strength	430,000 psi	23 g/d	2.9×10^{10} dyn/cm^2
Modulus	11,000,000 psi	600 g/d	7.7×10^{11} dyn/cm^2
Elongation	3.7%	3.7%	3.7%
Sound Velocity	31,300 ft/sec	–	9400 m/sec

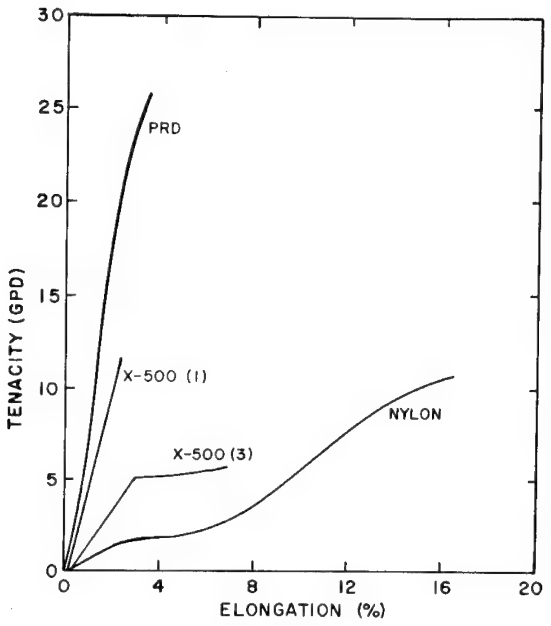

FIG. 4. Tensile stress-strain properties of new high modulus fibers at a strain rate of 5000%/sec.

estimate the theoretical strength possible in an organic polymer such as Fiber B. For this purpose the following assumptions have to be made: (a) bond breaking predominates; (b) the lowest bond energy involved is that of a C-C single bond, 5.5×10^{-12} erg/bond or 80 kcal/molecule; (c) the effective distance for force application is 0.2 Å; (d) the cross-section occupied by each polymer molecule is a square 10 Å by 10 Å. Based upon the above assumptions, the force involved in breaking each molecular chain would be 2.8×10^{-3} dyn. The theoretical strength can then be calculated from the product of the individual chain strength and the 10^{14} chains that can fit in 1 cm^2 cross-section. This product of 2.8×10^{11} dyn/cm^2 is equivalent to 4.1×10^6 psi in English units. For conversion to the unusual units used in the textile industry, it is necessary to introduce a density value of 1.45 g/cm^3. The figure thus obtained, 220 g/d, is almost 10 times that found for Fiber B. One conclusion from this comparison is that the 23 g/d achieved may only be the beginning for further improvements. Values of 30 to 40 g/d may be possible by breaking a larger fraction of molecules simultaneously. On the other hand, it is not likely that the theoretical value can be reached, since that requires that 100% of the chains break simultaneously. Even the observed strength of 23 g/d requires that over 10% of the chains break simultaneously. Because chain folding appears to be the rule in crystalline morphology, simultaneous breaking of many molecular chains does not occur.

It is proposed that the structure of the new aromatic polyamide polymers favors extended chains, in which simultaneous rupture is more likely than for

folded chains. Lindenmeyer has discussed chain folding in some detail, and has indicated some of the factors favoring this phenomenon. These factors include: (a) a single molecular weight species making up the material, (b) low molecular weight, (c) high temperature and pressure [19]. Actually, Lindenmeyer points out that folded chains are not favored energetically, because energy is needed to insert a crystalline fold. However, the energy required is more than compensated for by the decrease in energy resulting from the molecular portions brought into crystalline register. The ability for the extended chains to be brought into crystalline register is probably the real key to the behavior of the new polymers.

The previous discussion of properties is somewhat speculative, and it is useful to return to the SEM in an attempt to determine the morphological characteristics of the fractured PRD fibers. Figure 5 shows a single fiber from a yarn after tensile impact failure at 5000%/sec. Fiber B is much smaller in diameter than usual for industrial fibers. For example, Fiber B is less than 11.7 μm, whereas nylon tire cord fibers are over 27 μm. The microfibers produced by the tensile test, as shown in Figure 5, are approximately 1 μm in diameter. This fiber break-up can possibly be related to the high strength observed. The longitudinal splitting of the fibers nullifies the more conventional process, in which failure is propagated perpendicular to the fiber axis. This tendency to split rather than melt has been seen earlier with X-500 aromatic type fibers (Fig. 3), but the amount and degree of splitting was less pronounced [20]. Fibrillation of Fiber B is not limited to impact speeds. In Figure 6, Fiber B yarn fractured at a relatively slow tensile rate of straining at 1.67%/sec shows the same fibrillation, and the fibrils are again less than 1 μm in diameter.

The new high modulus fibers, such as X-500, PRD 49-III, and PRD 49-IV (Fiber B), were actually developed for applications in tire cord and laminates, where superior strength and modulus properties could produce longer wearing tires without flat spotting and composite structures with high strength and stiffness to weight ratios [21]. A laminate was prepared from Fiber B fabric and

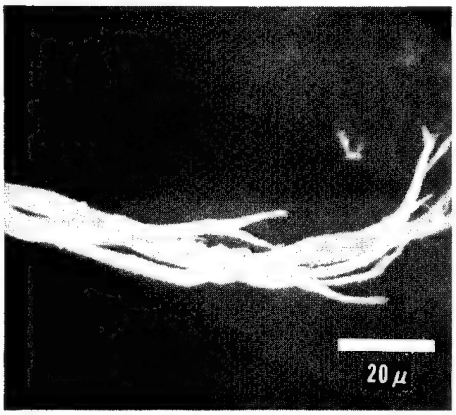

FIG. 5. Fibrillated appearance of PRD 49-IV fiber after tensile impact at 5000%/sec; 650X.

FIG. 6. Fibrillated fiber of PRD 49-IV after slow-speed test; 800X.

phenolic-modified polyvinyl butyral resin. The resulting laminate was impacted transversely with .22 caliber fragments of the type used by Susich [8]. A great deal of fibrillation was noted in the vicinity of the missile hole, as shown in Figure 7. Although changes were made in the structure, type of straining, and rate of impact, a similar type of fibrillation is observed in Figure 7 as had been shown in Figures 5 and 6.

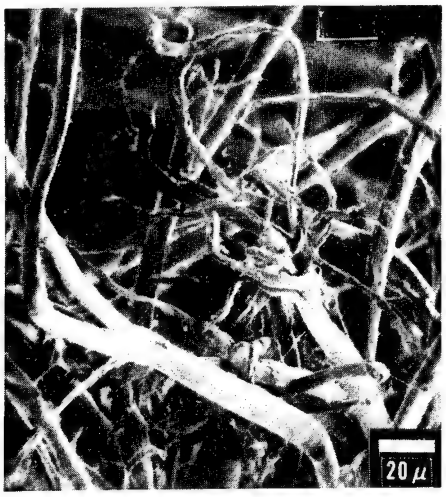

FIG. 7. Composite form of PRD 49-IV after impact with .22 Caliber missile; 360X.

SUMMARY

It has been shown that new organic fibers are now available with moduli as high as glass. The most successful to these, the PRD-49-type fiber developed by DuPont is probably based upon an all-para condensation product of p-phenylene diamine and terephthalic acid. The strengths exhibited, 20-25 g/d, are double those previously available commercially. SEM micrographs of the fractured fiber ends show that fibrillation appears to be characteristic, regardless of testing speed, type of impact, or lamination. The superior properties of PRD 49-IV fiber are probably due to (a) extended chain tie molecules, (b) a nearly perfect crystalline register, and (c) crack blunting through fibrillation.

REFERENCES

[1] W. J. Lyons, *Impact Phenomena in Textiles,* MIT Press, Cambridge, Massachusetts, 1963.
[2] R. Meredith, *J. Text. Inst., 45,* T-30 (1954).
[3] L. H. Hall, *J. Polym. Sci., 54,* 50 (1961).
[4] R. Laible and H. Morgan, *J. Polym. Sci., 54,* 53 (1961).
[5] R. Laible and H. Morgan, *J. Appl. Polym. Sci., 6,* 269 (1962).
[6] F. Figucia, L. I. Weiner, and R. C. Laible, *Polym. Eng. Sci., 11,* 289 (1971).
[7] A. F. Wilde, J. J. Ricca, and J. M. Rogers, *Polym. Eng. Sci., 12,* 41 (1972).
[8] G. Susich, L. M. Dogliotti, and A. S. Wrigley, *Text. Res. J., 28,* 360 (1958).
[9] W. K. Stone, H. F. Schiefer, and G. Fox, *Text. Res. J., 25,* 520 (1955).
[10] R. H. Wilfong and J. Zimmerman, *J. Appl. Polym. Sci., 17,* 2039 (1973).
[11] A. Peterlin, *Text. Res. J., 42,* 20 (1972).
[12] E. A. Tippetts and J. Zimmerman, *J. Appl. Polym. Sci., 8,* 2465 (1964).
[13] W. B. Black and J. Preston, *Man-Made Fibers,* vol. 2, H. F. Mark, S. M. Atlas, and E. Cernia, Eds., Interscience, New York, 1968, pp. 297–364.
[14] H. Hopff and A. Krieger, *Macromol. Chem., 47,* 93 (1961).
[15] V. E. Shashoua and W. M. Eakeckson, *J. Polym. Sci., 40,* 343 (1959).
[16] W. B. Black, J. Preston, H. S. Morgan, G. Rauman, and M. Lilyquist, *J. Macromol. Sci. Chem., A7,* 137 (1973).
[17] W. B. Black, *J. Macromol. Sci. Chem., A7,* 3 (1973).
[18] G. S. Fielding-Russell, *Text. Res. J., 41,* 861 (1971).
[19] P. H. Lindenmeyer, *J. Chem. Phys., 46,* 1902 (1967).
[20] R. Laible, F. Figucia, and J. Ferguson, *J. Macromol. Sci. Chem., A7,* 295 (1973).
[21] J. W. Moore, L. H. Miner, P. G. Riewald, and D. C. Wagle, paper presented at 4th National SAMPE Technical Conference, Palo Alto, California, October 17–19, 1972.

FIXING AND WETTING OF XEROGRAPHIC IMAGES ON PAPER–SCANNING ELECTRON MICROSCOPY STUDIES

L. H. LEE

Xerox Corporation, Wilson Center For Technology
Rochester, New York 14644

SYNOPSIS

In xerography, a thermoplastic toner is thermally fixed on paper to form an image. The fixing process can be examined with scanning electron microscopy. SEM is especially useful in determining the progress of fixing, wetting, and adhesion between toner and cellulose fibers. It shows that sintering, spreading, and penetration take place at different temperatures. The parameters controlling each step are briefly discussed. Viscosity appears to be the dominant factor for all three steps involved in the thermal fixing of xerographic toner.

INTRODUCTION

The word xerography originated from the Greek ξηρος, meaning dry, and γραφω, meaning writing, thus emphasizing the dry nature of the process as opposed to wet photographic methods [1]. By definition, xerography is "a process for copying printed material, pictures, etc., in which the latent image of the original material is transferred by the action of light to an electrically charged surface to which the image attracts oppositely charged dry ink particles, which are then fused in place on the copy paper, reproducing the original image" [2, 3]. The dry ink particles are technically also known as toner [4]. This study is related to the "wetting" of these "dry" ink particles on paper by a process similar to that by which a wet ink prints on paper.

Fixing of xerographic images actually involves three steps: (a) coalescence of polymer toner particles through sintering; (b) spreading of the coalesced melt; (c) penetration of the melt into the paper fiber. All three steps involve both surface-chemical and rheological parameters. In this paper we discuss briefly some of these parameters, and illustrate each step of the fixing process with scanning electron micrographs. In forthcoming papers we shall deal separately with sintering phenomena [5] and the spreading and penetration of toner melt [6].

EXPERIMENTAL

Our experimental toner was a styrene-acrylate copolymer and a carbon black. The xerographic images were prepared by radiant fusing of the toner, to

Applied Polymer Symposium No. 23, 193-200 (1974)

retain the free flow surface. The images were thermally fixed at 149°, 161°, 177°, and 193°C on Xerox paper. After the paper cooled to room temperature, a section of the image was cut with a sharp razor for examination with the SEM. The general techniques for preparing SEM samples have been described by Fernquist and Short [7]. The samples of paper were coated with a thin film (500-1000 Å) of gold. The coating operation took place at 6-20 V for 1-3 sec. Care was taken to prevent the polymer surface from being heated by radiation. The conductive surface could then be viewed directly in the SEM. The SEM was operated at 20 kV with specimen currents of 10^{-9} to 10^{-10} A.

RESULTS AND DISCUSSION

Frenkel, who first studied the physics of sintering, derived an approximate expression relating the driving force, γ, and the retardation force, η, of coalescence of two spherical particles in contact:

$$\frac{x^2}{a} = \frac{3}{2}\left(\frac{\gamma}{\eta}\right)t \tag{1}$$

where x is the radius of the interface as shown in Figure 1, a is the radius of the spheres, γ is the surface tension, η the viscosity, and t the time.

The presence of carbon black in a xerographic toner can change its flow characteristics. If the toner behaves like a non-Newtonian fluid, Equation (1) may not be adequate to describe the relationship between x^2/a and the sintering time t. In a forthcoming paper we shall elaborate on the effect of carbon black on the sintering of xerographic toner [5]. In general, eq. (1) describes the effect of surface tension and viscosity on sintering or coalescence of polymer particles. However, coalescence is usually more complex than described by the Frenkel equation. Toner particles are not only of different sizes but also of different shapes. We can clearly see the real situation in SEM micrographs of Figures 2 and 3.

Partial sintering can be observed in SEM micrographs of images fixed at 149°C. In figure 2 at 200X, there are both sintered and unsintered particles,

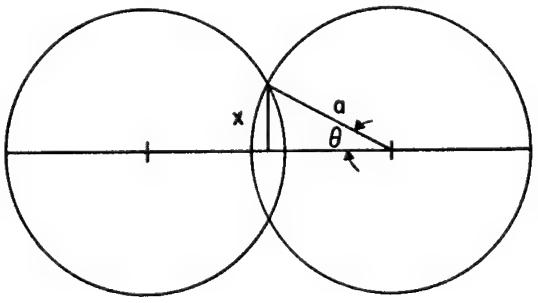

FIG. 1. Frenkel's model of sintering of two spheres.

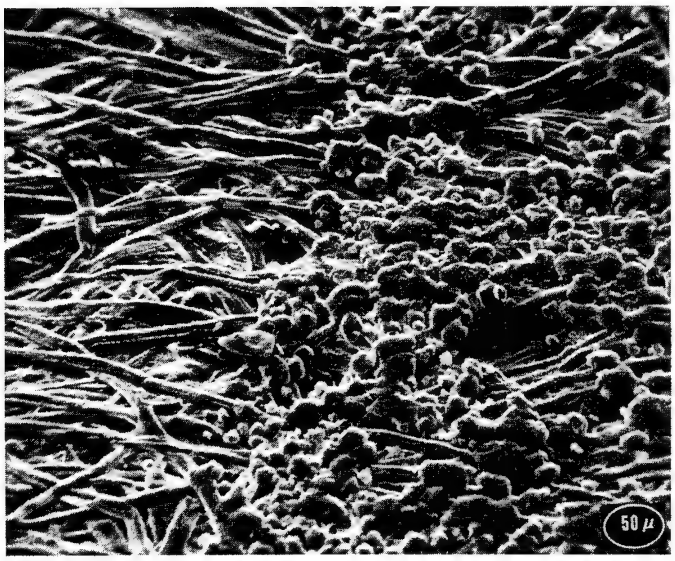

FIG. 2. Partial sintering of an experimental toner at 149°C; 200X.

where the sintered particles stick together in groups. Most particles have not formed a toner-paper bond. At high magnification, 1000X in Figure 3, we can identify the unsintered from the sintered particles, because they are loosely attached to the fibers.

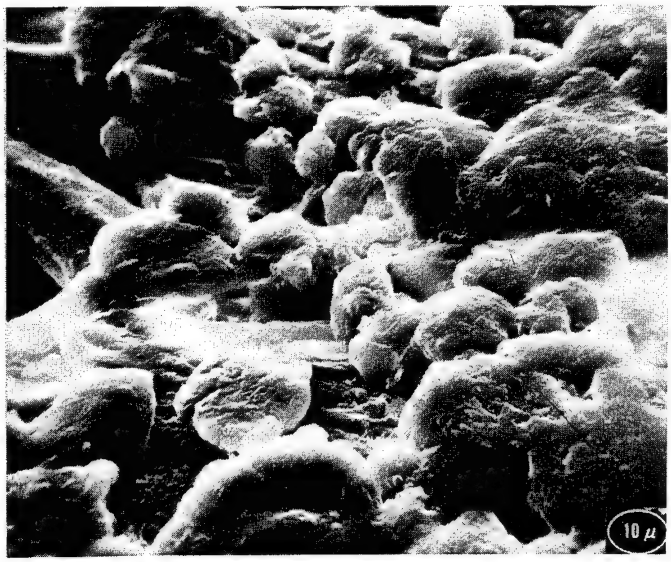

FIG. 3. Partial sintering of experimental toner at 149°C; 1000X.

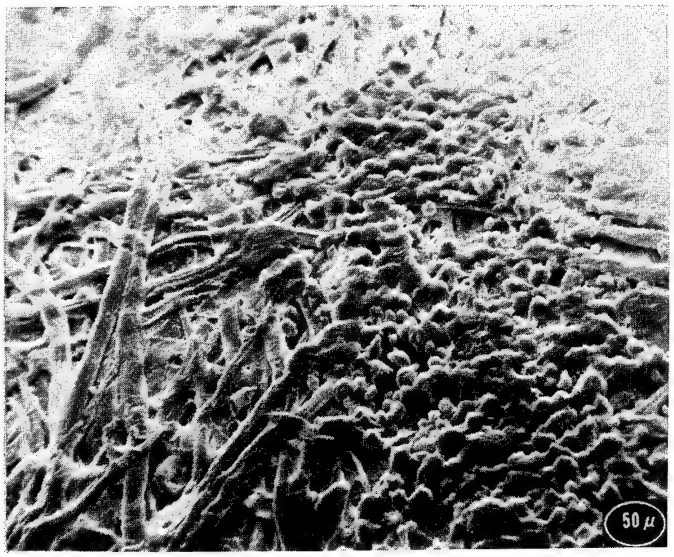

FIG. 4. Advanced sintering of experimental toner at 161°C; 200X.

At higher temperatures, the viscosity of the toner melt decreased, and advanced sintering took place. Figures 4 and 5 of the image obtained at 161°C show that there are fewer unsintered particles. The low magnification micrograph of Figure 4 shows a nearly completely sintered image joined together, like a band, from top to bottom. The top of each sintered particle can still be identified in the SEM at high magnification, as shown in Figure 5 at 1000X.

FIG. 5. Advanced sintering of experimental toner at 161°C; 1000X.

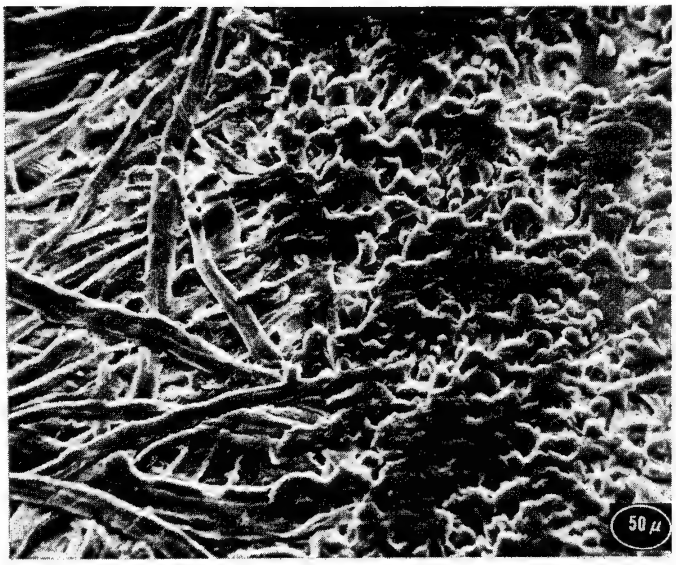

FIG. 6. Melting and wetting takes place at 177°C; 200X.

When the image was fixed at 177°C, the experimental toner began to wet the paper. This appearance of wetness is evident in Figures 6 and 7. At low magnification, 200X in Figure 6, we can see a darker and flatter toner melt in the center of the micrograph. The smoothness of the image is more distinguishable in Figure 7 at 1000X than in any of the previous figures.

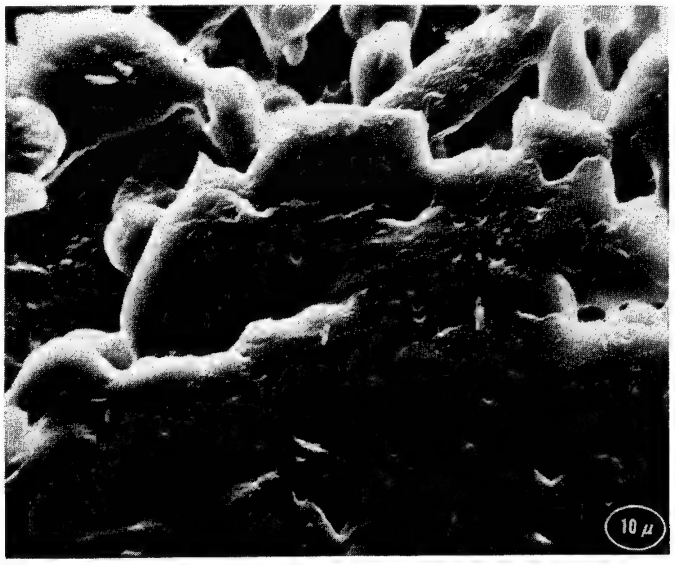

FIG. 7. Flow of toner is not complete at 177°C; 1000X.

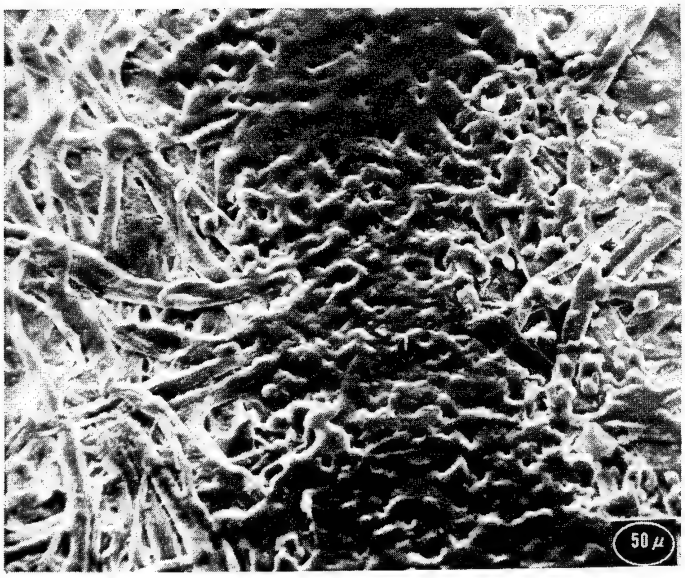

FIG. 8. Flow into the pores of the paper has become advanced at 193°C; 200X.

However, the image still contains pinholes and imperfections.

The third step of fixing, namely penetration, can be identified in images fixed at 193°C. Micrographs of such images are presented in Figures 8 and 9,

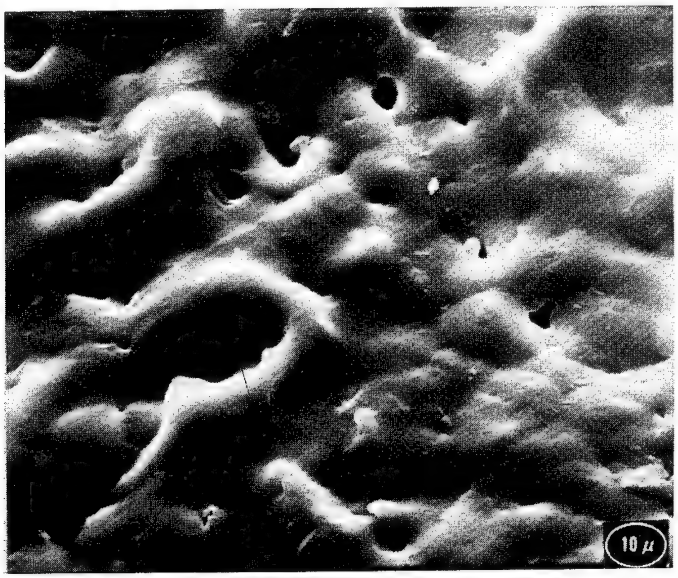

FIG. 9. Toner particles have fused completely, and penetration has made top surface rougher at 193°C; 1000X.

where the image does not only appear "wet", but also penetrates into the asperities formed by the cellulosic fibers. Penetration has also produced a rougher surface, but the fibers are better wetted than at lower temperatures, and a strong toner-fiber bond is finally formed.

By controlling the fixing temperature, and thus the viscosity of the toner, we could identify each fixing step in the SEM. Overlapping of steps, especially at high temperatures, were unavoidable. For example, Figures 8 and 9 do not just represent the penetration step, since all three steps take place simultaneously.

Equation (1) described the sintering phenomenon. Similar equations can be developed for spreading and penetration. For spreading, the velocity can be expressed generally by the following equation:

$$\langle V \rangle = f_1\left(\frac{\gamma \cos \theta_\infty}{\eta r_0}\right) \tag{2}$$

where γ is the surface tension and η the viscosity, r_0 is the radius of the sessile drop, and θ_∞ is the equilibrium contact angle.

To develop an equation for penetration it is necessary to first assume or identify the type of capillaries involved. Generally, an assumption of parallel slits or V-shaped grooves is sufficient to apply the proper equation. In the absence of an external pressure, the following expression describes the effect of various parameters on the penetration rate [10]:

$$\frac{d\ell}{dt} = f_2\left(\frac{\delta \gamma \cos \theta}{\eta \ell}\right) \tag{3}$$

where ℓ is the depth of penetration and δ the width of the slit.

In forthcoming papers [5, 6] we shall illustrate with actual examples that viscosity is more important than surface tension in controlling sintering, spreading, and penetration. Here we merely mention the effect of temperature on both viscosity and surface tension of a toner. A change of 10°C at the fusing level generally results in at least a factor 2 change in viscosity. But the same temperature change brings about only a 2% variation in the surface tension, assuming the surface tension temperature coefficient to be −0.06 to −0.07 dyn/cm/°C [11], and the surface tension to be 32 dyn/cm. Therefore, the viscosity appears to be the dominant factor governing all three steps of thermal fixing with respect to temperature change.

CONCLUSIONS

This preliminary study indicates that thermal fixing of a xerographic toner on paper involves three steps: (a) sintering, (b) spreading, and (c) penetration. By controlling the fixing temperature, it was possible to prepare images at different levels of development. Examination with scanning electron microscopy makes identification of each step possible. This technique is also suitable to

examine the toner-cellulose fiber bond and adhesion in general. For example, micrographs indicated that, for the experimental toner used, sintering took place between 141° and 161°C, slight spreading at 177°C, and penetration at 193°C.

The parameters controlling the three steps of thermal fixing were briefly discussed. Viscosity, rather than surface tension, appears to be the dominant factor for all three thermal fixing steps in the absence of any external force.

The author thanks R. G. Fernquist and Mrs. J. Dulmage for preparing the scanning electron micrographs.

REFERENCES

[1] R. M. Schaffert and C. D. Oughton, *J. Opt. Soc. Amer.*, 38 991 (1948).
[2] *Webster's New Twentieth Century Dictionary*, World Publishing, Cleveland, Ohio, 1971.
[3] J. H. Dessauer and H. E. Clark, *Xerography and Related Processes*, Focal Press, London and New York, 1965.
[4] L. E. Walkup, U. S. Pat. #2,618,551 (November 18, 1952).
[5] L. H. Lee, *Proc. 166th Meeting-ACS-Org. Coatings and Plastics Chem., 33*(2), 467 (1973).
[6] L. H. Lee, *Proc. 166th Meeting ACS, Org. Coatings and Plastic Chem., 33*(2), 479 (1973).
[7] R. G. Fernquist and J. M. Short, *Proc. 14th Annu. Conf. Soc. Vac. Coaters*, p. 26, 1971.
[8] J. Frenkel, *J. Phys. (U.S.S.R.)*, *9*, 385 (1945).
[9] H. VanOene, Y. F. Chang, and S. Newman, *J. Adhesion, 1*, 54 (1969).
[10] K. Kanmaru, *Kolloid-Z. Z. Polym., 192*, 51 (1963).
[11] R. J. Roe, *Proc. Nat. Acad. Sci., 6*, 56, 918 (1966).

AUTHOR INDEX

SUBJECT INDEX

Published Applied Polymer Symposia

1965	No. 1	High Speed Testing, Vol. V Co-Chaired by A. G. H. Dietz and Frederick R. Eirich
1966	No. 2	Thermoanalysis of Fibers and Fiber-Forming Polymers Edited by Robert F. Schwenker, Jr.
	No. 3	Structural Adhesives Bonding Edited by Michael J. Bodnar
1967	No. 4	Weatherability of Plastic Materials Edited by Musa R. Kamal
	No. 5	High Speed Testing, Vol. VI: The Rheology of Solids Co-Chaired by Rodney D. Andreqs, Jr., and Frederick R. Eirich
	No. 6	Fiber Spinning and Drawing Edited by Myron J. Coplan
1968	No. 7	Polymer Modification of Rubbers and Plastics Edited by Henno Keskkula
1969	No. 8	International Symposium on Polymer Modification Edited by K. A. Boni and F. A. Sliemers
	No. 9	High Temperature Resistant Fibers from Organic Polymers Edited by J. Preston
	No. 10	Analysis and Characterization of Coatings and Plastics Edited by Claude A. Lucchesi
	No. 11	New Polymeric Materials Edited by Paul F. Bruins
	No. 12	High Speed Testing, Vol. VII: The Rheology of Solids Co-Chaired by Rodney D. Andrews, Jr., and Frederich R. Eirich
1970	No. 13	Membranes from Cellulose and Cellulose Derivatives Edited by Albin F. Turbak
	No. 14	Silicone Technology Edited by Paul F. Bruins
	No. 15	Polyblends and Composites Edited by Paul F. Bruins
1971	No. 16	Scanning Electron Microscopy of Polymers and Coatings Edited by L. H. Princen
	No. 17	Mechanical Performance and Design in Polymers Edited by O. Delatycki
	No. 18	Proceedings of the Fourth International Wool Textile Research Conference Edited by Ludwig Rebenfeld
1972	No. 19	Processing for Adhesives Bonded Structures Edited by Michael J. Bodnar
1973	No. 20	United States–Japan Seminar on Polymer Processing and Rheology Edited by D. C. Bogue, M. Yamamoto, and J. L. White
	No. 21	High-Temperature and Flame-Resistant Fibers Edited by J. Preston and J. Economy
	No. 22	Polymeric Materials for unusual Service Conditions Edited by Morton A. Golub and John A. Parker
1974	No. 23	Scanning Electron Microscopy of Polymers and Coatings. II Edited by L. H. Princen

More on Polymers-
from Wiley-Interscience

1. Structured Polymer Properties

The Identification, Interpretation, and Application of Crystalline Polymer Structure

By Robert J. Samuels, *Hercules, Inc.*

This book compiles many varied physical methods and describes them in a systematic, interdependent form. By using the data from the same series of samples to describe all techniques, the author shows the value of each method. The reader will understand the total structural picture of a crystalline polymer process, and learn how the quantitative use of these techniques, in conjunction with process information from sample preparation, can reveal the intimate structural patterns that control properties.

1974 (approx.) 272 pages $19.95 (tent.)

2. Polymer Stabilization

By Lincoln W. Hawkins, *Bell Telephone Laboratories, Inc., New Jersey*

Polymer Stabilization presents a mechanistic approach to the problems of polymer stabilization in order to combat the major environmental factors responsible for deterioration. The approach shows the reader how to make a scientific choice of a stabilizer or stabilization system suitable for protection against degradation.

1971 452 pages $27.50

3. Macromolecular Syntheses, Volume 5

Edited by Emerson L. Wittbecker, *E. I. DuPont DeNemours Co., Inc., Delaware*

A volume in the Wiley-Interscience series on Macromolecular Syntheses, edited by C. G. Overberger

This volume presents syntheses that have been checked for reproducibility, and offers detailed descriptions of the preparation and characterization of a wide variety of the polymeric structures. The polymers described range from well known structures to new and unusual ones.

1974 approx. 96 pages In Press

4. Molecular Weight Distributions in Polymers, Volume 18

By Leighton H. Peebles, Jr., *Chemstrand Research Center, Inc.*

A volume in the Wiley-Interscience series of Polymer Reviews, edited by H. F. Mark and E. H. Immergut

Here is a comparative summary of the various molecular weight distributions in polymers that are derived from kinetic or statistical arguments. Written for engineers and polymer characterization chemists involved in the manufacture of commercial polymers, this book helps them find out how changes in the manufacturing process affect the molecular weight distribution of the polymers.

1971 331 pages $19.75

5. Introduction to Polymer Viscoelasticity

By John J. Aklonis, *University of Southern California, Los Angeles*, William J. MacKnight, *University of Massachusetts*, and Mitchel Shen, *University of California, Berkeley*

Presents the fundamental concepts of molecular viscoelasticity in the bulk phase of polymers. Following an introduction, the book treats time-temperature correspondence, transition and relaxation in amorphous polymers, statistics of a polymer chain, rubber elasticity, viscoelastic models, and chemical stress relaxation.

1972 249 pages $15.75

WILEY-INTERSCIENCE, a division of John Wiley & Sons, Inc.
605 Third Avenue, New York, N.Y. 10016
In Canada: 22 Worcester Road, Rexdale, Ontario

Prices subject to change without notice. 092 A4530-WI